RESONANCE MEETING
MAY 30 TO JUNE 1, 1999
NATIONAL CENTER FOR PHYSICAL ACOUSTICS
THE UNIVERSITY OF MISSISSIPPI

VOLUME 2. TRANSPARENCIES

Proceedings of a Symposium Sponsored by the Office of Naval Research

Compiled by
Elizabeth A. Furr
National Center for Physical Acoustics
The University of Mississippi
University, MS 38677

NCPA Report Number: LF1000-01

TABLE OF CONTENTS

ELASTICITY OF LEUCITE THROUGH HIGH-TEMPERATURE PHASE TRANSITIONS

DONALD ISAAK[1], ANDY SHEN[2], ORSON ANDERSON[1], JOHN CARNES[1]
[1]UNIVERSITY OF CALIFORNIA AT LOS ANGELES
[2]UNIVERSITY OF CAMBRIDGE, UK

Preview

- Elasticity of Leucite
  - Phase transition
- Rutile
  - Info on K′ from high-T RUS
- RUS and pressure - SiO_2

Yes	No
Leucite	**Lucite**
⇒ **White, gray mineral $KAlSi_2O_6$** ⇒ **Important constituent in alkali rocks (esp. lava)**	⇒ **Trademark name for a transparent synthetic resin: polymerized methyl methacrylate**

Phase Transitions in Leucite

cooling →		← heating
$Ia3d$	$I4_1/acd$	$I4_1/a$

~ 938 K	~ 918 K
(Volume change)	(Ferroelastic)

Cubic	Tetragonal	Tetragonal

Sample Description

- Locality: Vesuvius, Italy
- Density: 2.461 g/cm^3
- Dimensions: 1.739 mm x 1.944 mm x 1.969 mm
- Starting elastic moduli for the high temperature phase ($Ia3d$)

C_{11} = 170 GPa
C_{12} = 67 GPa
C_{44} = 20 GPa

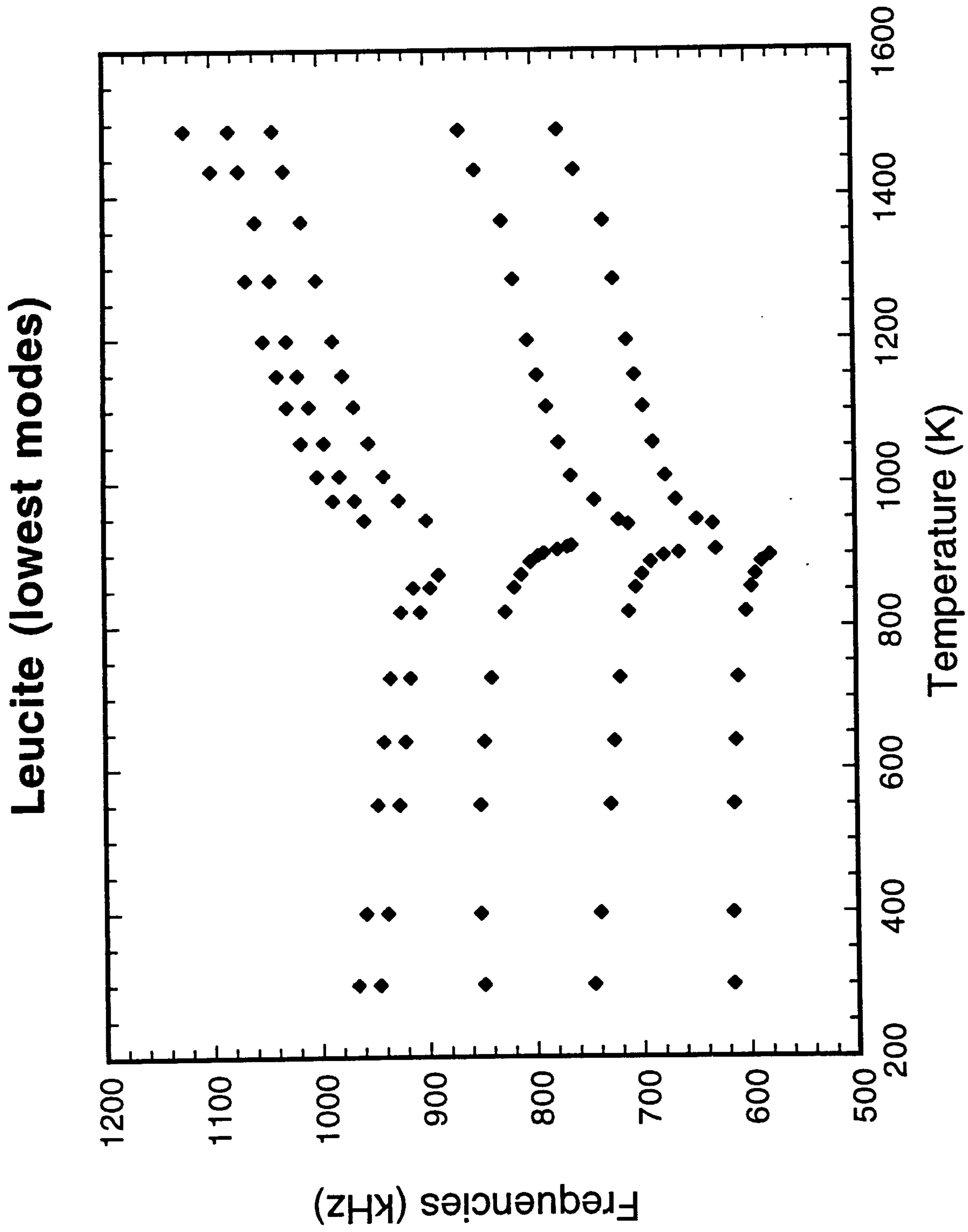
Leucite (lowest modes)
Frequencies (KHz)
1200
1100
1000
900
800
700
600
500
Temperature (K)
200
400
600
800
1000
1200
1400
1600

- Leucite -
Variation of Frequencies with C_{44}

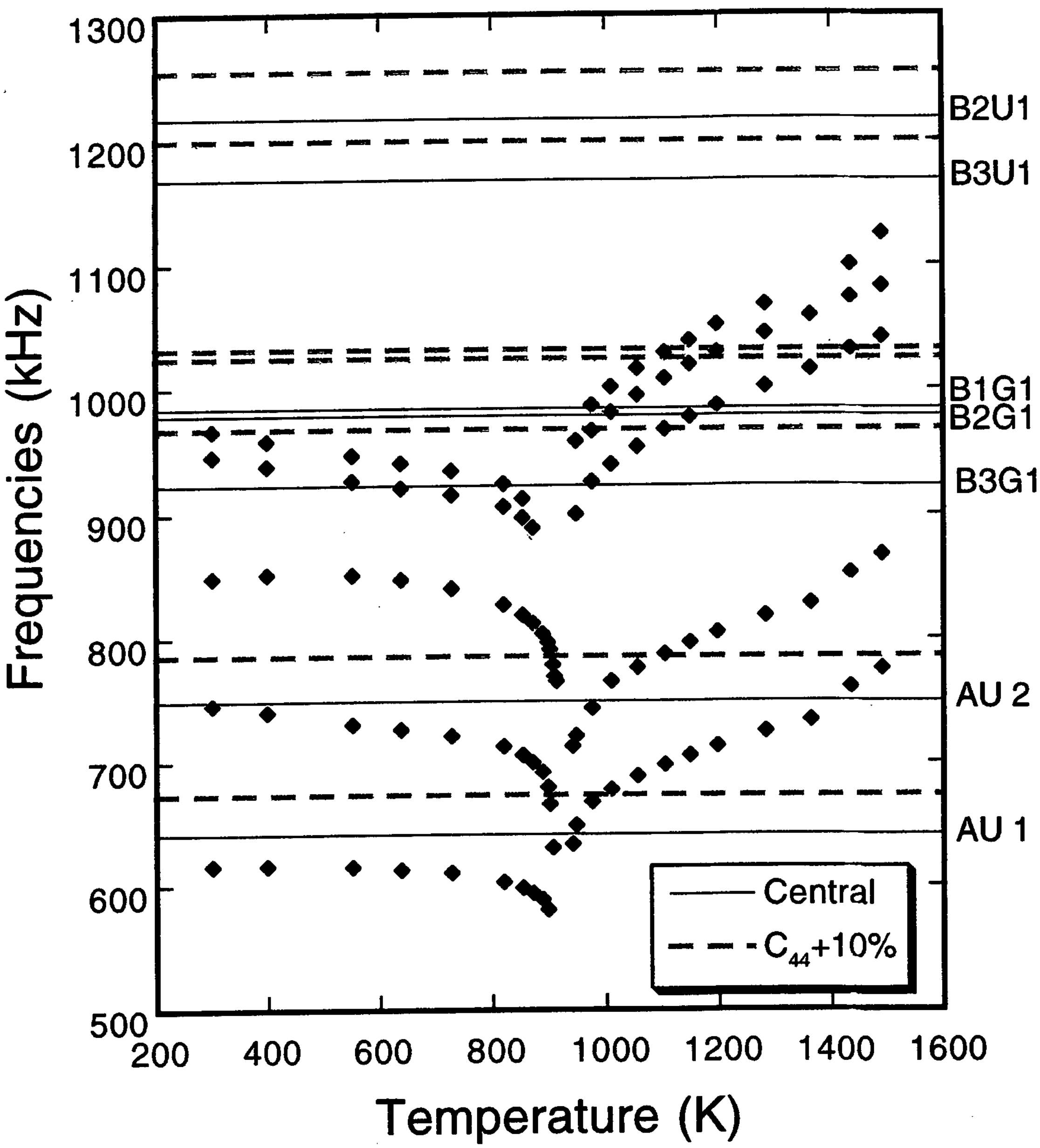

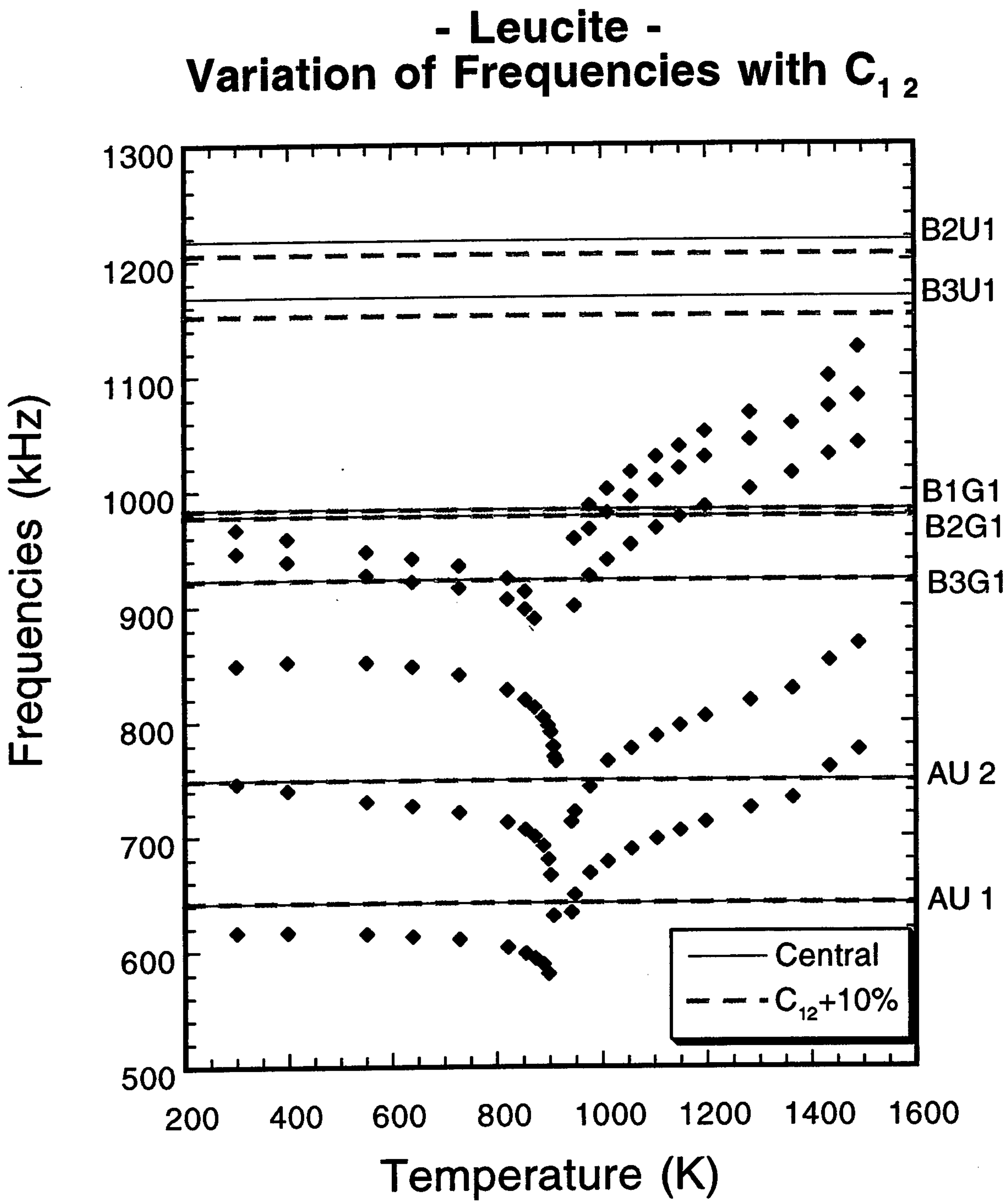

- Leucite -
Variation of Frequencies with C_{12}
Frequencies (kHz)
1300
1200
1100
1000
900
800
700
600
500
200
400
600
800
1000
1200
1400
1600
Temperature (K)
B2U1
B3U1
B1G1
B2G1
B3G1
AU 2
AU 1
Central
C_{12}+10%

TR-7

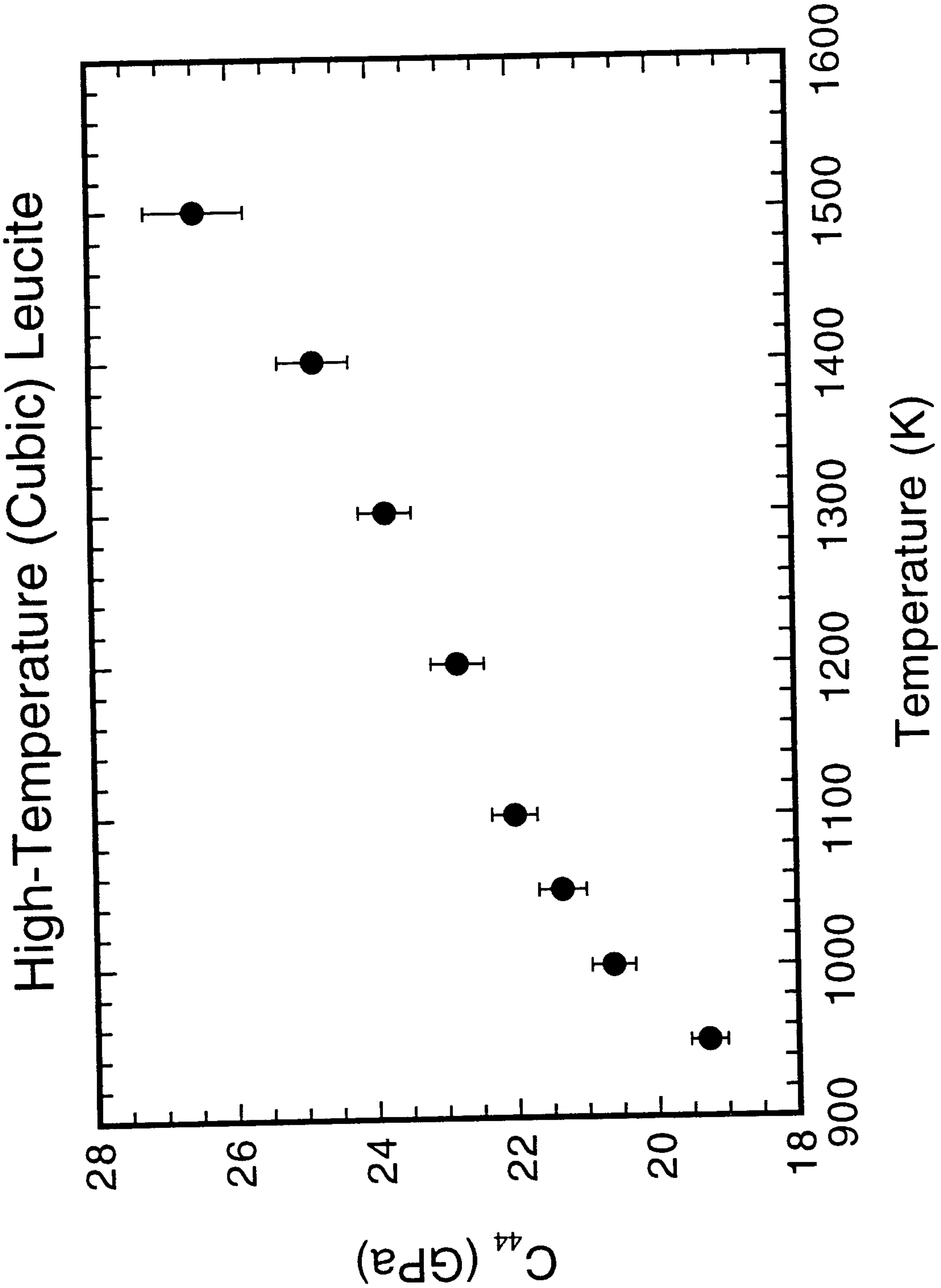
High-Temperature (Cubic) Leucite
C44 (GPa)
Temperature (K)
18
20
22
24
26
28
900
1000
1100
1200
1300
1400
1500
1600

TR-8

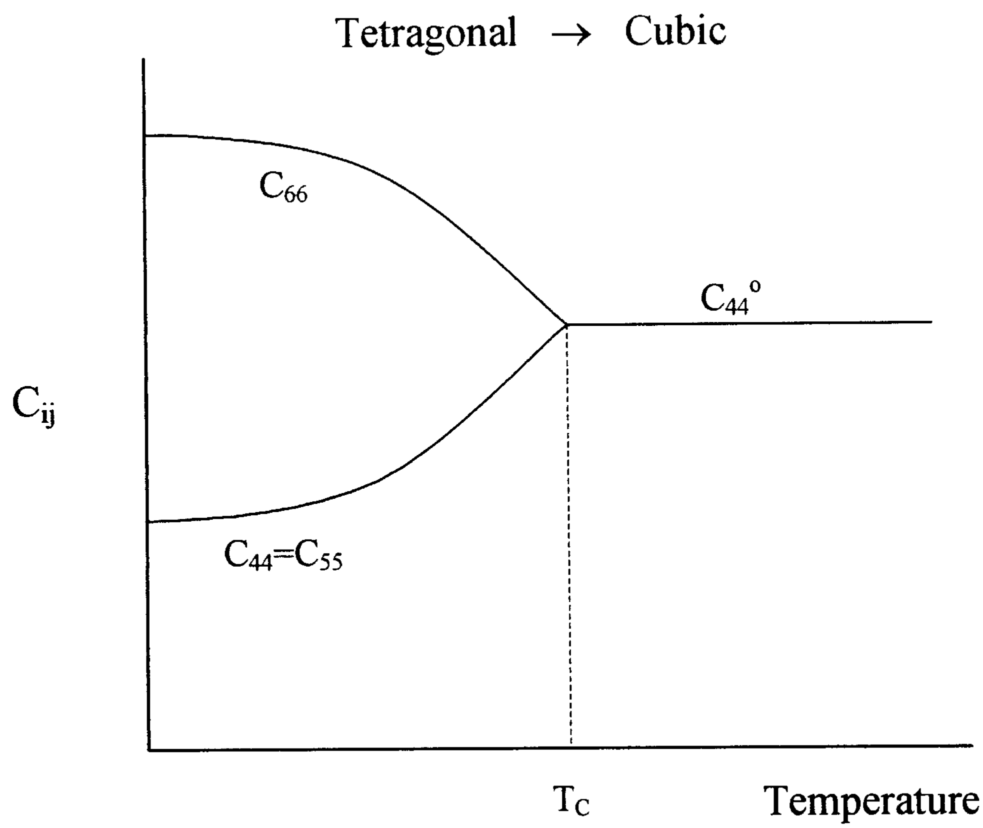

After T_C:

$C_{44} = C_{55} = C_{66} = C_{44}^{o}$

C_{44}^{o} is the normal C_{44} without influence from transition

(See Carpenter et al., *Eur. J. Mineral.*, *10*, 621-691, 1998)

Our Observations with Leucite:

- Wide range of T over which T_C influences C_{44} in leucite (Compare to Migliori et al. 1993)

- C_{44} does not equal C_{44}^{o} unless d $C_{44}/\mathrm{d}T > 0$ (which seems implausible)

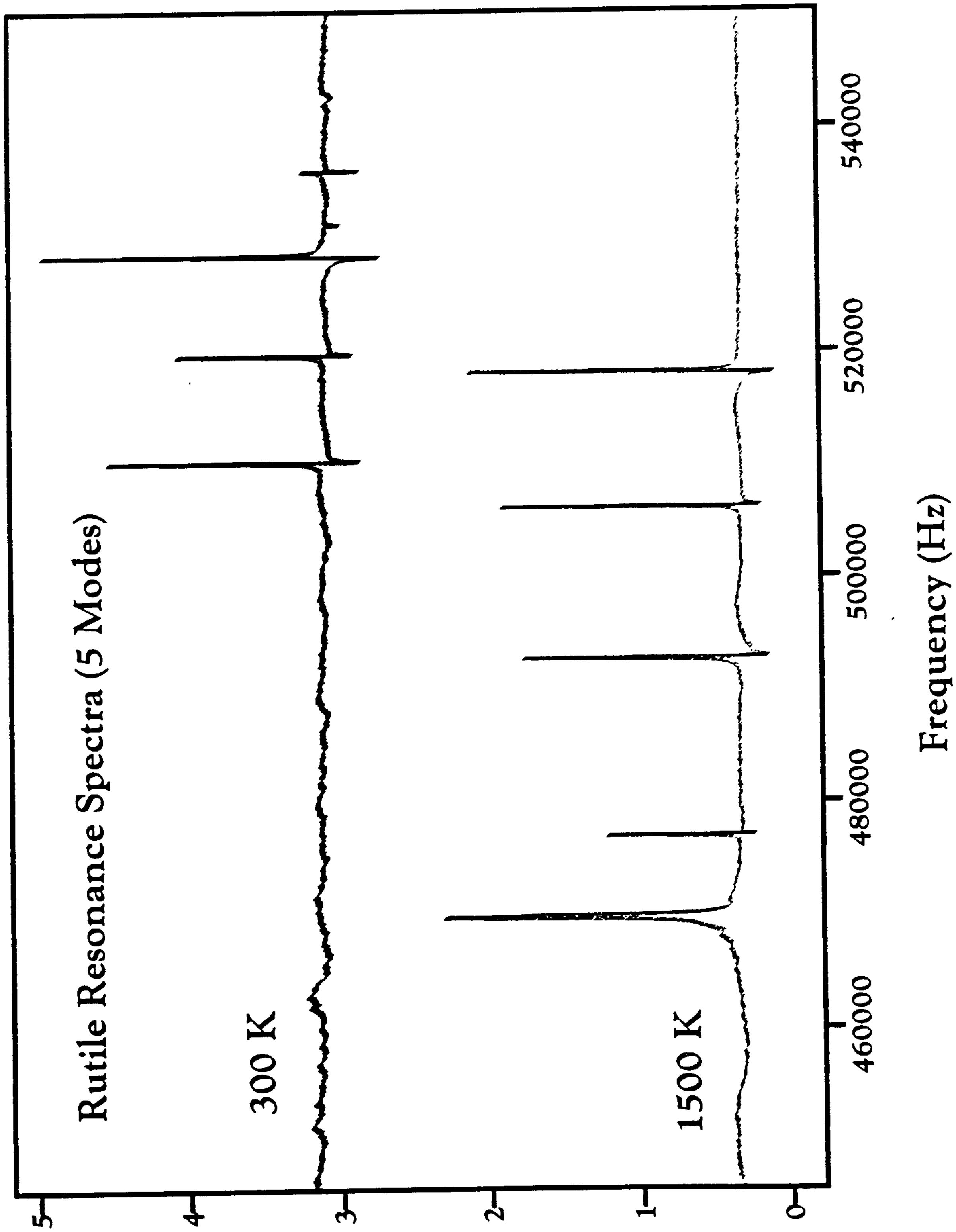
Rutile Resonance Spectra (5 Modes)
300 K
1500 K
Frequency (Hz)
460000
480000
500000
520000
540000
0
1
2
3
4
5

TR-10

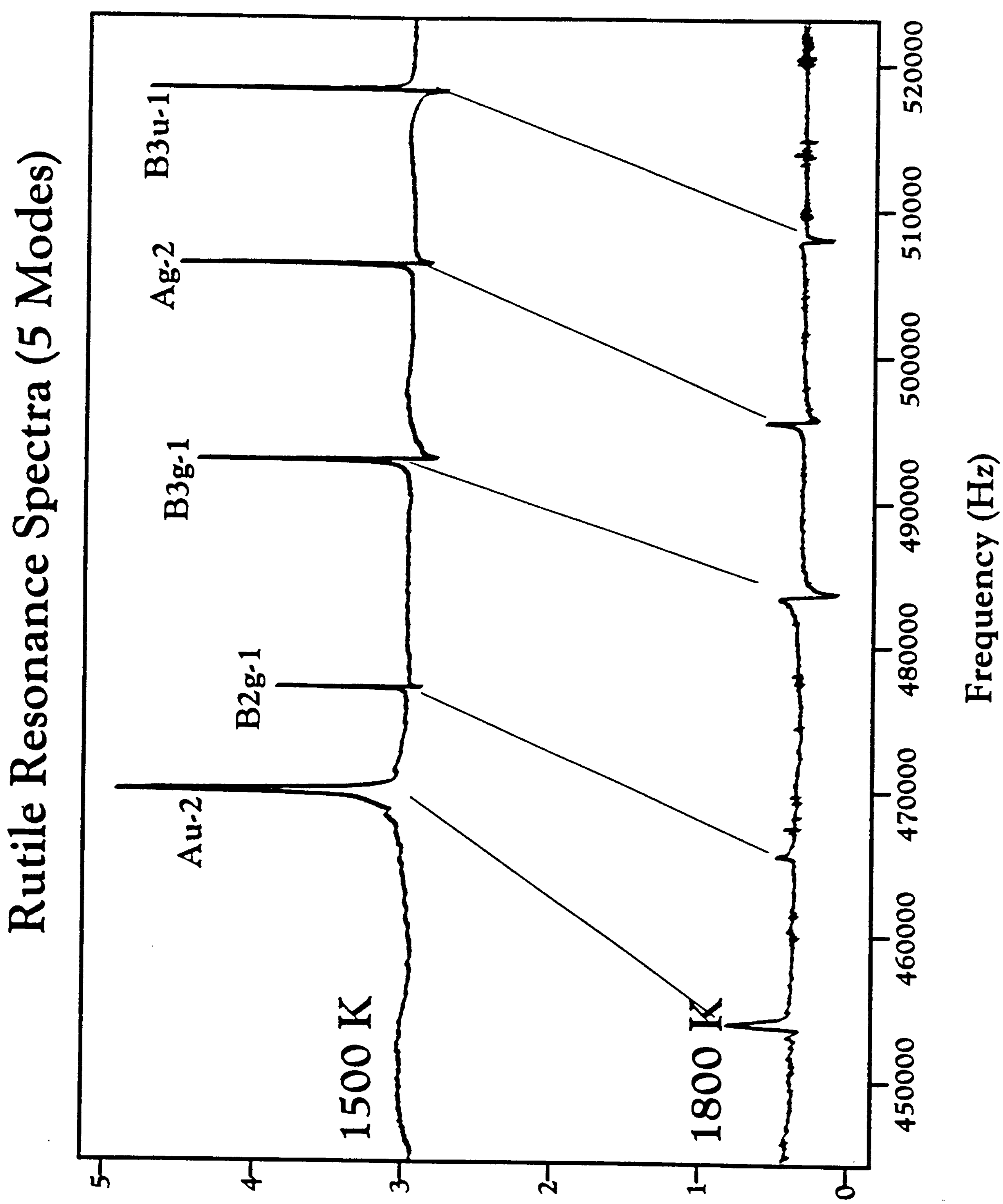
Rutile Resonance Spectra (5 Modes)
1500 K
1800 K
Au-2
B2g-1
B3g-1
Ag-2
B3u-1
Frequency (Hz)
450000
460000
470000
480000
490000
500000
510000
520000
0
1
2
3
4
5

Temperature Variation of Modes

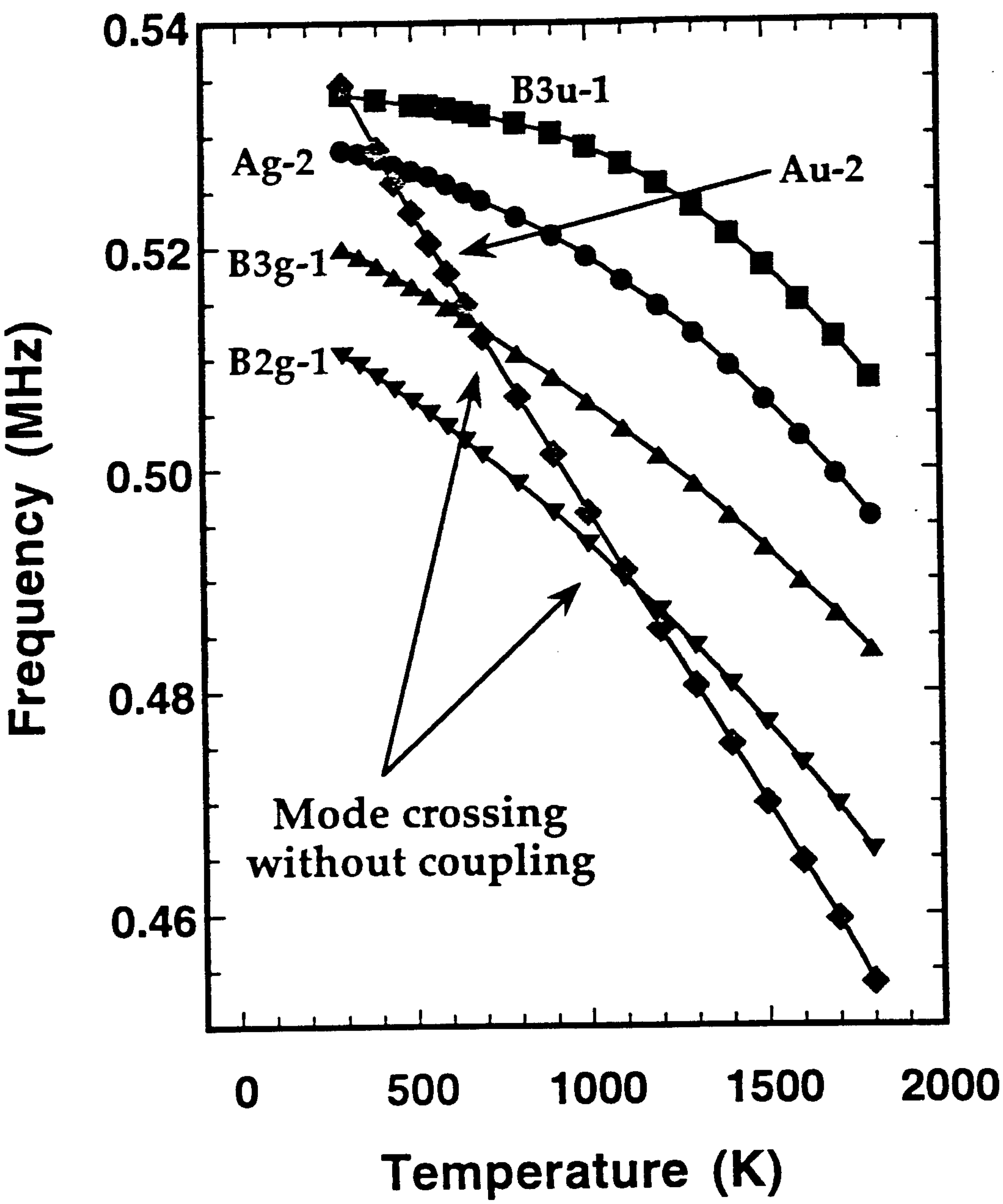

TR-12

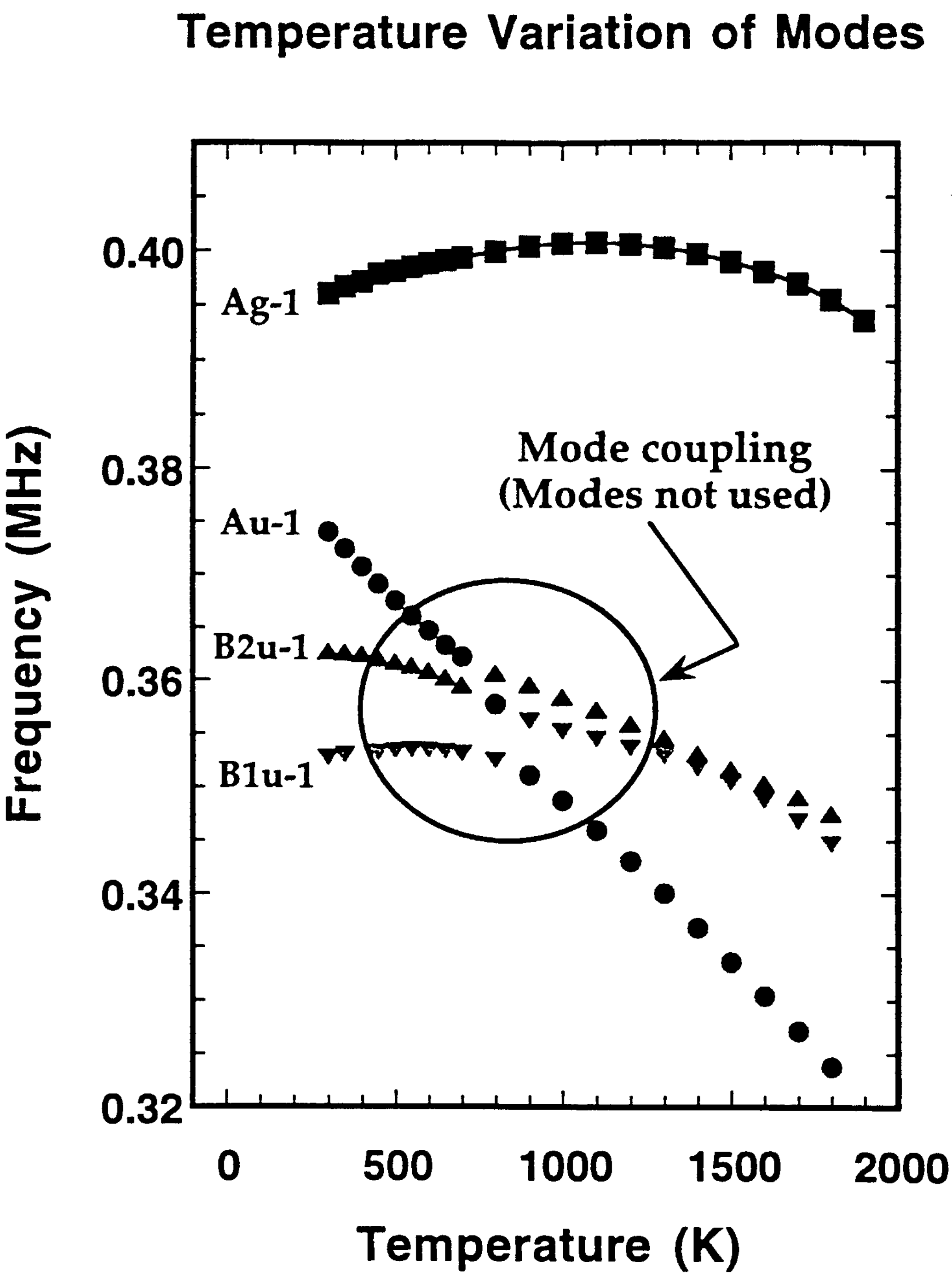

Temperature Variation of Modes
Frequency (MHz)
0.40
0.38
0.36
0.34
0.32
Ag-1
Au-1
B2u-1
B1u-1
Mode coupling
(Modes not used)
0
500
1000
1500
2000
Temperature (K)

TR-13

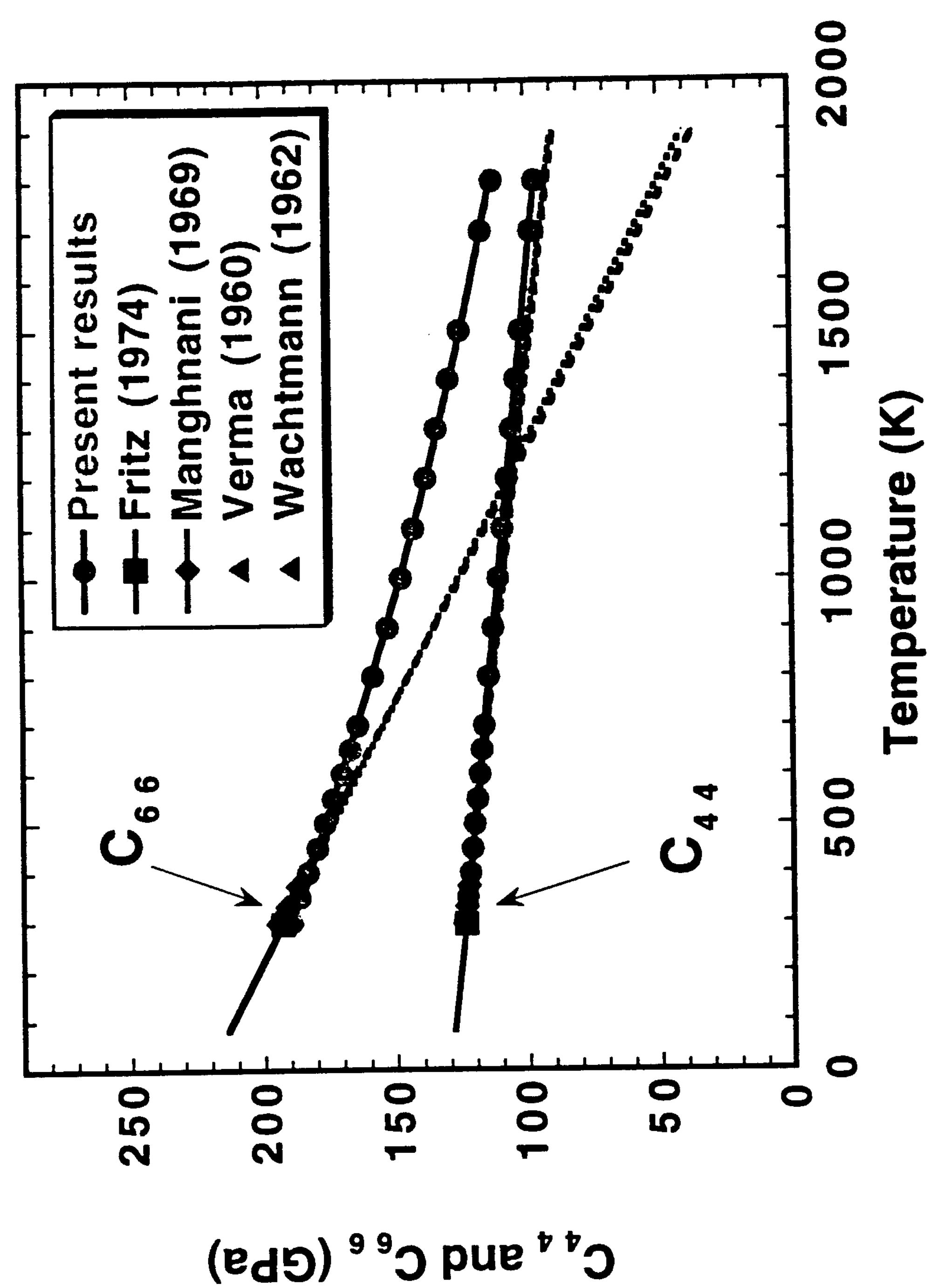
Present results
Fritz (1974)
Manghnani (1969)
Verma (1960)
Wachtmann (1962)
C_{66}
C_{44}
Temperature (K)
C_{44} and C_{66} (GPa)
0
500
1000
1500
2000
50
100
150
200
250

TR-14

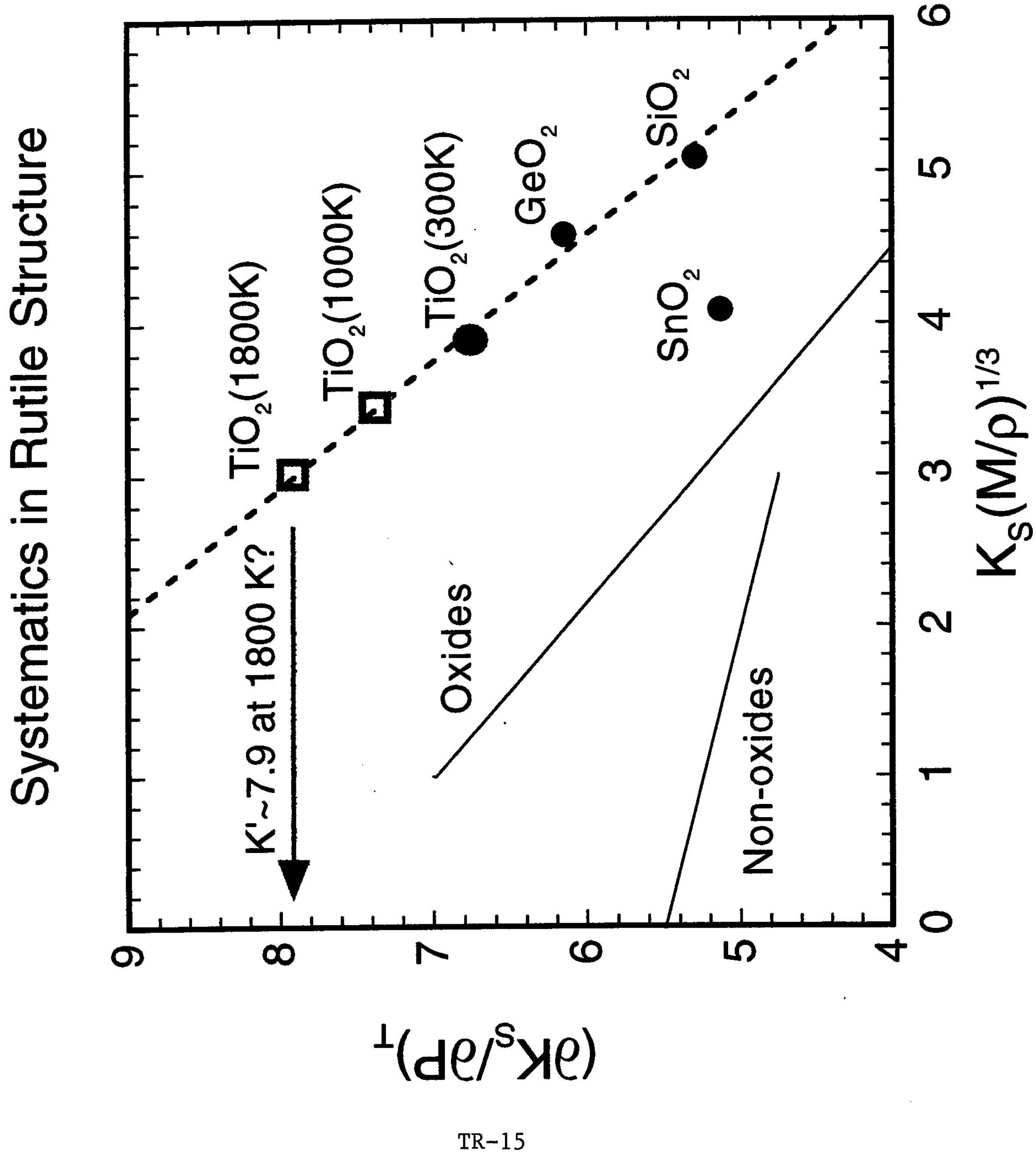

Systematics in Rutile Structure
K'~7.9 at 1800 K?
TiO$_2$(1800K)
TiO$_2$(1000K)
TiO$_2$(300K)
GeO$_2$
SiO$_2$
SnO$_2$
Oxides
Non-oxides
$(\partial K_s/\partial P)_T$
$K_S(M/\rho)^{1/3}$

TR-15

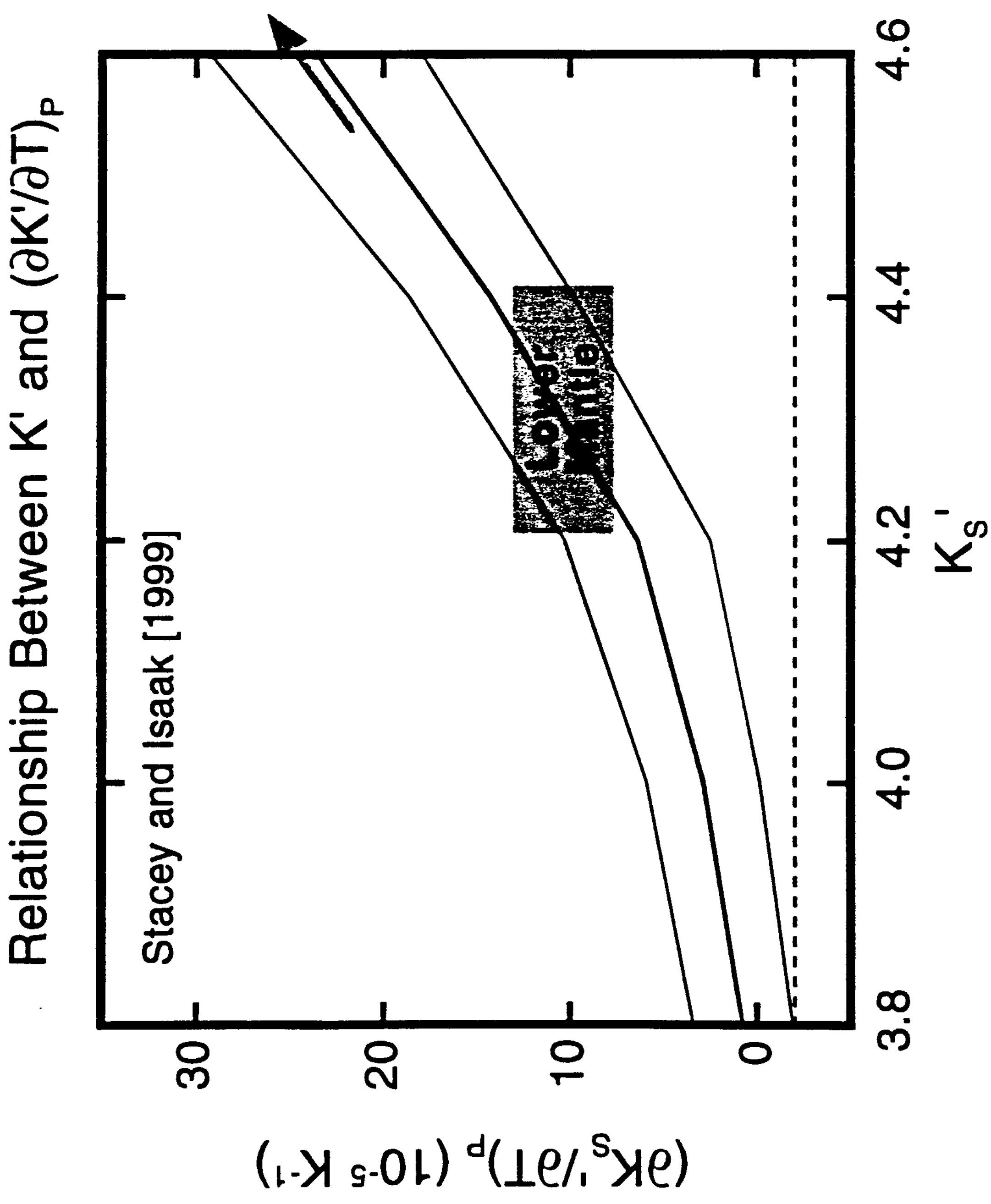
Relationship Between K' and (∂K'/∂T)P
Stacey and Isaak [1999]
Lower Mantle
(∂KS'/∂T)P (10-5 K-1)
30
20
10
0
3.8
4.0
4.2
4.4
4.6
KS'

TR-16

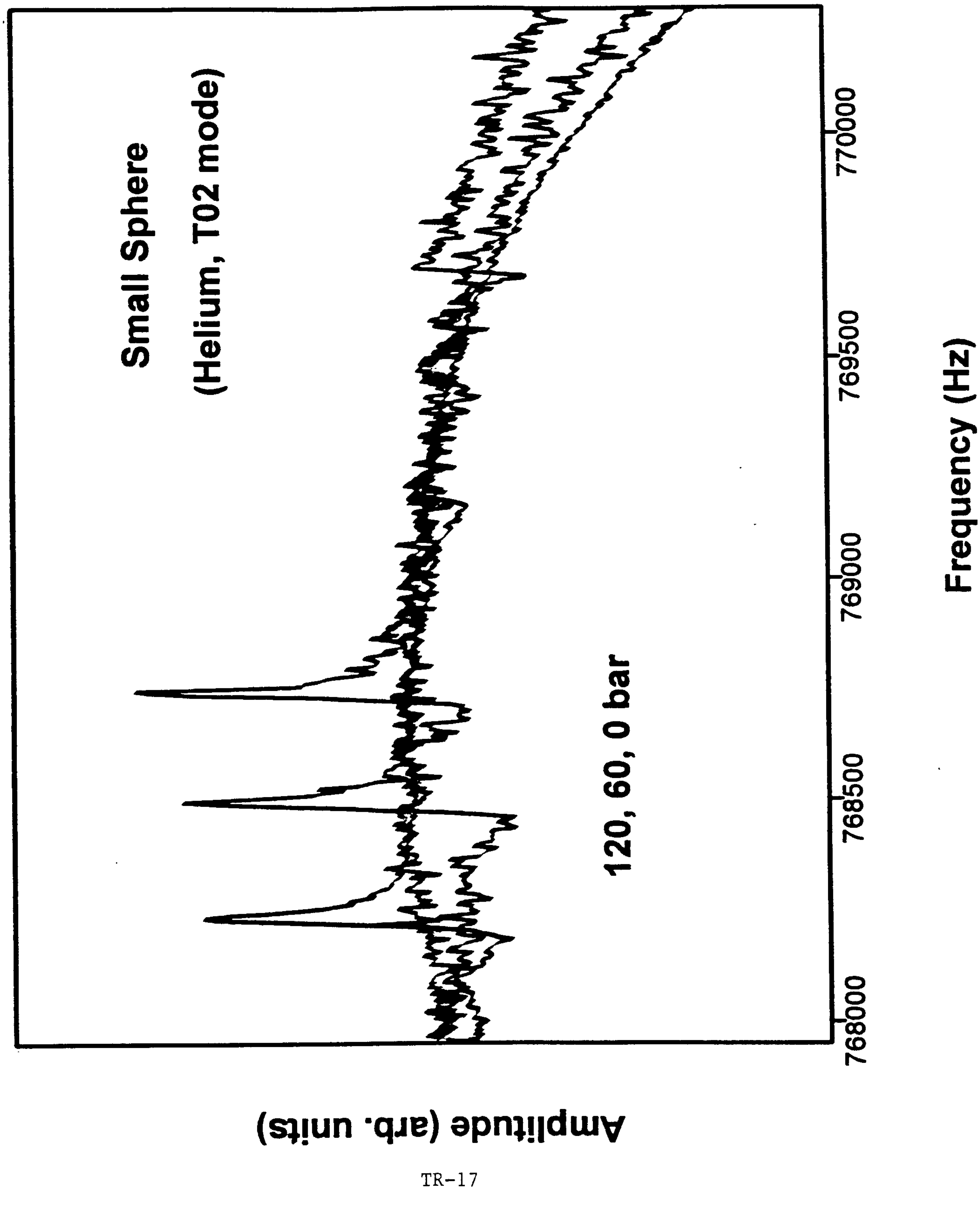

Small Sphere
(Helium, T02 mode)
120, 60, 0 bar
768000
768500
769000
769500
770000
Frequency (Hz)
Amplitude (arb. units)

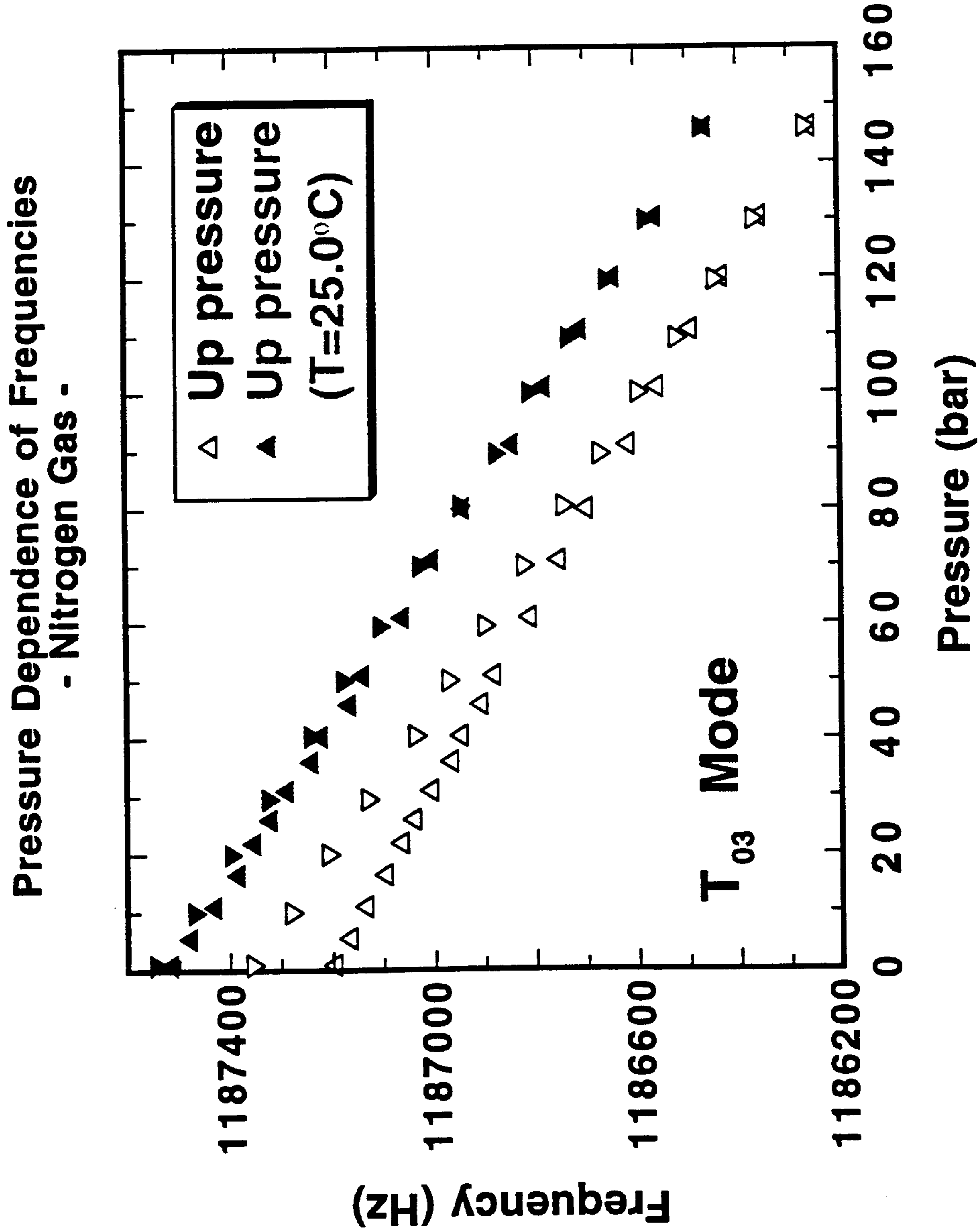

Pressure Dependence of Frequencies
- Nitrogen Gas -
Up pressure
Up pressure
(T=25.0°C)
T03 Mode
Pressure (bar)
Frequency (Hz)
0
20
40
60
80
100
120
140
160
1187400
1187000
1186600
1186200

TR-18

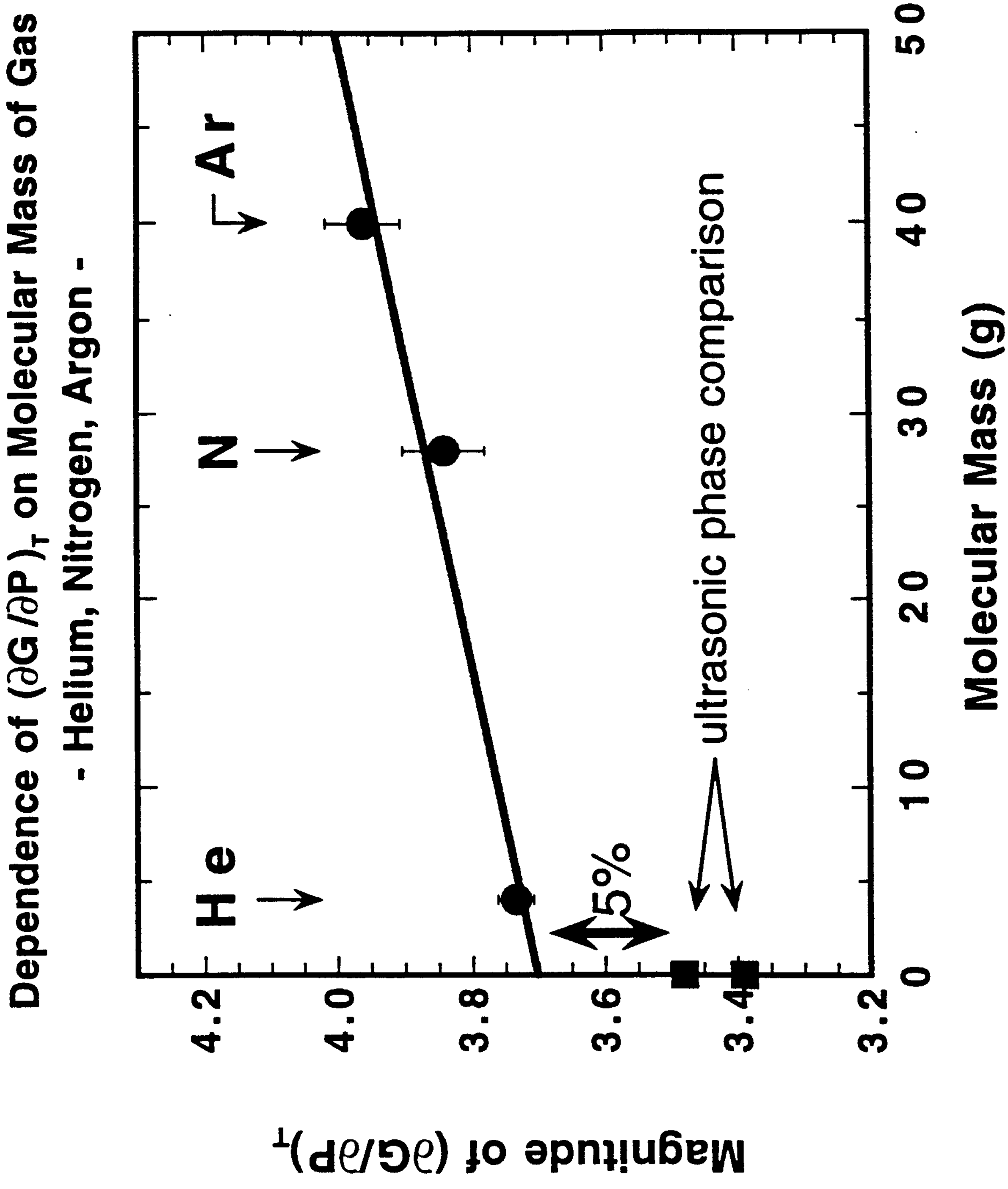
Dependence of (∂G/∂P)$_T$ on Molecular Mass of Gas
- Helium, Nitrogen, Argon -
He
N
Ar
5%
ultrasonic phase comparison
Molecular Mass (g)
Magnitude of (∂G/∂P)$_T$
0
10
20
30
40
50
3.2
3.4
3.6
3.8
4.0
4.2

Basic Equations

- **Frequency, *f*, depends on *G* and *r***

$$\delta f = \left(\frac{\partial f}{\partial G}\right)_{r,m} \delta G + \left(\frac{\partial f}{\partial r}\right)_{G,m} \delta r$$

- **Include pressure, *P*, and do algebra**

$$\boxed{\frac{dG}{dP} = \frac{\dfrac{df}{dP} + \dfrac{f}{6K_T}}{\left(\dfrac{\partial f}{\partial G}\right)_{r,m}}}$$

TR-20

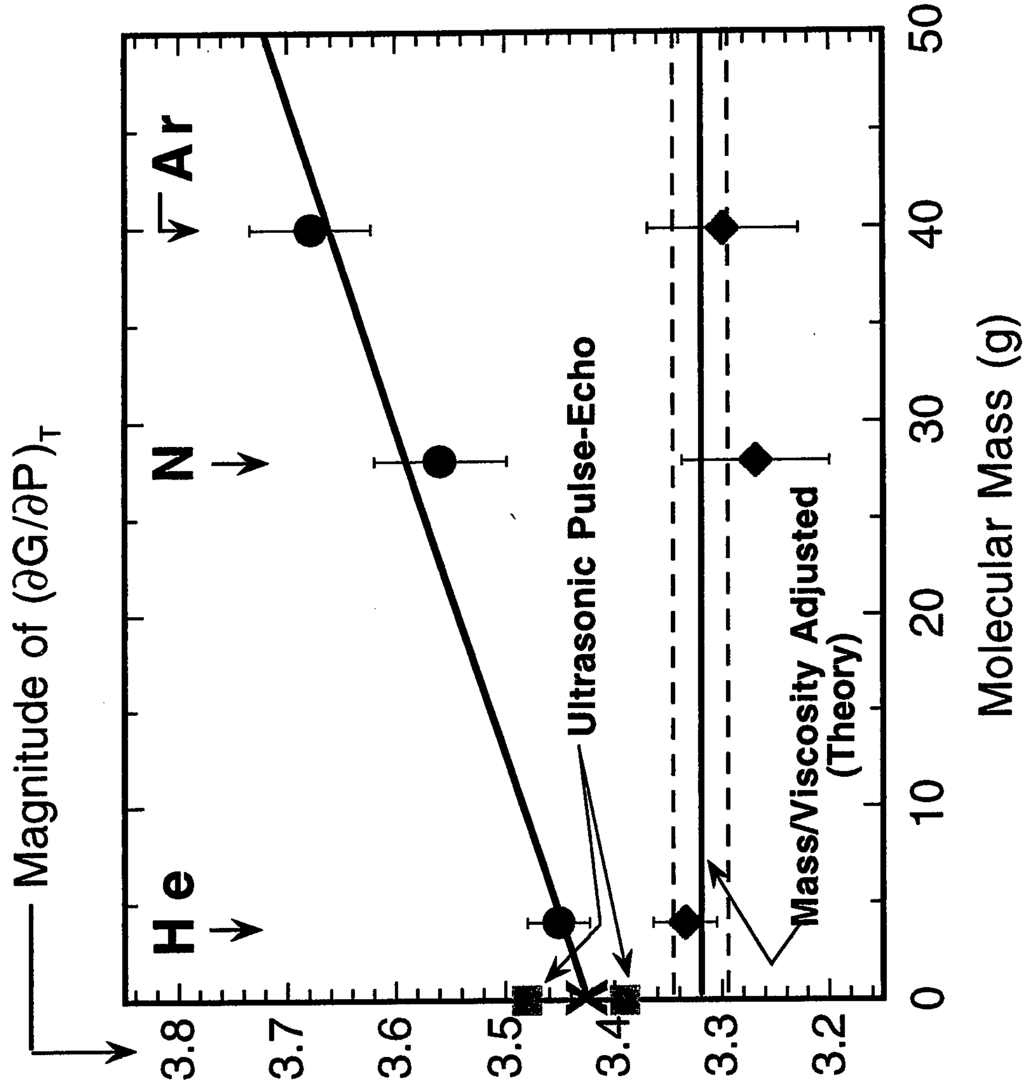
Magnitude of $(\partial G/\partial P)_T$
3.8
3.7
3.6
3.5
3.4
3.3
3.2
0
10
20
30
40
50
Molecular Mass (g)
He
N
Ar
Ultrasonic Pulse-Echo
Mass/Viscosity Adjusted
(Theory)

TR-21

$$\delta \mathrm{f} = \left(\frac{\partial f}{\partial G}\right)_{r,m} \delta \mathrm{G} + \left(\frac{\partial f}{\partial r}\right)_{G,m} \delta \mathrm{r} + \left(\frac{\partial f}{\partial m}\right)_{G,r} \delta \mathrm{m}$$

$$\frac{\mathrm{dG}}{\mathrm{dP}} = \frac{\frac{\mathrm{df}}{\mathrm{dP}} + \frac{f}{6K_T} + \left(\frac{f}{2m}\right)\left(\frac{\mathrm{dm}}{\mathrm{dP}}\right)}{\left(\frac{\partial f}{\partial G}\right)_{r,m}}$$

where $$\frac{\mathrm{dm}}{\mathrm{dP}} = \frac{\mathrm{dm}_g}{\mathrm{dP}} = \frac{d(\rho_g V_g)}{\mathrm{dP}}$$

$$= \frac{2\sqrt{\pi}\, r^2}{P} \sqrt{\frac{\rho_g \eta_g}{f}}$$

Resonant Ultrasound Spectroscopy of Metal-Hydrogen Systems

Bob Leisure
Department of Physics
Colorado State University

Acknowledgments
Keir Foster - *Colorado State University*
Joel Shaklee - *Colorado State University*
Ken Kelton - *Washington University*
J.Y. Kim - *Washington University*
Alexander Skripov - *Ekaterinburg, Russia*
Albert Migliori - LANL

Research supported by NSF Grant No. 95-9501550

TR-1

OUTLINE

A. Background

1. Metal-hydrogen systems
2. Hydrogen motion and ultrasonic attenuation

B. Measurements on a Laves phase material, TaV_2, containing hydrogen(deuterium)

C. Measurements on a Ti-Zr-Ni quasicrystal and a Ti-Zr-Ni crystalline approximant containing hydrogen

D. Summary

METAL-HYDROGEN SYSTEMS

- Many metals absorb large amounts of hydrogen.
  e.g. transition metals, rare earths, actinides

- H typically sits on interstitial sites of host metal lattice.

O

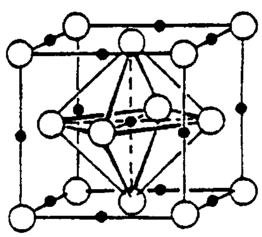

T

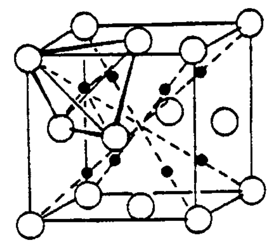

Octahedral and tetrahedral sites in the fcc lattice

- Site occupancy may be random (solid solution), or ordered (hydrides).

- H is often highly mobile and diffuses by hopping between interstitial sites.

- Many physical effects and practical applications are associated with hydrogen in metals, e.g.
  - Hydrogen storage
  - Metal hydride batteries
  - Switchable optical and magnetic properties
  - Hydrogen embrittlement

HYDROGEN MOTION

- H motion is studied by a variety of techniques.

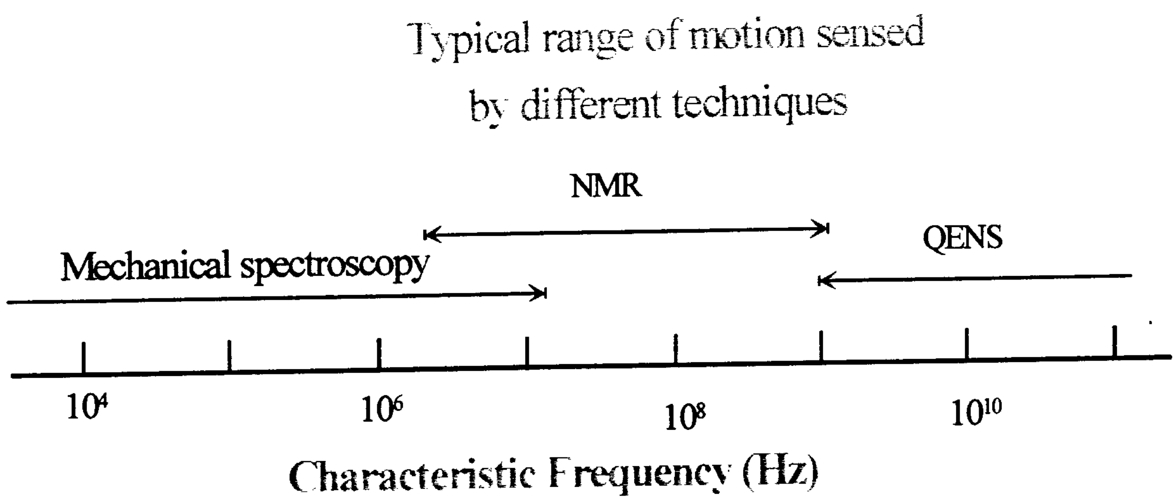

- Ultrasonic attenuation arises due to a stress-induced rearrangement of H on the interstitial sites (relaxation).

- Defect symmetry must be lower than crystal symmetry for relaxation attenuation to occur (*Anelastic relaxation in crystalline solids*, Nowick and Berry).

Illustration of relaxation effects for sites on the face of a simple cubic lattice

I. With no stress, all interstitial sites energetically equal

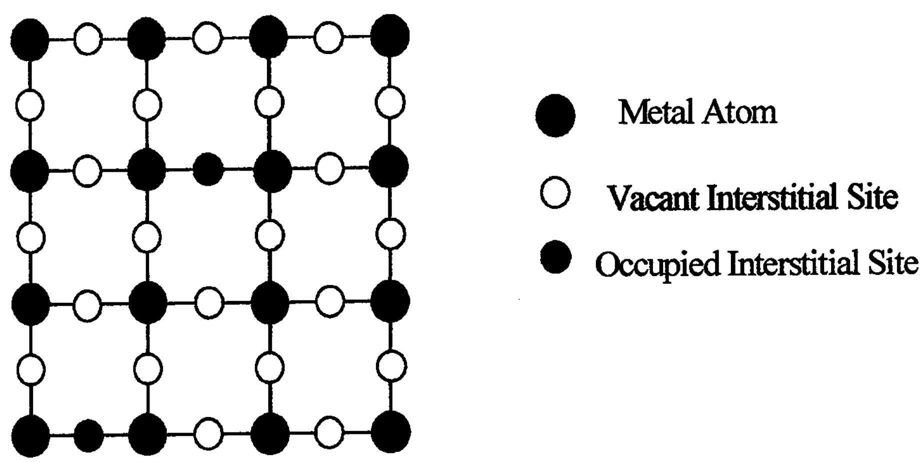

II. With stress, sites no longer energetically equal, rearrangement of interstitial atoms occurs.

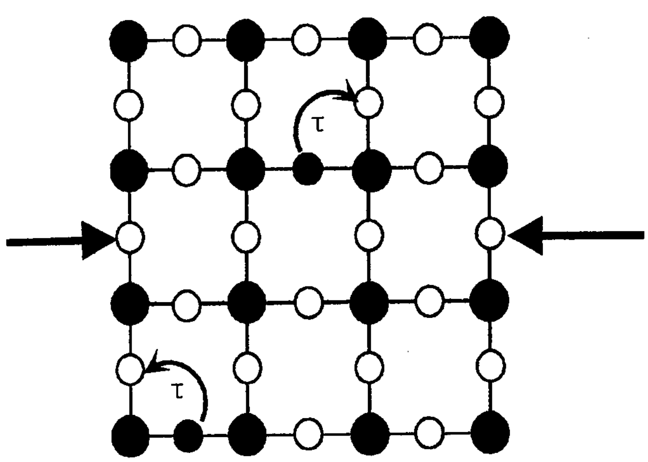

TR-5

RELAXATION ATTENUATION

- The loss is given by

$$\frac{1}{Q} = \frac{\Delta C}{C} \frac{\omega \tau_R}{1 + \omega^2 \tau_R^2} \quad . \text{ Usually } \frac{\Delta C}{C} \propto \frac{1}{T}$$

- Hydrogen can "hop" between sites by several different processes.

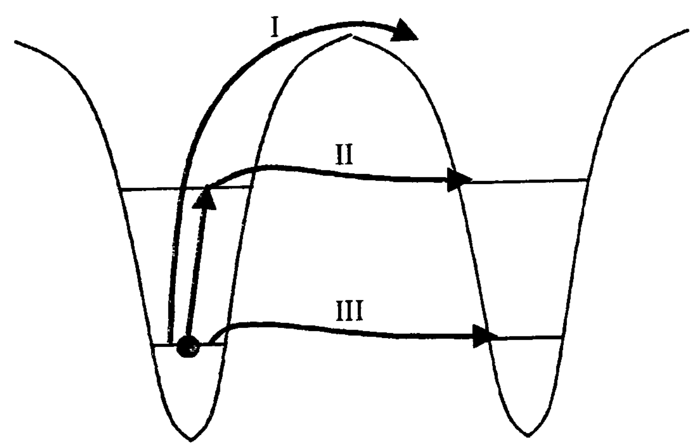

- Classical Arrhenius behavior may be observed at high temperatures, process I.

$$\tau_R = \tau_{Ro} \exp(E_a / kT)$$

A distribution of E_a is frequently required.

- Deviation from classical behavior is common, especially at lower temperatures.

TR-6

Resonant Ultrasound Spectroscopy

I. Sample-Transducer Arrangement

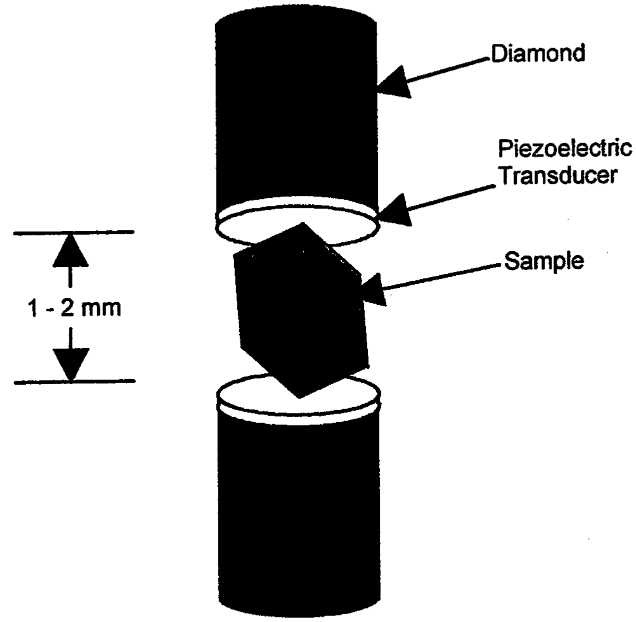

II. Spectrometer

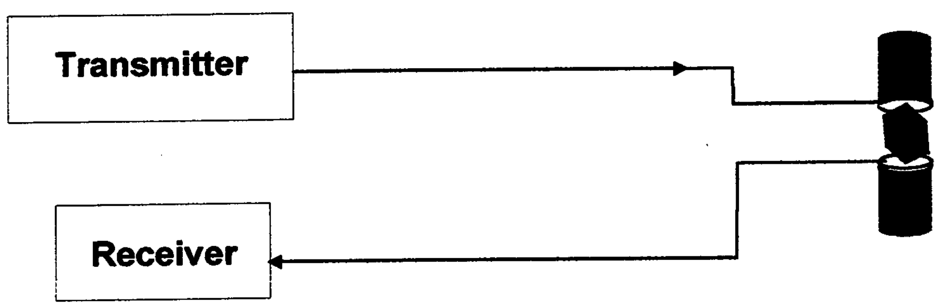

III. Typical Modes

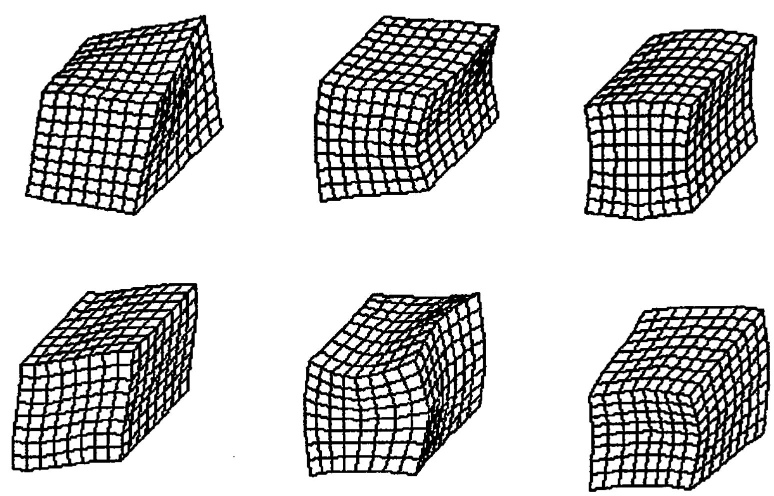

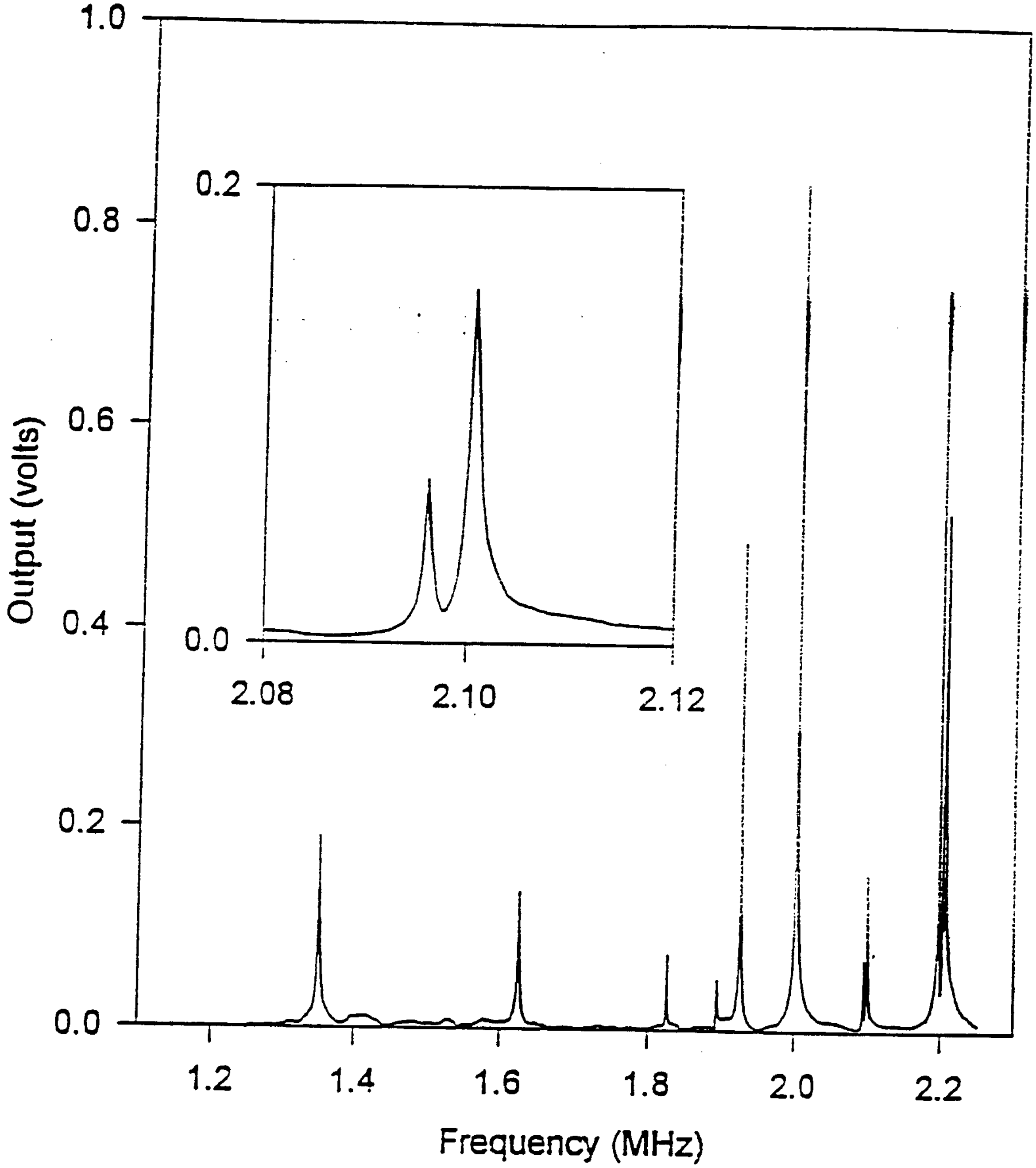
1.0
0.8
0.6
0.4
0.2
0.0
Output (volts)
0.2
0.0
2.08
2.10
2.12
1.2
1.4
1.6
1.8
2.0
2.2
Frequency (MHz)

TR-8

The C-15 Laves-phase compound TaV_2

- Many C-15 materials, including TaV_2, absorb large amounts of hydrogen.
- The hydrogen is highly mobile.
- Large number of tetrahedral sites.

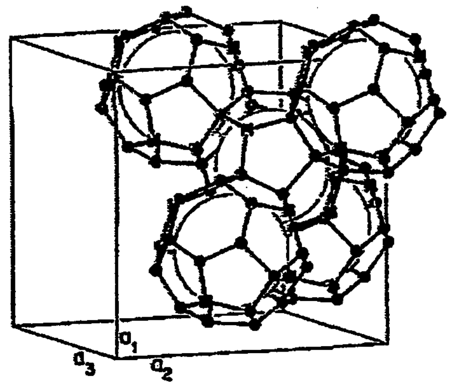

Interstitial sites in TaV_2

- Previous neutron scattering and NMR work suggests two types of motion in these materials: I. "Slow", Long range; II. "Fast", Local

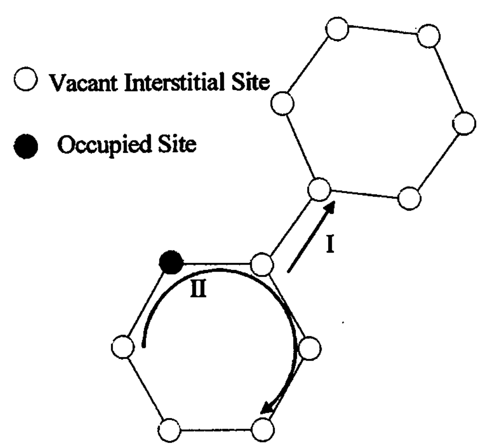

2-D representation of H(D) in TaV_2

- Objective of present study - Investigate this motion in a different frequency range using RUS

TR-9

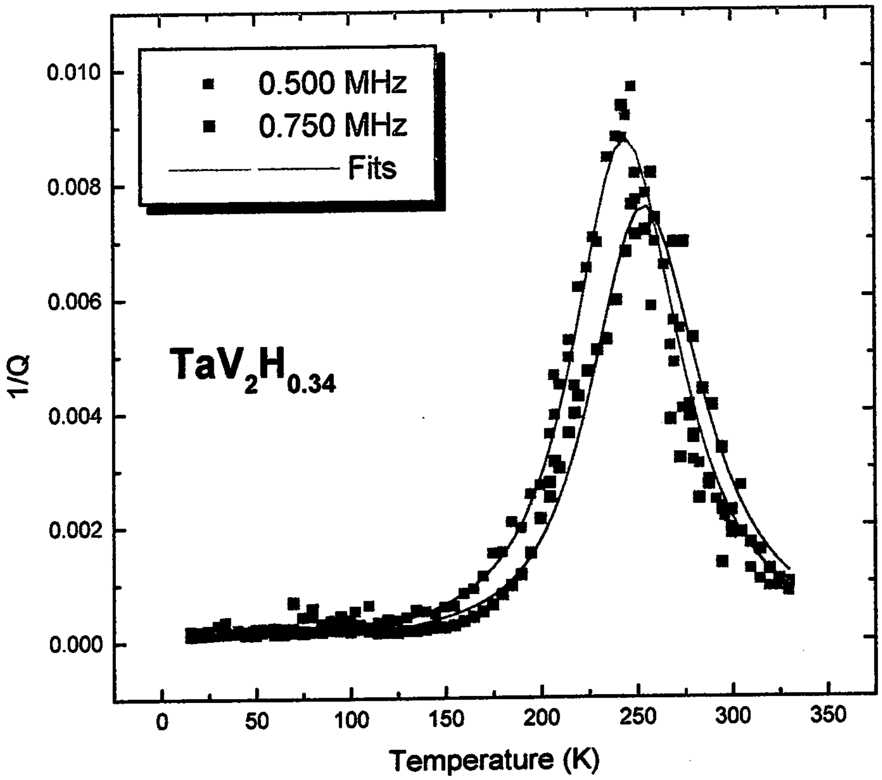

0.500 MHz
0.750 MHz
Fits
$TaV_2H_{0.34}$
1/Q
Temperature (K)

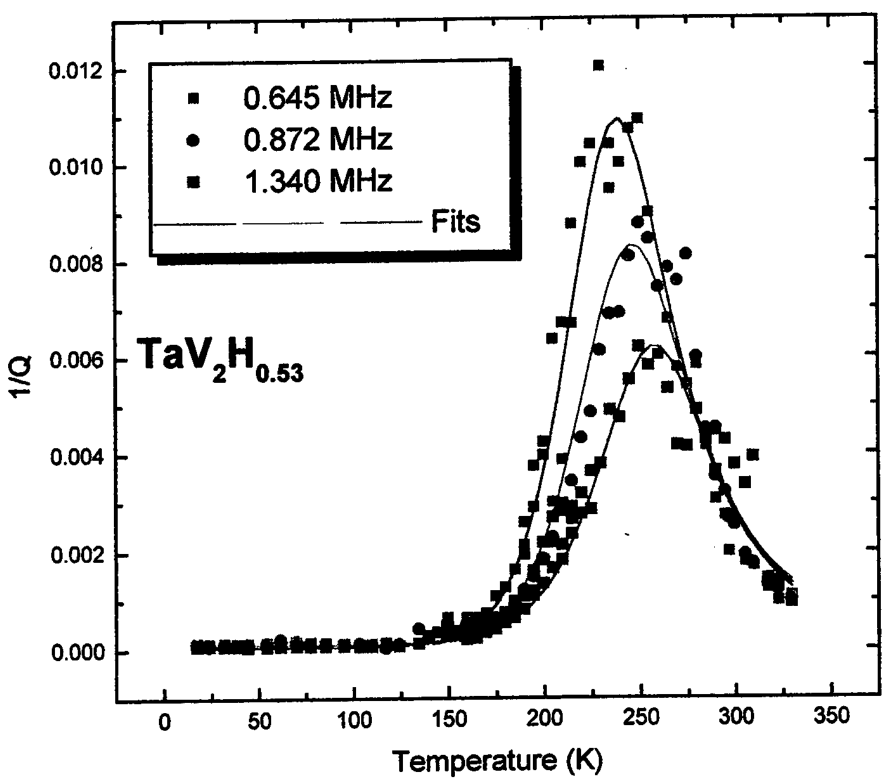

0.645 MHz
0.872 MHz
1.340 MHz
Fits
$TaV_2H_{0.53}$
1/Q
Temperature (K)

TR-10

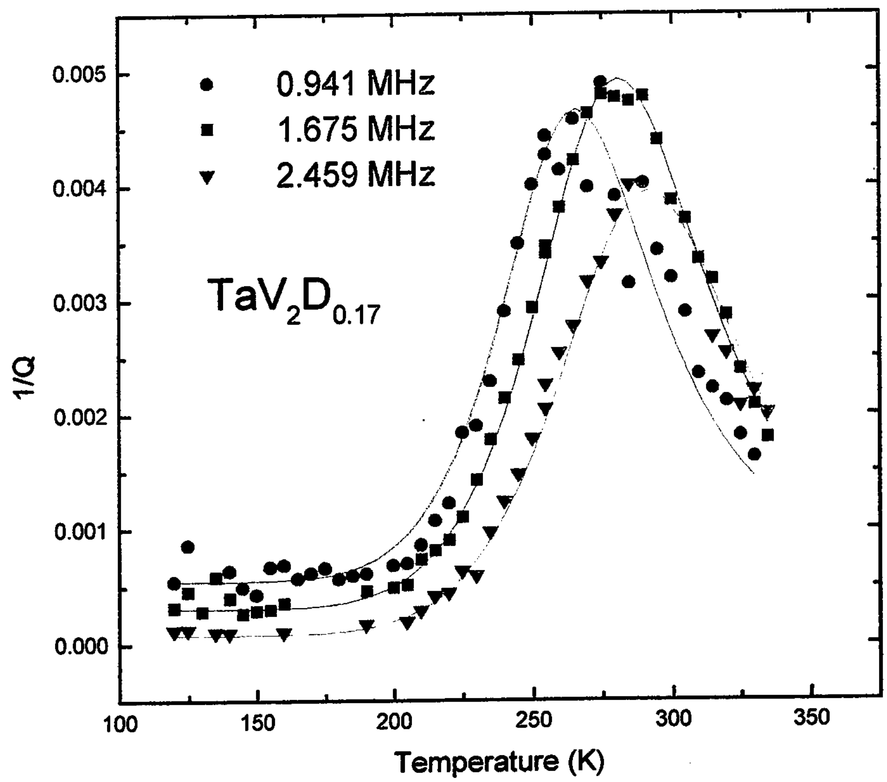
0.941 MHz
1.675 MHz
2.459 MHz
TaV2D0.17
1/Q
Temperature (K)

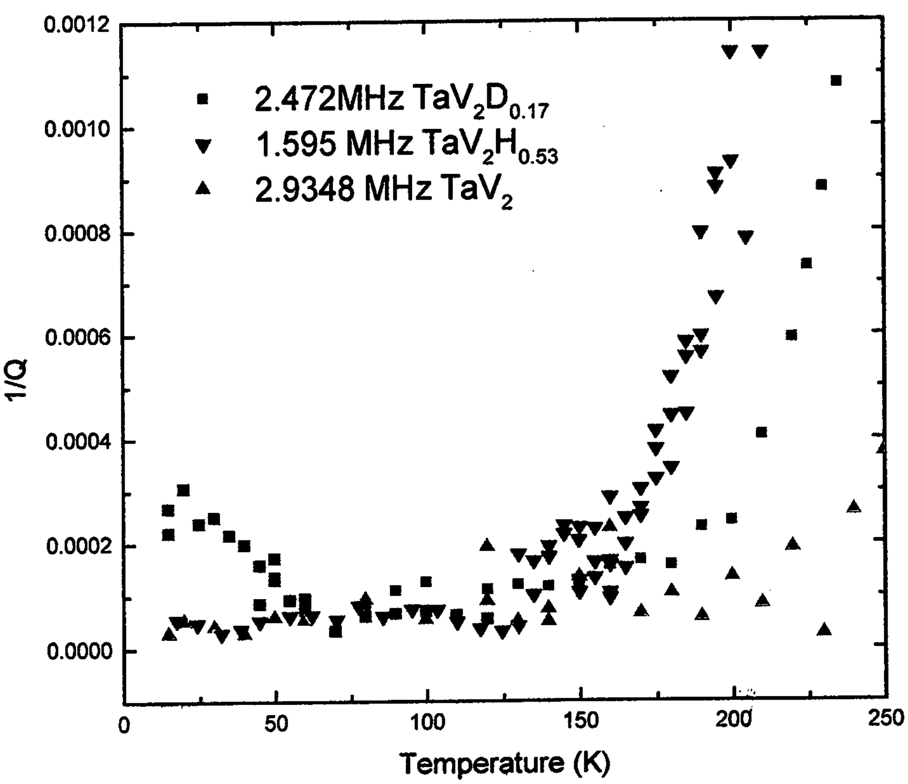
2.472MHz TaV2D0.17
1.595 MHz TaV2H0.53
2.9348 MHz TaV2
1/Q
Temperature (K)

TR-11

Ti-based quasicrystals and crystalline approximants

- Can absorb H up to H/M = 1.6
- Little previous study of H motion in such materials.
- Offers opportunity to study diffusion in a non-periodic lattice.
- Materials studied

  i-phase quasicrystal $Ti_{41.5}Zr_{41.5}Ni_{17}$
  Loaded with hydrogen to H/M = 0.79

  W-phase 1/1 approximant $Ti_{44}Zr_{40}Ni_{16}$
  Loaded with hydrogen to H/M = 0.20

- H enters in solid solution.

Ultrasonic loss data versus temperature for Ti-Zr-Ni phase quasicrystal.

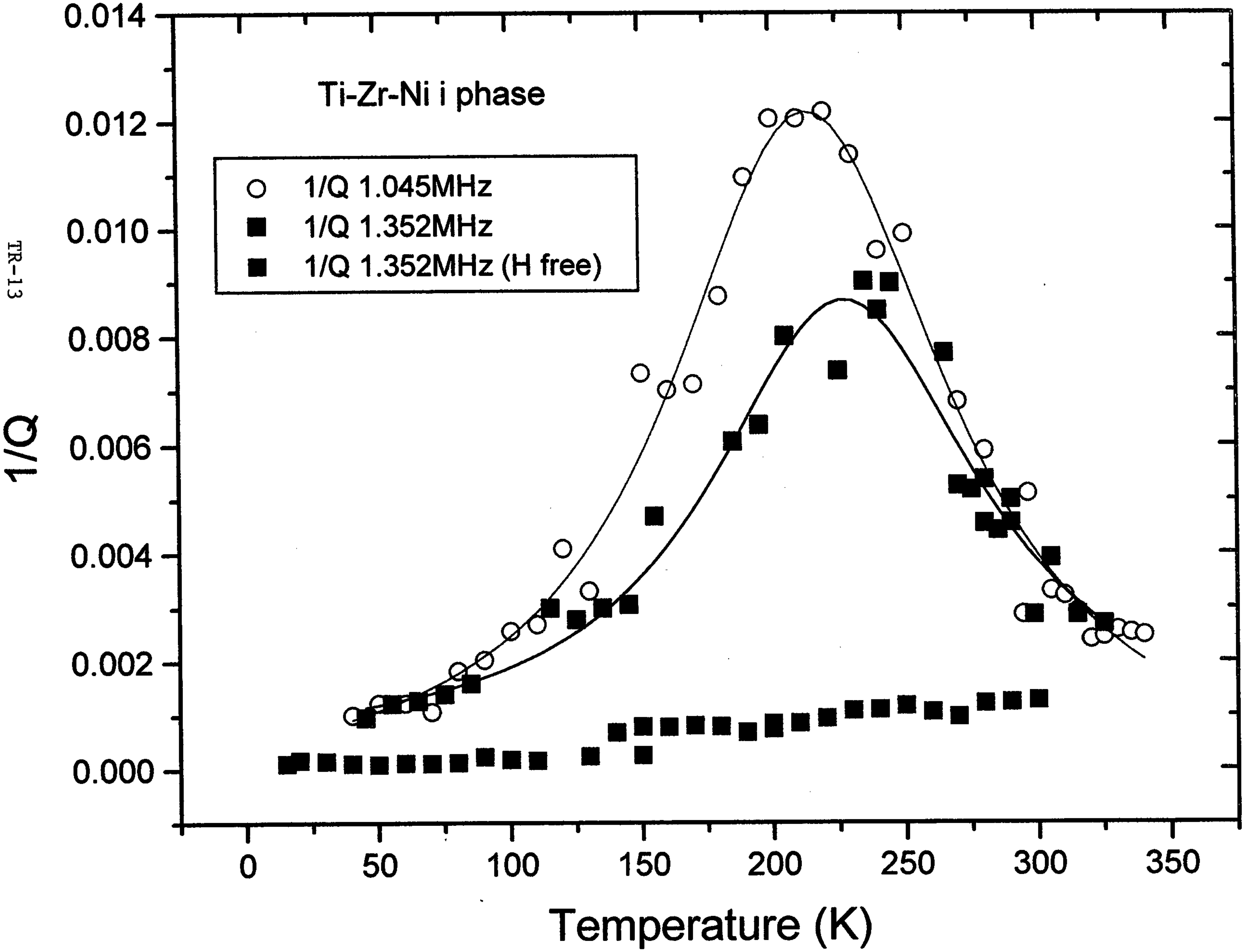

TR-13

Ultrasonic loss data versus temperature for Ti-Zr-Ni 1/1 crystal approximant.

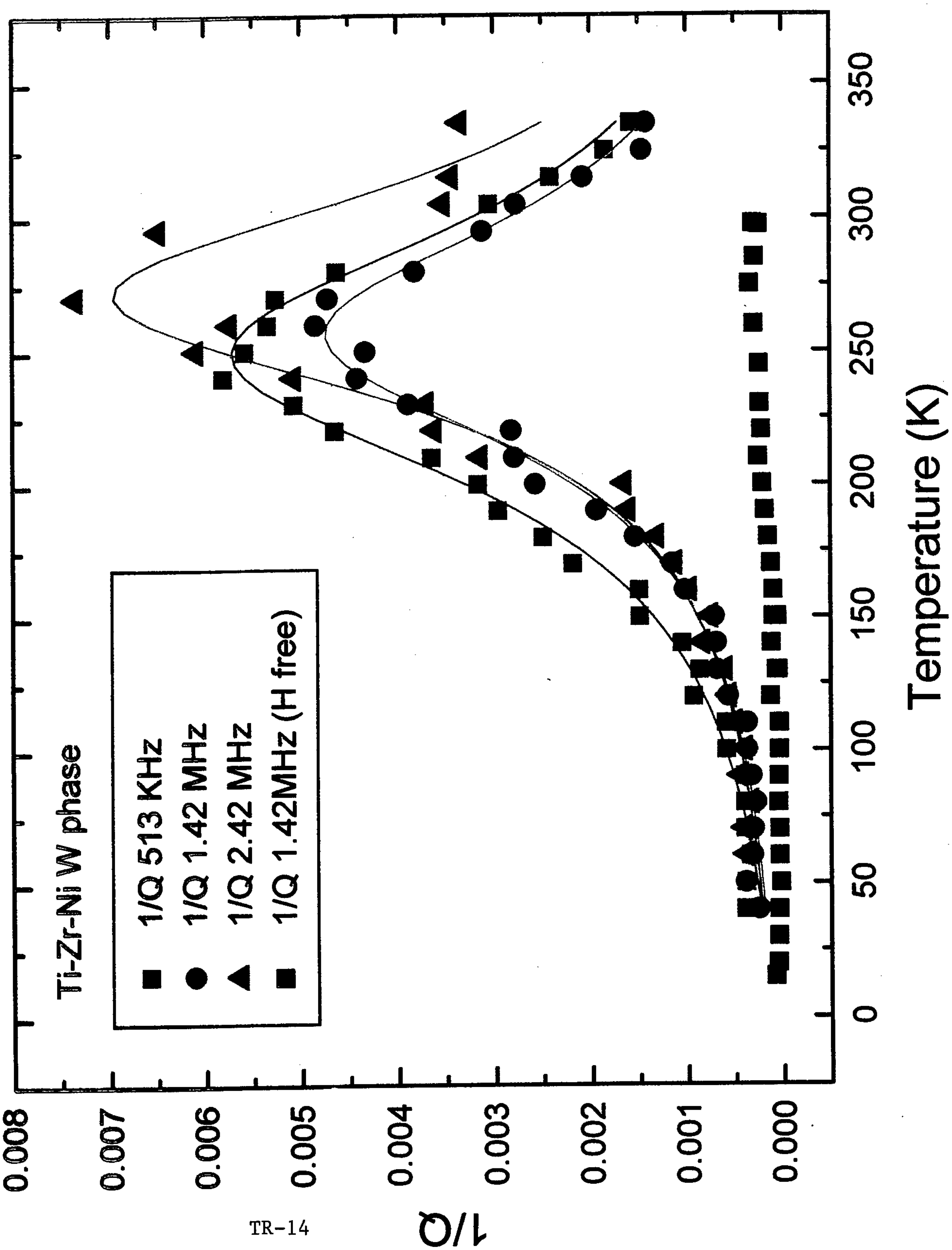

TR-14

SUMMARY

- Evidence for two types of motion in TaV_2D_x with different characteristic frequencies.
- First ultrasonic measurements of H motion in quasicrystals. Evidence for a distribution of activation energies.
- Resonant ultrasound spectroscopy is a sensitive probe of internal motion in solids in a frequency range which is complementary to NMR and neutron scattering.

$TaV_2H(D)_x$ Fitting Parameters

- TaV_2H_x

$$\tau_R^{-1} = \tau_1^{-1} + \tau_2^{-1}$$

$$\tau_i = \tau_{io} \exp(E_i / k_B T)$$

	E_{a1} (eV)	$\tau_{o1}(10^{-12}$sec)	E_{a2} (eV)	$\tau_{o1}(10^{-8}$sec)
$TaV_2H_{0.34}$	0.25	3.1	0.082	3.6
$TaV_2H_{0.53}$	0.23	4.8	0.091	1.9

- $TaV_2D_{0.17}$

$$\tau_R = \tau_{Ro} \exp(E_a / k_B T)$$

$$\tau_{Ro} = 3.4x10^{-12} \text{ sec} \qquad E_a = 0.25\text{eV}$$

Industrial Applications

Sort good vs defective parts during manufacturing

- Types of defects
- Existing methods for inspection of parts
- RUS
- Problems
- The future

Defect Types

Cracks

Chips

Dimensional variations

Material Composition

Microcracking

Hardness

Existing Methods

- Eddy Current
  - Metals only
- Dye Penetrant
  - Messy, environmental issues, visual
- Mag Particle
  - Visual
- X-Ray
  - Training, certification

Inspection via RUS

- Works on many materials
  - Ceramics
  - Metals
  - Glass
- Environmentally friendly
- Not limited to surface defects
- Automated

NDT & RUS

Must use known good and defective parts to define spectra

Determine differences in spectra between good and bad sets of parts

Sort unknown parts based on measured resonances

"Good" parts may contain defects

2 Good, 1 cracked cups

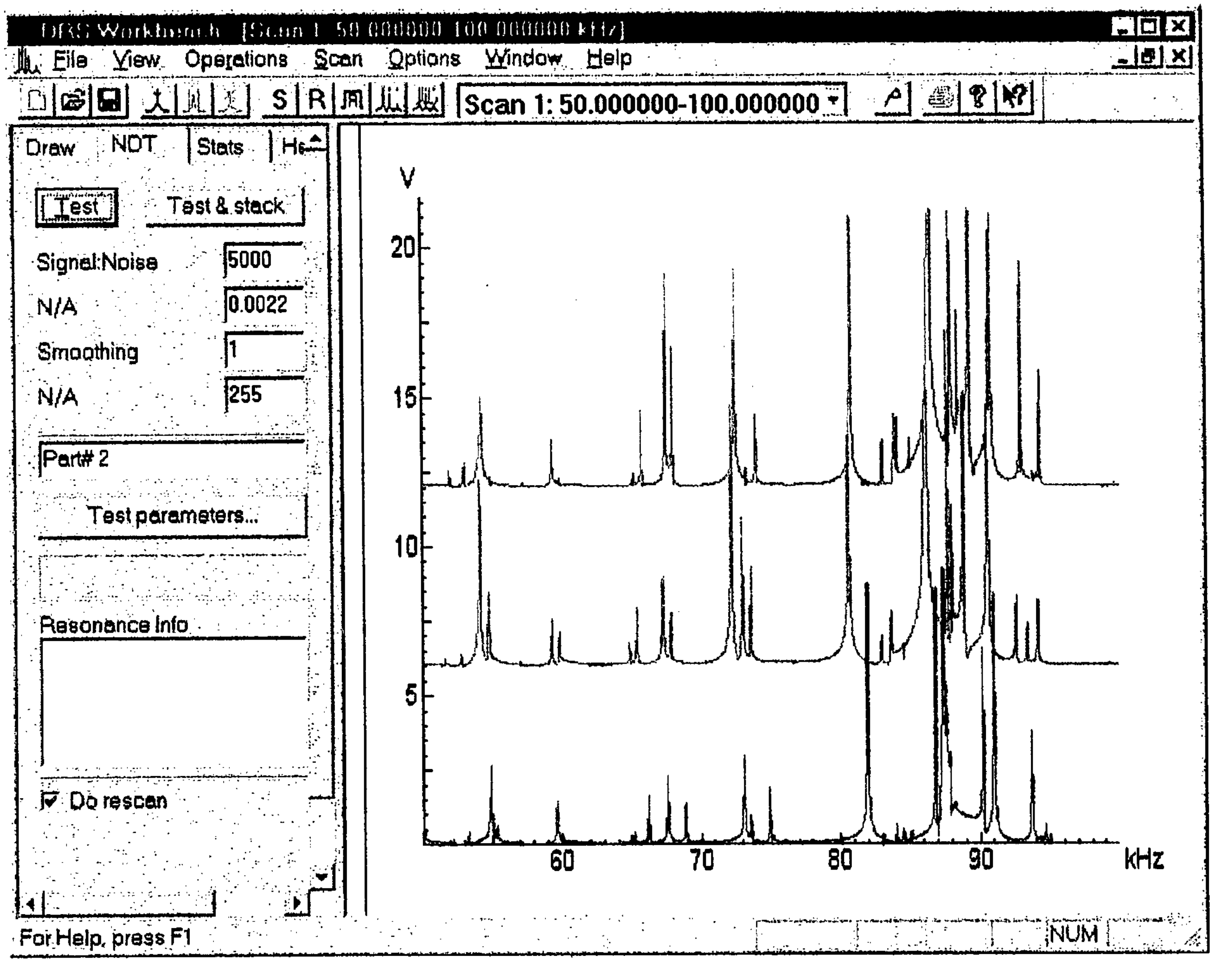

Types of Tests (Patterns)

- Simple position
  - Correct number of peaks in a frequency region
- Doublet
  - 2 peaks separated by the correct amount
    - An ideal part might only show 1 peak
    - Separation of doublet may be related to size of defect

More test types

- Linked peaks
  - 2 peaks linearly related
  - Can also be used to correct for density or other variations
- Q
- Amplitude
- Phase

Successful Applications

Ceramic Gas Seal

- ~14 mm diameter ceramic 'o-ring'
- Tolerance on diameters ~0.006"
- Saw correlation between chip size and doublet separation
- Tolerance on diameters dV~9 mm^3 same as ~2 mm diameter chip
- Could detect chips down to ~1 mm^3

Gas Seal

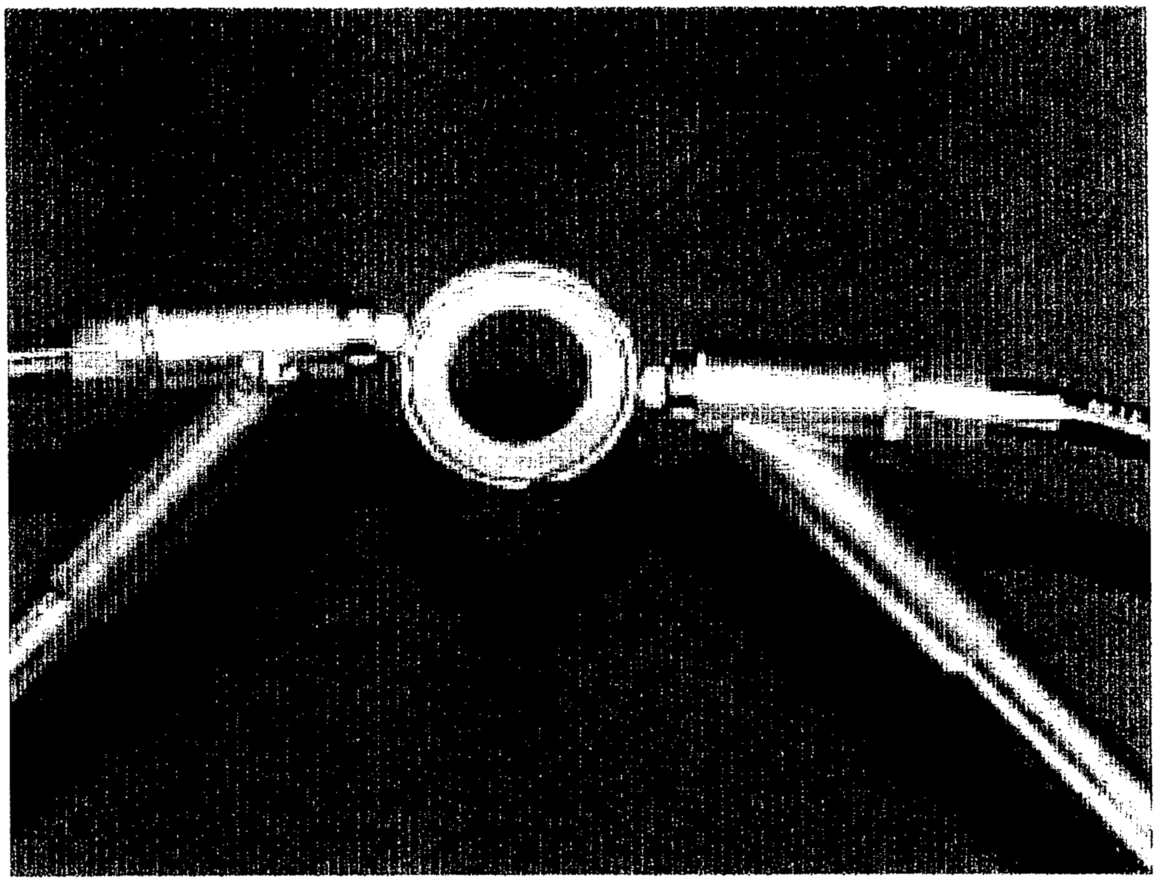

Gas Seal

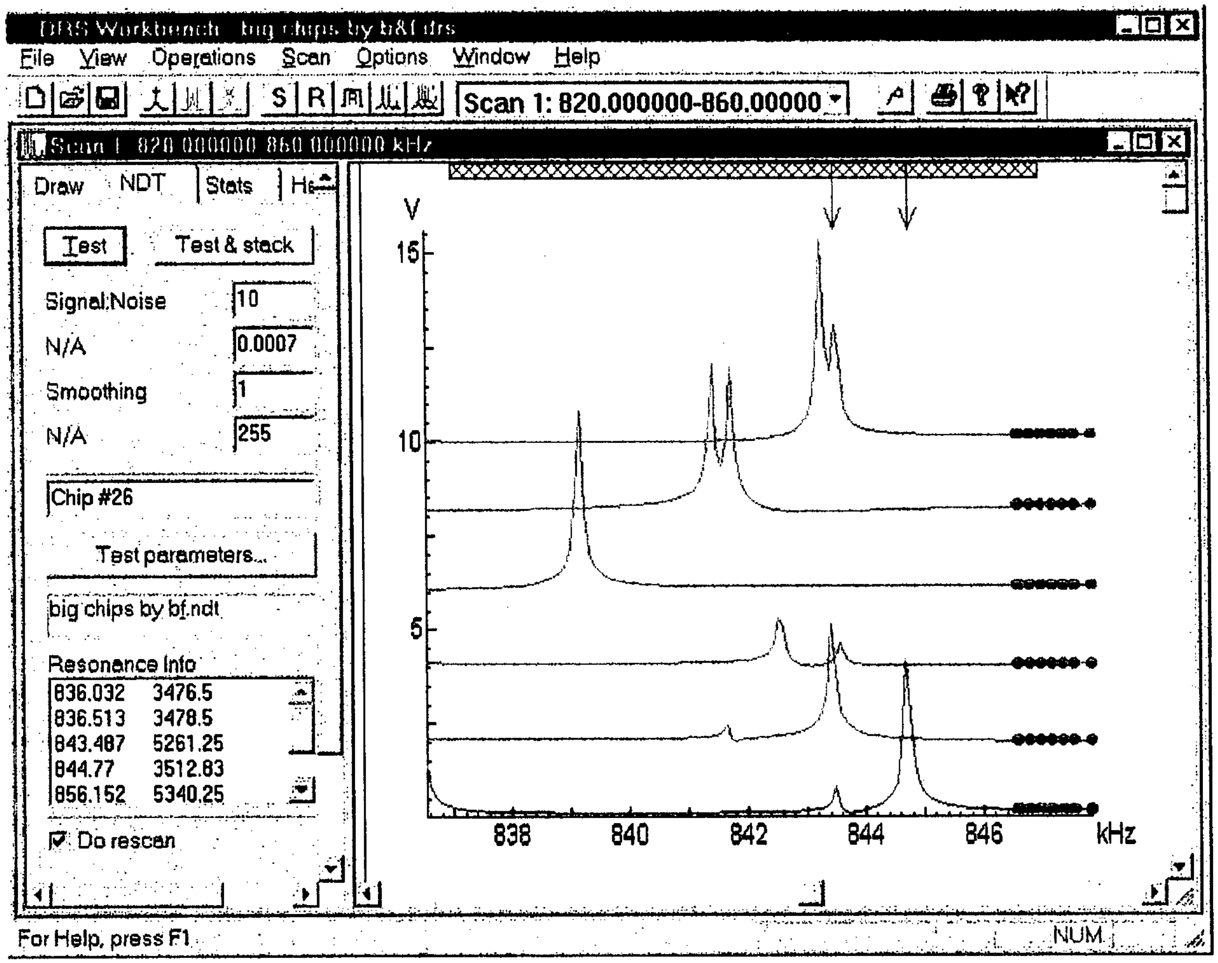

DRS Workbench big chips by b&f drs
File View Operations Scan Options Window Help
S R
Scan 1: 820.000000-860.00000
Scan 1 820.000000 860.000000 kHz
Draw NDT Stats
Test
Test & stack
Signal:Noise 10
N/A 0.0007
Smoothing 1
N/A 255
Chip #26
Test parameters...
big chips by bf.ndt
Resonance Info
836.032 3476.5
836.513 3478.5
843.487 5261.25
844.77 3512.83
856.152 5340.25
Do rescan
V
15
10
5
838
840
842
844
846
kHz
For Help, press F1
NUM

Successful Applications

- Machined steel bearing race
  - Grinding burns were the primary defect sought
  - Combined 2 simple position tests to improve sort

Bearing Race

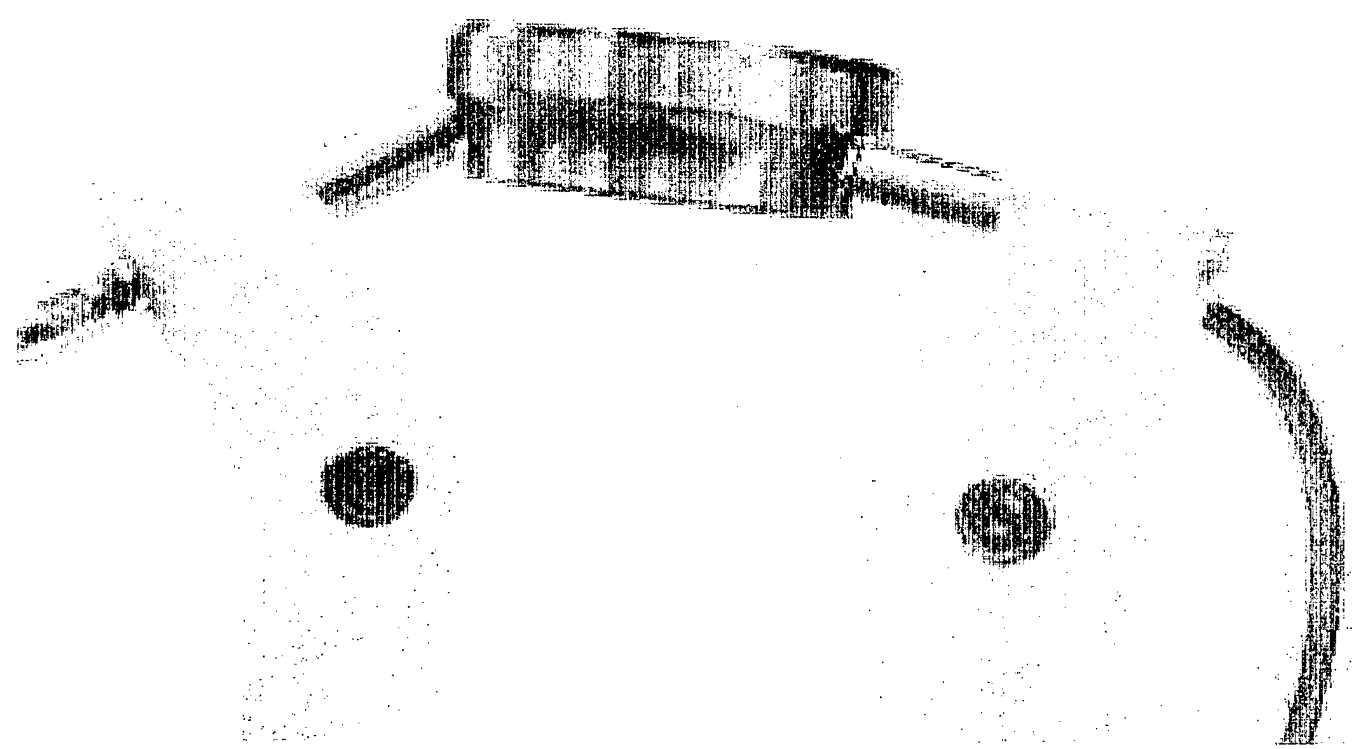

Bearing Race

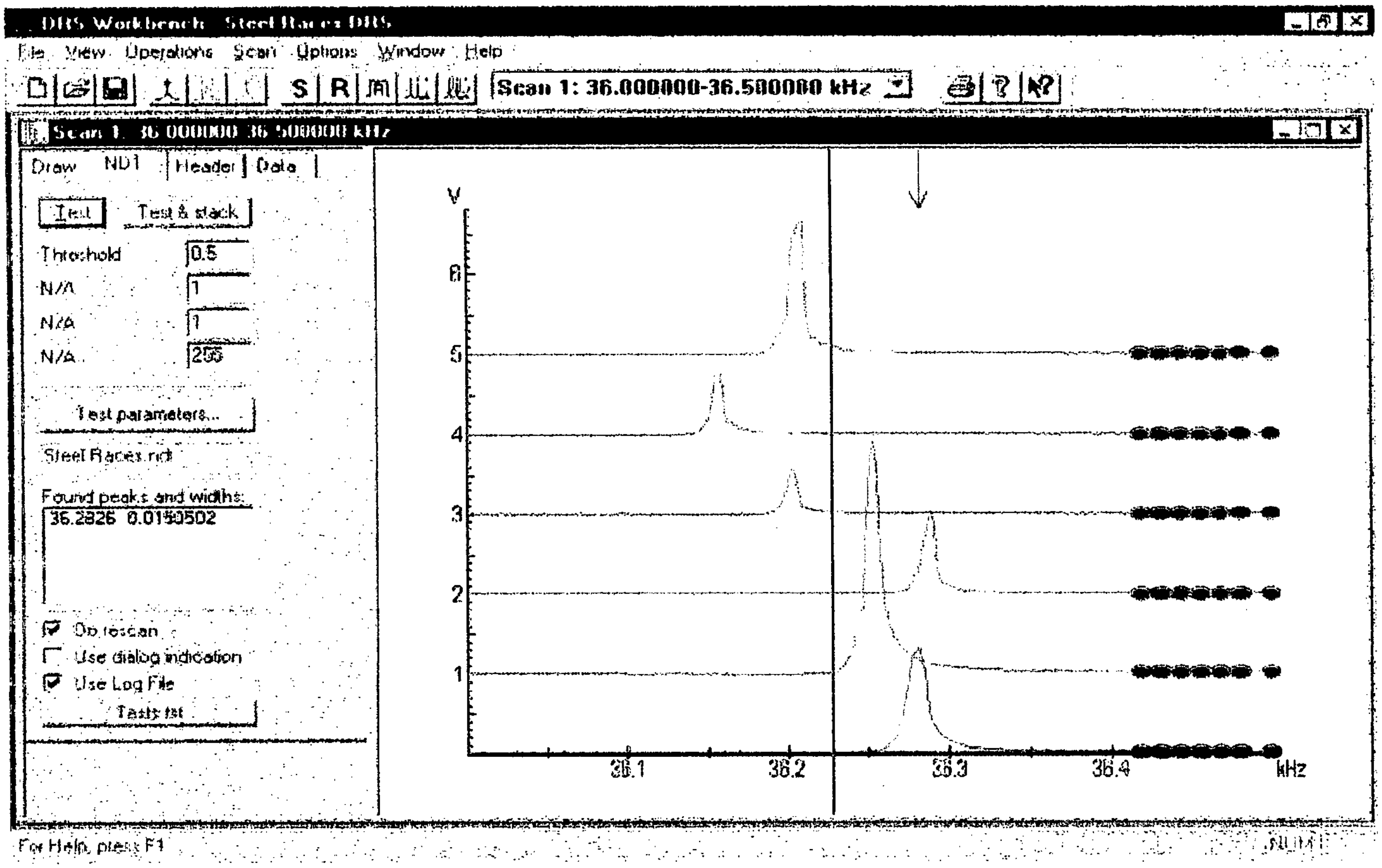

Problems

- Pattern recognition
  - Peaks do not line up - variations in material or density
  - Peaks missing - High density of modes in many cases
  - Parts are large - Lowest resonances often at 100's Hz
  - Combinations of tests may be needed

Problems

- Powdered Metal Parts
  - Composition varies?
- All parts
  - Patterns may be due to dimensional variations
  - Good parts often contain defects

Next Generation System(s)

Lower Frequency

Broad Spectrum
- Do FFT on complicated signal

Advanced pattern recognition

The Future

Tolerances on parts will be tighter

Quality of raw materials will improve

Manufacturing process control will improve

All will make RUS easier to implement and more reliable

Thin Film Characterization Using Resonant Ultrasound Spectroscopy

J. D. Maynard, Jason White, and Jin Hyun So
The Pennsylvania State University

Objective

- To study physical properties, through measurements of elastic stiffness and damping, for thin films deposited on substrates.

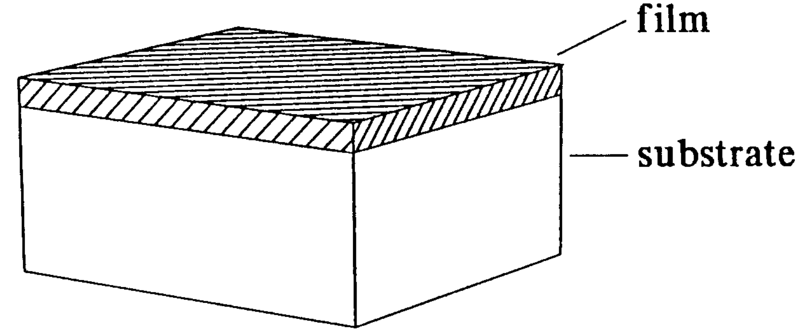

Applications

- Thin films in magnetic recording media
- Protective or lubricating coatings, such as diamond, quasicrystalline, or carbon nanotube films
- Superconducting films
- Micro- (nano-) electronics

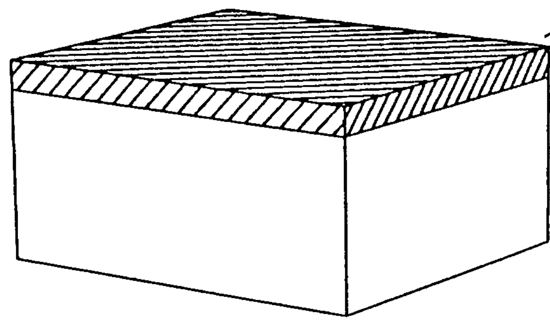

Scientific Issues

- The physics of thin deposited films is effected by:
  - the reduced dimensionality of the film (2D rather than 3D)
  - the influence of the substrate, such as strain or disorder induced in the film by lattice mismatch, magnetic interactions, etc.
- Novel properties of unique systems such as mats of carbon nanotubes
- Determine properties for practical applications, such as elastic constants, friction, and damping

Approach

Use Resonant Ultrasound Spectroscopy to measure elastic constants and damping for the film, assuming known properties of the substrate.

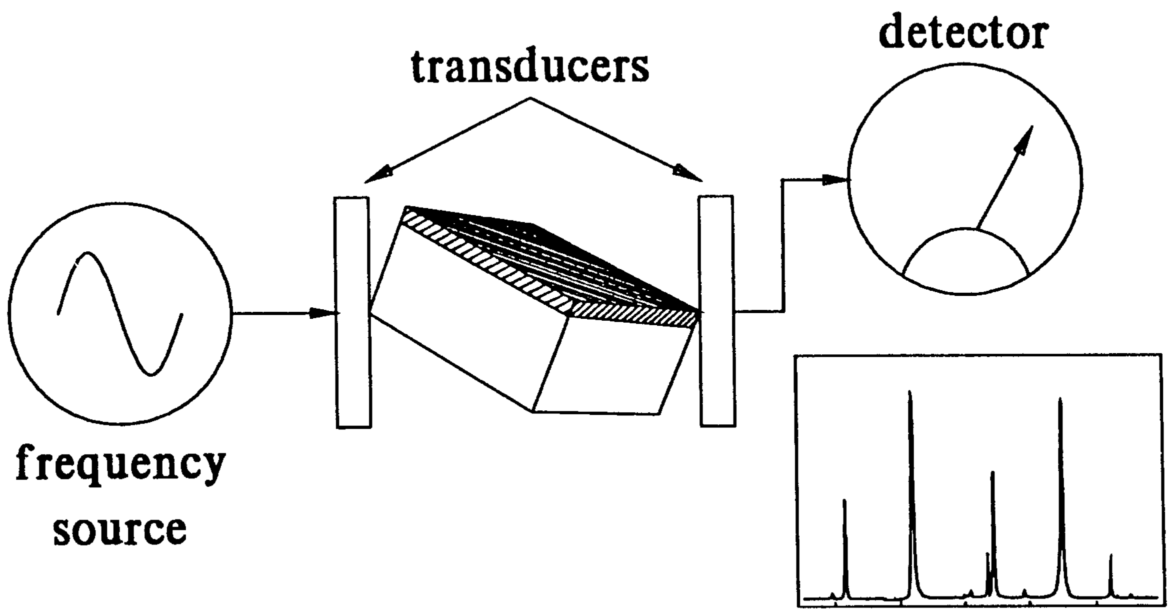

Approach, cont.

Measurements are made for the substrate with and without the film.

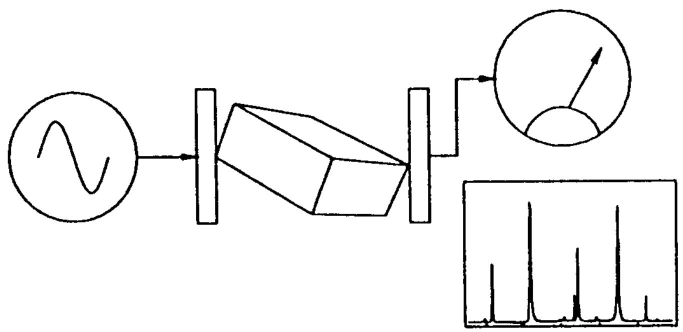

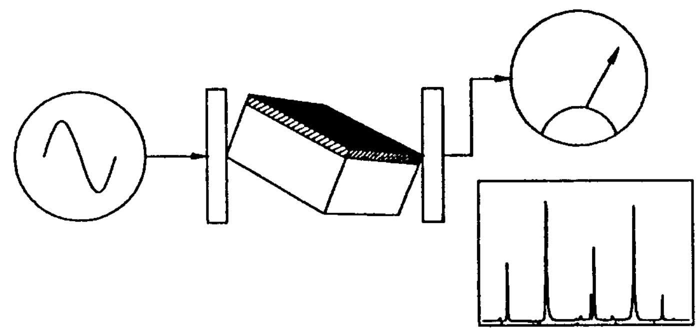

Challenges

- The film must be a suitable fraction of the thickness of the sample
  - Typically: 100 nm films on 100 μm substrates
- For anisotropic films, the lateral dimensions should be small as well
  - Necessary to excite thickness modes of film

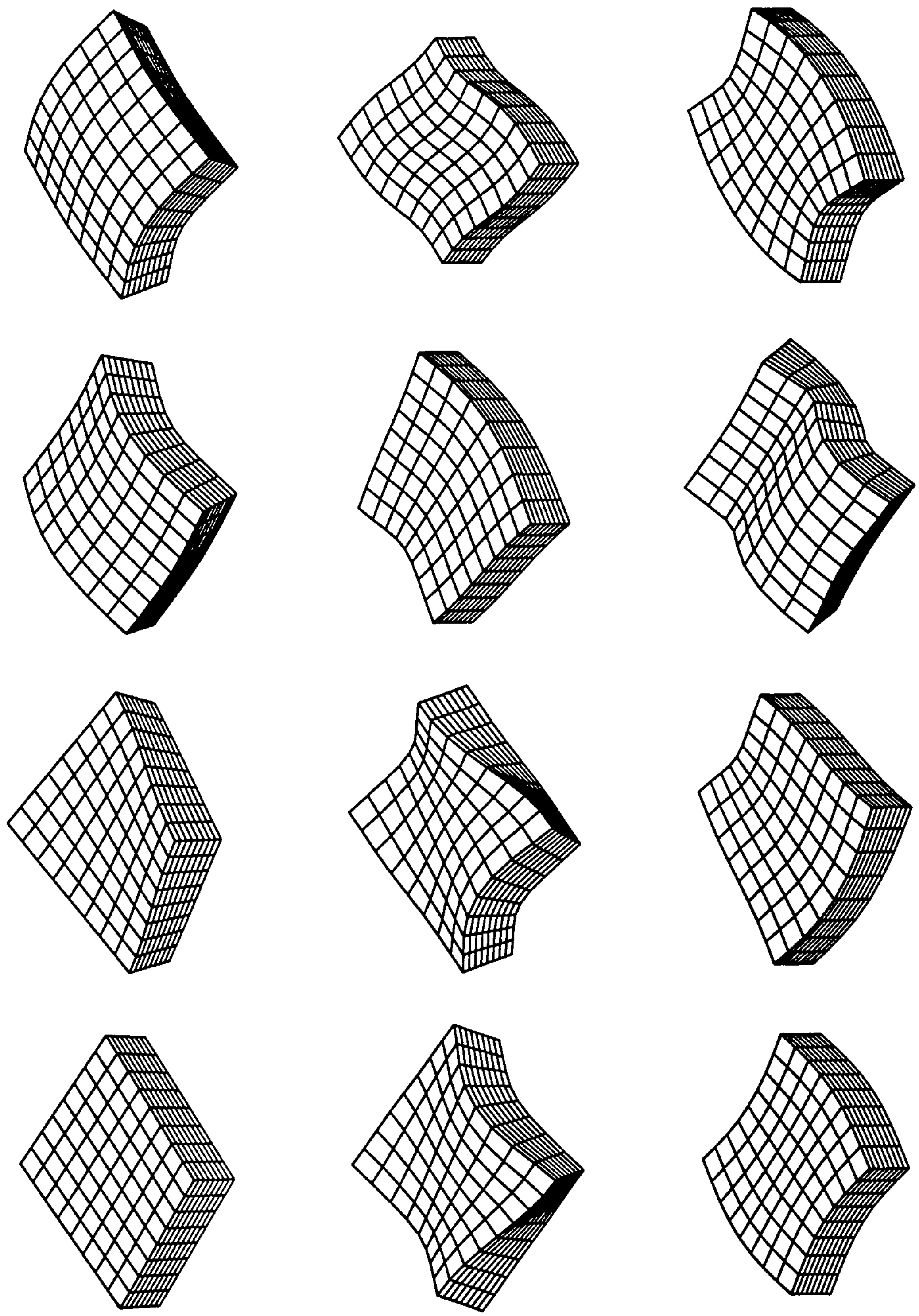

TR-5

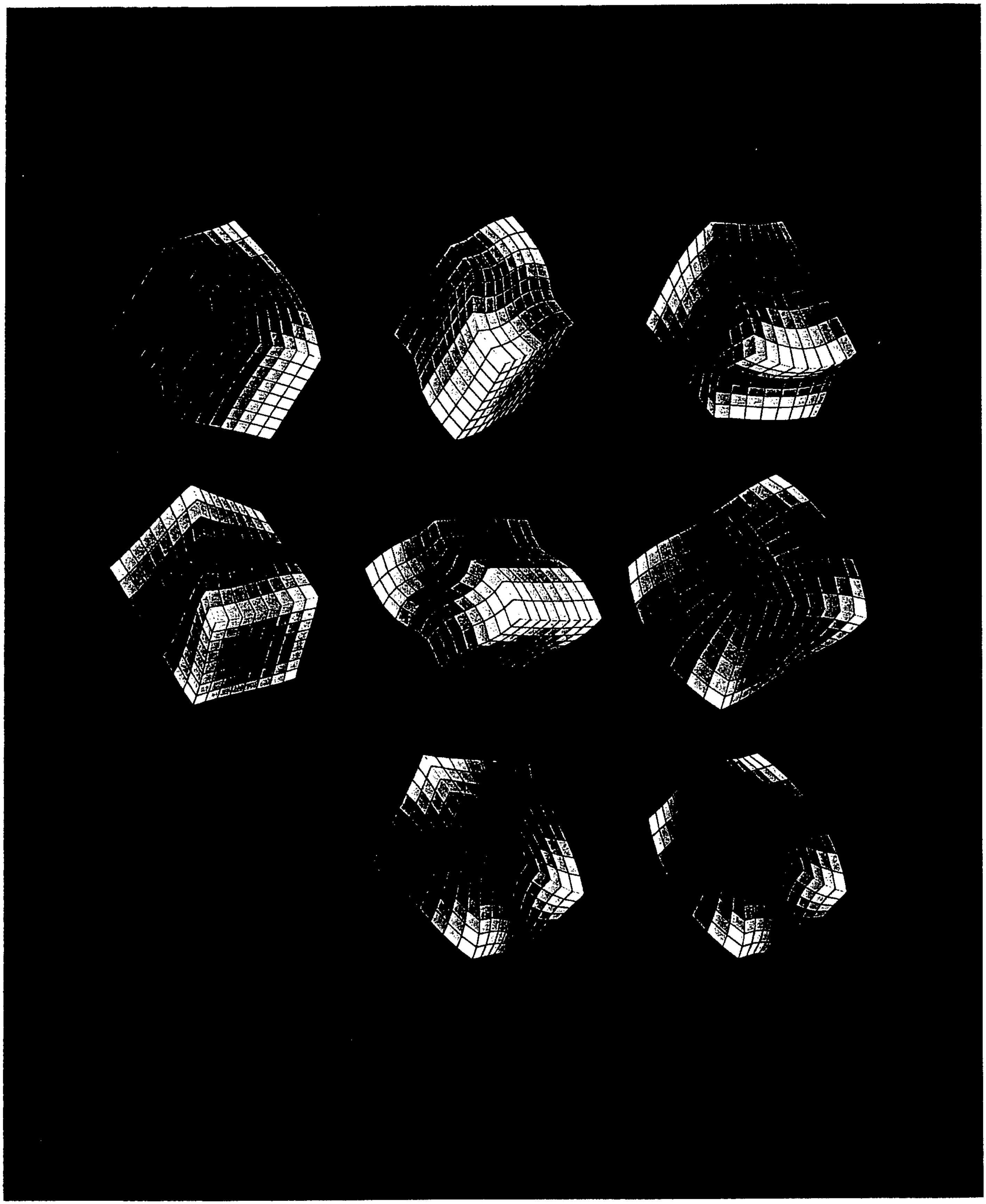

TR-6

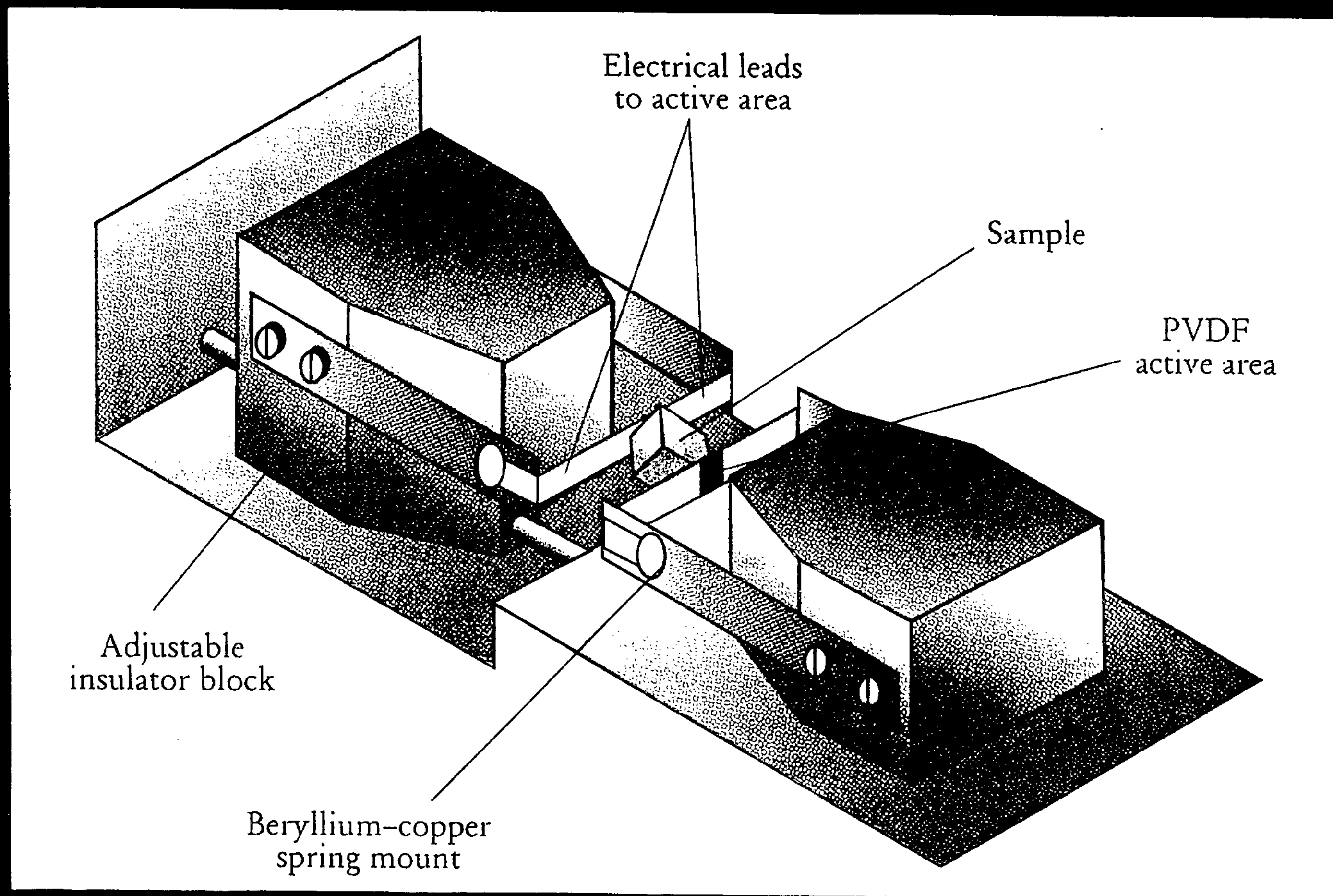
Electrical leads
to active area
Sample
PVDF
active area
Adjustable
insulator block
Beryllium–copper
spring mount

Small transducers for small samples

Piezoelectric Film: Polyvinylidene Fluoride (PVDF, tradename Kynar)
Available in 9 μm thick sheets

	units	BaTiO	Quartz	PVDF
Electric field/Pressure	Vm/N	5	50	200
Quality factor	Q	10^3	10^5	10
Acoustic impedance, ρc	10^6 kg/m^2-s	30	15	3
Frequency responce		MHz	MHz	GHz

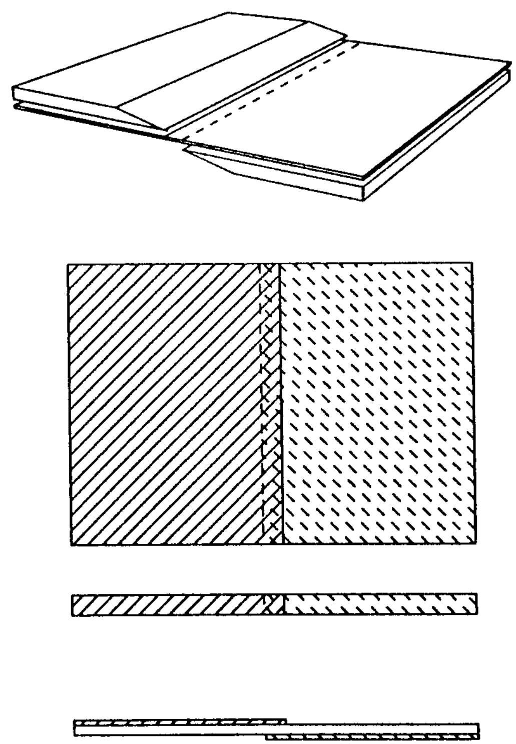

(a) (b) (c) (d)

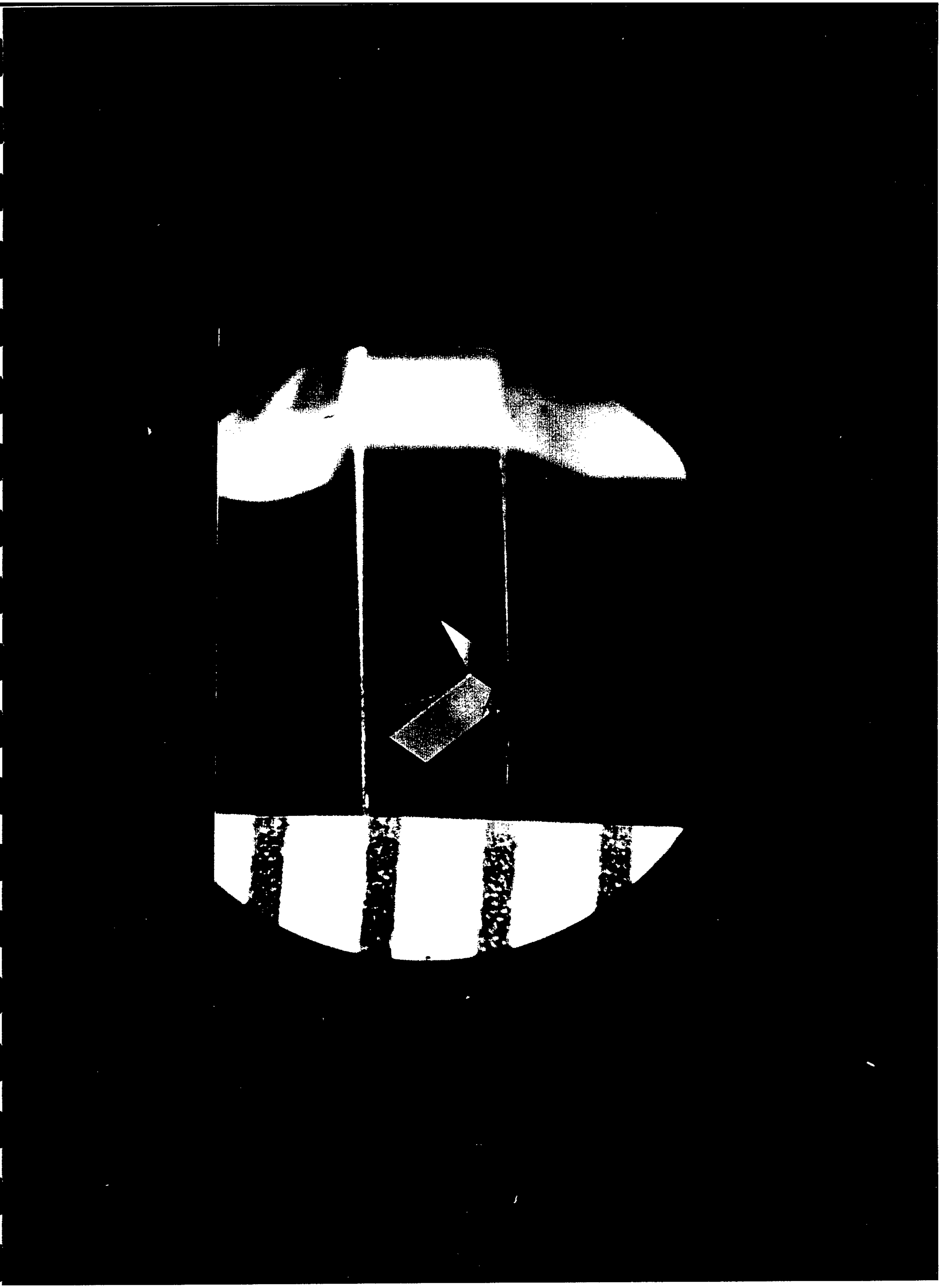

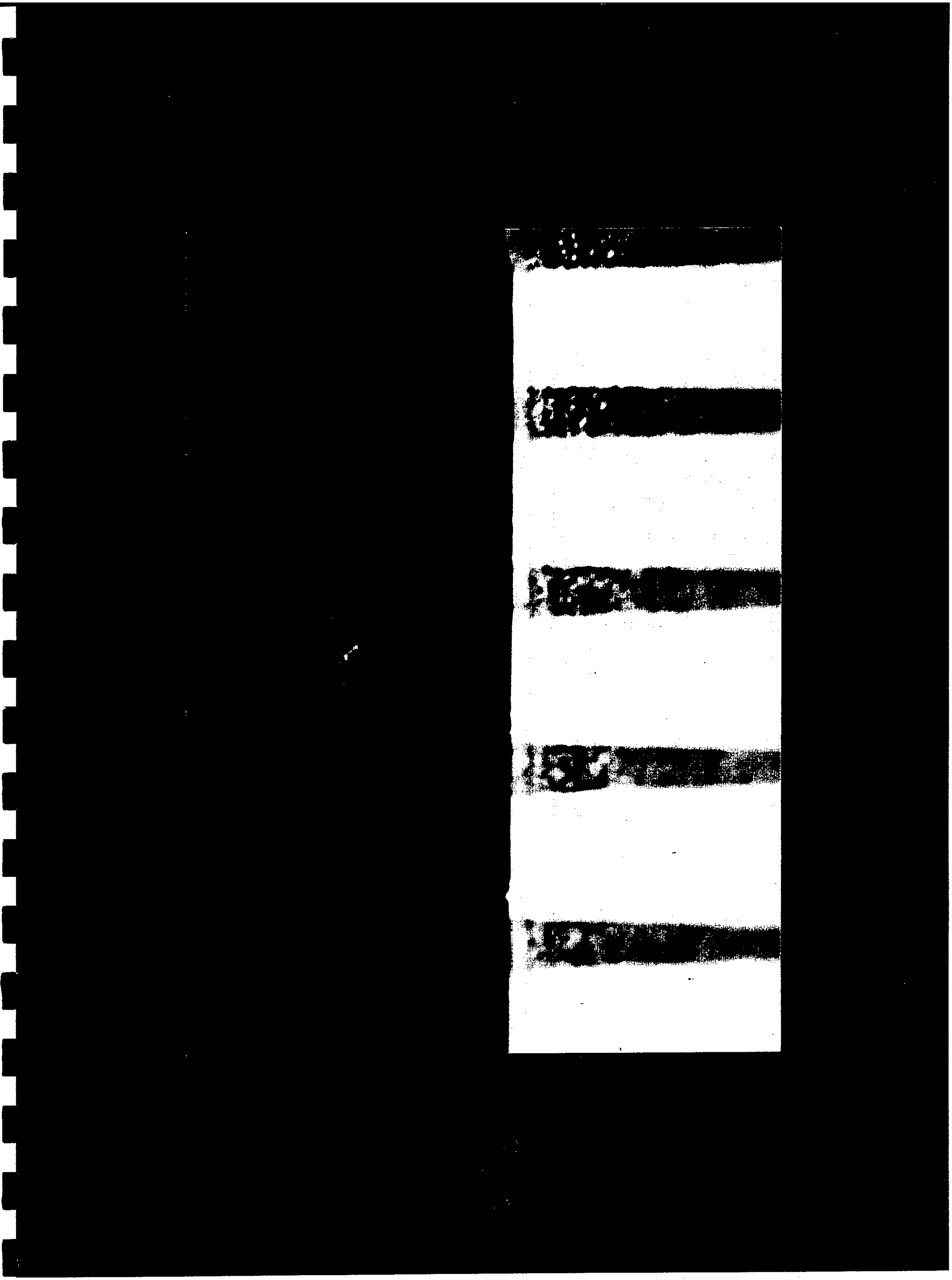

Feasibility

The elastic constants for the film, c'_{ij}, should be measured with suitable precision

$$\frac{\Delta c'_{ij}}{c'_{ij}} = \frac{\Delta f}{f} \left[\frac{c'_{ij}}{f} \frac{\partial f}{\partial c'_{ij}} \right]^{-1}$$

Problem: Measuring the substrate with and without the film may require mounting and remounting the sample.

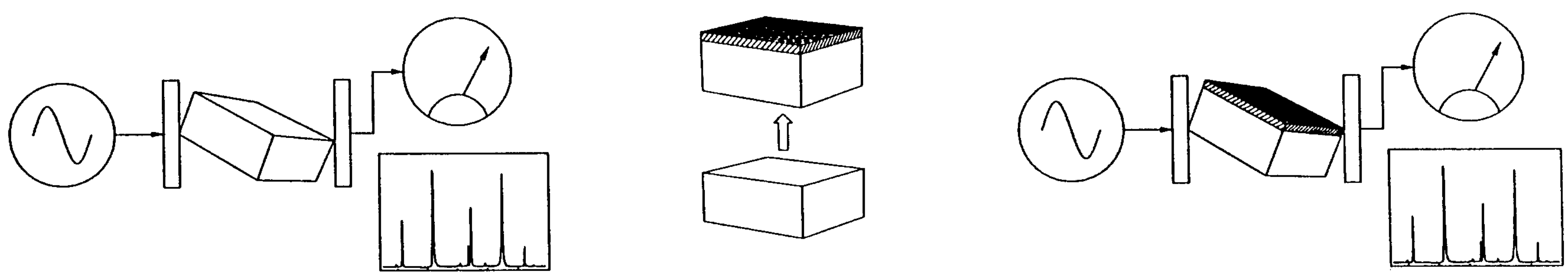

- The precision in measuring frequency, $\Delta f / f$, may be limited by changes resulting from remounting.

Reproducibility in Mounting and Remounting Sample

Silicon sample #1: a = 768 μm, b = 640 μm, c = 97 μm

Mode	1st	2nd	3rd	4th	Avg	ppm
1	1.334500	1.334500	1.333750	1.333750	1.333750	375
2	1.919250	1.920000	1.919625	1.919250	1.919373	221
3	2.137250	2.137250	2.136500	2.136875	2.136833	193
4	2.502500	2.503000	2.501500	2.501500	2.136833	362
5	3.407250	3.407625	3.406500	3.406500	3.406500	220
6	3.859750	3.859375	3.860500	3.860875	3.860125	153
7	4.069375	4.069000	4.068625	4.068625	4.068775	94
8	4.142125	4.142500	4.141750	4.141375	4.141643	134
10	4.780000	4.780500	4.779250	4.779000	4.781000	192
11	5.223375	5.223750	5.219625	5.227500	5.224375	494
12	5.463000	5.464875	5.465250	5.464900	5.464375	180

Reproducibility in Mounting and Remounting Sample

Strontium titanate sample #2: a = 804 μm, b = 722 μm, c = 445 μm

Mode	1st	2nd	3rd	Avg	ppm
1	2.373750	2.373625	2.373625	2.373667	25
2	3.051250	3.051625	3.051250	3.051375	58
3	3.661500	3.661375	3.661375	3.661417	16
4	3.787750	3.787750	3.787750	3.787750	00
7	4.273500	4.273500	4.273625	4.273542	14
8	4.368625	———	4.368750	4.368688	14
9	4.520812	4.520687	4.520937	4.520812	23
10	4.714000	4.714375	4.714750	4.714375	65
11	4.777500	4.777500	4.778000	4.777667	49
12	5.138250	5.138625	5.138625	5.138500	34
14	———	5.429875	5.430000	5.429938	12

Precision in Determining Film Elastic Constants

Strontium titanate sample #2: $a = 804\ \mu m$, $b = 722\ \mu m$, $c = 445\ \mu m$

Film thickness $t = 450$ nm

Mode	Freq	$\partial f/\partial t$	$\Delta 11\%$	$\Delta 12\%$	$\Delta 44\%$
1	2.372141	-0.792E-03	-	-	3.61
2	3.047371	-0.111E-02	4.28	7.03	-
3	3.667886	-0.382E-03	5.00	9.71	-
4	3.778126	-0.875E-03	-	-	-
5	4.007881	-0.379E-03	-	-	-
6	4.210928	-0.450E-03	-	-	-
7	4.278163	-0.366E-03	4.61	9.03	-
8	4.370969	-0.898E-03	2.19	3.98	4.65
9	4.520948	-0.960E-03	2.70	4.57	-
10	4.691540	-0.370E-03	-	-	-
11	4.793241	-0.477E-03	-	-	-
12	5.152972	-0.491E-03	7.52	-	-
13	5.195106	-0.252E-03	-	-	-
14	5.445382	-0.421E-03	3.52	8.41	-

Review of Basic RUS analysis

Assume stress-free boundary conditions and $\cos(\omega t)$ time dependence ($\omega = 2\pi f$):

Strain $$\epsilon_{ij} = \frac{1}{2}\left(\frac{\partial\psi_i}{\partial x_j} + \frac{\partial\psi_j}{\partial x_i}\right)$$

Hooke's Law $$\sigma_{ij} = c_{ijkl}\epsilon_{kl} = c_{ijkl}\frac{\partial\psi_k}{\partial x_l}$$

Newton's Law $$\rho\omega^2\psi_i + c_{ijkl}\frac{\partial^2\psi_k}{\partial x_j \partial x_l} = 0$$

Stress-free boundary condition $$\sigma_{ij}n_j = c_{ijkl}\frac{\partial\psi_k}{\partial x_l}n_j = 0$$

Boundary value problem has eigenvalues $\omega_n \rightarrow$ resonant frequencies $f_n = \omega_n/2\pi$

Equivalent to minimizing the Lagrangian:

$$L = \int\int\int \left(\rho\omega^2\psi_i\psi_i - c_{ijkl}\frac{\partial\psi_i}{\partial x_j}\frac{\partial\psi_k}{\partial x_l}\right) dV$$

Rayleigh-Ritz Approximation

Expand with basis functions $$\psi_i = \sum_{p=1}^{N} a_{pi}\Phi_p$$

Lagrangian $$L = \left(\omega^2 E_{piqj} - \Gamma_{piqj}\right) a_{pi}a_{qj}$$

where $$E_{piqj} = \delta_{ij} \int\int\int \rho \Phi_p \Phi_q dV$$

and $$\Gamma_{piqj} = \int\int\int c_{ikjl} \frac{\partial \Phi_p}{\partial x_k} \frac{\partial \Phi_q}{\partial x_l} dV$$

Let μ represent the combination pi, and ν represent qj. Minimizing L with respect to the coefficients a_μ yields the $3N$ x $3N$ matrix eigenvalue problem

Matrix eigenvalue problem $$\Gamma_{\mu\nu} a_\nu = \omega^2 E_{\mu\nu} a_\nu$$

Visscher Basis Set:

Use $\Phi_p = x^l y^m z^n$: Integrals for $\Gamma_{\mu\nu}$ and $\mathrm{E}_{\mu\nu}$ may be evaluated analytically for prisms, spheroids, ellipsoids, shells, bells, eggs, potatoes, sandwiches, and others. Normalize to improve matrix conditioning:

$$\Phi_p = \left(\frac{x}{a}\right)^l \left(\frac{y}{b}\right)^m \left(\frac{z}{c}\right)^n$$

where a, b, c are half the edge lengths of the sample. The integrals, with fixed limits (-1,1), become simple expressions.

Consequences of Symmetry

- If the elastic tensor has orthorhombic symmetry or better, then the matrices become **block diagonal.**
- Result of parity of $(x/a)^l$ (odd or even)
- Nearly eight-fold reduction of computation time

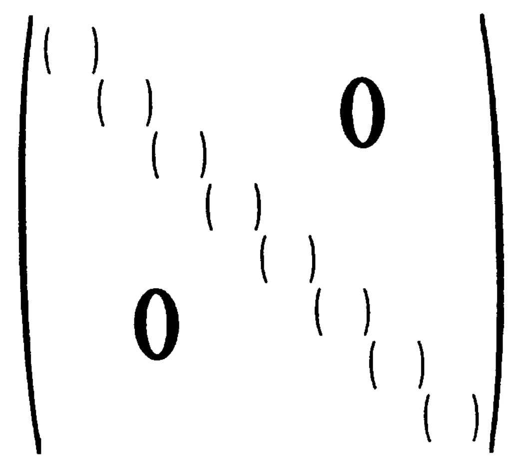

Modifications for Substrate with Film

Let $\alpha =$ (film thickness)/(half edge length), $\zeta = (\rho' - \rho)/\rho$, and $d_{ijkl} = c'_{ijkl} - c_{ijkl}$.

$$\frac{1}{\rho}E_{piqj} = \delta_{ij}\left[\int\int\int_{-1}^{1}\Phi_p\Phi_q dxdydz + \zeta\int\int_{-1}^{1}\int_{(1-\alpha)}^{1}\Phi_p\Phi_q dxdydz\right]$$

$$\Gamma_{piqj} = c_{ijkl}\int\int\int_{-1}^{1}\frac{\partial\Phi_p}{\partial x_k}\frac{\partial\Phi_q}{\partial x_l}dxdydz + d_{ijkl}\int\int_{-1}^{1}\int_{(1-\alpha)}^{1}\frac{\partial\Phi_p}{\partial x_k}\frac{\partial\Phi_q}{\partial x_l}dxdydz$$

Consequences of Reduced Symmetry

- Because of the film, parity symmetry is lost in the z-direction.
- Parity symmetry remains for the x- and y-directions.
- The matrix is block-diagonal with four blocks.

$$\begin{pmatrix} (\quad) & & \mathbf{0} & \\ & (\quad) & & \\ & & (\quad) & \\ \mathbf{0} & & & (\quad) \end{pmatrix}$$

```
C*********************************************************************
C
      PROGRAM XYZMRQ
C
C*********************************************************************
C
C     Read data file
C
      OPEN(3,FILE='xyzmrq.dat',STATUS='OLD',ERR=101)
      GO TO 102
101   WRITE(*,'(A)') ' Error opening xyzmrq.dat.'
      GO TO 9000
C
102   READ(3,*,ERR=101) C11,C12,C44,E1,E2,E3
      READ(3,*,ERR=101) (IA(I),I=1,6)
      READ(3,*,ERR=101) RHO,NN,NMDS
      DO 103 I=1,NMDS
      READ(3,*,ERR=101) FDATA(I)
103   CONTINUE
      CLOSE(3,ERR=9000)
C
      NDATA=0
      DO 105 I=1,NMDS
      IF(FDATA(I).LE.0.0) GO TO 104
      NDATA=NDATA+1
      X(NDATA)=FLOAT(I)
      Y(NDATA)=FDATA(I)
      GO TO 105
104   FDATA(I)=-FDATA(I)
105   CONTINUE
C
C     Parameter setup
C
      CALL INIT
C
      ALAMDA=-1.
      SUMSQ=1.D23
      ITER=0
C
200   ITER=ITER+1
      OLAMDA=ALAMDA
      CHI0=SUMSQ
      WRITE(*,'(A20,I2)') '     Iteration number',ITER
C
      CALL MRQMIN(X,Y,SIG,NDATA,A,IA,MA,COVAR,ALPHA,MMAX,
     & SUMSQ,FREQS,ALAMDA)
C
      CHANGE=ABS((SUMSQ-CHI0)/CHI0)
      WRITE(*,'(5E12.4)') OLAMDA,ALAMDA,CHI0,SUMSQ,CHANGE
C
      IF(CHANGE.GT.TOL) GO TO 200
C
      DO 8200 I=1,NMDS
      ERR=0.0
      IF(FDATA(I).GT.0.) ERR=100.*((FDATA(I)-WSAV(I))/WSAV(I))
      WRITE(3,'(I3,2F10.5,F8.3)') I,FDATA(I),WSAV(I),ERR
8200  CONTINUE
C
9000  STOP
      END
```

```
C*********************************************************************
C
      SUBROUTINE FREQS(XVAL,A,YMOD,DYDA,MA)
C
C*********************************************************************
C
10    DO 11 I=1,MA
      IF(A(I).NE.ALST(I)) GO TO 100
11    CONTINUE
      GO TO 200
C
100   CALL XYZBLK(A,MA,WSAV)
C
      DO 112 I=1,MA
      IF(IA(I).EQ.0) GO TO 112
      A0=A(I)
      A(I)=A0*(1.D0+EPS(I))
      DA=A(I)-A0
      CALL XYZBLK(A,MA,WTMP)
      DO 111  J=1,NDATA
      JX=NINT(X(J))
      DYDAA(I,JX)=(WTMP(JX)-WSAV(JX))/DA
111   CONTINUE
      A(I)=A0
112   CONTINUE
C
      DO 113 I=1,MA
      ALST(I)=A(I)
113   CONTINUE
C
200   IX=NINT(XVAL)
      YMOD=WSAV(IX)
      DO 201 I=1,MA
      DYDA(I)=DYDAA(I,IX)
201   CONTINUE
C
      RETURN
      END
```

```
C*********************************************************************
C
      SUBROUTINE XYZBLK(A,MA,WSAV)
C
C*********************************************************************
C
C     Loop for eight blocks
C
      DO 8000 L0=1,2
      DO 8000 M0=1,2
      DO 8000 N0=1,2
C
      IG=0
      DO 2 I=1,3
      LMN(1)=L0
      LMN(2)=M0
      LMN(3)=N0
      LMN(I)=LMN(I)+1
      IF(LMN(I).EQ.3) LMN(I)=1
      DO 2 L=LMN(1),NNP1,2
      DO 2 M=LMN(2),NNP1,2
      DO 2 N=LMN(3),NNP1,2
      IF(L+M+N.GT.NNP3) GO TO 2
      IG=IG+1
      IC(IG)=I
      LB(IG)=L-1
      MB(IG)=M-1
      NB(IG)=N-1
2     CONTINUE
      NR=IG
C
C calculate Gamma and E
C
      DO 3 IG=1,NR
      DO 3 JG=IG,NR
      E(IG,JG)=0.D0
      GAMMA(IG,JG)=0.D0
      I=IC(IG)
      J=IC(JG)
      LS=LB(IG)+LB(JG)
      MS=MB(IG)+MB(JG)
      NS=NB(IG)+NB(JG)
      GAMMA(IG,JG)=
     & C(I,1,J,1)*DFLOAT(LB(IG)*LB(JG))*F(LS-2,MS,NS)*E11
     & +C(I,2,J,2)*DFLOAT(MB(IG)*MB(JG))*F(LS,MS-2,NS)*E22
     & +C(I,3,J,3)*DFLOAT(NB(IG)*NB(JG))*F(LS,MS,NS-2)*E33
     & +(C(I,1,J,2)*DFLOAT(LB(IG)*MB(JG))+C(I,2,J,1)*
     & DFLOAT(MB(IG)*LB(JG)))*F(LS-1,MS-1,NS)*E12
     & +(C(I,1,J,3)*DFLOAT(LB(IG)*NB(JG))+C(I,3,J,1)*
     & DFLOAT(NB(IG)*LB(JG)))*F(LS-1,MS,NS-1)*E13
     & +(C(I,2,J,3)*DFLOAT(MB(IG)*NB(JG))+C(I,3,J,2)*
     & DFLOAT(NB(IG)*MB(JG)))*F(LS,MS-1,NS-1)*E23
      GAMMA(JG,IG)=GAMMA(IG,JG)
      IF(I.EQ.J) E(IG,JG)=F(LS,MS,NS)
      E(JG,IG)=E(IG,JG)
3     CONTINUE
C
      CALL EIGEN(GAMMA,E,WSAV)
C
      DO 8020 I=1,NMDS
      WSAV(I)=DSQRT(WSAV(I)/RHO)/TWOPI
8020  CONTINUE
C
9000  RETURN
      END
C
      FUNCTION F(IP,IQ,IR)
C
      F=0.00D+00
      IF((IP.LT.0).OR.(IQ.LT.0).OR.(IR.LT.0)) RETURN
      IF((MOD(IP,2).NE.0).OR.(MOD(IQ,2).NE.0).OR.(MOD(IR,2).NE.0))
     & RETURN
      F=8.D0/DFLOAT((IP+1)*(IQ+1)*(IR+1))
      RETURN
      END
```

```
C*****************************************************
C
      SUBROUTINE XYZBLK(A,MA,WSAV,NDATA)
C
C*****************************************************
C
C  normalization factors for the calculation of Gamma
C
      E11=4.D0/(E1*E1)
      E22=4.D0/(E2*E2)
      E33=4.D0/(E3*E3)
      E23=4.D0/(E2*E3)
      E13=4.D0/(E1*E3)
      E12=4.D0/(E1*E2)
C
C  Loop for block matrices
C
      DO 8000 L0=1,2
      DO 8000 M0=1,2
      DO 8000 N0=1,2
C
      IG=0
      DO 2 I=1,3
      LMN(1)=L0
      LMN(2)=M0
      LMN(3)=N0
      JLMN=1
      IF(LMN(I).EQ.1) JLMN=2
      LMN(I)=JLMN
C
      DO 2 L=LMN(1),NN+1,2
      DO 2 M=LMN(2),NN+1,2
      DO 2 N=LMN(3),NN+1,2
      IF(L+M+N.GT.NN+3) GO TO 2
      IG=IG+1
      IC(IG)=I
      LB(IG)=L-1
      MB(IG)=M-1
      NB(IG)=N-1
2     CONTINUE
C
```

```
C**********************************************************
C
      SUBROUTINE XYZBLK(A,MA,WSAV,NDATA)
C
C**********************************************************
C
C  normalization factors for the calculation of Gamma
C
      E11=4.D0/(E1*E1)
      E22=4.D0/(E2*E2)
      E33=4.D0/(E3*E3)
      E23=4.D0/(E2*E3)
      E13=4.D0/(E1*E3)
      E12=4.D0/(E1*E2)
C
C  Loop for block matrices
C
      DO 8000 L0=1,2
      DO 8000 M0=1,2
C
      IG=0
      DO 2 N0=1,2
      DO 2 I=1,3
      LMN(1)=L0
      LMN(2)=M0
      LMN(3)=N0
      JLMN=1
      IF(LMN(I).EQ.1) JLMN=2
      LMN(I)=JLMN
C
      DO 2 L=LMN(1),NN+1,2
      DO 2 M=LMN(2),NN+1,2
      DO 2 N=LMN(3),NN+1,2
      IF(L+M+N.GT.NN+3) GO TO 2
      IG=IG+1
      IC(IG)=I
      LB(IG)=L-1
      MB(IG)=M-1
      NB(IG)=N-1
2     CONTINUE
C
```

```
C
C
C  calculate Gamma
C
        NR=IG
        DO 3 IG=1,NR
        DO 3 JG=IG,NR
        E(IG,JG)=0.D0
        GAMMA(IG,JG)=0.D0
        I=IC(IG)
        J=IC(JG)
        LS=LB(IG)+LB(JG)
        MS=MB(IG)+MB(JG)
        NS=NB(IG)+NB(JG)
        GAMMA(IG,JG)=
     &  C(I,1,J,1)*DFLOAT(LB(IG)*LB(JG))*F(LS-2,MS,NS)*E11
     & +C(I,2,J,2)*DFLOAT(MB(IG)*MB(JG))*F(LS,MS-2,NS)*E22
     & +C(I,3,J,3)*DFLOAT(NB(IG)*NB(JG))*F(LS,MS,NS-2)*E33
     & +(C(I,1,J,2)*DFLOAT(LB(IG)*MB(JG))+C(I,2,J,1)*
     & DFLOAT(MB(IG)*LB(JG)))*F(LS-1,MS-1,NS)*E12
     & +(C(I,1,J,3)*DFLOAT(LB(IG)*NB(JG))+C(I,3,J,1)*
     & DFLOAT(NB(IG)*LB(JG)))*F(LS-1,MS,NS-1)*E13
     & +(C(I,2,J,3)*DFLOAT(MB(IG)*NB(JG))+C(I,3,J,2)*
     & DFLOAT(NB(IG)*MB(JG)))*F(LS,MS-1,NS-1)*E23
     & +D(I,1,J,1)*DFLOAT(LB(IG)*LB(JG))*G(LS-2,MS,NS)*E11
     & +D(I,2,J,2)*DFLOAT(MB(IG)*MB(JG))*G(LS,MS-2,NS)*E22
     & +D(I,3,J,3)*DFLOAT(NB(IG)*NB(JG))*G(LS,MS,NS-2)*E33
     & +(D(I,1,J,2)*DFLOAT(LB(IG)*MB(JG))+D(I,2,J,1)*
     & DFLOAT(MB(IG)*LB(JG)))*G(LS-1,MS-1,NS)*E12
     & +(D(I,1,J,3)*DFLOAT(LB(IG)*NB(JG))+D(I,3,J,1)*
     & DFLOAT(NB(IG)*LB(JG)))*G(LS-1,MS,NS-1)*E13
     & +(D(I,2,J,3)*DFLOAT(MB(IG)*NB(JG))+D(I,3,J,2)*
     & DFLOAT(NB(IG)*MB(JG)))*G(LS,MS-1,NS-1)*E23
C
        GAMMA(JG,IG)=GAMMA(IG,JG)
        IF(I.EQ.J) E(IG,JG)=F(LS,MS,NS)+DRHO*G(LS,MS,NS)
        E(JG,IG)=E(IG,JG)
 3      CONTINUE
C
```

```
C
C***************************************************************************
C
      FUNCTION F(IP,IQ,IR)
C
C***************************************************************************
      IMPLICIT INTEGER (I-N)
      IMPLICIT REAL*8 (A-H,O-Z)
C
      F=0.00D+00
      IF((IP.LT.0).OR.(IQ.LT.0).OR.(IR.LT.0)) RETURN
      IF((MOD(IP,2).NE.0).OR.(MOD(IQ,2).NE.0).OR.(MOD(IR,2).NE.0)) RETURN
C
      IP1=IP+1
      IQ1=IQ+1
      IR1=IR+1
C
      F=8.D0/DFLOAT(IP1*IQ1*IR1)
      RETURN
      END
C
C***************************************************************************
C
      FUNCTION G(IP,IQ,IR)
C
C***************************************************************************
      IMPLICIT INTEGER (I-N)
      IMPLICIT REAL*8 (A-H,O-Z)
      COMMON /ALPHA/ ALPHA
C
      G=0.00D+00
      IF((IP.LT.0).OR.(IQ.LT.0).OR.(IR.LT.0)) RETURN
      IF((MOD(IP,2).NE.0).OR.(MOD(IQ,2).NE.0)) RETURN
C
      IP1=IP+1
      IQ1=IQ+1
      IR1=IR+1
C
      G=(4.D0/DFLOAT(IP1*IQ1*IR1))*(1.D0-(1.D0-ALPHA)**(IR1))
      RETURN
      END
```

Application: Mats of Carbon Nanotubes

Single Walled Nanotubes (SWNT):

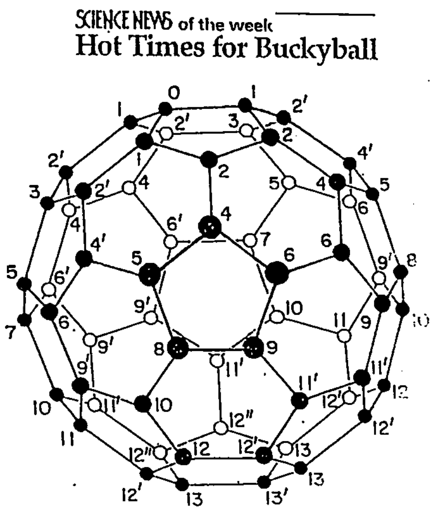

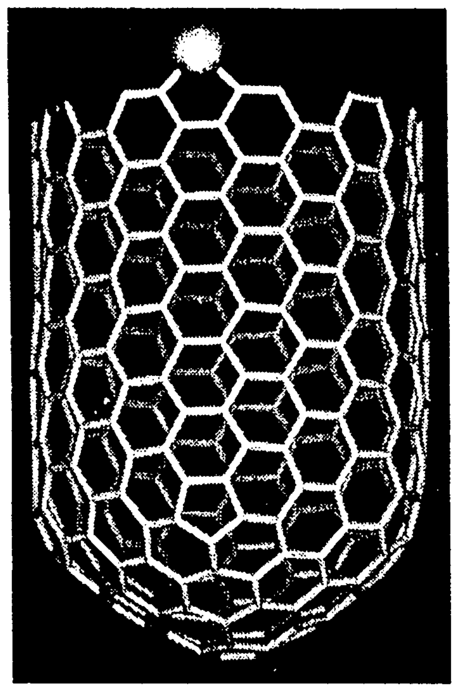

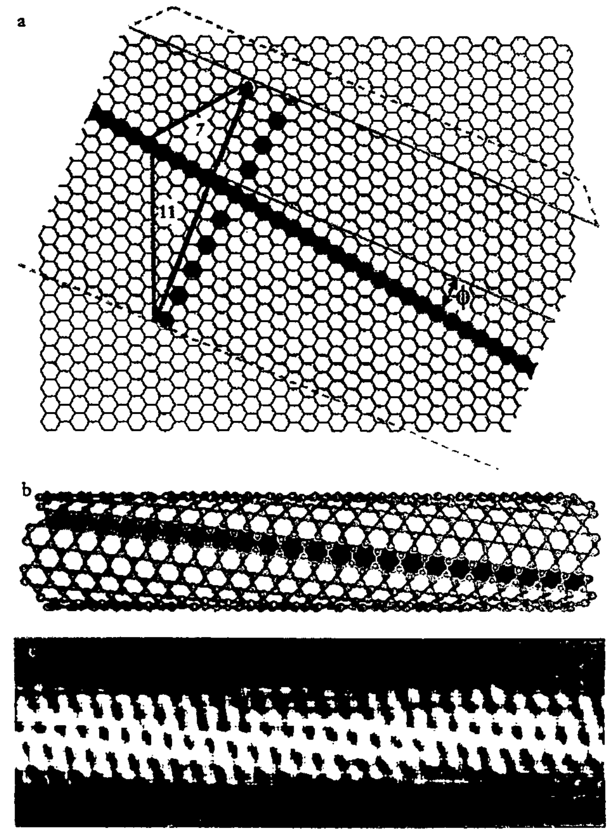

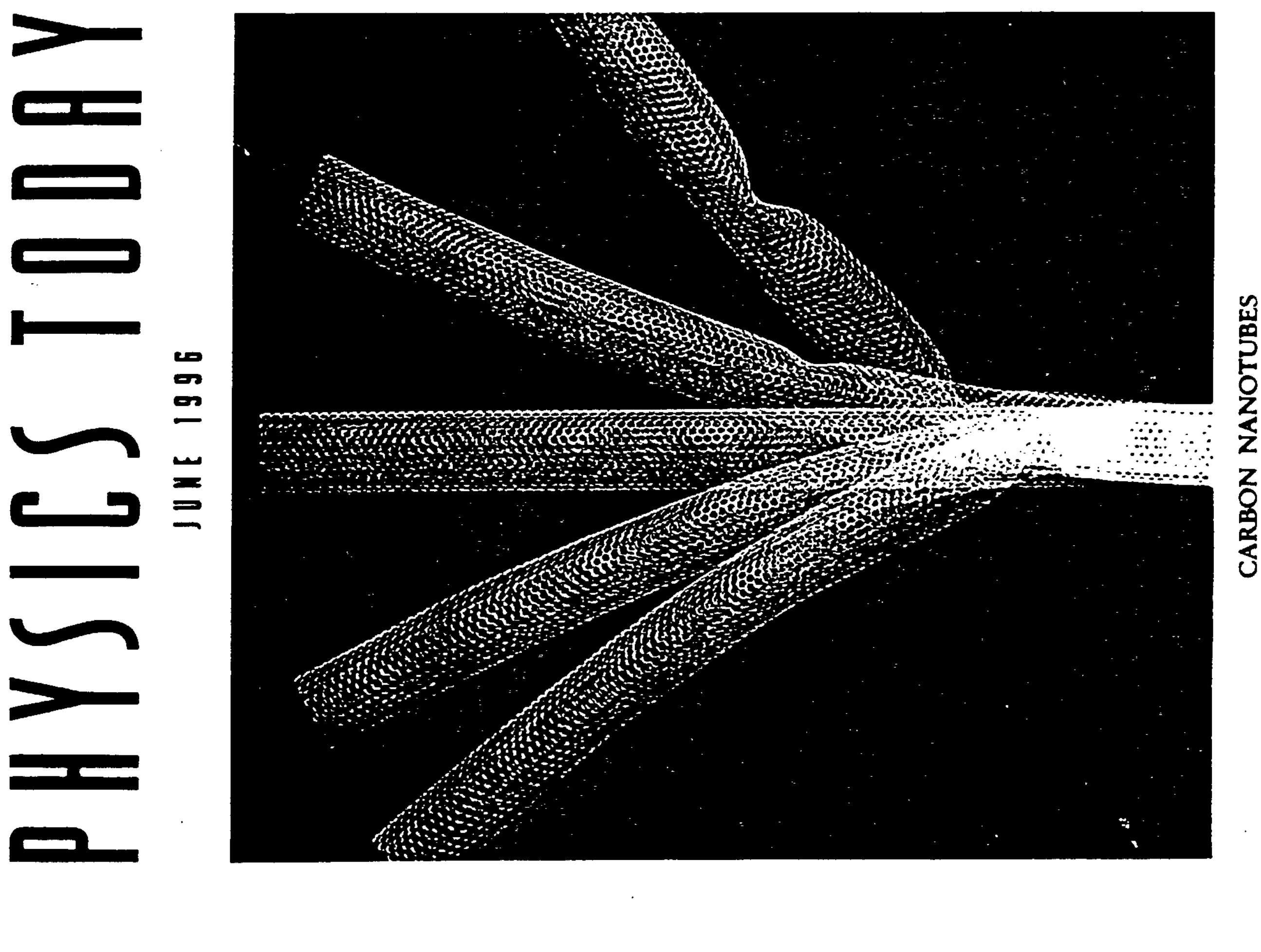
PHYSICS TODAY
JUNE 1996
CARBON NANOTUBES

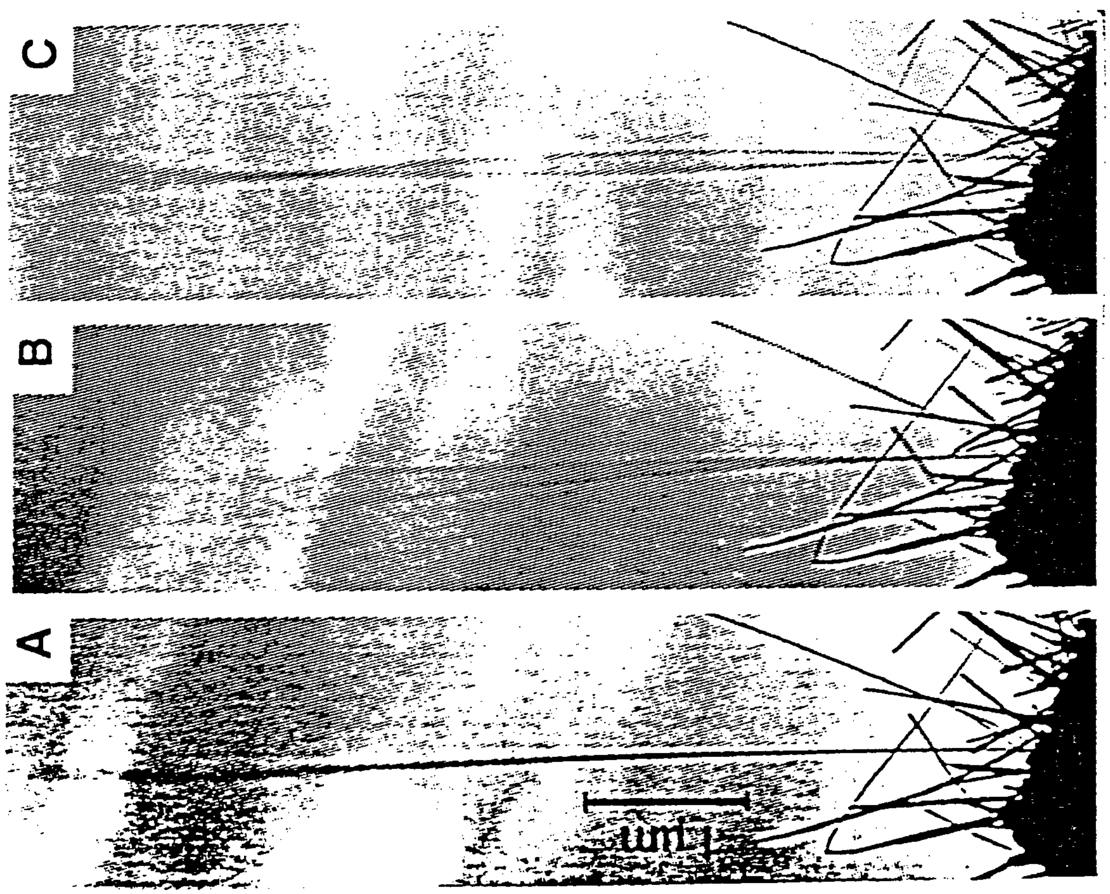
A
B
C
1 µm

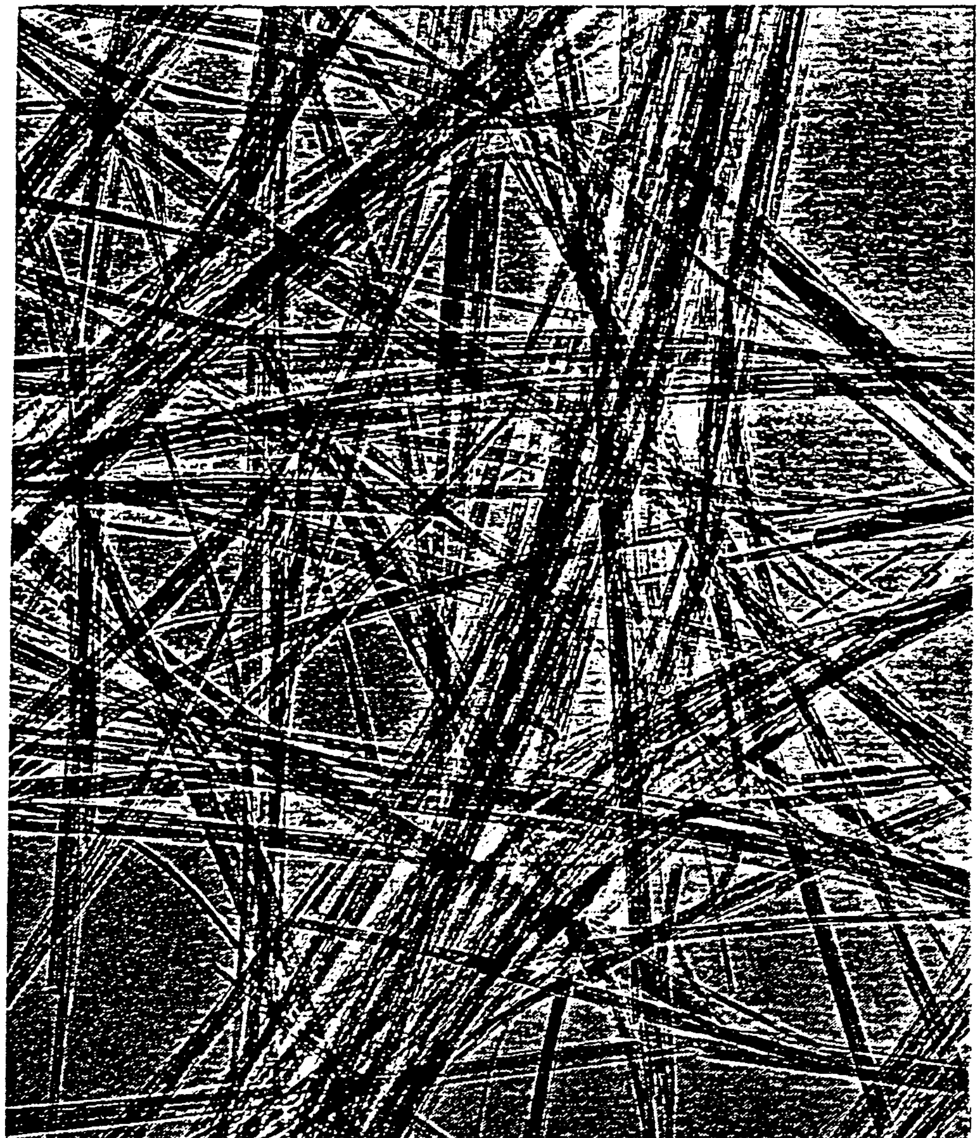

TR-26

Elasticity of steel and silica glass spheres under gas pressure by RUS

I. Ohno[1], M. Abe[1], M. Kimura[2], Y. Hanayama[3], H. Oda[4] and I. Suzuki[4]

1 Department of Earth Sciences, Ehime University, Matsuyama 790-8577, Japan
2 Department of Material Science and Engineering, Ehime University, Matsuyama 790-8577, Japan
3 Department of Mechanical Engineering, Ehime University, Matsuyama 790-8577, Japan
4 Department of Earth Sciences, Okayama University, Okayama 700-0082, Japan

ABSTRACT

Elasticity of minerals under high pressure are of great importance from geophysical view point. In order to develop a new method to measure pressure dependence of elastic constants, resonant ultrasound spectroscopy (RUS) were applied to the condition of gas pressure. We used a three-layered spherical shell assembly of spherical sample-thin gas layer-spherical cavity container, which works to give a well-defined boundary condition in the analysis. The samples measured were spheres of steel and silica glass with diameter of 4-5 mm. Several modes, not only torsional but also spheroidal modes, were observed at least up to 200MPa (2kbar) under helium gas pressure, and pressure shifts of frequencies were obtained definitely in both samples. The data of the slope of pressure shift of frequency yield pressure derivatives of bulk modulus and shear modulus, dK/dP and dG/dP, which are in good agreement with previous data.

1. Method

Resonant Ultrasound Spectroscopy (RUS)
with spherical sample

Two kinds of data acquisition

1) Continuous Wave (CW) method

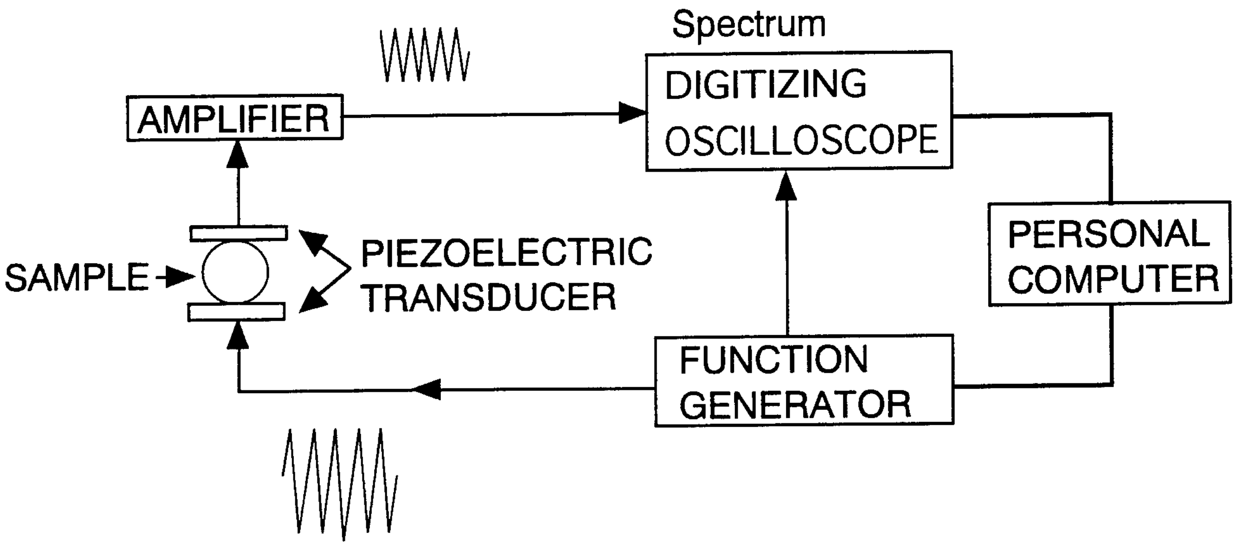

2) Fourier Transform (FT) method

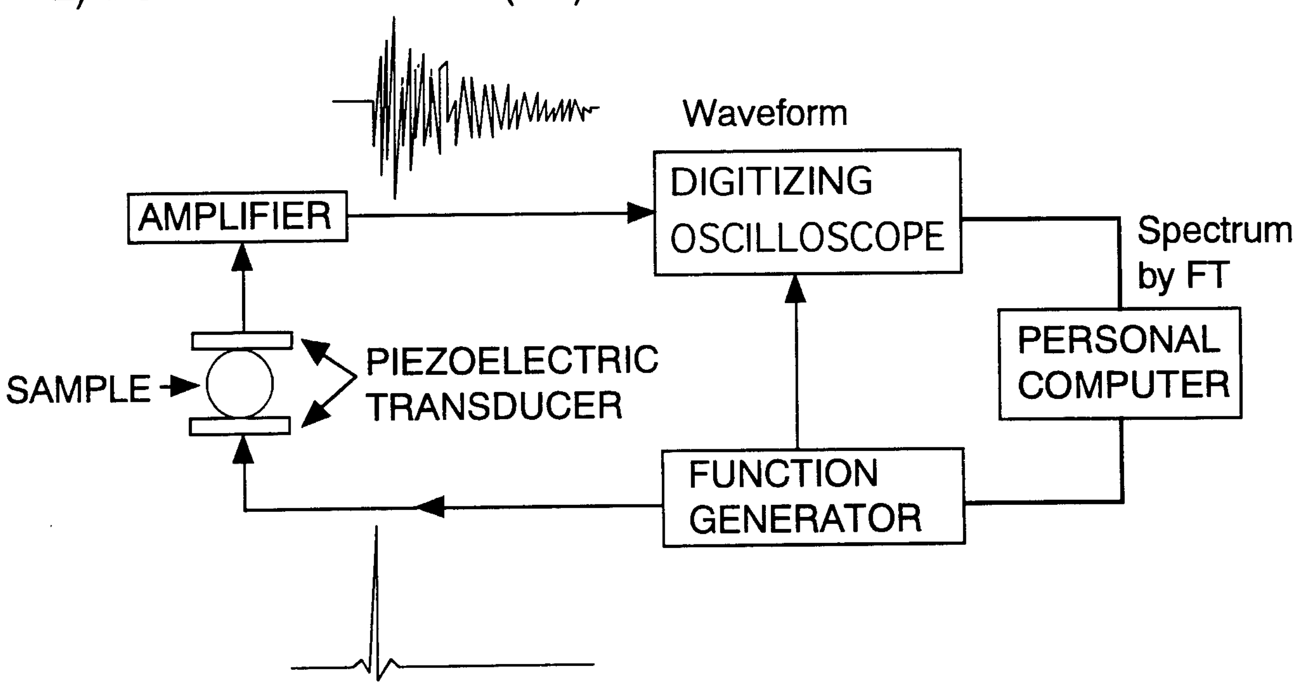

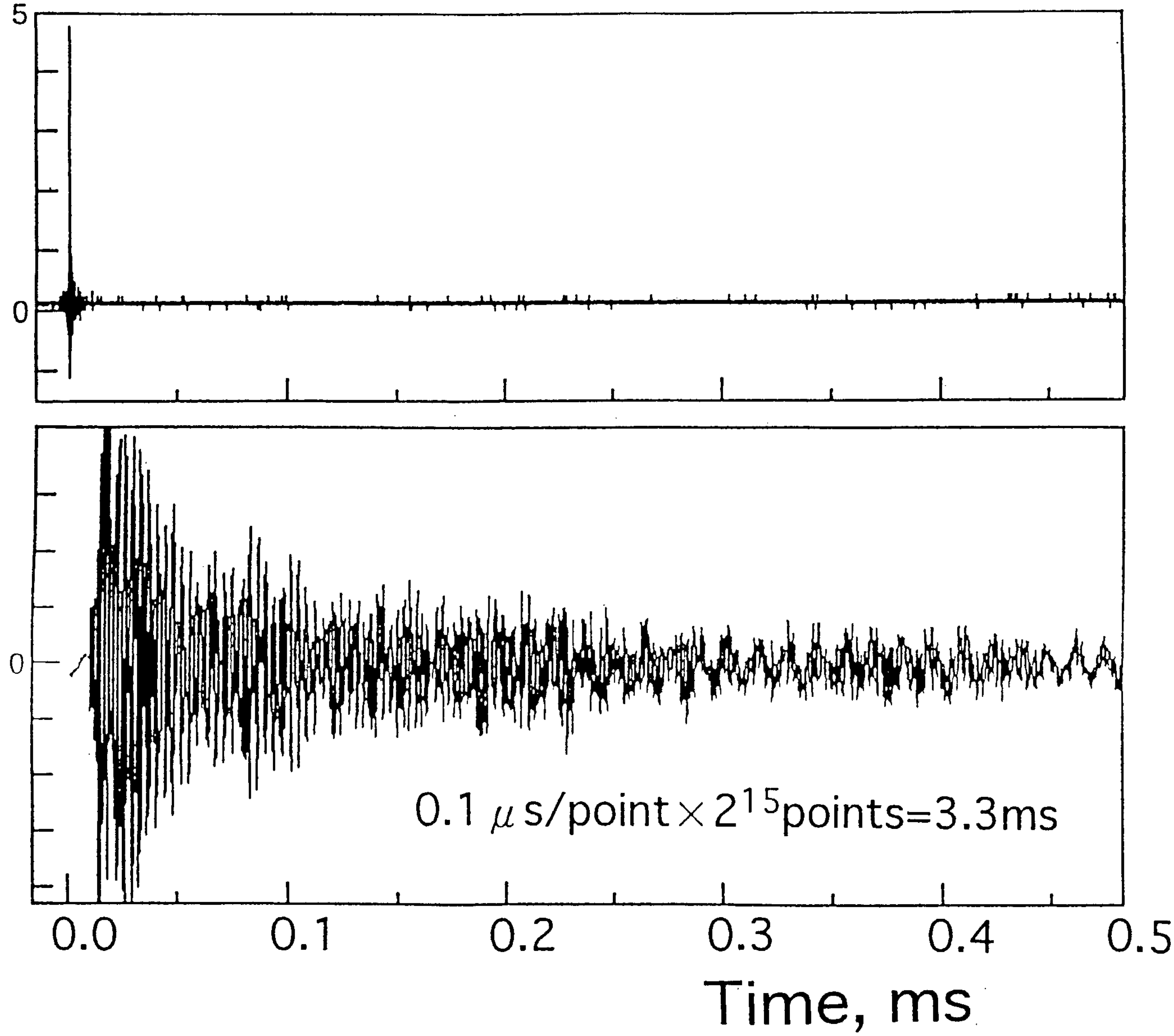

An example of input impulse (top) and output responsee(bottom) in FT method.

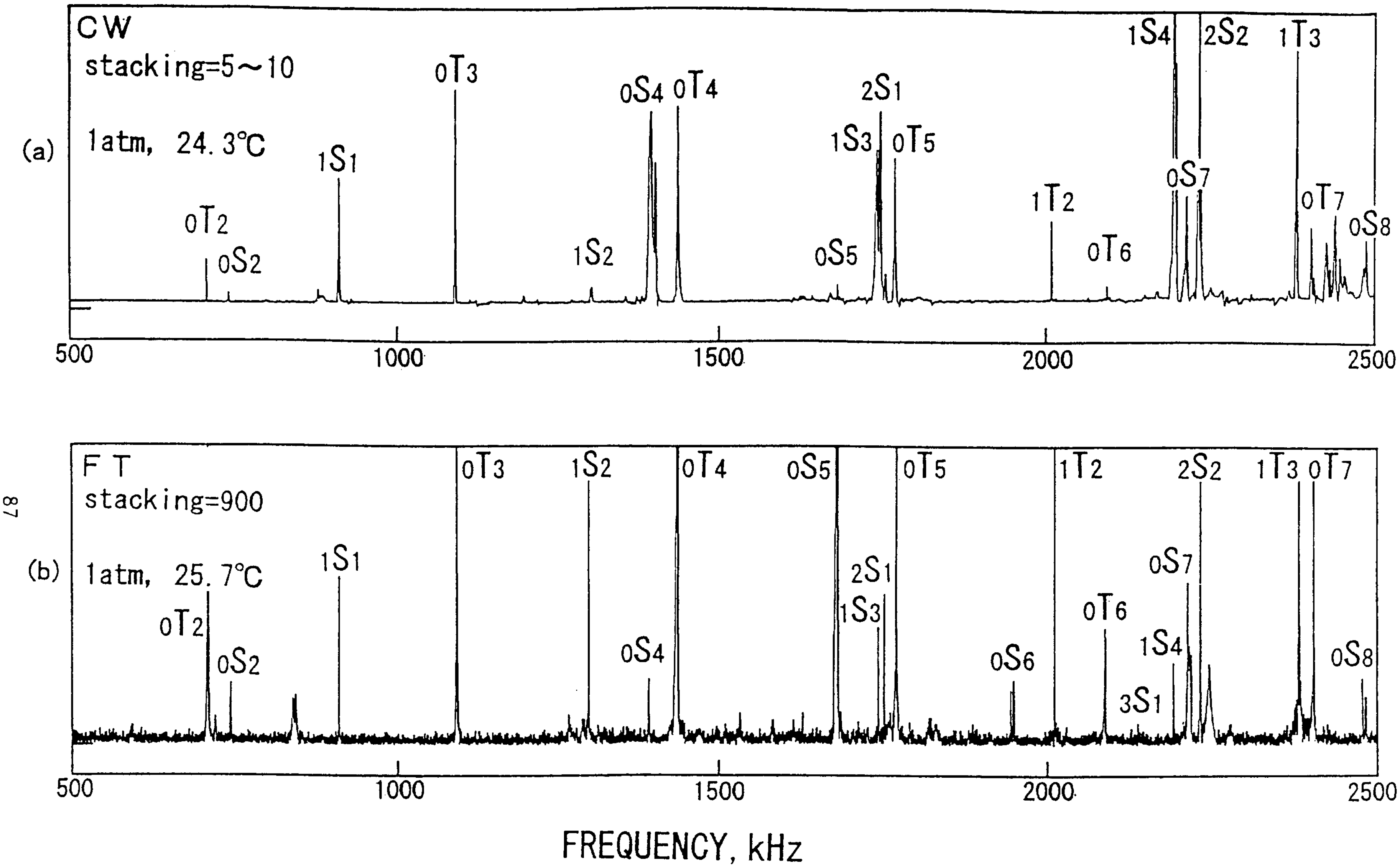

Comparison between spectra acquired by CW method (top) and FT method (bottom).
sample: silica glass sphere.

2. Samples

	Silica Glass Sphere	Steel Sphere
Diameter	4.245 mm	4.766 mm
Density	2.21_4 g/cm^3	7.798 g/cm^3
Poisson's Ratio	0.164	0.293
Shear Velocity	3.76_8 km/s	3.19_4 km/s
Bulk Modulus	36.2_4 GPa	$165._5$ GPa
Rigidity	31.3_8 GPa	79.5_6 GPa

3. Measurement under Gas Pressure

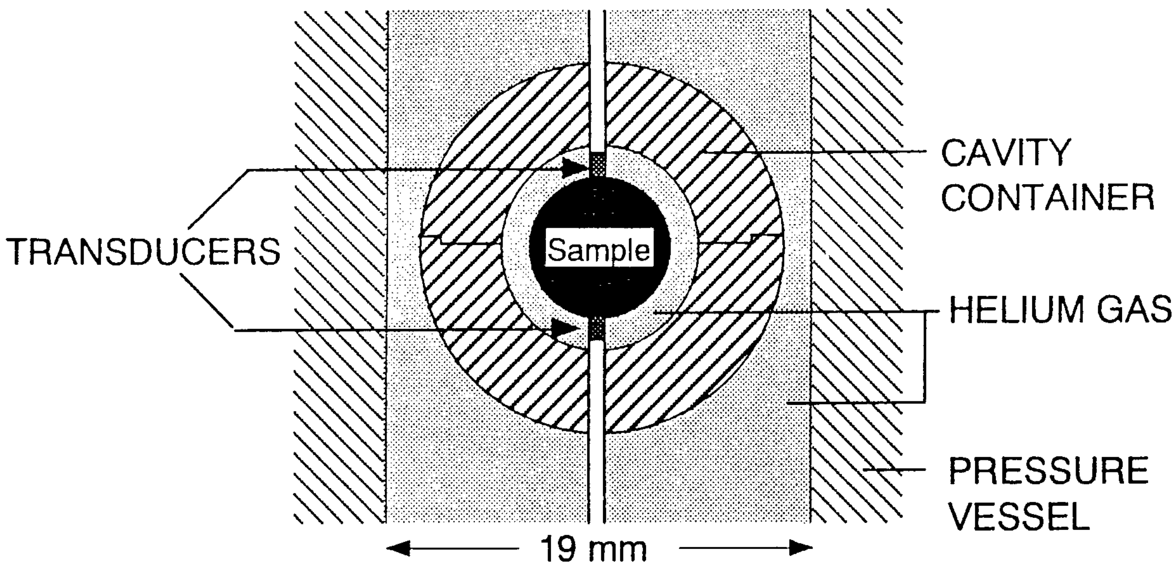

Sample assembly for measurement under pressure.

- cavity container: 5mm in inner, and 17mm in outer diameter
- transducer: PZT, shear type, 2.5MHz
- pressure range: 1atm - 200MPa (2kbar)

Eigenfrequencies of the sample-cavity(gas layer)-cavity container system were measured under gas pressure. The cavity container was used to make a well-defined bountary condition. The pressure shift of frequency of torsional mode gives G_0', and those of spheroidal mode gives K_0'.

4. Result on Steel Sphere

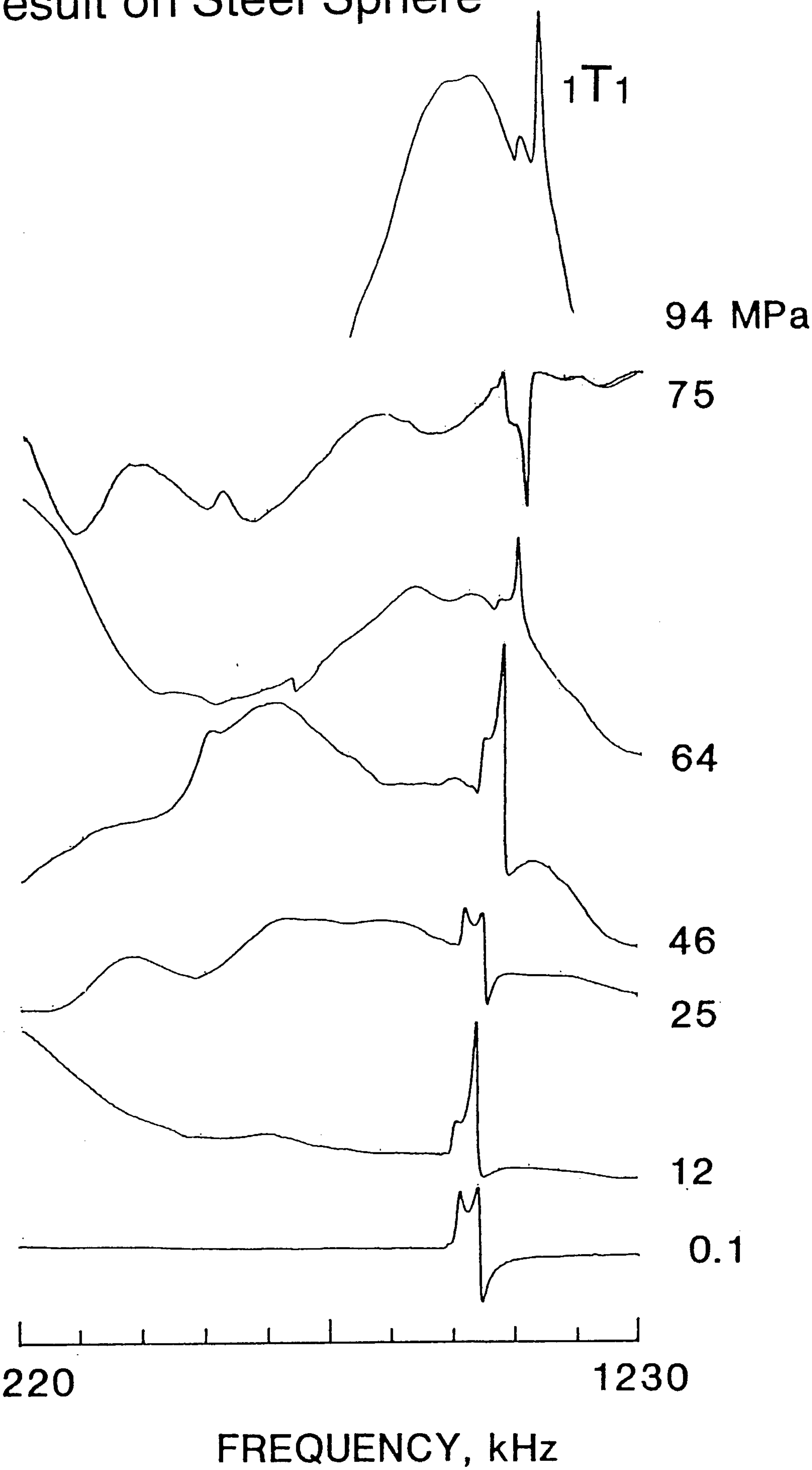

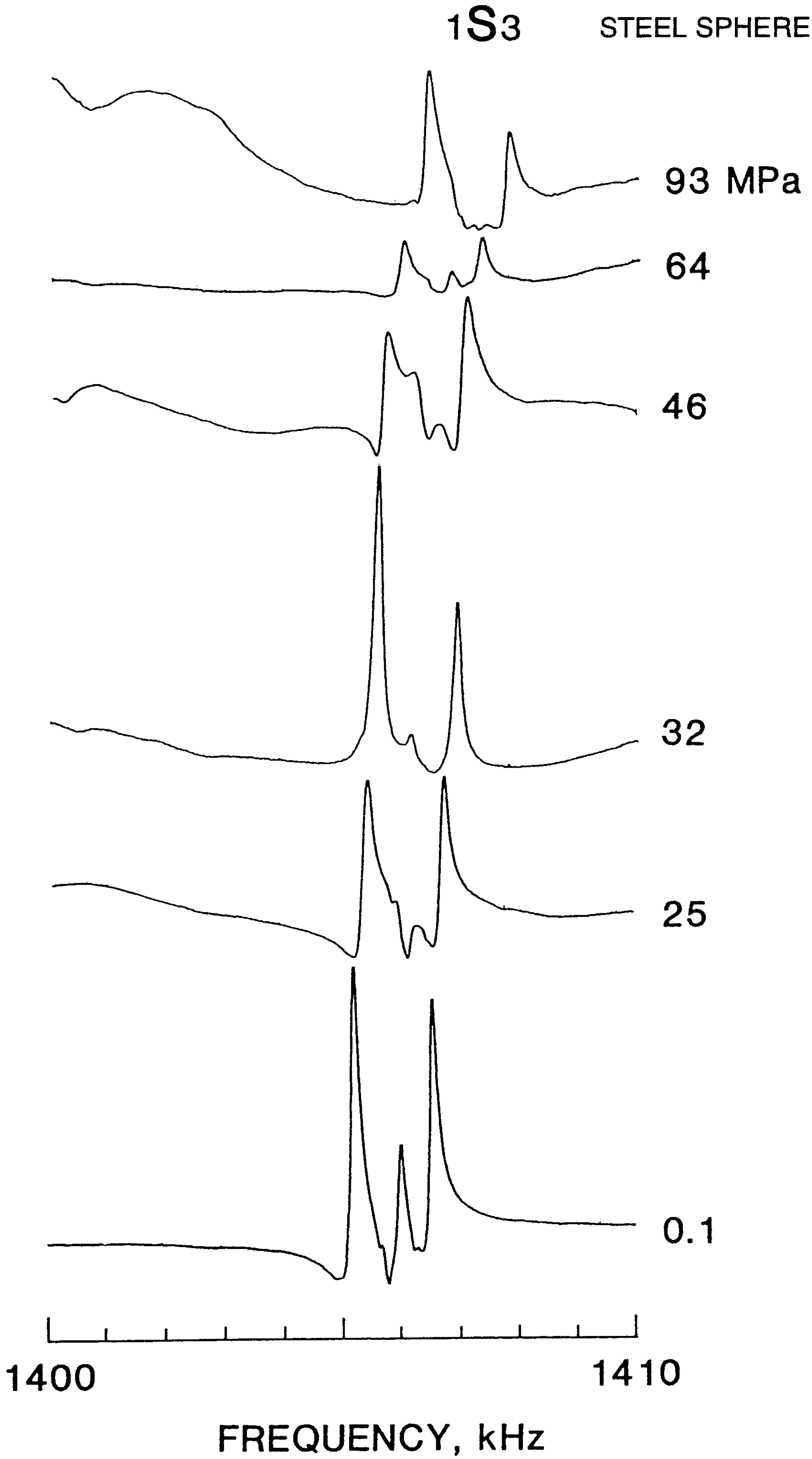
1S3
STEEL SPHERE
93 MPa
64
46
32
25
0.1
1400
1410
FREQUENCY, kHz

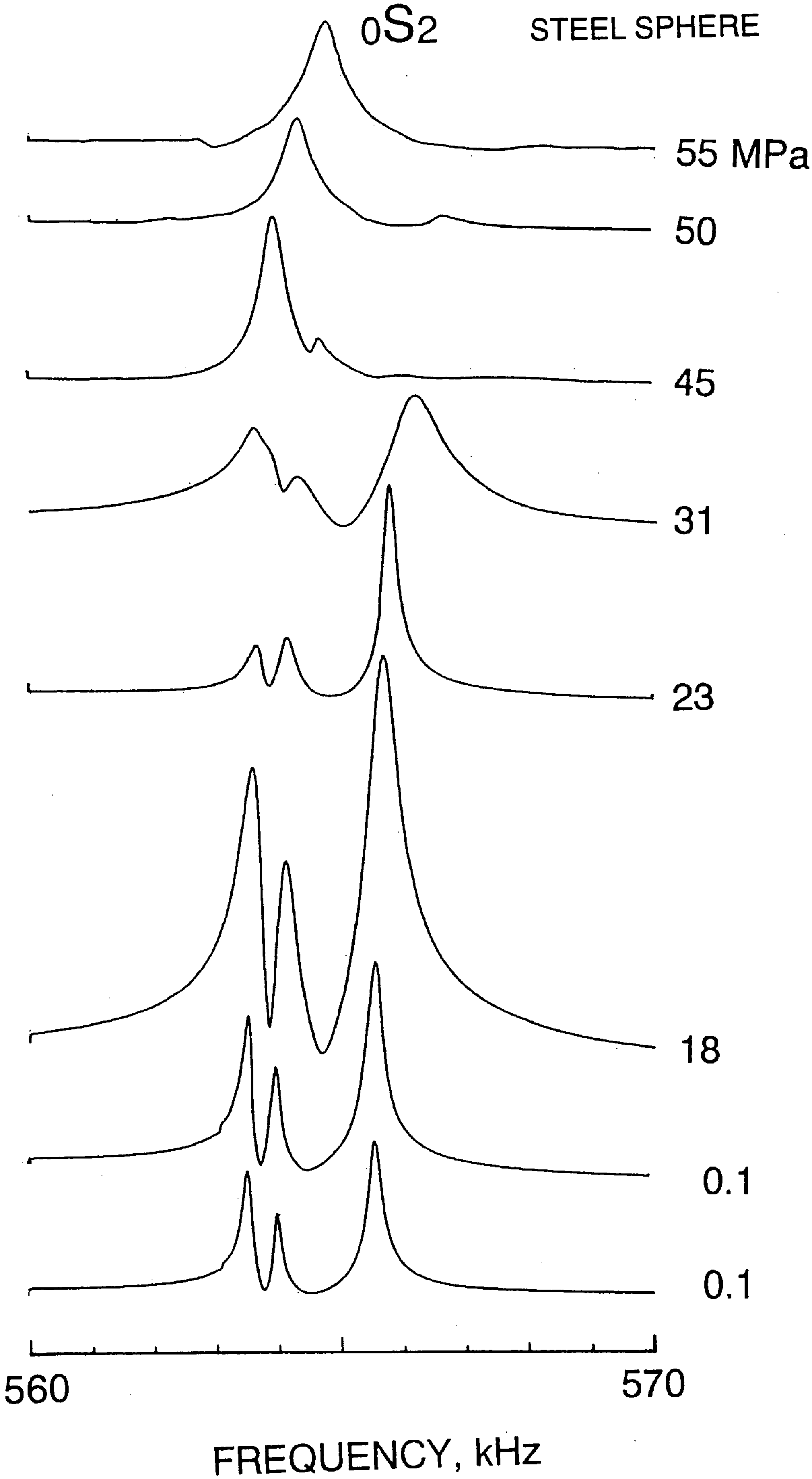

$_0S_2$
STEEL SPHERE
55 MPa
50
45
31
23
18
0.1
0.1
560
570
FREQUENCY, kHz

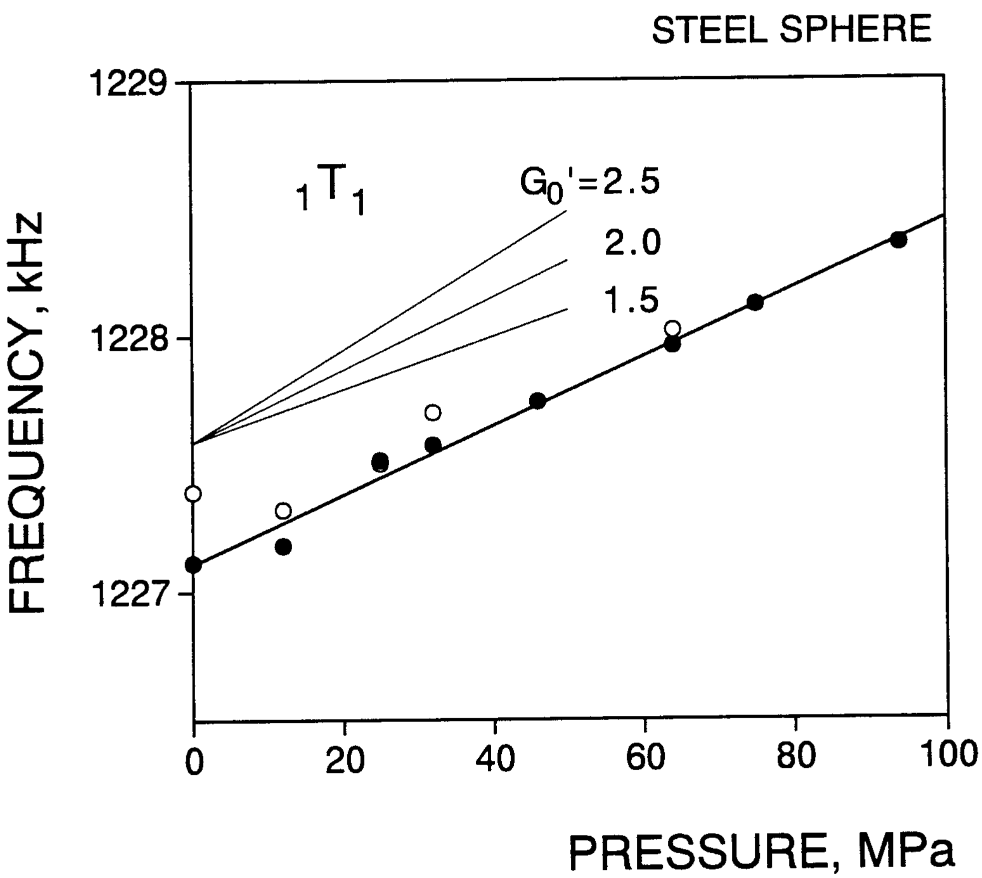

STEEL SPHERE
1229
1228
1227
$_1T_1$
$G_0'=2.5$
2.0
1.5
FREQUENCY, kHz
0
20
40
60
80
100
PRESSURE, MPa

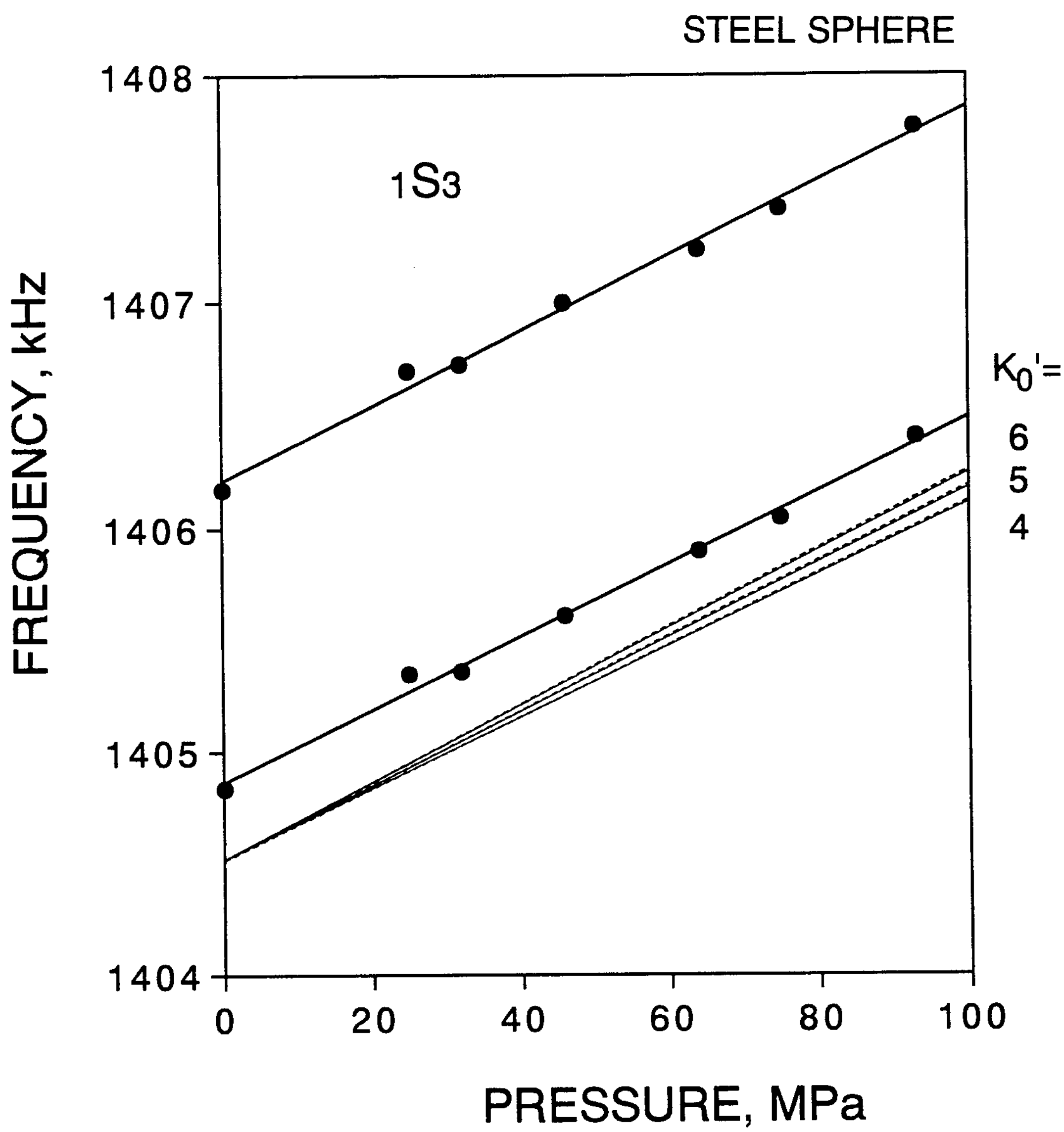
STEEL SPHERE
1408
1407
1406
1405
1404
$_1S_3$
FREQUENCY, kHz
K_0'=
6
5
4
0
20
40
60
80
100
PRESSURE, MPa

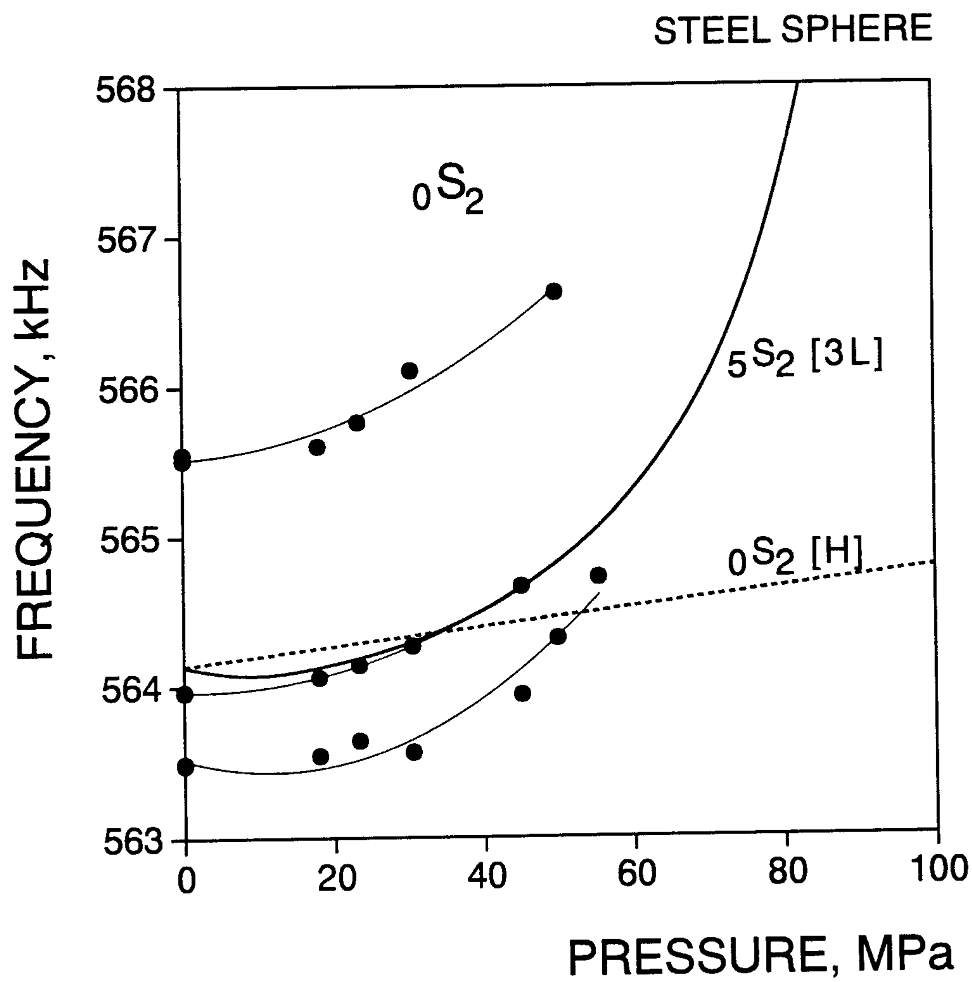

STEEL SPHERE
568
567
566
565
564
563
0
20
40
60
80
100
$_0S_2$
$_5S_2$ [3L]
$_0S_2$ [H]
FREQUENCY, kHz
PRESSURE, MPa

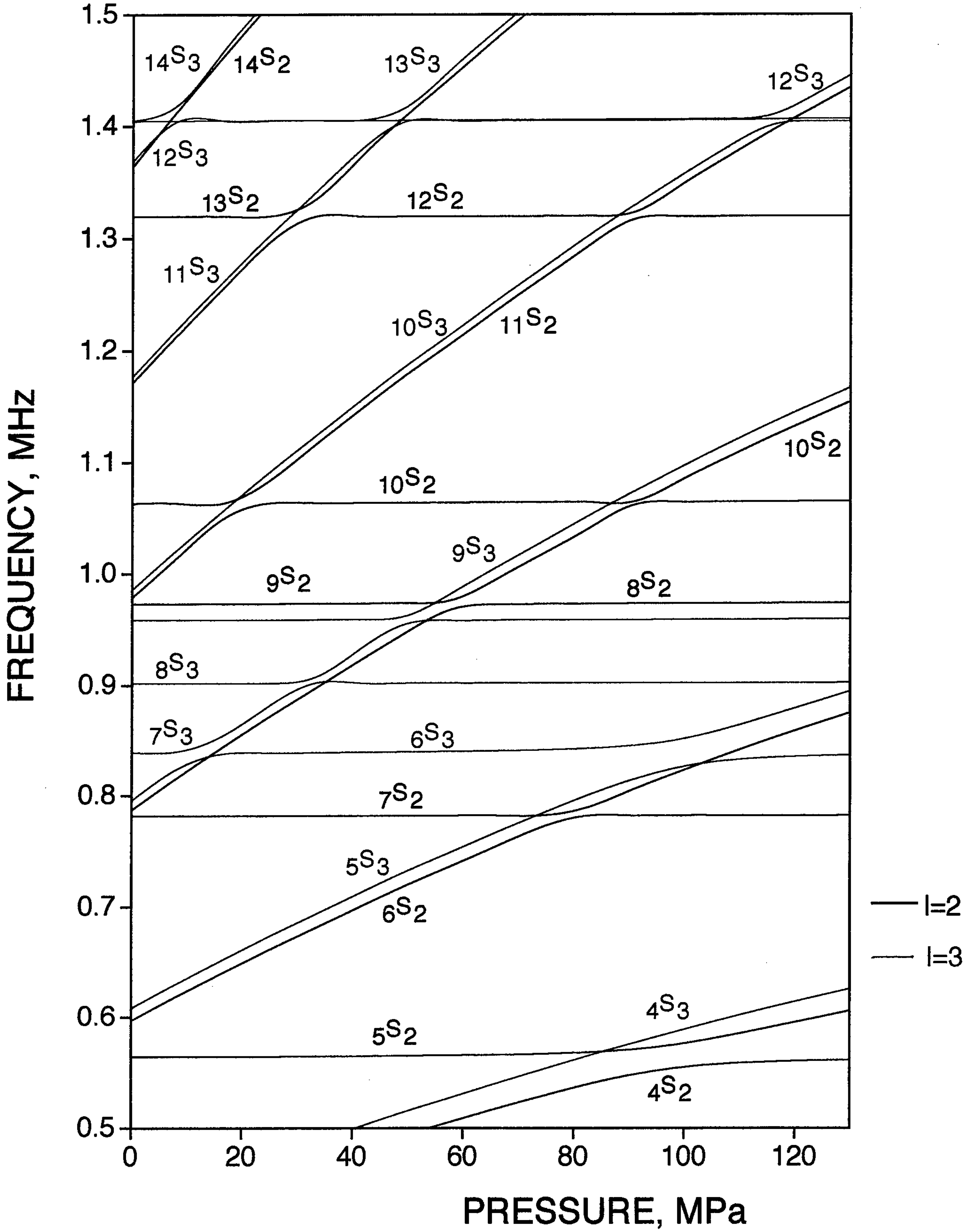

Theoretical eigenfrequencies of the three-layered spherical structure. Steel sphere is 4.245 mm and the cavity is 10 mm in diameter.

STEEL SPHERE

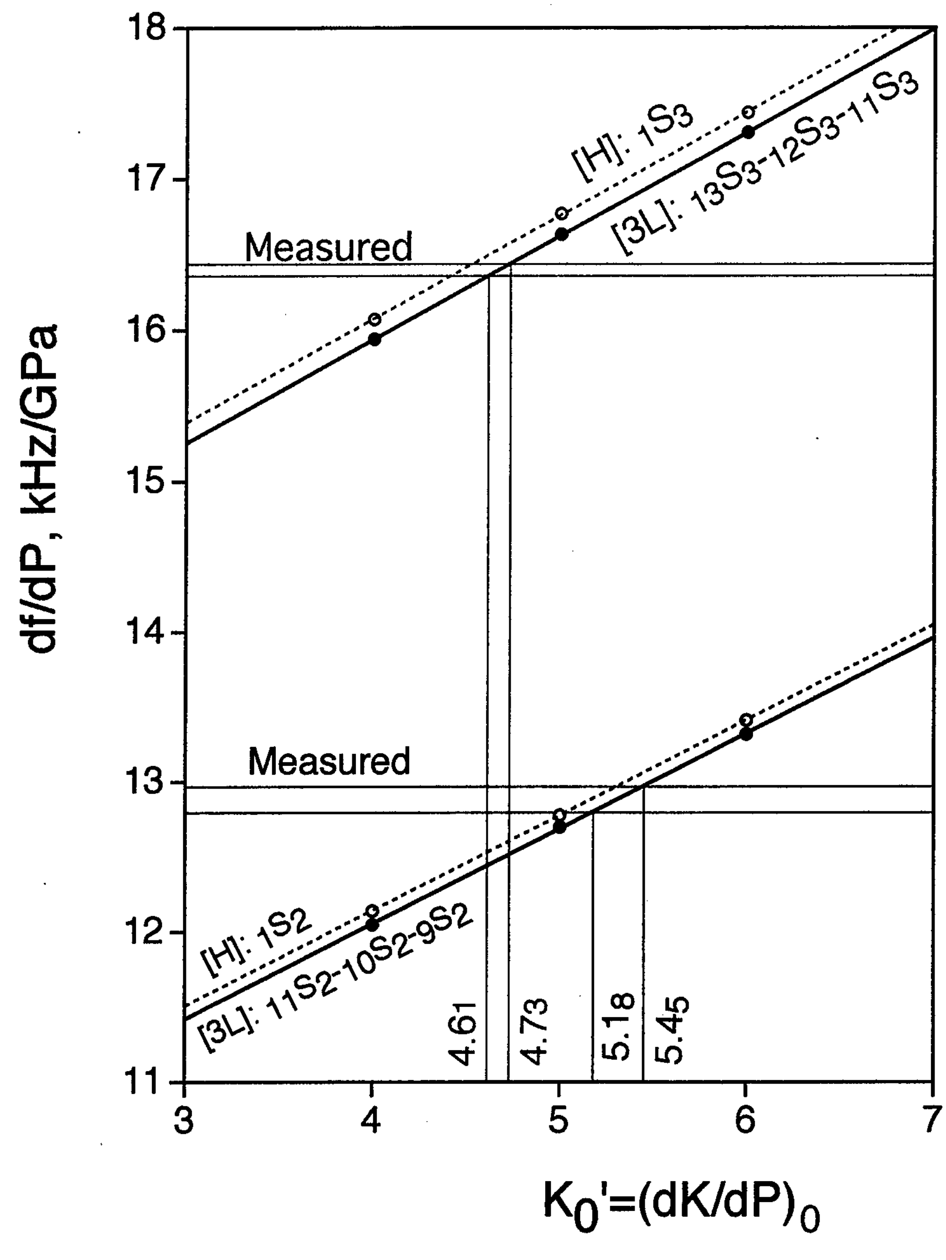

STEEL SPHERE

$\partial f/\partial P$ of torsional mode and G_0'

Mode	Frequency kHz	$\partial f/\partial P$ kHz/GPa	$G_0'=(\partial G/\partial P)_0$
${}_0T_4$	1087.0	13.4(7)	2.12
${}_1T_1$	1227.1	13.5(6)	1.91
${}_0T_5$	1335.9	15.1(9)	1.96
${}_0T_5$	1336.4	15.7(7)	2.03
${}_0T_5$	1337.0	15.8(6)	2.01
		Ave.	2.01(8)

$\partial f / \partial P$ of spheroidal mode and K_0'

Mode	Frequency	$\partial f / \partial P$	$K_0' = (\partial K / \partial P)_0$	
	kHz	kHz/GPa	[H]	[3L]
${}_1S_2$	1063.1	12.97(4)	5.28	5.45
${}_1S_2$	1064.1	12.79(5)	4.88	5.18
${}_1S_3$	2138.7	16.35(6)	4.39	4.61
${}_1S_3$	2214.1	16.43(7)	4.49	4.73
		Ave.	4.76	4.99

[H] : Analyzed as homogeneous sphere of sample only

[3L] : Analyzed as three-layered spherical structure

5. Result on Silica Glass Sphere

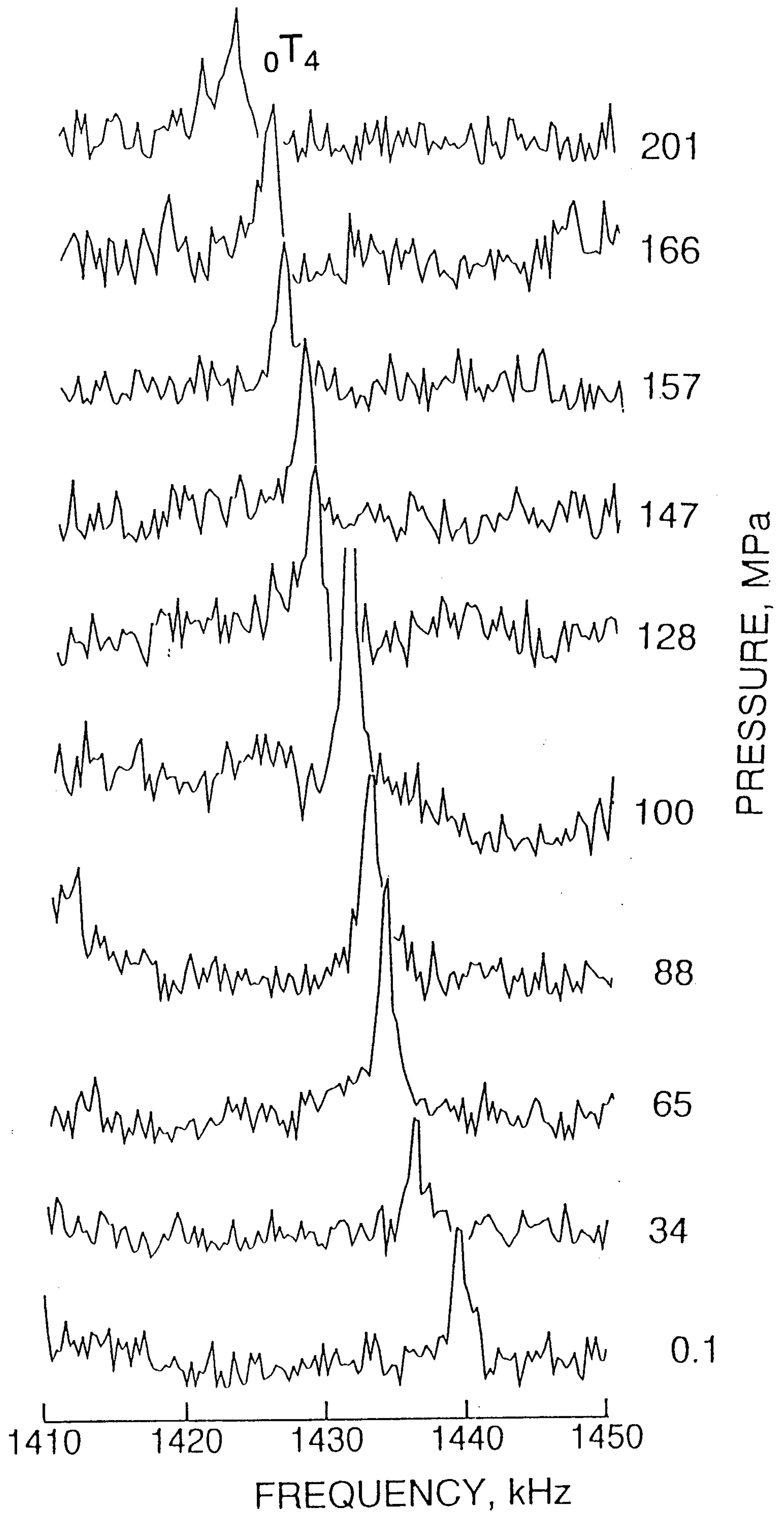

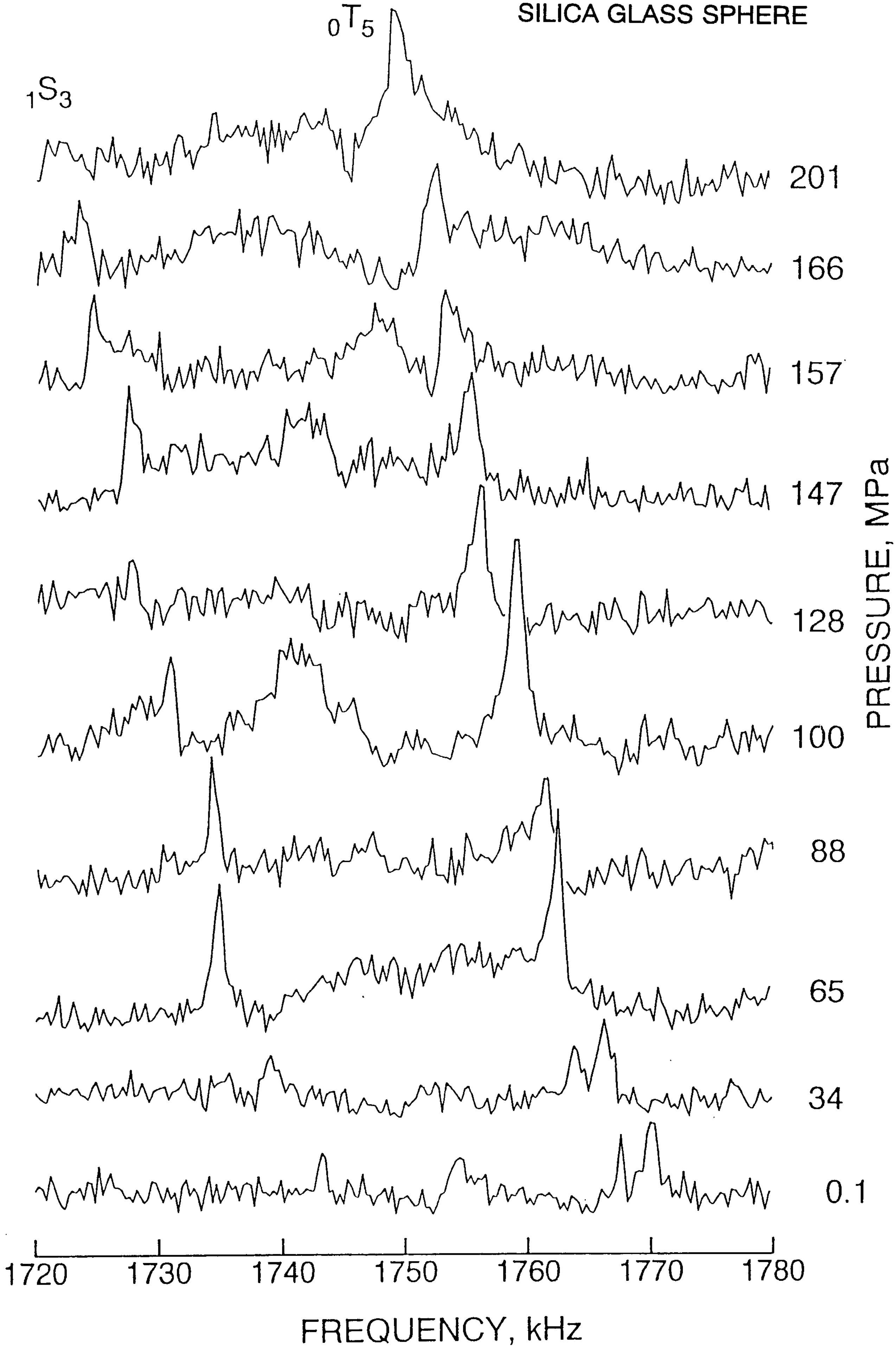

SILICA GLASS SPHERE
$_0T_5$
$_1S_3$
201
166
157
147
128
100
88
65
34
0.1
PRESSURE, MPa
1720
1730
1740
1750
1760
1770
1780
FREQUENCY, kHz

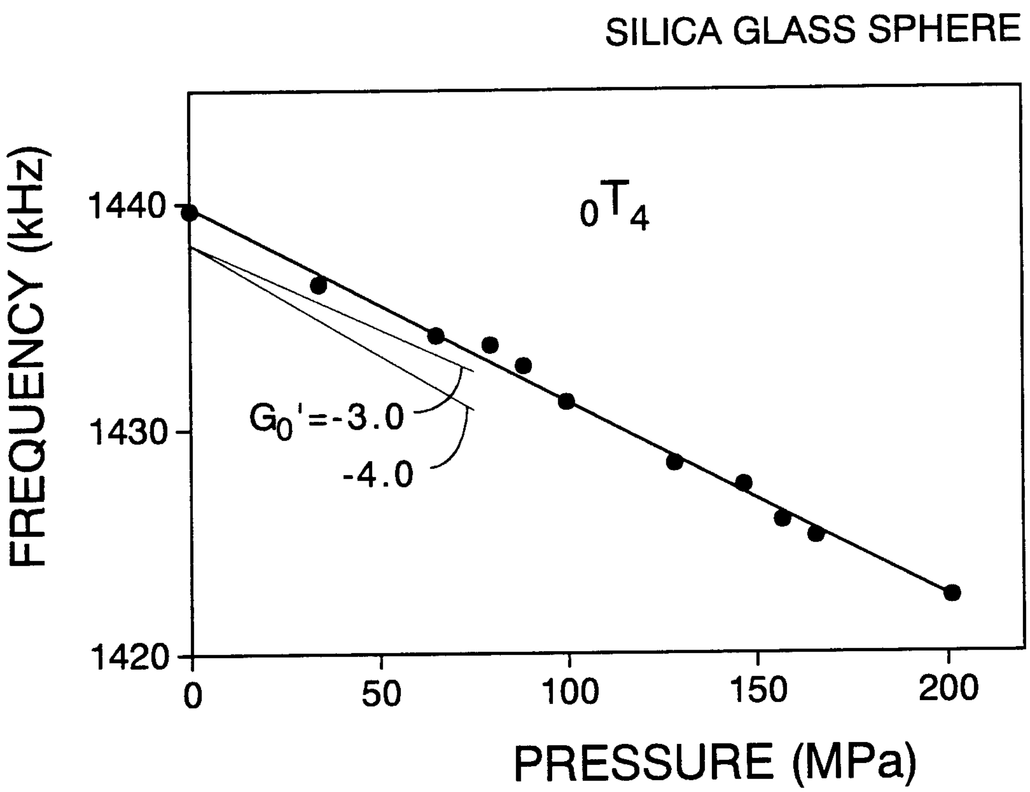

SILICA GLASS SPHERE
$_0T_4$
1440
1430
1420
G_0'=-3.0
-4.0
0
50
100
150
200
FREQUENCY (kHz)
PRESSURE (MPa)

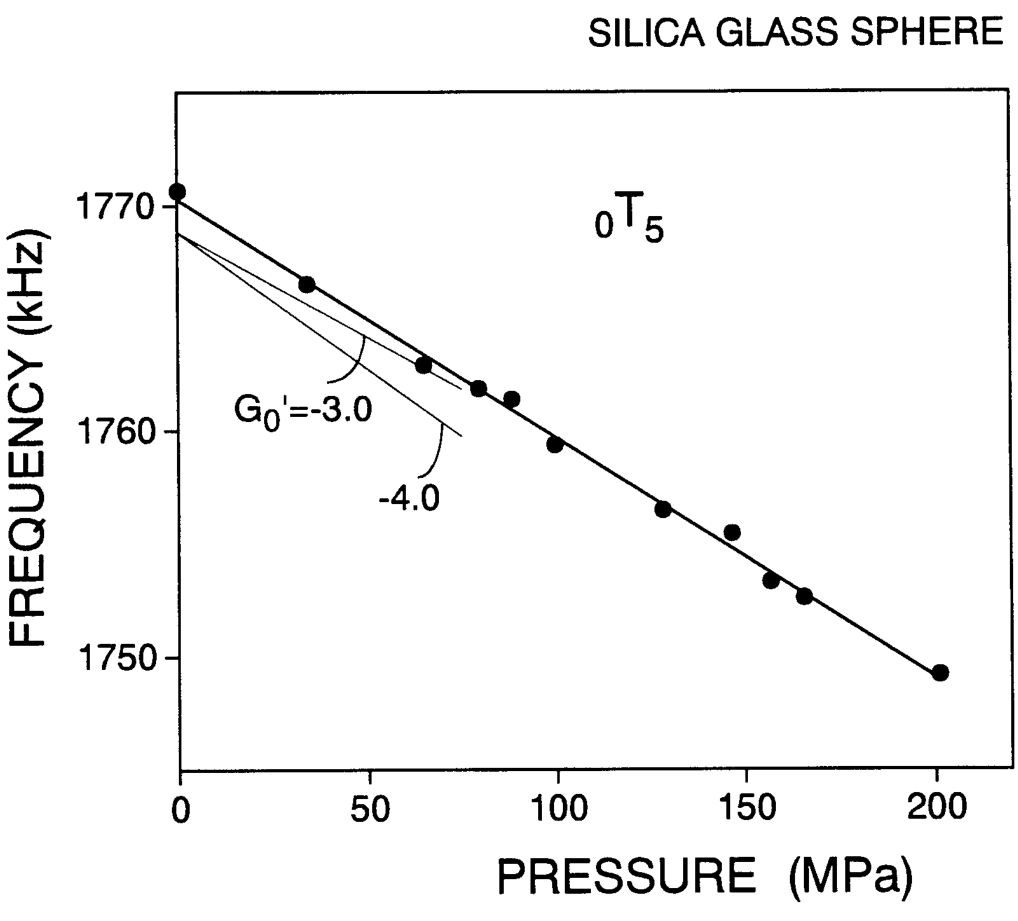
SILICA GLASS SPHERE
$_0T_5$
G_0'=-3.0
-4.0
1770
1760
1750
FREQUENCY (kHz)
0
50
100
150
200
PRESSURE (MPa)

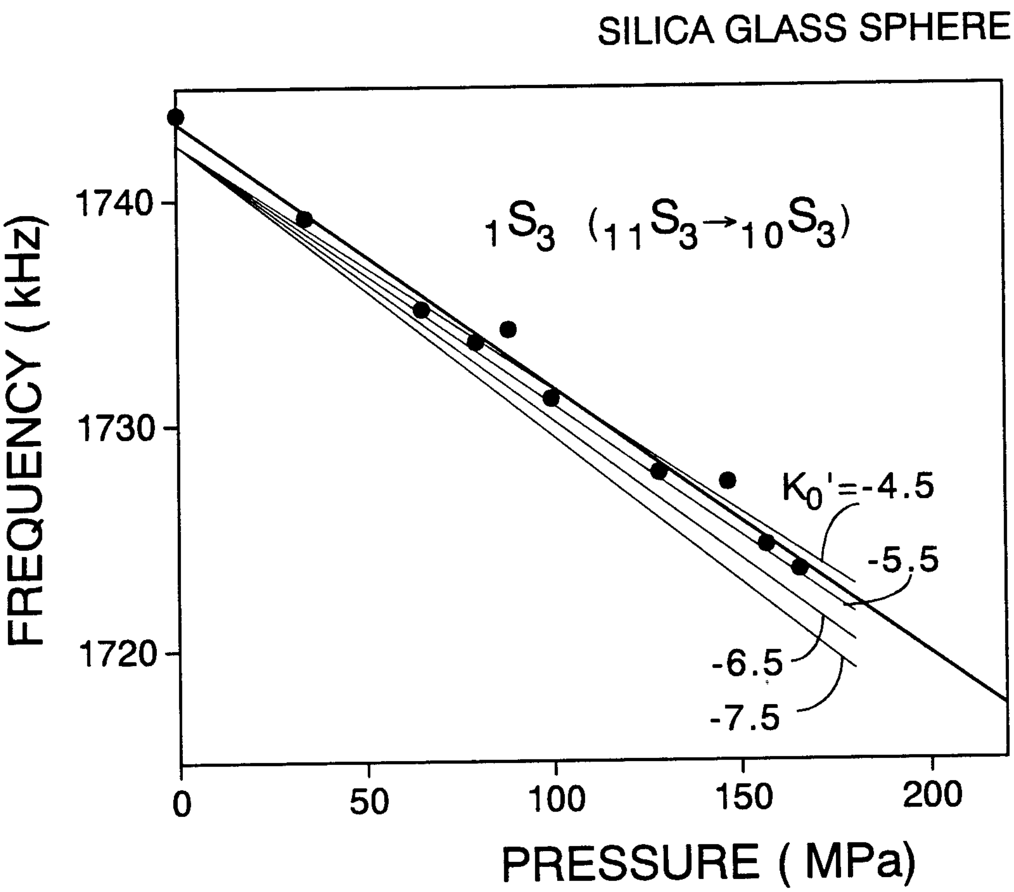
SILICA GLASS SPHERE
$_1S_3$ ($_{11}S_3 \rightarrow {}_{10}S_3$)
K_0'=-4.5
-5.5
-6.5
-7.5
1740
1730
1720
FREQUENCY (kHz)
0
50
100
150
200
PRESSURE (MPa)

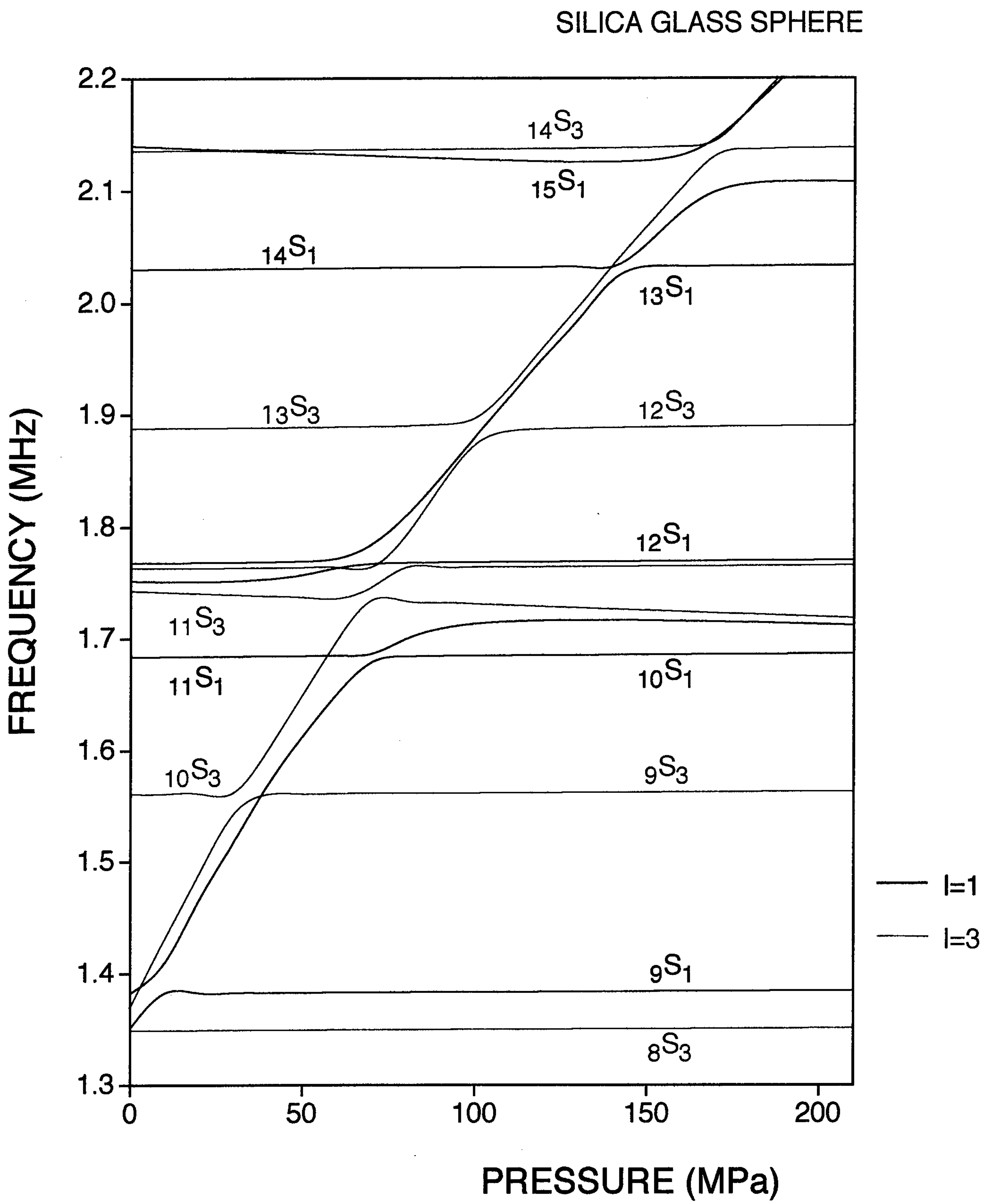

Theoretical eigenfrequencies of the three-layered spherical structure. Silica glass sphere is 4.764 mm and the cavity is 5 mm in diameter.

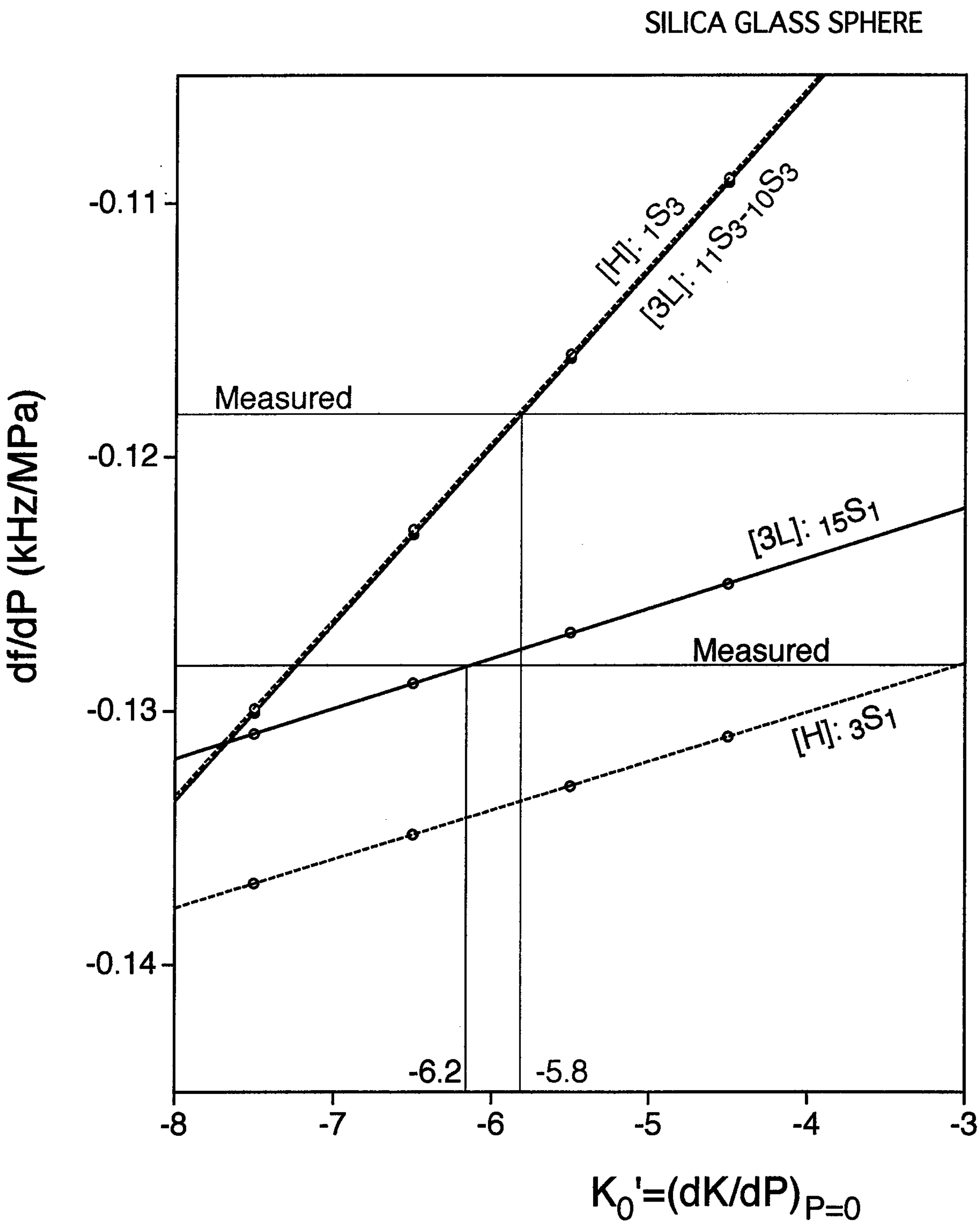

SILICA GLASS SPHERE
df/dP (kHz/MPa)
-0.11
-0.12
-0.13
-0.14
[H]: $_1S_3$
[3L]: $_{11}S_3$-$_{10}S_3$
Measured
[3L]: $_{15}S_1$
Measured
[H]: $_3S_1$
-6.2
-5.8
-8
-7
-6
-5
-4
-3
$K_0'=(dK/dP)_{P=0}$

$\partial f / \partial P$ of torsional mode and G_0'

Mode	Frequency kHz	$\partial f / \partial P$ kHz/GPa	$G_0' = (\partial G / \partial P)_0$
${}_0T_2$	709.9	-49(1)	-4.04
${}_0T_3$	1093.9	-69(2)	-3.67
${}_0T_4$	1439.7	-86(2)	-3.46
${}_1T_1$	1626.2	-94(2)	-3.61
${}_0T_5$	1770.6	-106(2)	-3.47
${}_0T_6$	2091.5	-119(4)	-3.28
${}_1T_3$	2382.3	-132(5)	-3.19
${}_0T_7$	2407.0	-141(4)	-3.39
		Ave.	-3.51

$\partial f / \partial P$ of spheroidal mode and K_0'

Mode	Frequency	$\partial f / \partial P$	$K_0' = (\partial K / \partial P)_0$	
	kHz	kHz/GPa	[H]	[3L]
$_1S_3$	1742.8	-118(4)	-5.8_5	-5.8_2
$_3S_1$	2138.7	-128(6)	-3.1	-6.2
		Ave.		-6.0

[H] : Analyzed as homogeneous sphere of sample only

[3L] : Analyzed as three-layered spherical structure

Silica Glass

G_0'	K_0'	Press. Range GPa	Reference
-3.25	-6.15	0.1	Peselnick et al. (1967)
-3.48	-6.31	1.8	Gerlich & Kennedy (1978)
-3.4	-6.0	0.1	Meister et al. (1980)
-2.71	-3.21	3.8	Suito et al. (1994)
-3.32		0.015	Isaak et al. (1998)
-3.5	-6.0	0.2	This Study

NONLINEAR MESOSCOPIC ELASTICITY

R. A. GUYER and P. A. JOHNSON
UMASS — LANL
KRM, K vdA, JT
TJS, ES, GB, LBL, ...

... sand | soil | ~~rock~~ | concrete | ceramic | ...

1. Is a generalization possible?
2. Rock as prototype
3. focus on "signatures" of unusual elastic behavior

I. DEEP BACKGROUND; quasi-static + dynamic

II SIGNATURES
1. NL - H - DM
2. $\Delta f \propto |\epsilon|$
3. log (t); slow dynamics

III A BEGINNING

I. DEEP BACKGROUND:

TEXTBOOK:

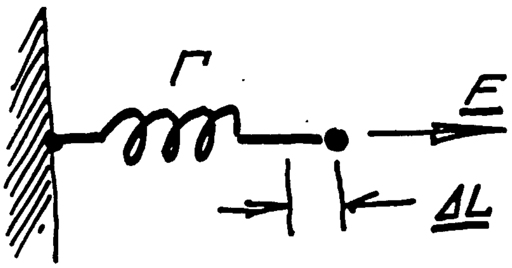

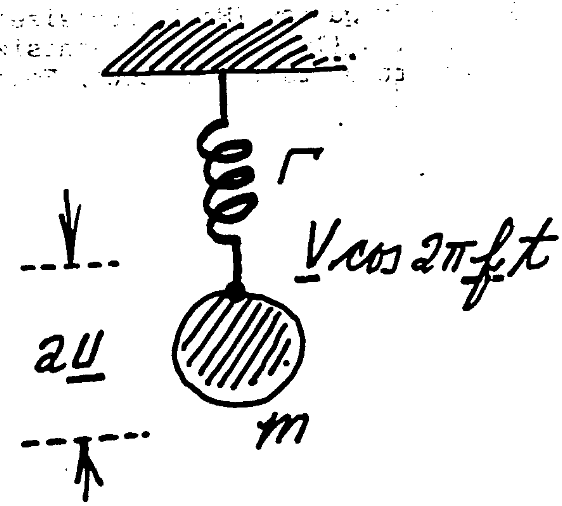

QUASI-STATIC MEASUREMENT

DYNAMIC MEASUREMENT

vary F, measure ΔL

fix V, vary f, measure U

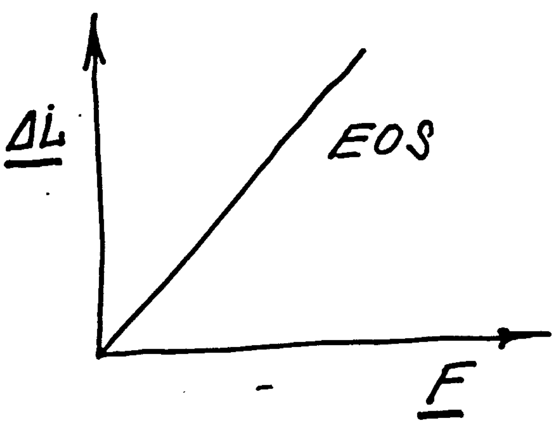

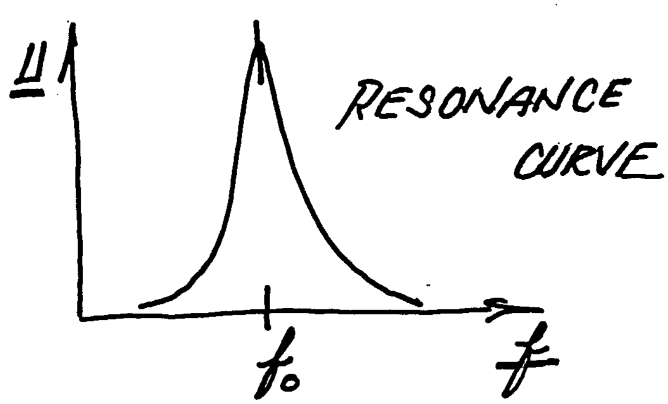

$$\boxed{\Delta L = \frac{1}{\Gamma} F}$$

$$\boxed{2\pi f_0 = \sqrt{\frac{\Gamma}{m}}}$$

REAL LIFE

1.

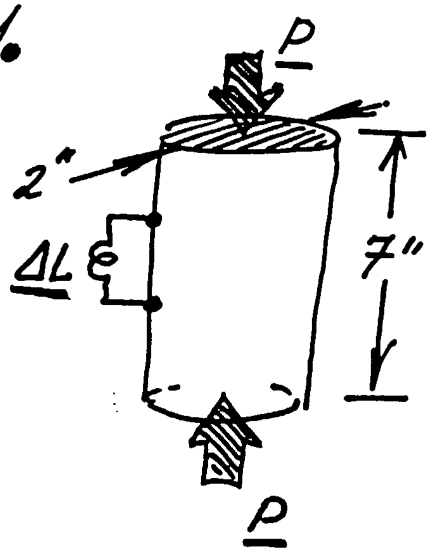

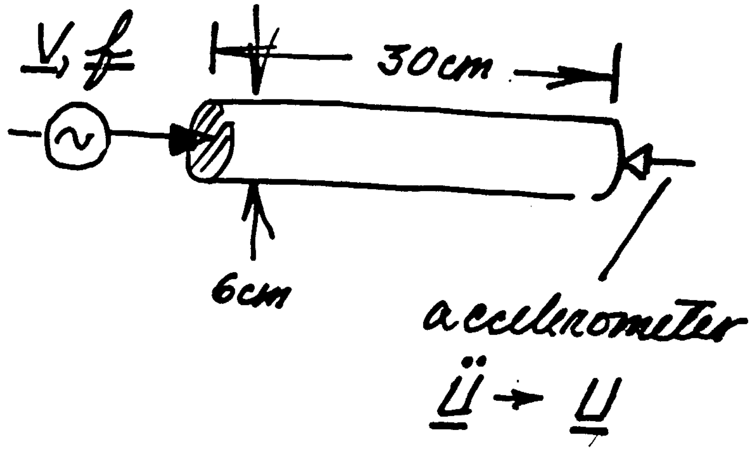

2.

3.

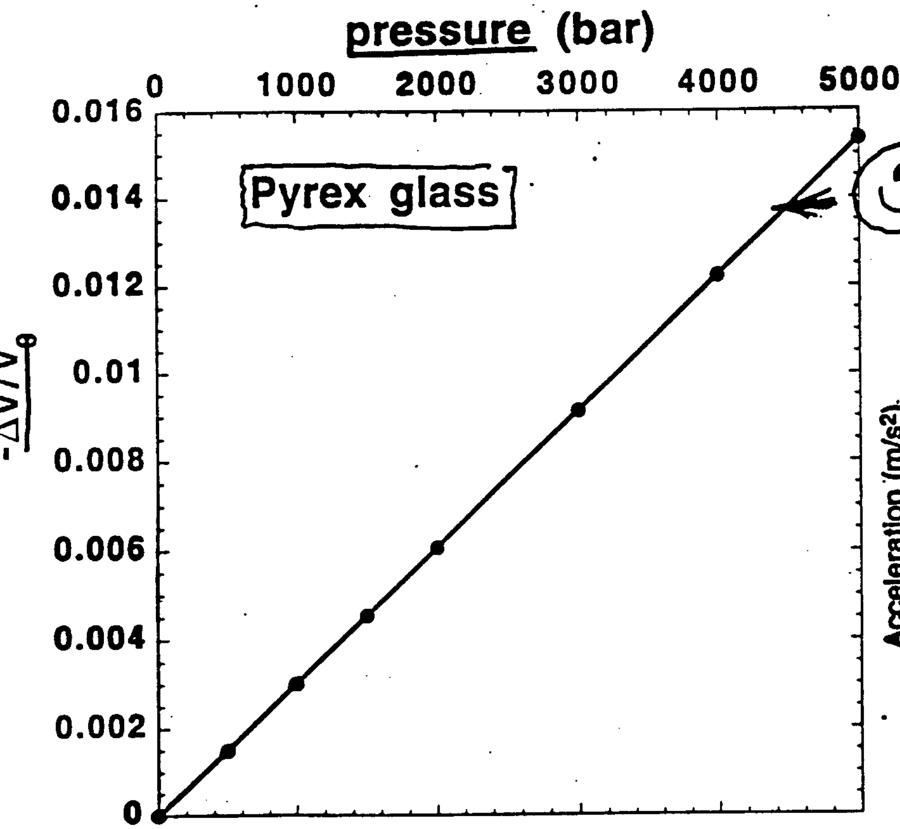
pressure (bar)
Pyrex glass
$-\Delta V/V_0$
0.016
0.014
0.012
0.01
0.008
0.006
0.004
0.002
0
0
1000
2000
3000
4000
5000

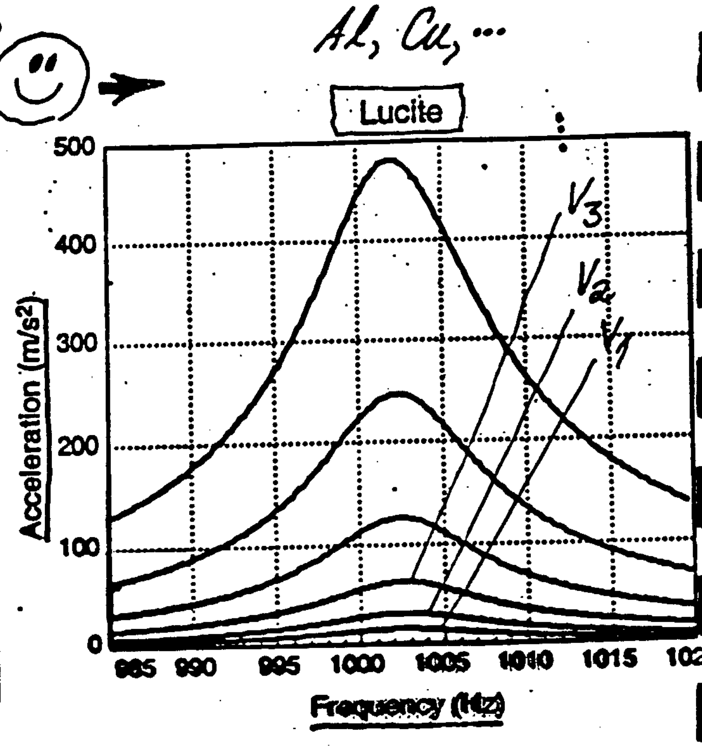
Al, Cu, ...
Lucite
Acceleration (m/s²)
Frequency (Hz)
V_3
V_2
V_1
500
400
300
200
100
0
985
990
995
1000
1005
1010
1015
102

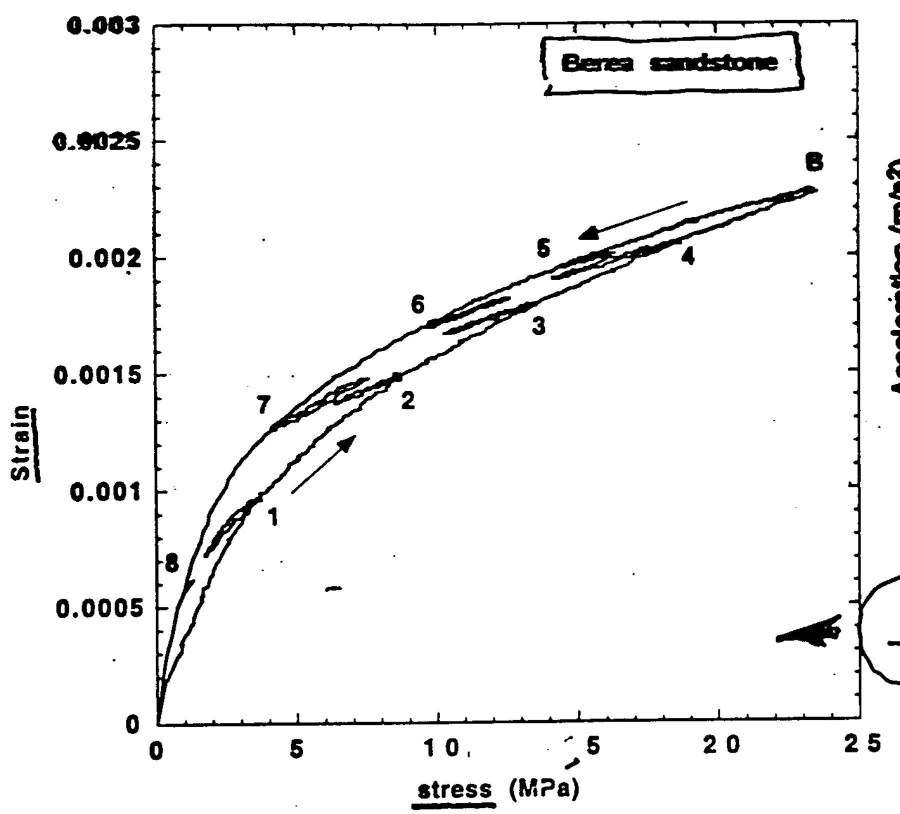
Berea sandstone
Strain
stress (MPa)
0.003
0.0025
0.002
0.0015
0.001
0.0005
0
0
5
10
15
20
25
1
2
3
4
5
6
7
8
B

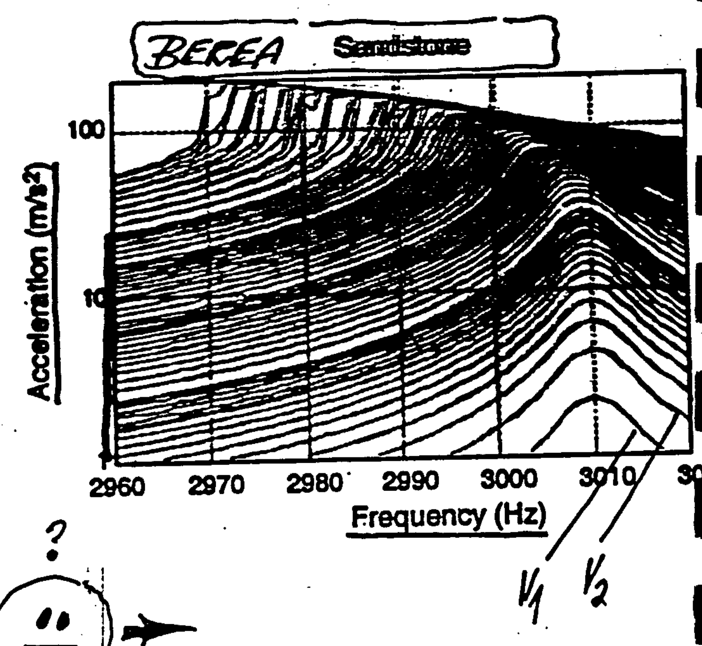
BEREA Sandstone
Acceleration (m/s²)
Frequency (Hz)
100
10
2960
2970
2980
2990
3000
3010
V_1
V_2
?

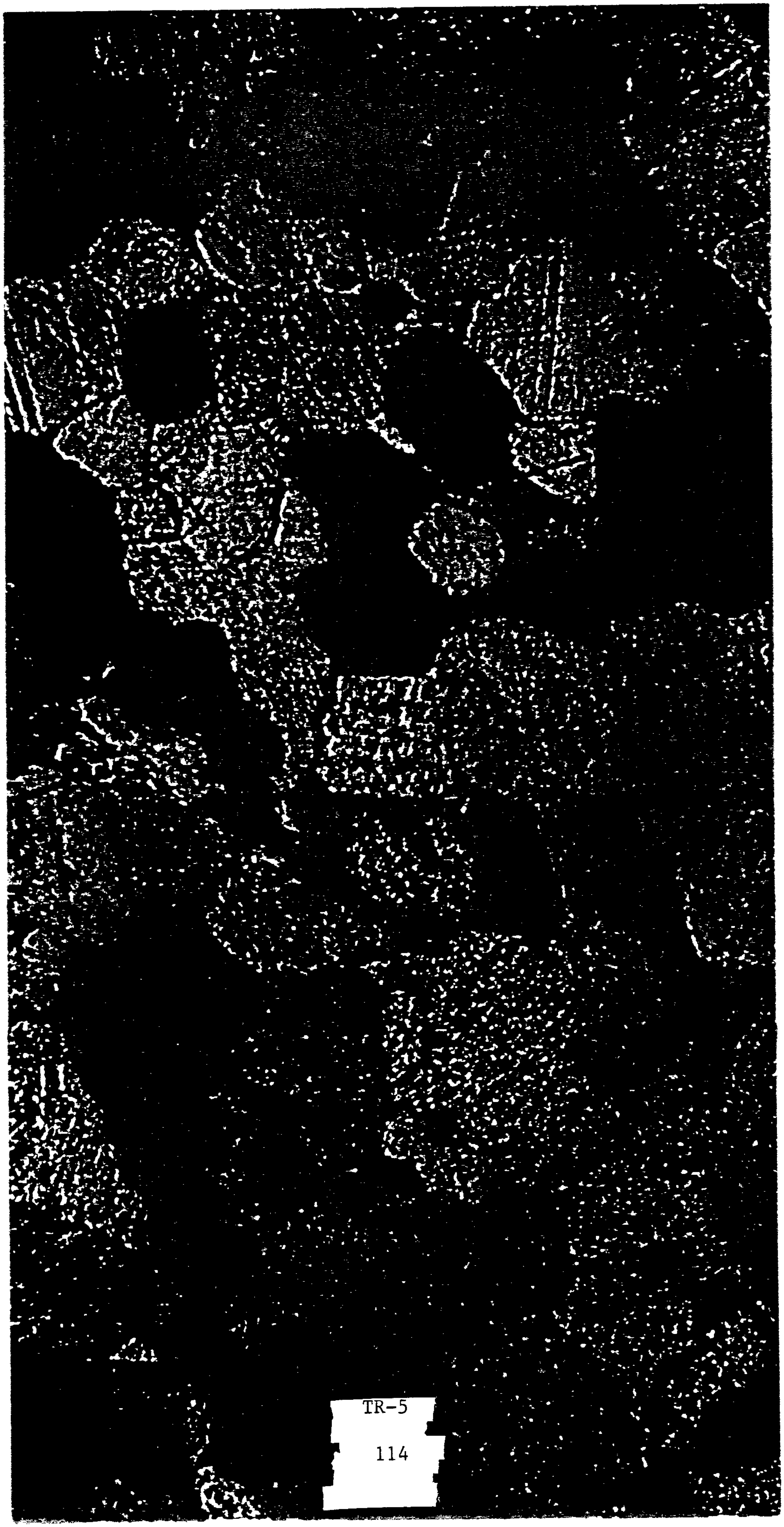

TR-5

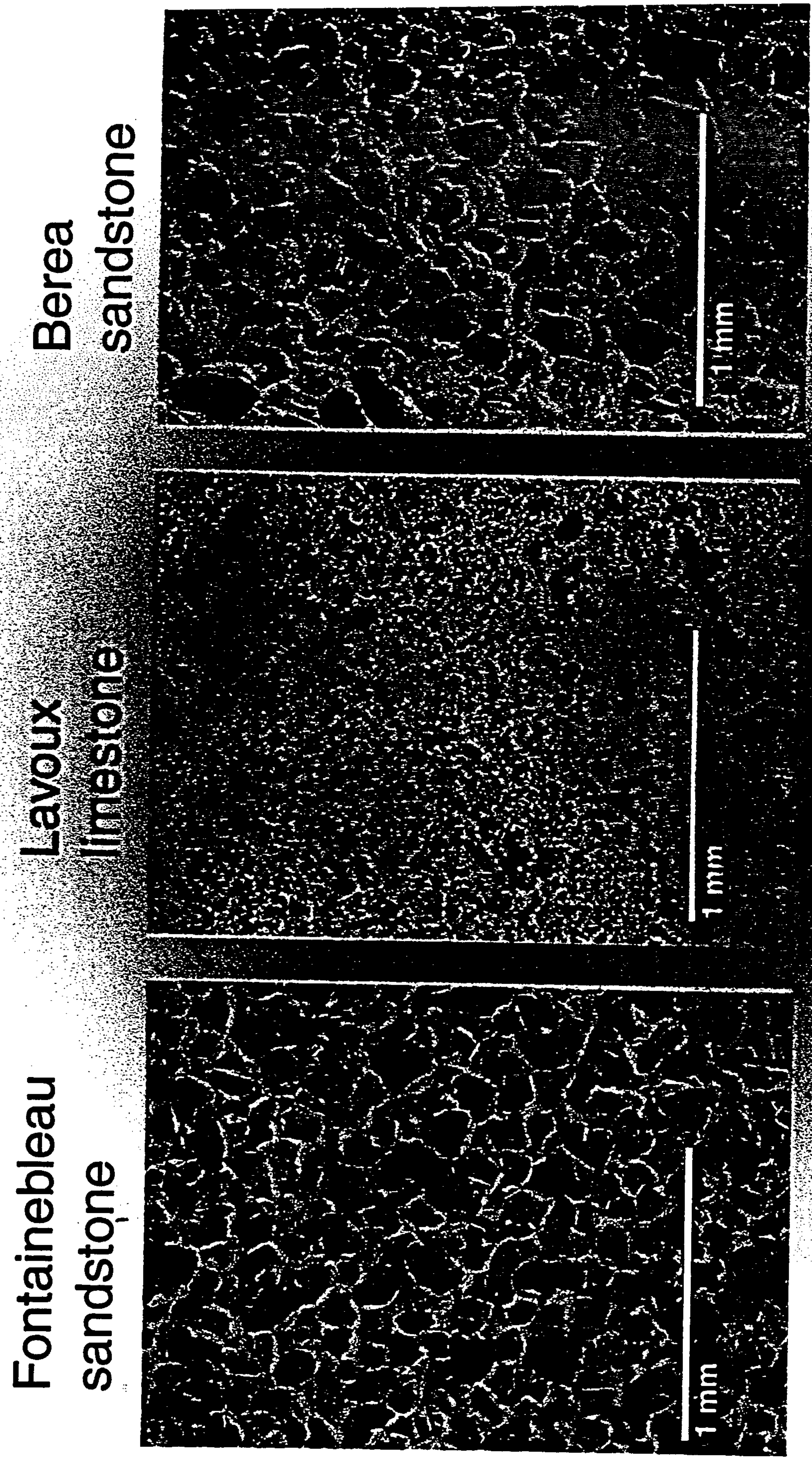
Berea sandstone
1 mm
Lavoux limestone
1 mm
Fontainebleau sandstone
1 mm

AN ABSTRACTION:

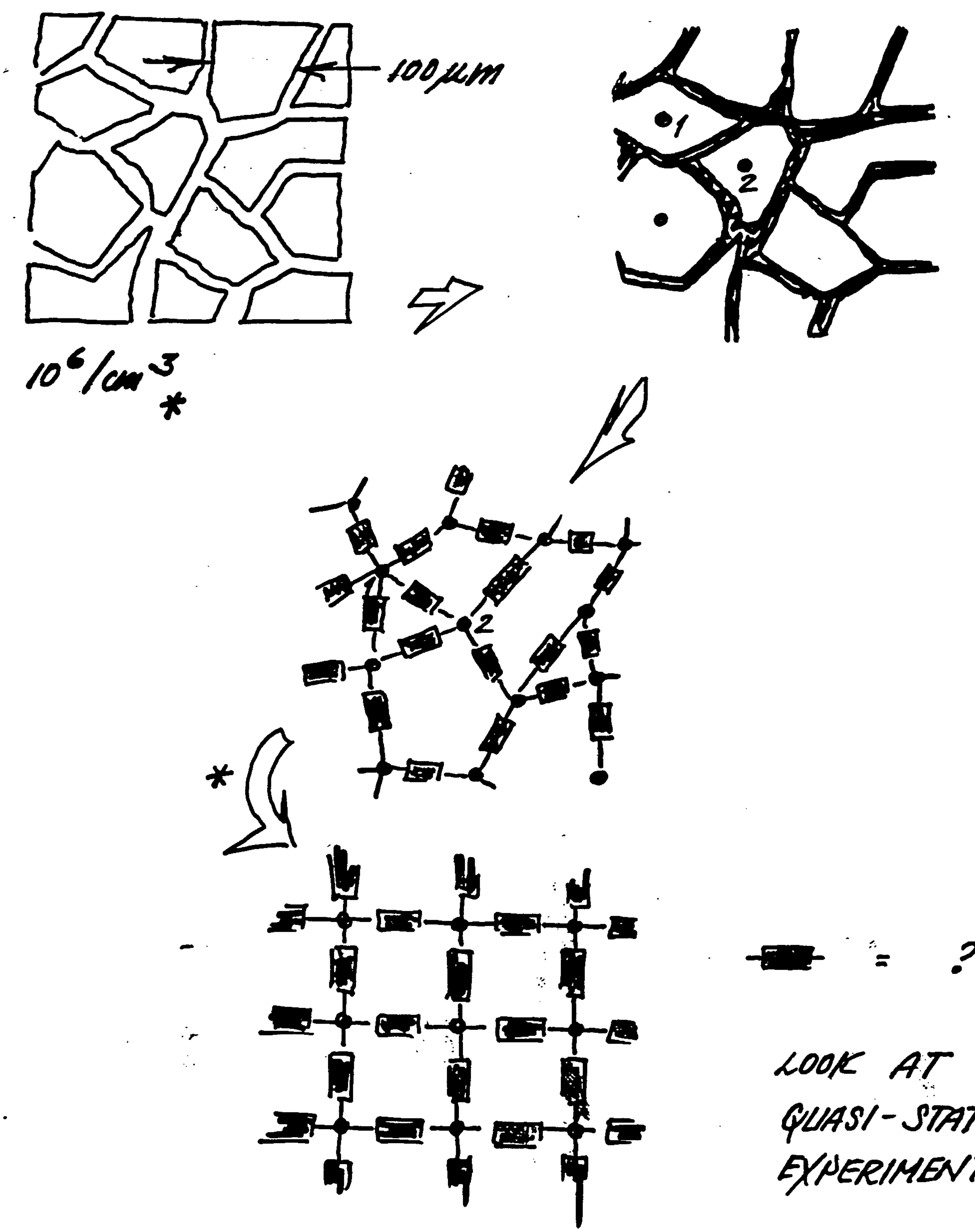

LOOK AT
QUASI-STATIC
EXPERIMENTS

1. NON - LINEAR (VERY)

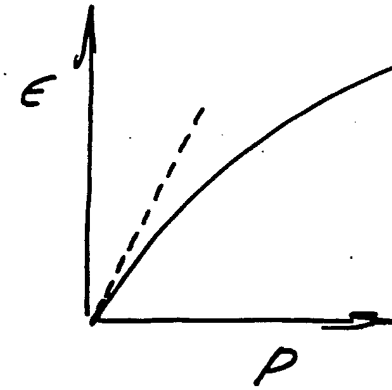

2. HYSTERETIC

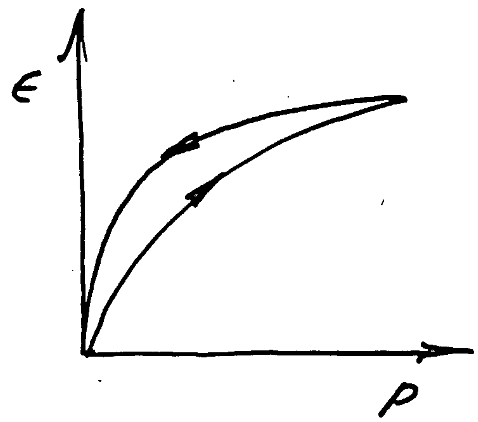

3. DISCRETE MEMORY

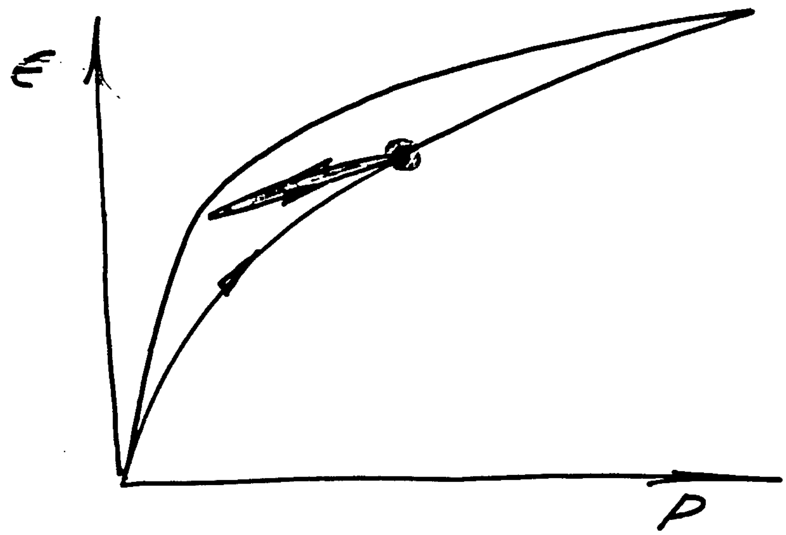

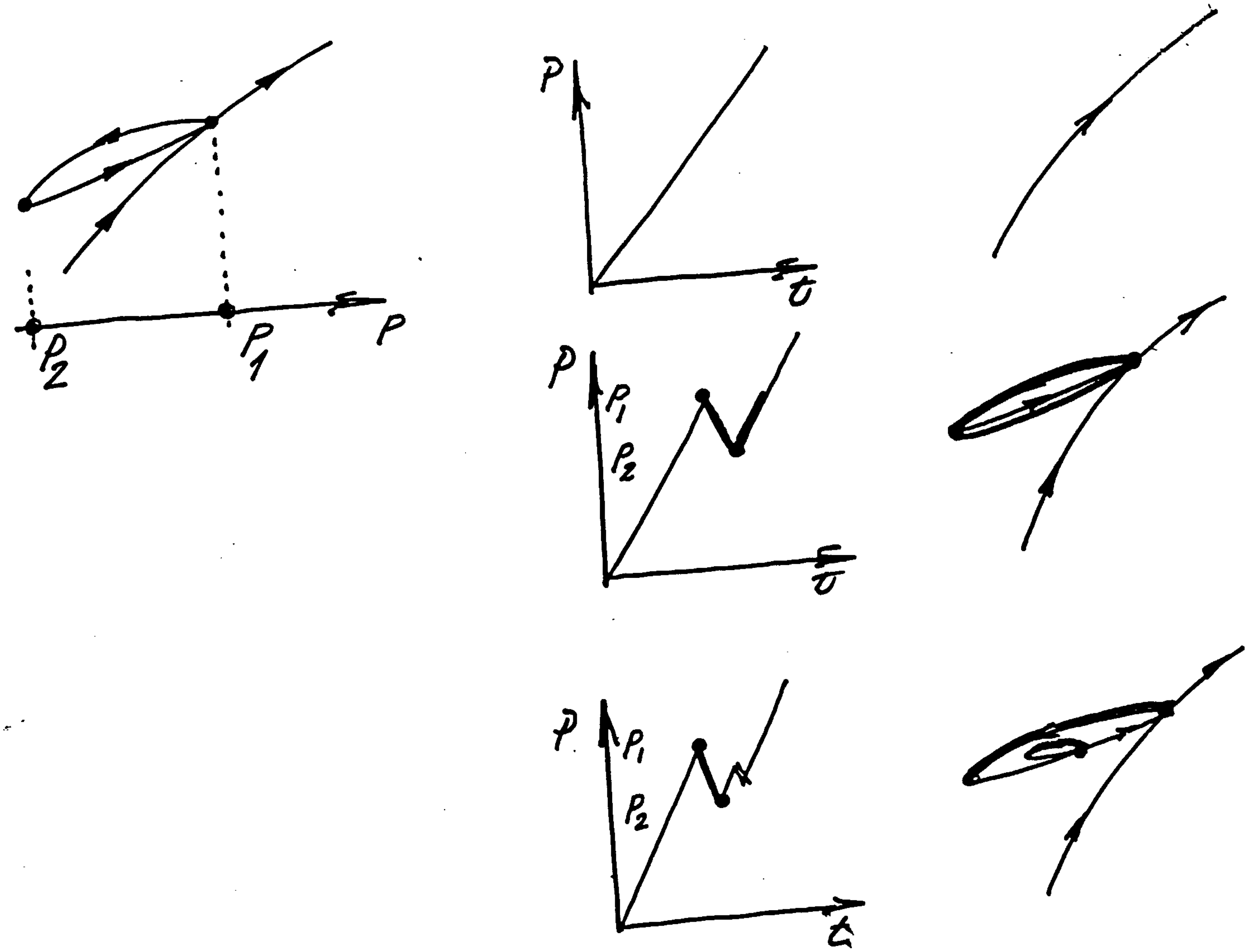

discrete memory, D
[end point memory]

SUMMARY I.:

1. THE ELASTICITY OF ROCKS EXHIBIT <u>NL</u>, <u>H</u>, <u>DM</u> IN QUASI-STATIC MEASUREMENTS

2. A PHENOMENOLOGY TO EXPLAIN THIS HAS BEEN DEVELOPED [GUYER and M^cCALL].

   P-M SPACE MODEL, "<u>AN ASSEMBLAGE OF HYSTERETIC ELASTIC BONDS</u>"

   — [redacted] —

   *BOITNOTT

3. THIS PHENOMENOLOGY PREDICTS BEHAVIOR FOR <u>NON-LINEAR RESONANCE</u> THAT HAS BEEN CONFIRMED IN EXPERIMENT.

   *TENCATE

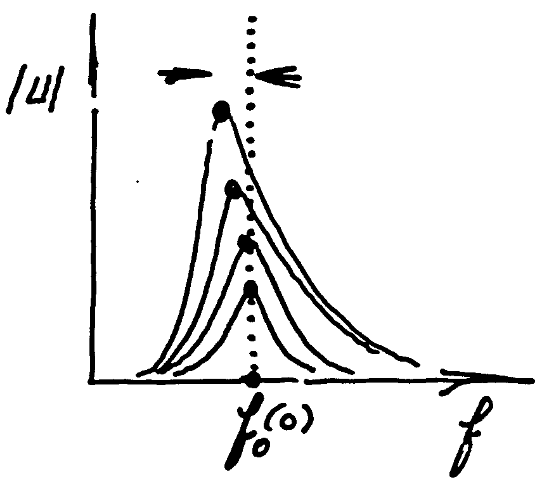

$$\boxed{f_0(0) - f_0(u) = c_F\,\underline{|u|}}$$

GM^{c}CB

!

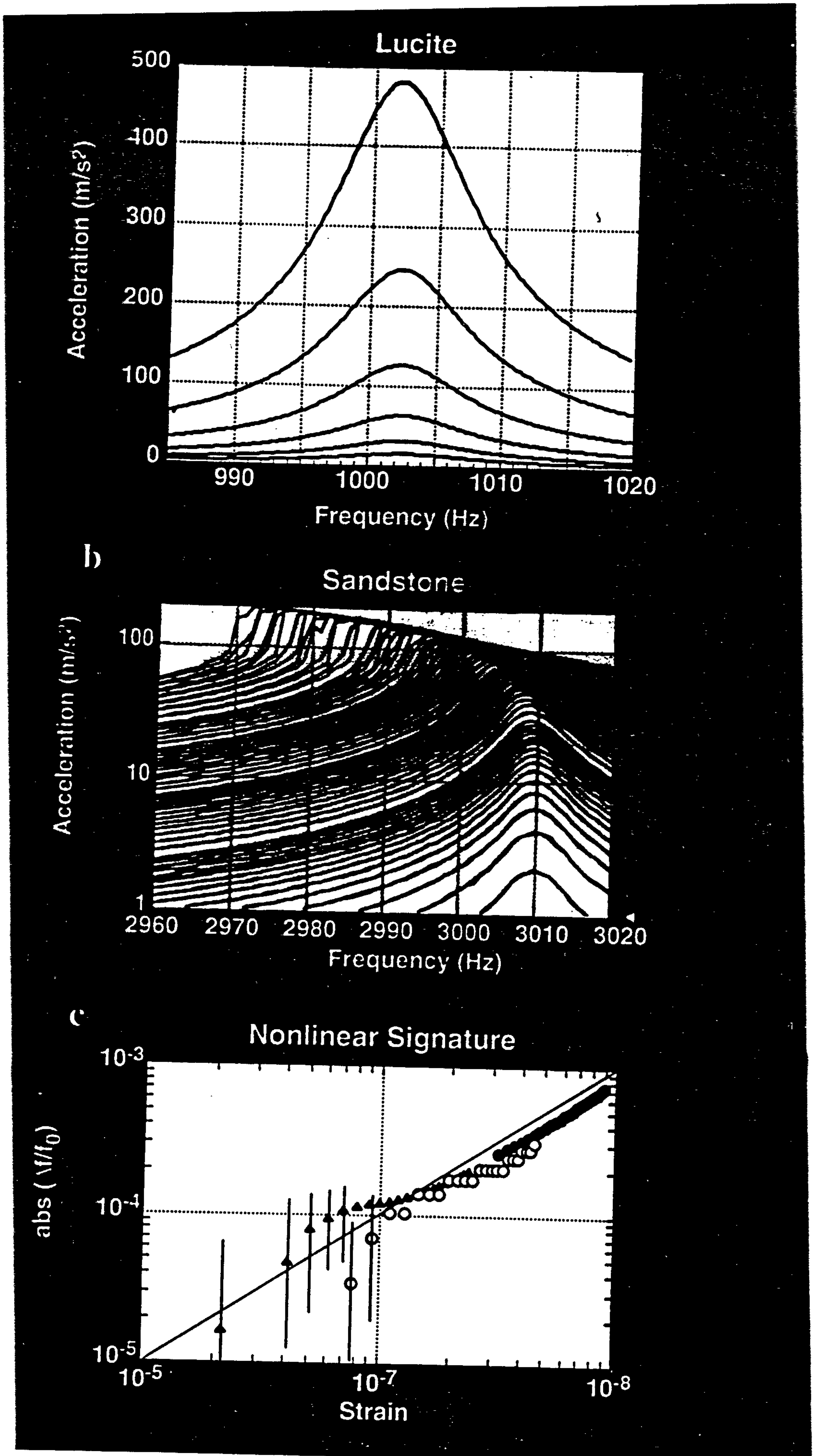

Lucite
Acceleration (m/s²)
500
400
300
200
100
0
990
1000
1010
1020
Frequency (Hz)
b
Sandstone
100
10
1
2960
2970
2980
2990
3000
3010
3020
Frequency (Hz)
c
Nonlinear Signature
abs (Δf/f0)
10-3
10-4
10-5
10-5
10-7
10-8
Strain

4. SLOW DYNAMICS

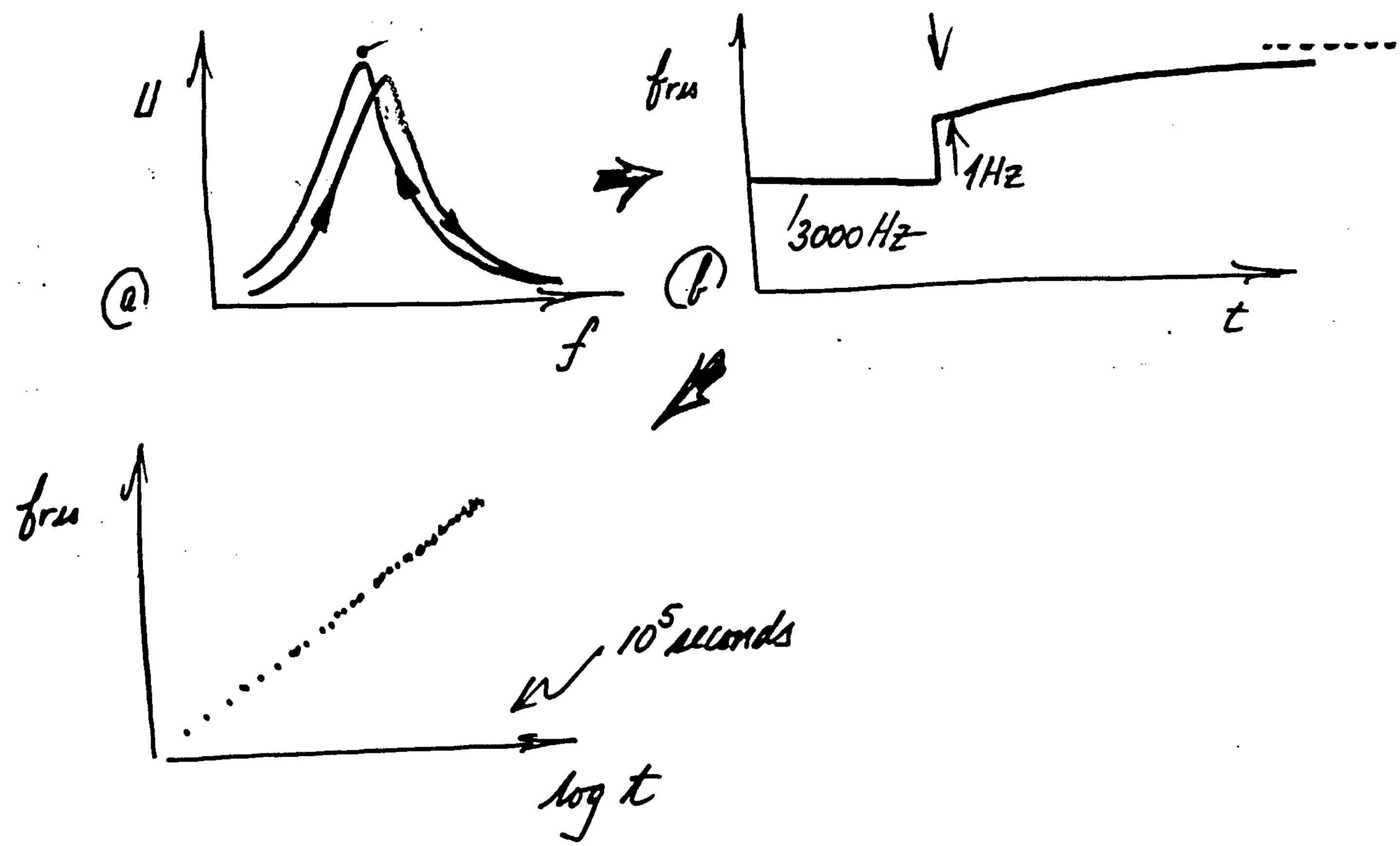

5. SIGNATURES

<u>NLHDM</u>

↕ PM

$\boxed{\Delta f \propto |\epsilon|}$

↕

ln(t)

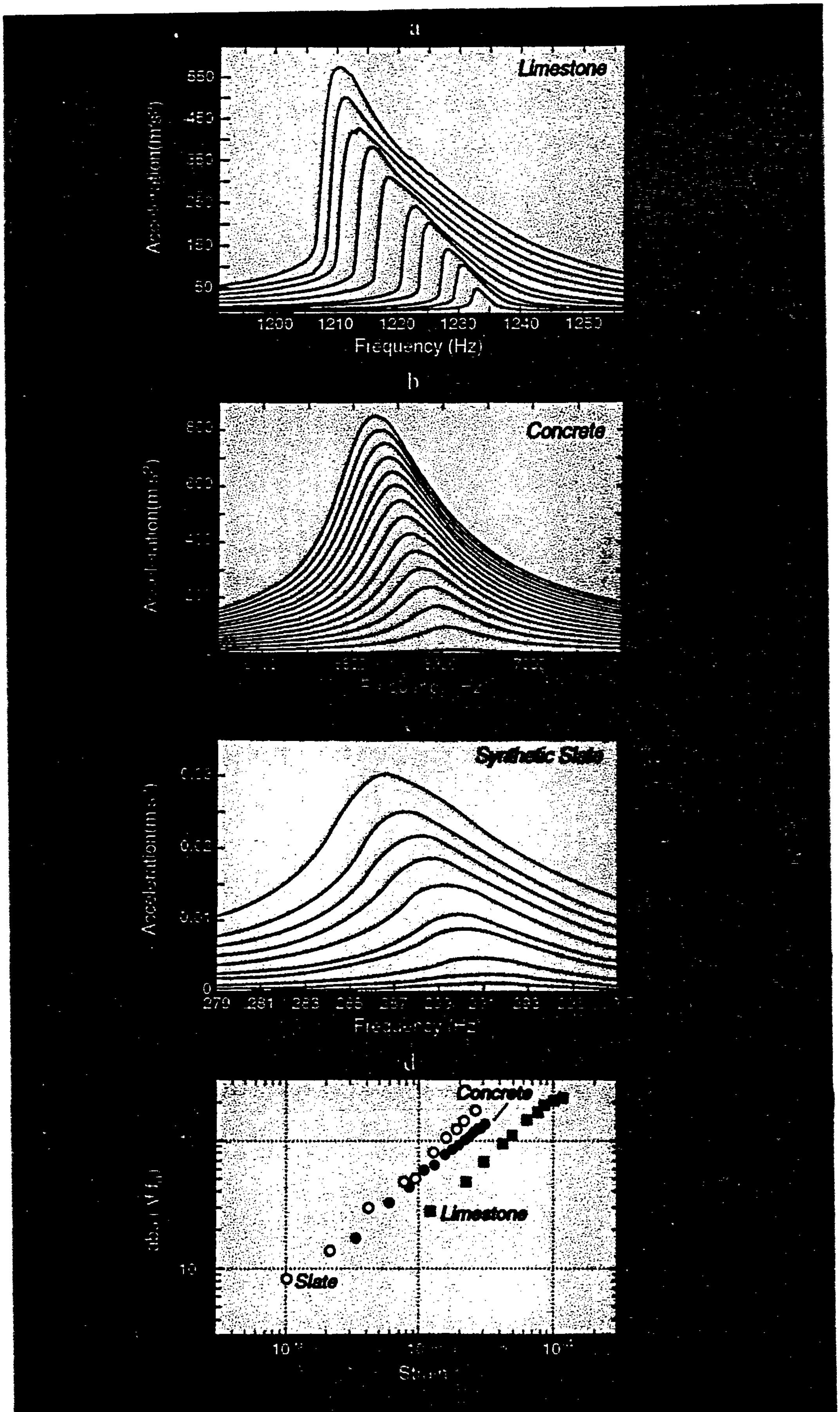
a
Limestone
550
450
350
250
150
50
1200
1210
1220
1230
1240
1250
Frequency (Hz)
b
Concrete
c
Synthetic Slate
0.03
0.02
0.01
0
279
281
283
285
287
289
291
293
Frequency (Hz)
d
Concrete
Limestone
Slate
10

WHO ELSE DOES IT?

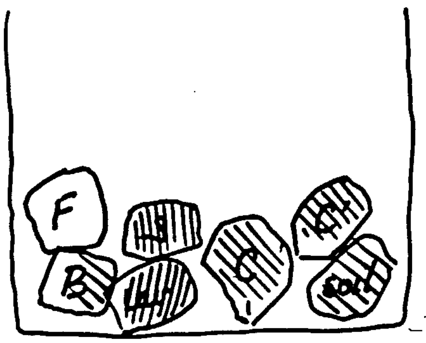

soil, VEUCETIC, ...

slate, Lavoux, Fontainebleau, concrete,

$\Delta f \propto |\epsilon|$

Berea, Lavoux, Fontainebleau, concrete, concrete' '99

$\log(t)$

AN ELASTICITY UNIVERSALITY CLASS?

At a level where the details are blurred there is common behavior. The description of this behavior for one should work for all.

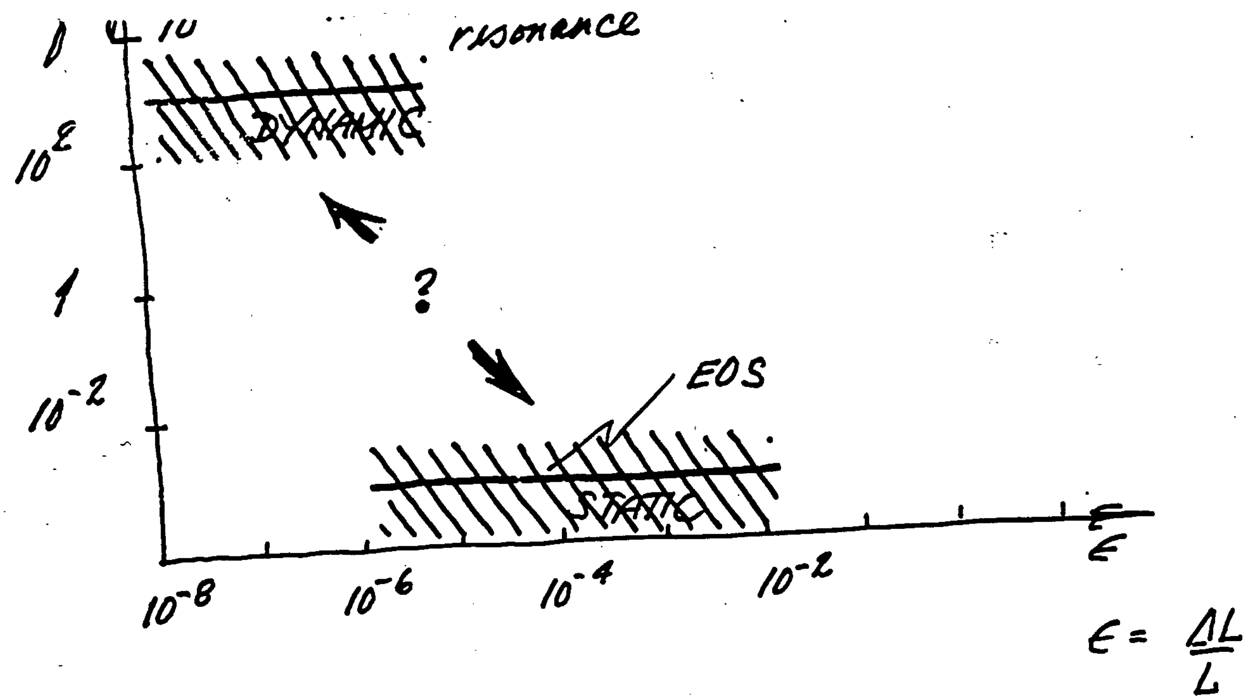

BROADER CONTEXT:

(a) kinds of materials

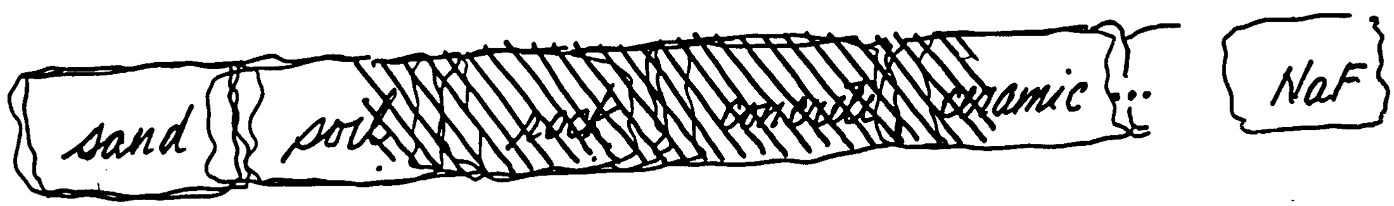

(b) strong motion

verification

NDE

logging

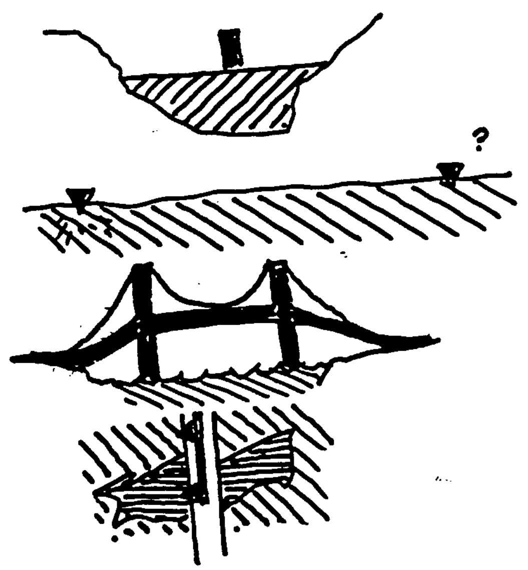

RUS and Rocks

K R McCall
TJ Ulrich

University of Nevada, Reno

TR-1

Outline

I. History

II. Experimental Details

III. Numerical Modeling

IV. Experimental Results

V. Future Work

I. History

A. Empirical Evidence: Macroscopically inhomogeneous materials are elastically nonlinear (R A Guyer, previous talk)

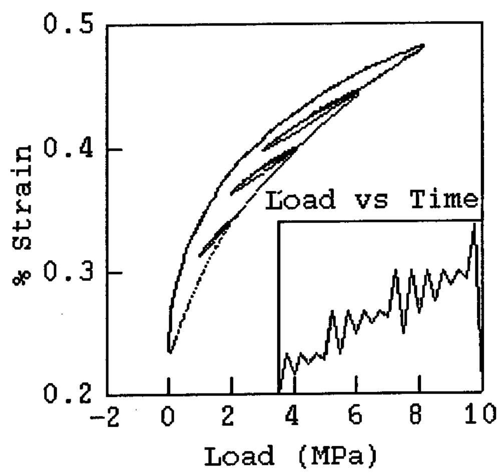

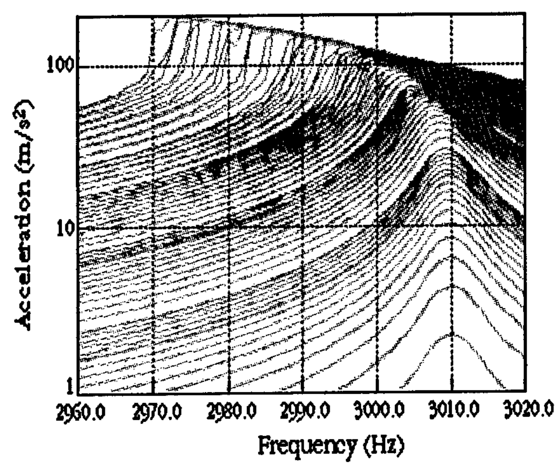

B. Theoretical Models: The elastic modulus is nonlinear and hysteretic.

$$\sigma = K\varepsilon$$

$$\boxed{K = K_o[1+\beta\varepsilon+\delta\varepsilon^2+\alpha(|\Delta\varepsilon|\pm\varepsilon)\ldots]}$$

TR-3

C. Hypothesis: Reliable measurements of linear moduli are the basis for quantitative study of nonlinear moduli.

1. Rock Mechanics

$$K = \frac{\sigma}{\varepsilon}$$

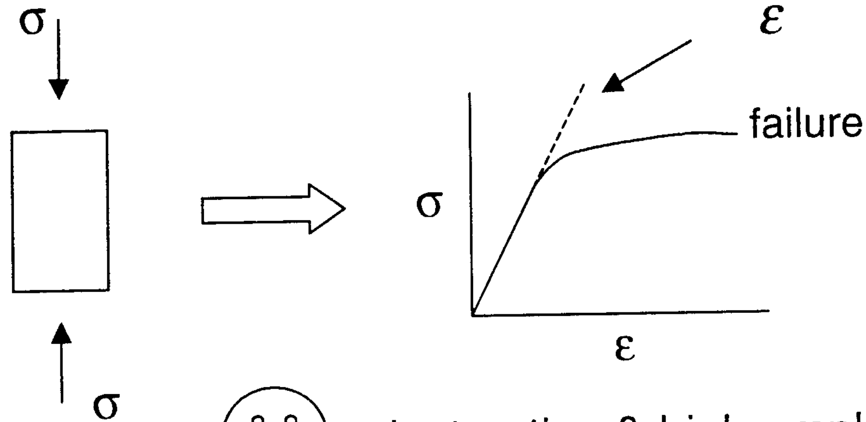

destructive & high amplitude

2. Time of flight

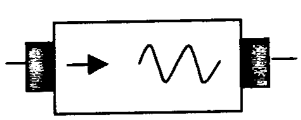

$c = \frac{\Delta l}{\Delta t} \rightarrow K = c^2 \rho$

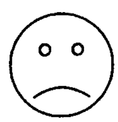

path dependent (vs. average K)

3. Resonant Ultrasound Spectroscopy

?

II. Experimental Details

A. RUS System by Dynamic Resonance Systems, Inc.

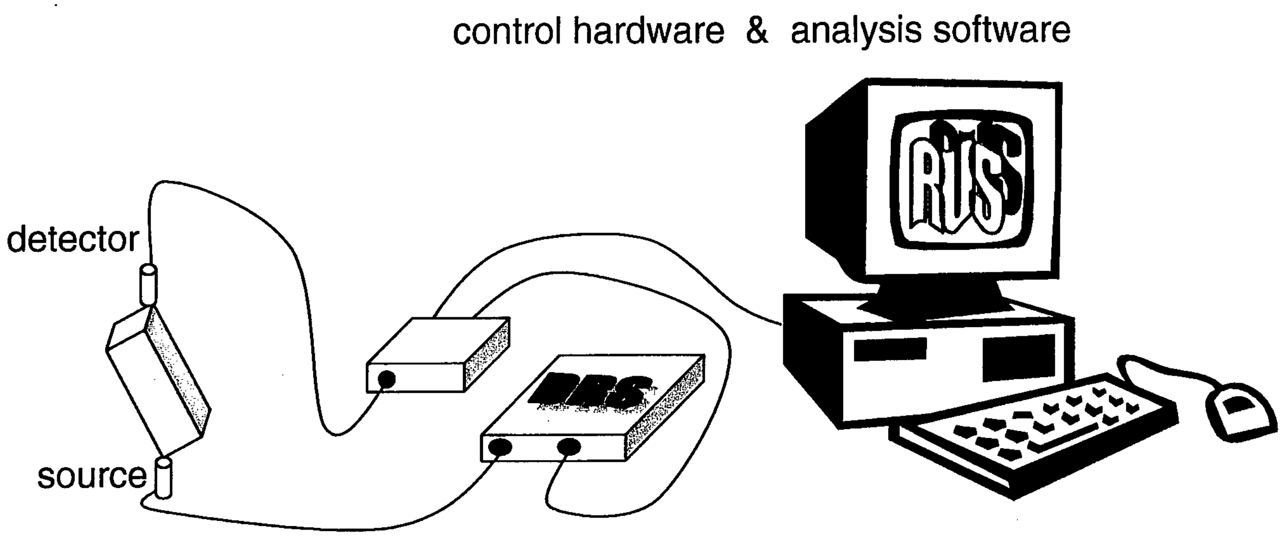

B. Analysis Software Assumptions

1. Free boundaries on sample
2. Homogeneous sample
3. Parallelepiped sample

C. Conditions for Optimal Results

4. Distinct resonance peaks
5. C_{11} dependence in low modes

TR-5

III. Numerical Modeling

(to explore the implications of the experimental conditions)

A. <u>Free boundaries on sample</u>

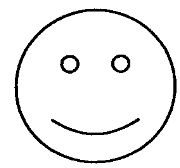

B. <u>Homogeneous sample</u>: Scale of inhomogeneity (ξ) should be smaller than wavelength of resonance (λ).

Example: 1-d system

$$\lambda = \frac{2L}{n} > \xi$$

For 10 resonances, $n = 10$

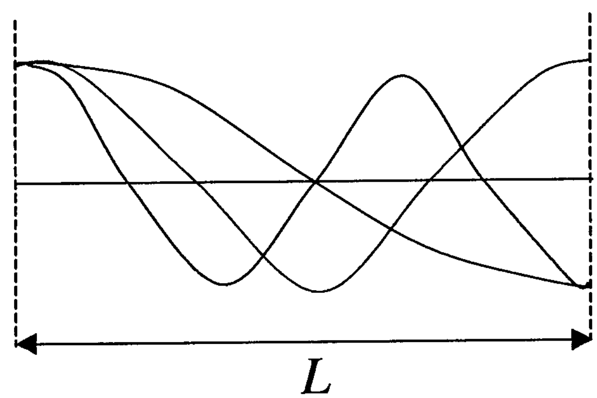

$$\boxed{L > 5\xi}$$

limiting sample size

C. <u>Parallelepiped samples</u>: Rock samples are cut on a diamond saw with limited accuracy, high probability of chips, nonparallel sides.

<u>*Perturbation Theory*</u>: 1st order evaluation of induced error (R A Guyer)

$$\boxed{\frac{\omega^2 - \omega_n^2}{\omega_n^2} = \langle u_n | \Delta\rho | u_n \rangle}$$

u_n = eigenmode

$\Delta\rho$ = density change

	mass imperfection		amount	frequency change
1	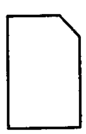	nick at corner	1%	0.15%
2	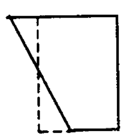	symmetric distortion	5%	~ 0%
3	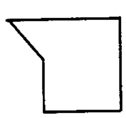	asymmetric distortion	5%	<1.5%

1 & 2 most likely ⇨ may be minor contributor to error

D. <u>Distinct Resonance Peaks</u>: Low Q means broad peaks. Use aspect ratio to separate peaks.

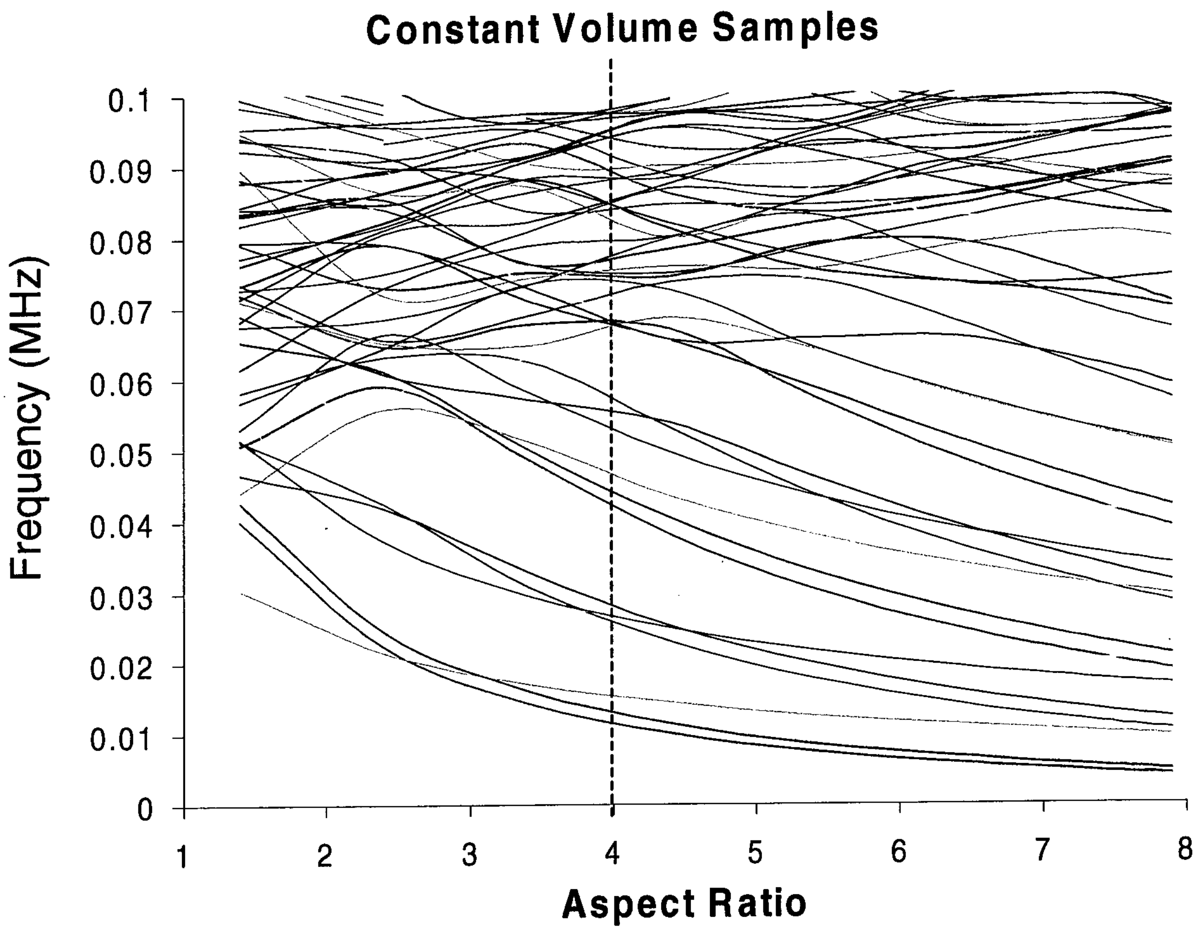

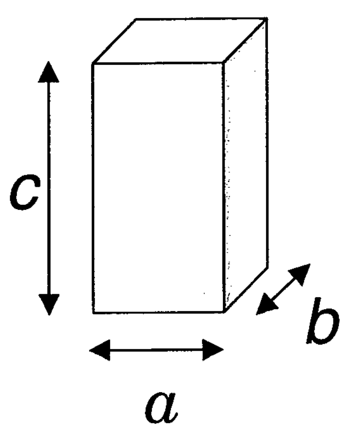

$b = 1.2a$

$$\text{Aspect Ratio} = \frac{c}{a}$$

(basalt c_{11} and c_{44})

TR-8

E. C_{11} dependence in low modes: Low Q limits number of discernable resonances. Use aspect ratio to increase C_{11} dependence.

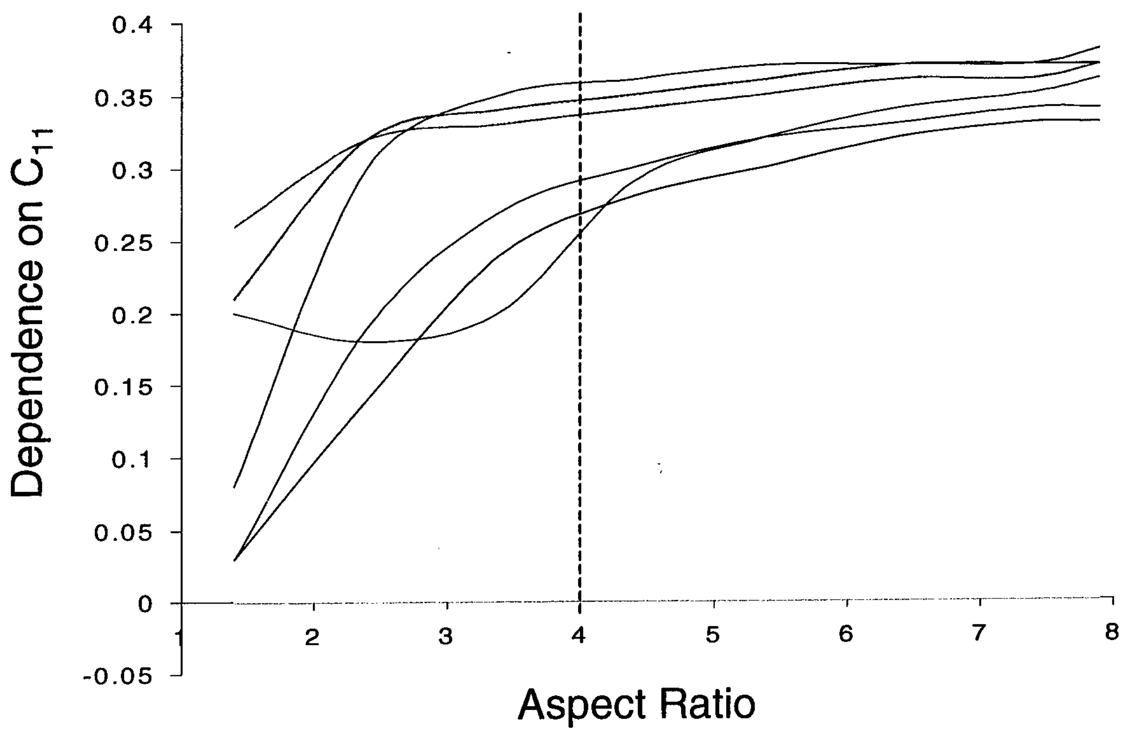

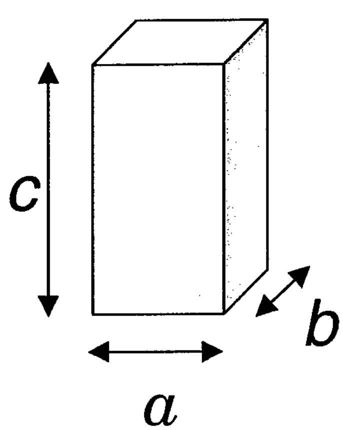

$b = 1.2a$

$$\text{Aspect Ratio} = \frac{c}{a}$$

(basalt c_{11} and c_{44})

IV. Experimental Results

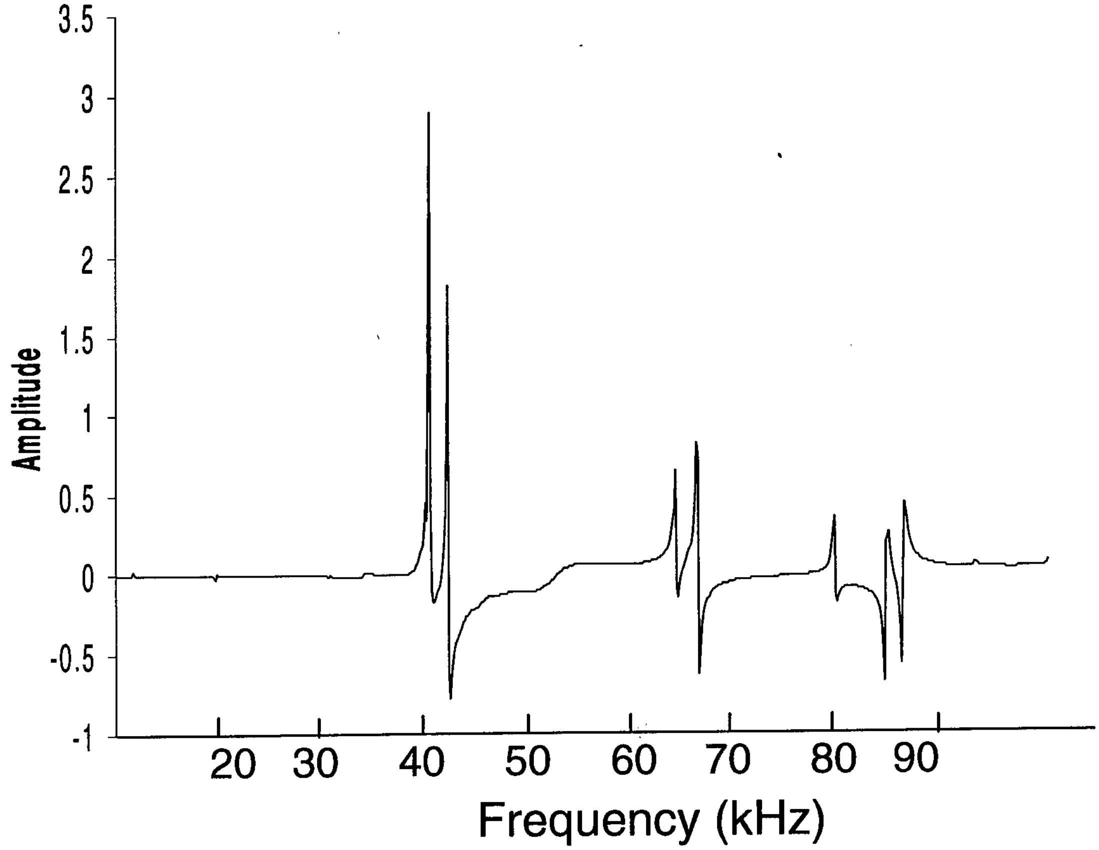

f_{exp} (kHz)	f_{fit} (kHz)
17.988	17.864
19.586	19.649
23.522	23.493
39.786	39.692
40.143	40.161
41.877	42.071
46.944	46.917
63.858	63.810
65.925	66.142

<u>Basalt Sample</u>

Aspect Ratio = 4

% error = 0.313

# of modes = 10

Basalt $C_{11} = 87$ GPa $C_{44} = 32$ GPa

$\frac{c}{a}$	a (cm)	b (cm)	c (cm)	ξ	modes	C_{11} (GPa)	C_{44} (GPa)	% err	<Q>
1.5	2.13	2.44	3.04	0.61	12	88.1	31.3	0.632	276
1.7	2.72	2.74	4.70	0.39	10	88.4	31.7	1.967	242
2.0	2.78	3.04	5.43	0.11	11	87.3	31.6	0.709	256
4.0	1.73	1.98	6.69	0.11	10	87.2	31.5	0.313	336

Sierra White Granite $C_{11} = 43$ GPa $C_{44} = 19$ GPa

$\frac{c}{a}$	a (cm)	b (cm)	c (cm)	ξ	modes	C_{11} (GPa)	C_{44} (GPa)	% err	<Q>
1.5	3.68	4.16	5.64	0.66	11	37.6	18.7	1.238	146
1.6	2.77	3.11	4.51	0.66	10	43.2	18.6	2.023	140
3.3	0.96	1.20	3.17	0.44	11	20.8	21.3	17.29	149
4.0	1.69	2.02	6.82	0.28	12	37.5	19.1	0.630	142

V. Future Work

A. <u>Same analysis for cylindrical samples</u>.

(Izabela Santos, Senior Thesis)

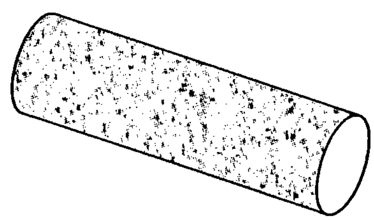

B. <u>Temperature and Saturation Control</u>.

(TJ Ulrich, PhD Thesis)

C. <u>Provide baseline for nonlinear analysis</u>.

CONSTANT STRAIN ANALYSIS

R. A. GUYER UMASS / LANL

JIM TENCATE LANL

ERIC SMITH LANL

1. a rock

2. traditional theory → L

3. PM-space "model → R

4. to confirm quasi-static ↔ dynamic connection

5. an expt and analysis

TR-1

TRADITIONAL THEORY OF NONLINEAR ELASTICITY, THE STRAW MAN.

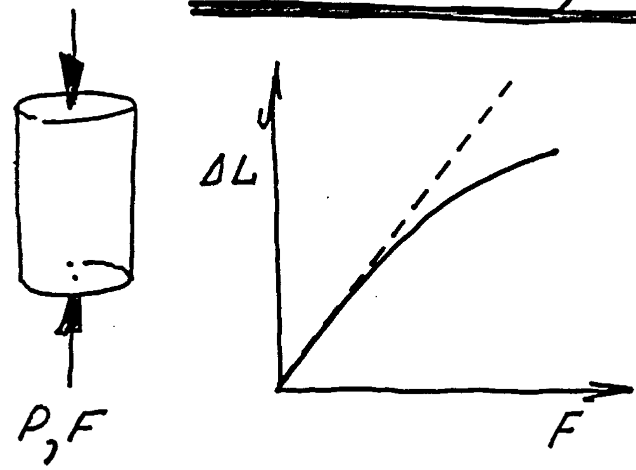

EOS

$$F = \underbrace{\Gamma(\Delta L)}\,\Delta L$$

$$F = \Gamma_0\left[1 + \beta\frac{\Delta L}{L_0} + \delta\left(\frac{\Delta L}{L_0}\right)^2 + \cdots\right]\Delta L$$

same springs work here as here**

WAVE EQUATION

$$\rho\frac{\partial^2 u}{\partial t^2} = K\frac{\partial}{\partial x}\left[\underbrace{\frac{\partial u}{\partial x}}_{\text{LINEAR}} + \underbrace{\beta\left(\frac{\partial u}{\partial x}\right)^2}_{\text{CUBIC NL}} + \underbrace{\delta\left(\frac{\partial u}{\partial x}\right)^3}_{\text{QUARTIC NL}} + \cdots\right] \quad \cdots$$

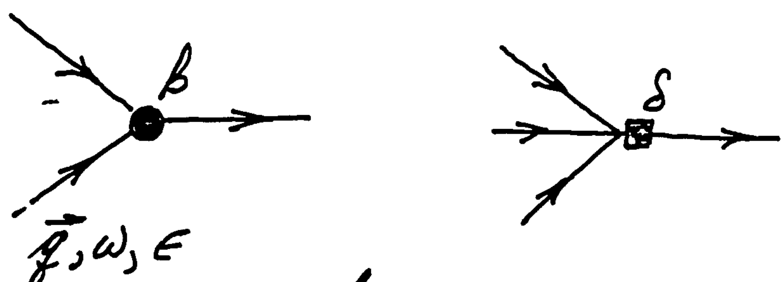

basic physical process is due to β, δ, ...
"coalesence" of strain fields

TRADITIONAL THEORY OF LINEAR and NONLINEAR ELASTICITY IS VERY ELABORATE, e.g LANDAU + LIFSHITZ, BECAUSE THE BASIC FIELD, the strain field, IS A TENSOR

$$\epsilon = \frac{\Delta L}{L} \leftrightarrow \frac{\Delta L_x}{L_y} = \epsilon_{xy}, \dots$$

OTHERWISE: TTNLE = TAYLOR SERIES EXPANSION

BUT:

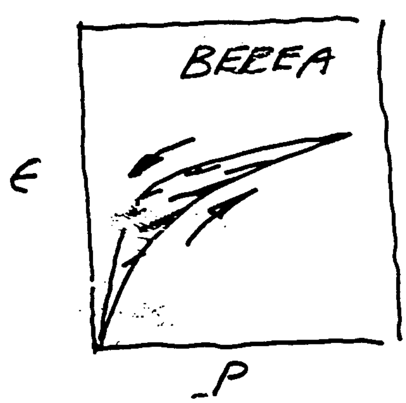

NL/H/DM

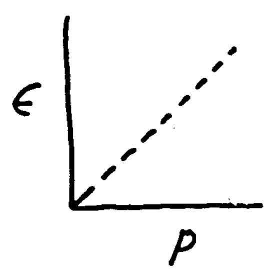

nonlinear, NL

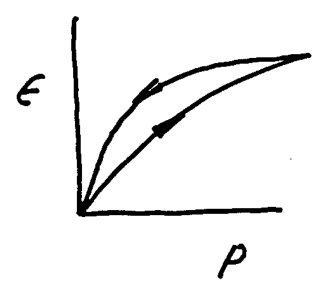

hysteresis, H

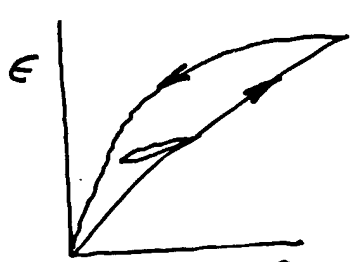

discrete memory, DM

THE ELASTICITY OF **ROCKS** IS CHARACTERIZED

SOILS
CONCRETE
CERAMICS ?
⋮
?

BY **NL / H / DM**

MAGNETS, RFIM
MARTENSITES
FLUID CONFIGURATIONS
IN A PORE SPACE
⋮
*

There is a **generic*** explanation of the elasticity of rocks; **details** are specific to rock elasticity; **essential features** shared by $\boxed{}$;

*ALL OF THESE SYSTEMS HAVE **MACROSCOPIC** BEHAVIOR THAT IS DUE TO AN ASSEMBLY OF

MESOSCOPIC
HYSTERETIC **MICROSCOPIC** UNITS.

magnet = 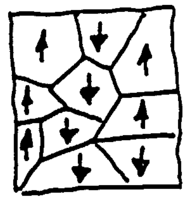 domains ↑ ↓

fluid in a pore space = 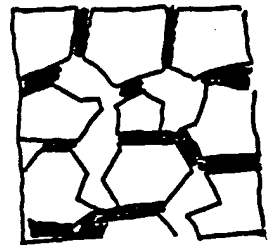 pore full empty

rock elasticity = ? elastic bonds ? ?

A PHENOMENOLOGY FOR DESCRIBING THE ELASTICITY OF ROCKS: PM-SPACE.

PREISACH '35 M-H
MAYERGOYZ '85

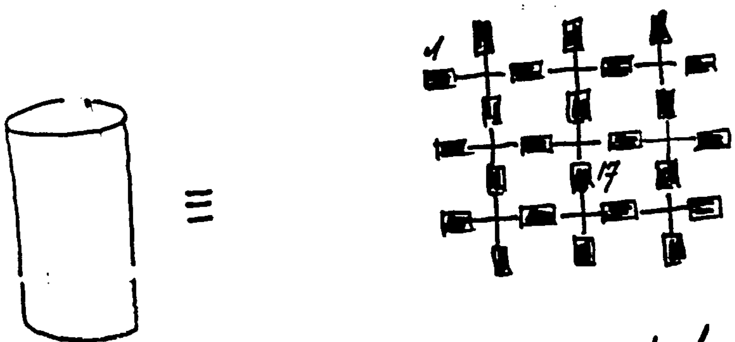

assembly of hysteretic elastic bonds

central construct: PM space, a space where you keep track of the state of each elastic bond

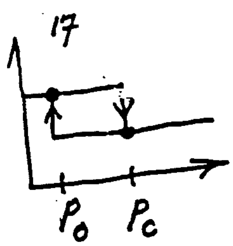

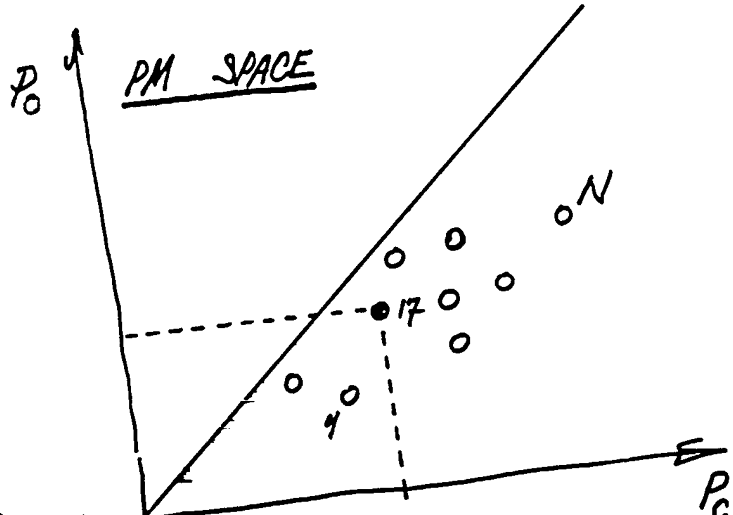

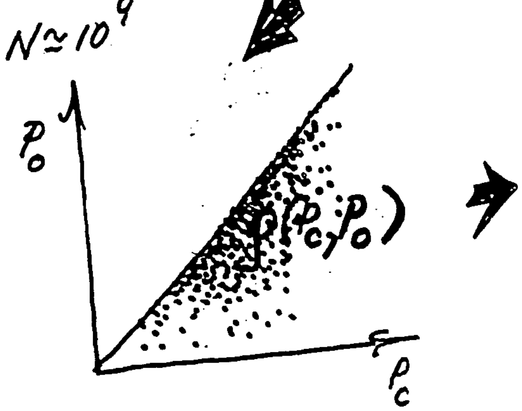

$\rho(P_c, P_o)$ = DENSITY OF ELASTIC BONDS IN PM SPACE IS THE MOST IMPORTANT QUANTITY.

FEATURES OF THE PM-SPACE MODEL:

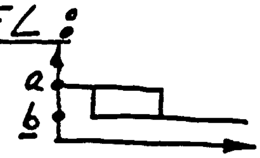

1. $\boxed{\epsilon(P) = \epsilon_0 F(\underline{P})}$

"fraction" of elastic bonds in state (closed, $\underline{b}$).

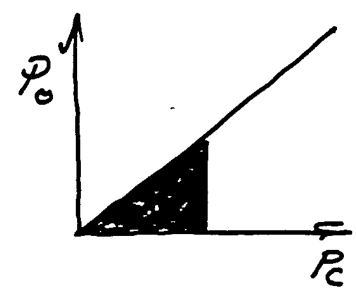

2. When $\rho(P_c, P_o)$ is known you can find the response to any pressure protocol.

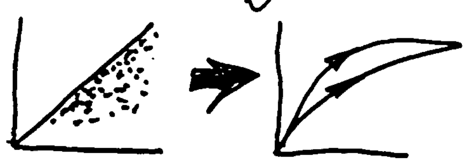

3. There is an inverse problem: from suitable ϵ-P data you can find $\rho(P_c, P_o)$

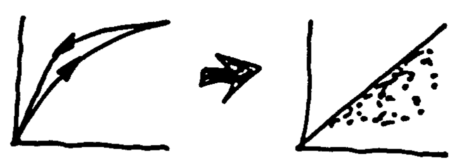

4. A sound wave is a pressure protocol.

THE PROGRAM

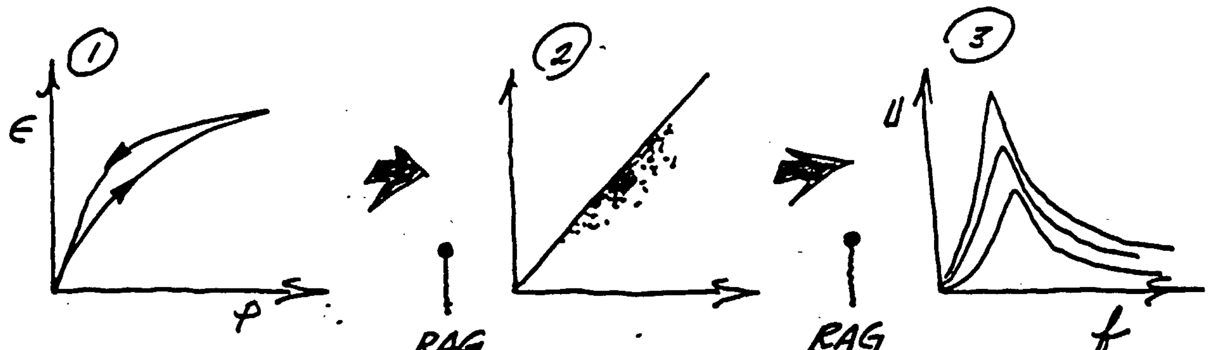

G BOITNOTT, NER

J TENCATE, LANL
RAG
E SMITH

WHAT DO YOU EXPECT FOR 3?

TRADITIONAL THEORY

Δf = frequency shift

$$\Delta f \sim \delta |U|^2_{max}$$

$$\frac{1}{Q} - \frac{1}{Q(0)} \sim \delta |U|^2_{max}$$

$$\delta \sim 10^{6}$$

quartic anharmonicity

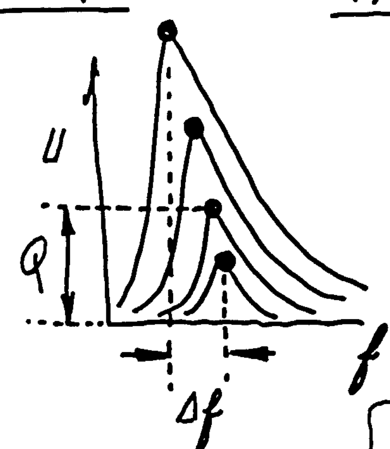

PM-SPACE MODEL

$\frac{1}{Q}$ = attenuation

$$\Delta f = C_1 |U|_{max}$$

$$\frac{1}{Q} - \frac{1}{Q(0)} = C_2 |U|_{max}$$

$C_1 \sim C_2 \sim$ [redacted]

2

J. TENCATE, LANL '98

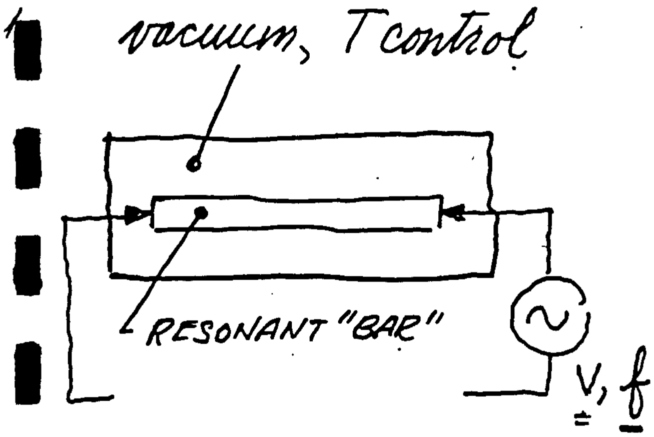

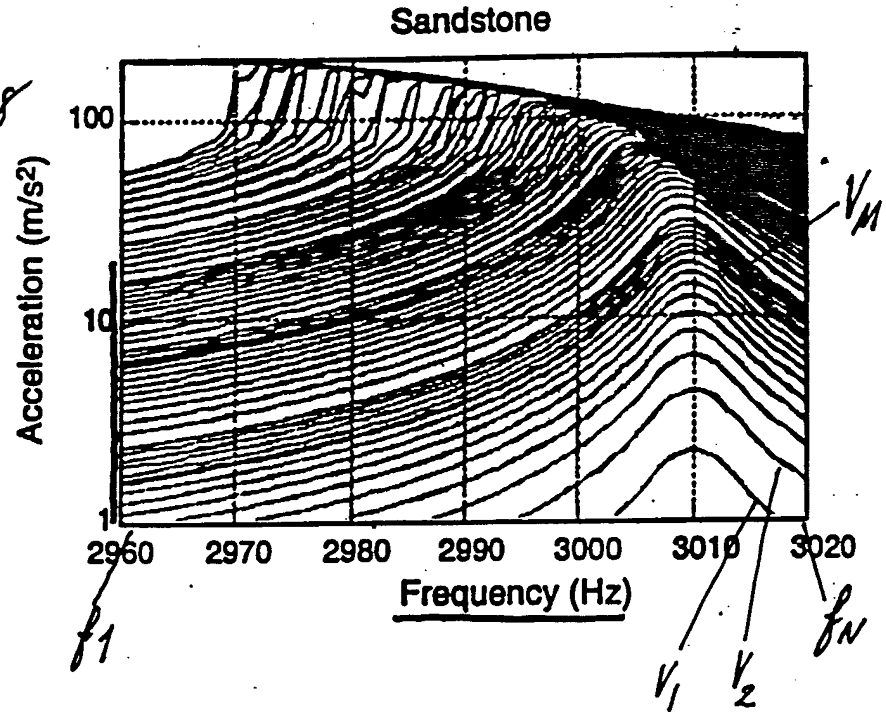

detect a(t),
report a(f); amplitude of motion at drive frequency

2. STUDY THE RESONANCE CURVES:

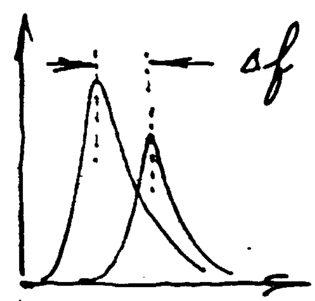

(a) rigorous acceptance criterion

V_1, f_1, f_2, ⋯ f_N ⋯ f_1

V_2, f_1, f_2, ⋯ f_N ⋯ f_1

⋮

V_M, f_1, f_2, ⋯ f_N f_1

⋮

V_1, f_1, ⋯ f_N ⋯ f_1

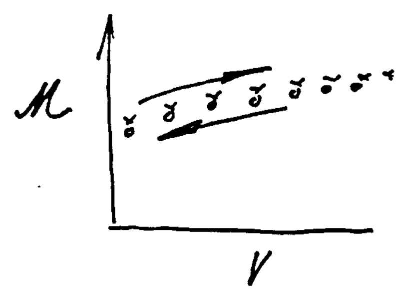

at V_i, f_j

(b) measure $\underline{A_{ij}}$, $\underline{B_{ij}}$

in phase   out of phase

$i = 1 \cdots M \leftrightarrow V_1, V_2, \cdots V_M$

$j = 1 \cdots N \leftrightarrow f_1, f_2, \cdots f_N$

$\underline{U_{ij}} = \sqrt{\underline{A_{ij}}^2 + \underline{B_{ij}}^2}$

essentially the amplitude of the strain field in the bar

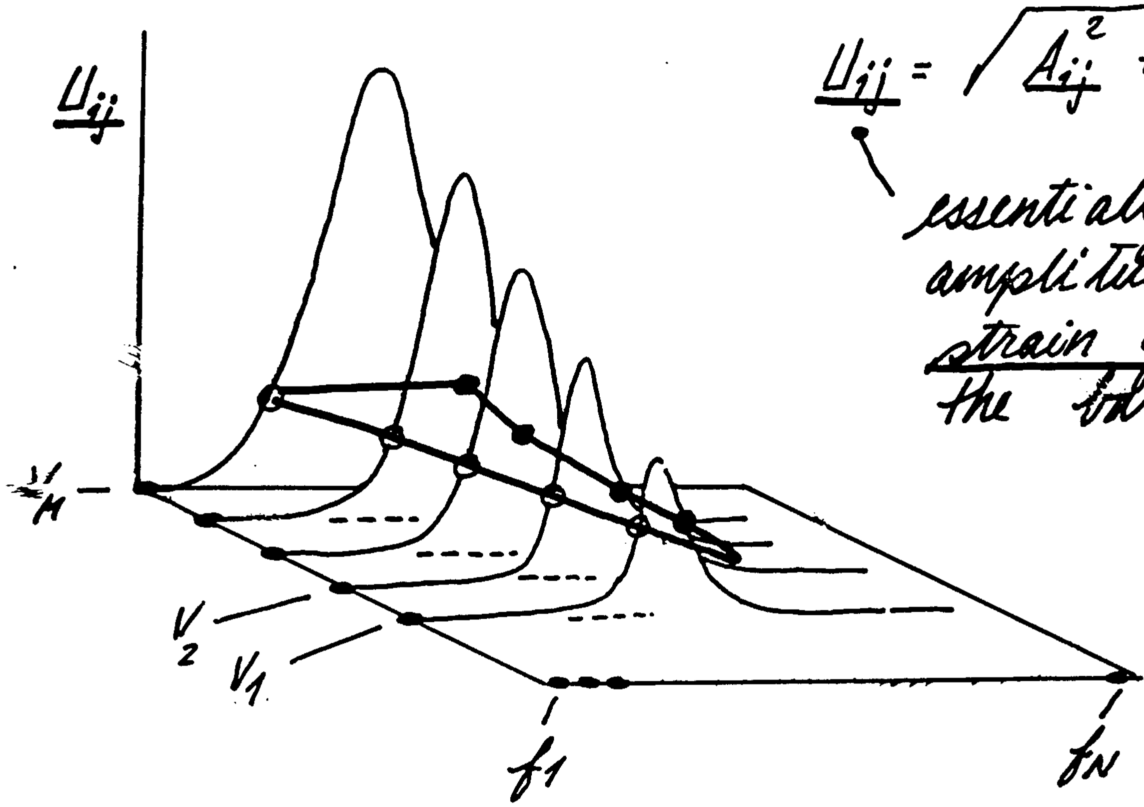

physical state of rock is set by the strain field in the rock - rock is in the same physical state along ——

when nonlinear - state ↔ strain : it makes

<u>no</u> sense to analyze curves of constant V!

DO THIS :

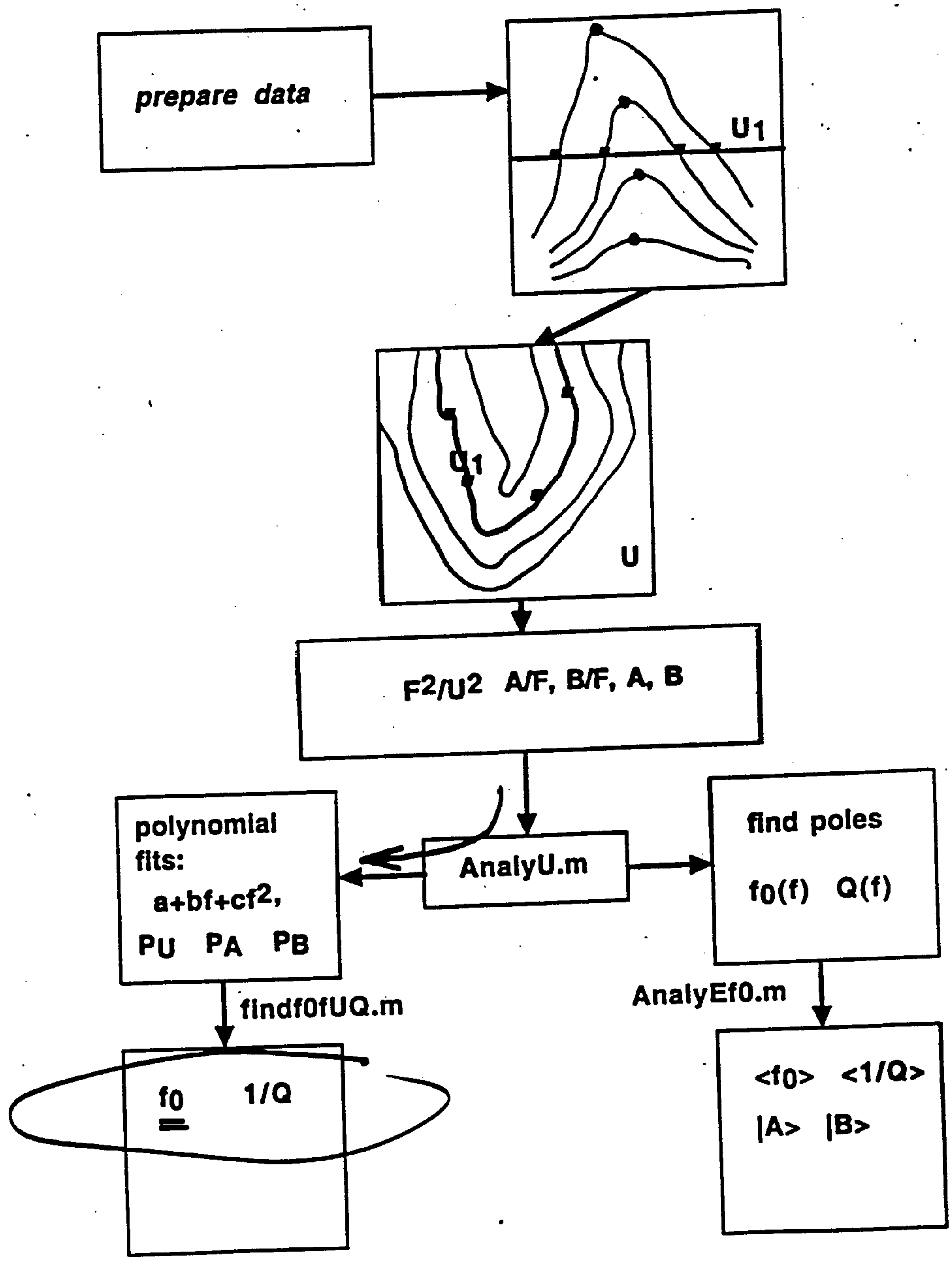

Some algebra ;

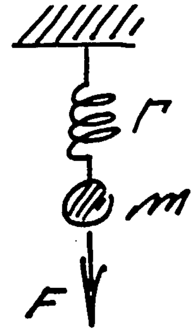

$$\omega_0^2 = \Gamma / m ,$$

$$\Omega = \omega / \omega_0 ,$$

$$f = \frac{F}{m\omega_0^2} .$$

$$A = \frac{1-\Omega^2}{\boxed{(1-\Omega^2)^2 + \frac{\Omega^2}{Q^2}}} f ,$$

$$B = -\frac{\Omega}{Q} \frac{1}{\boxed{(1-\Omega^2)^2 + \frac{\Omega^2}{Q^2}}} f ,$$

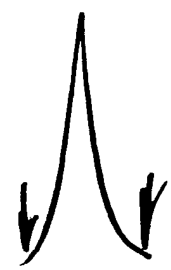

$$|U| = \sqrt{A^2+B^2} = \frac{1}{\sqrt{\boxed{(1-\Omega^2)^2 + \frac{\Omega^2}{Q^2}}}} f .$$

$$\boxed{\left\{ \begin{aligned} \frac{1}{|U|^2} A &\propto 1-\Omega^2 \\ \frac{1}{|U|^2} B &\propto -\frac{\Omega}{Q} \end{aligned} \right.}$$

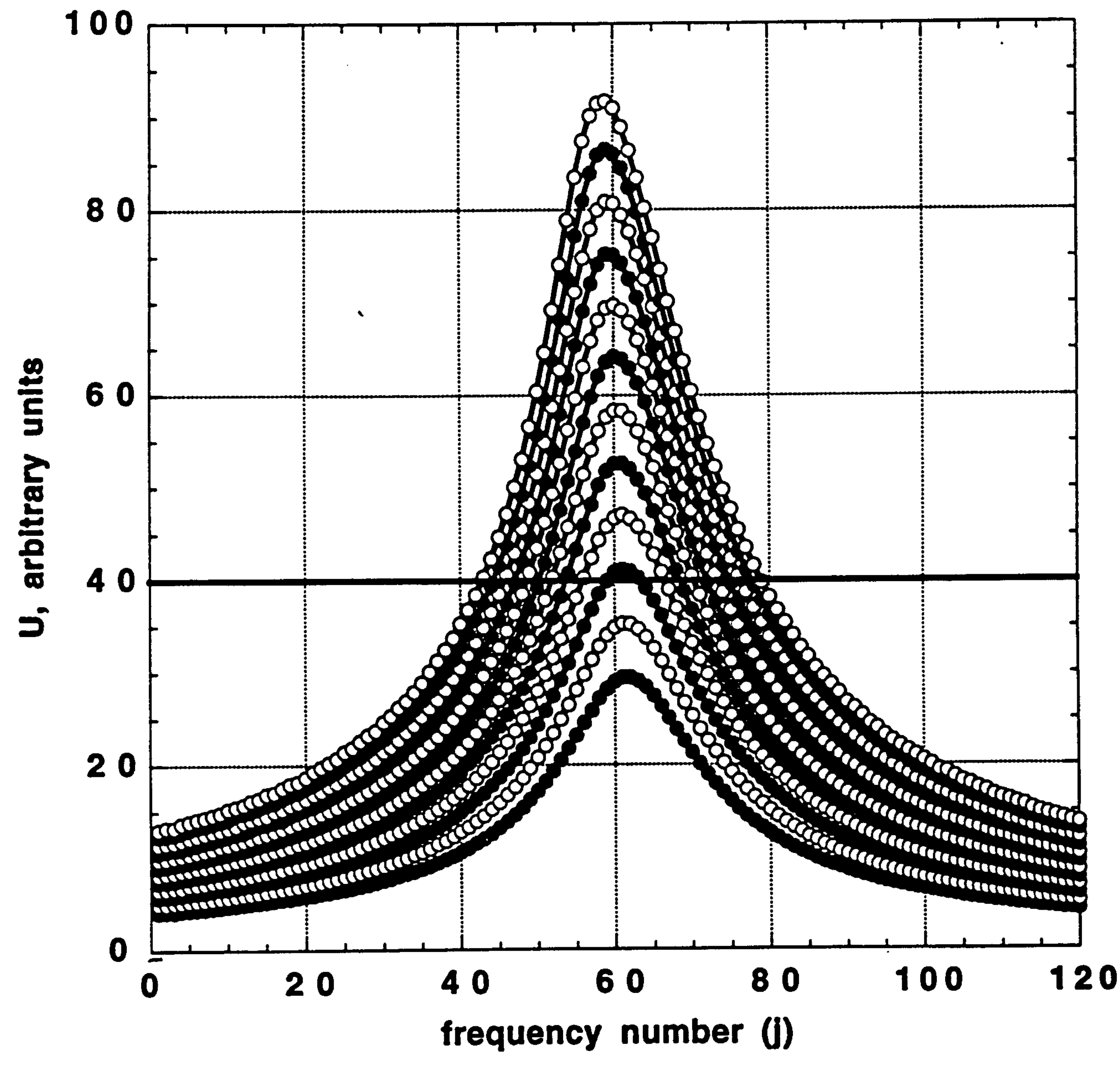
100
80
60
40
20
0
0
20
40
60
80
100
120
U, arbitrary units
frequency number (j)

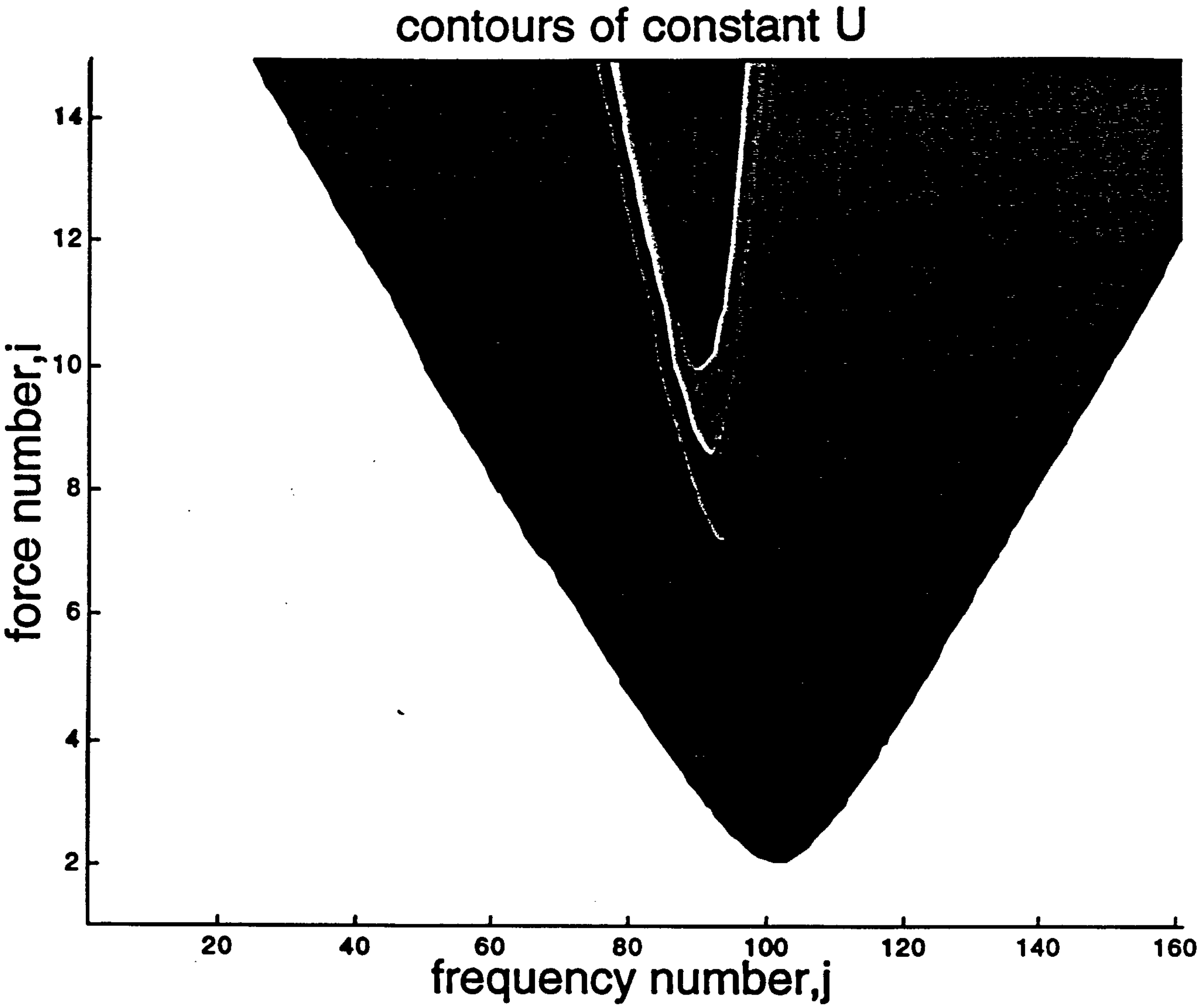
contours of constant U
force number,i
frequency number,j
14
12
10
8
6
4
2
20
40
60
80
100
120
140
160

RESULTS:

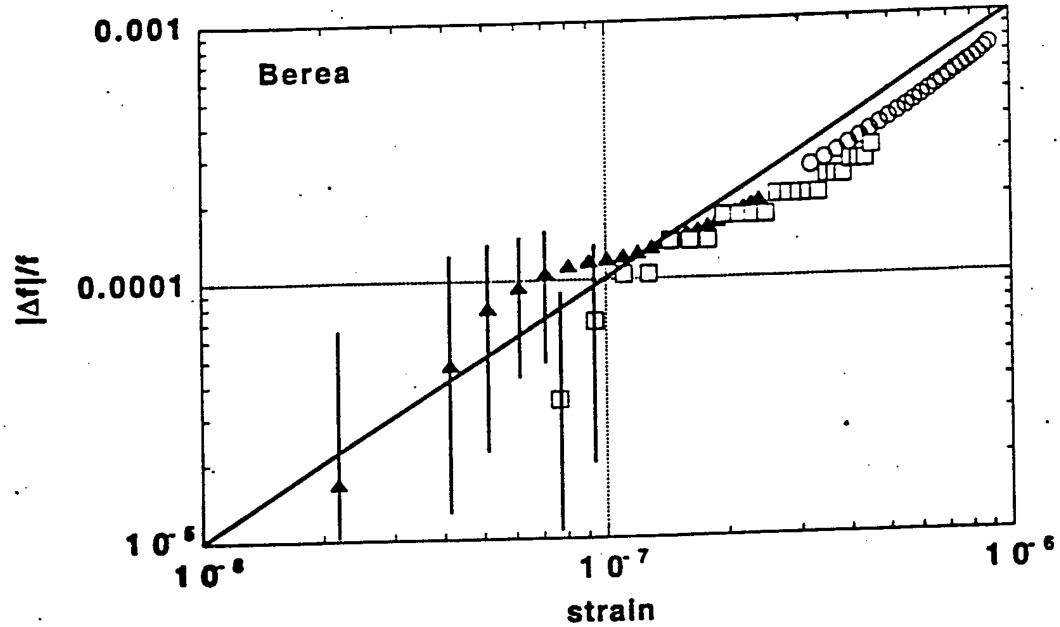

Berea
0.001
0.0001
10^{-5}
$|\Delta f|/f$
10^{-8}
10^{-7}
10^{-6}
strain

Δf

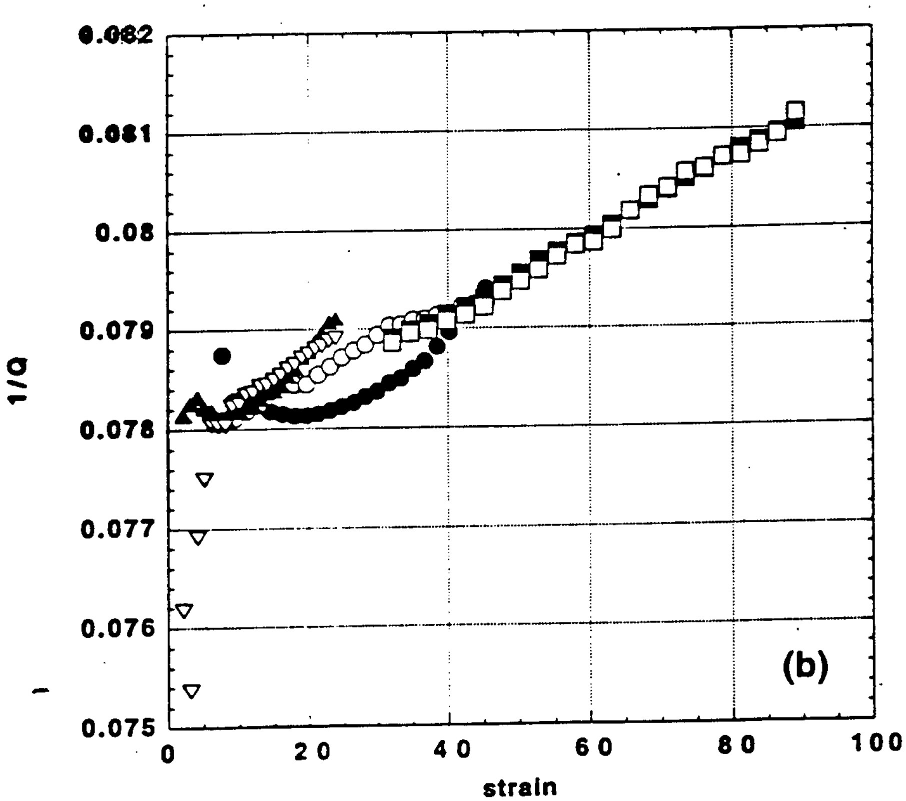

0.082
0.081
0.08
0.079
0.078
0.077
0.076
0.075
1/Q
0
20
40
60
80
100
strain
(b)

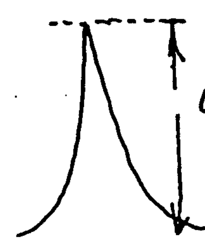

Q

$$\frac{\Delta f}{f_0} \simeq C_f \, \underline{|\epsilon|} \simeq \frac{3\ Hz}{3000\ Hz}$$

$$\frac{1}{Q(\epsilon)} - \frac{1}{Q(0)} \simeq C_Q \, \underline{|\epsilon|}$$

$$C_f \simeq C_Q \simeq 2\,C_1 \simeq \underline{2000}$$

$$2\times 10^{-8} \lesssim |\epsilon| \lesssim 10^{-6}$$

excellent agreement with PM-space picture.

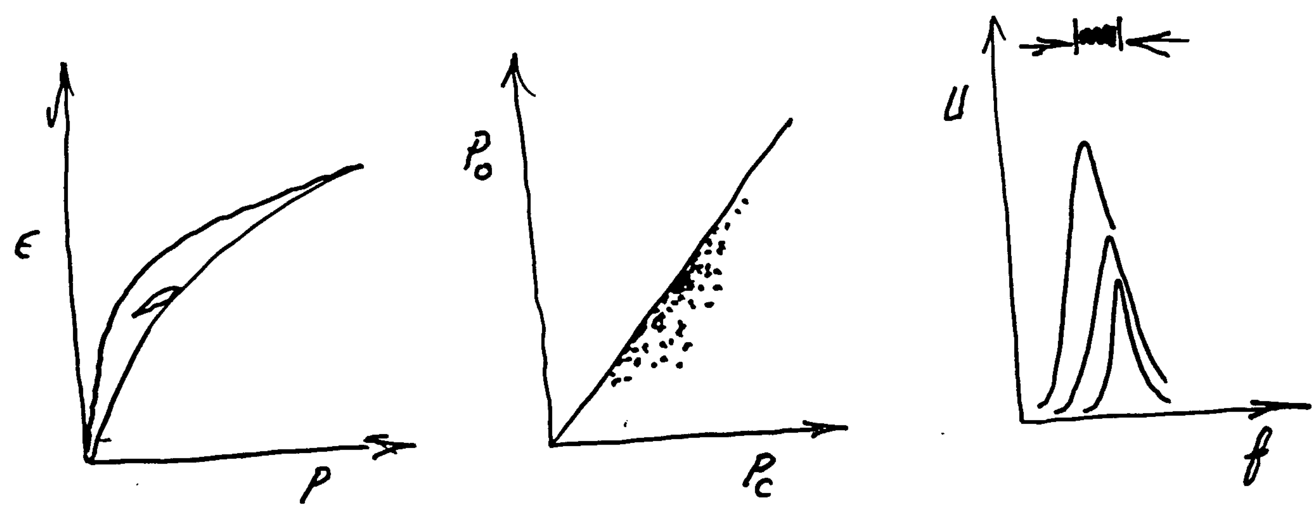

Global Symmetry, the Phonon Density of States, and RUS

Tim Darling and Albert Migliori

LANL

RUS measures a tiny piece of the phonon DOS and can determine a global elastic symmetry.

Many physical properties depend on the entire DOS and the meso- or microscopic symmetry.

How good is the connection?

> For when you are put into the Vortex you are given just one momentary glimpse of the entire unimaginable infinity of creation, and somewhere in it a tiny little marker, a microscopic dot on a microscopic dot, which says 'You are here.'

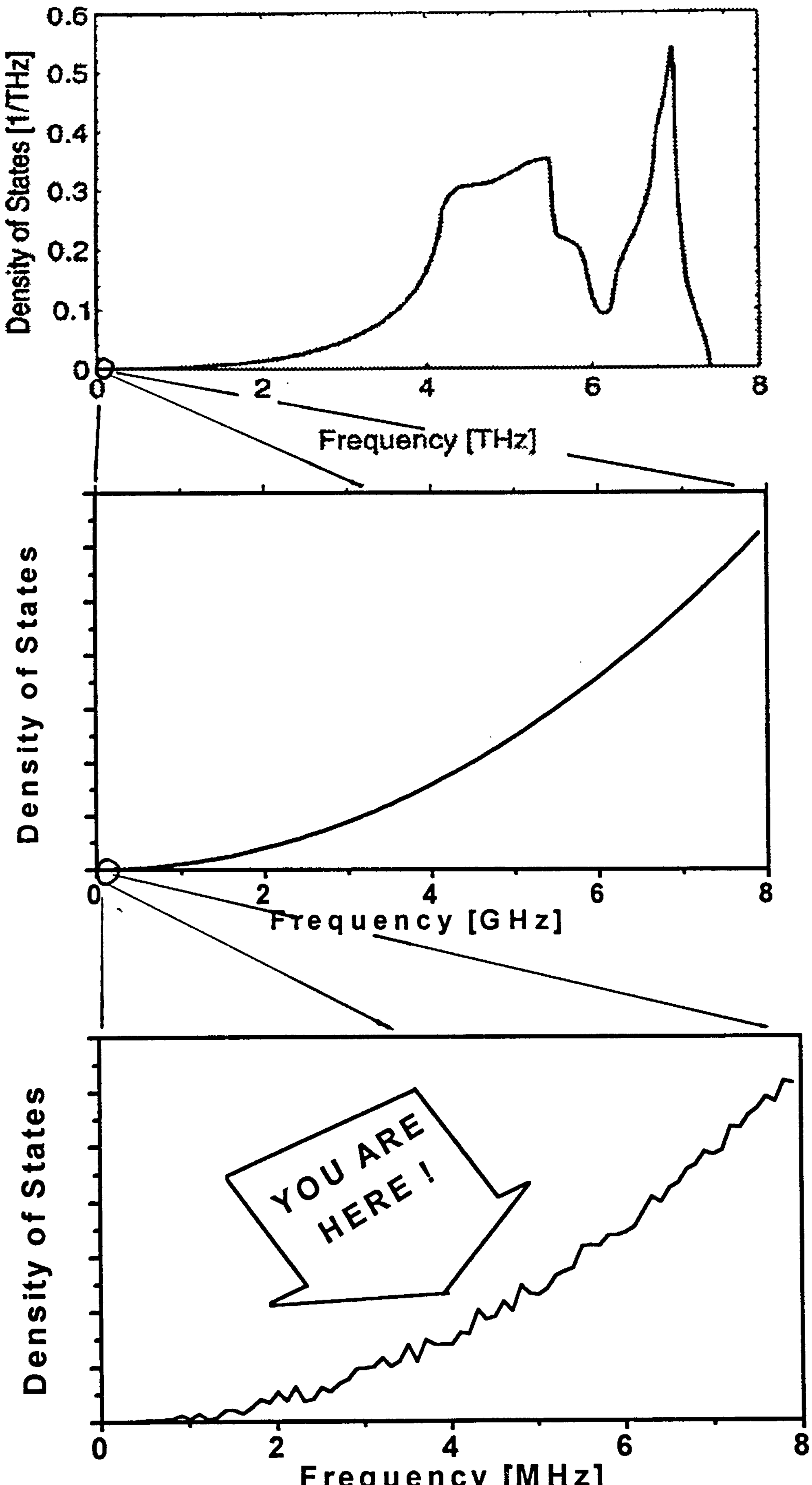

Density of States [1/THz]
0.6
0.5
0.4
0.3
0.2
0.1
0
0
2
4
6
8
Frequency [THz]
Density of States
0
2
4
6
8
Frequency [GHz]
Density of States
YOU ARE HERE !
0
2
4
6
8
Frequency [MHz]

TR-2

Harmonic approximation:

Replace 3N degrees of freedom by 3N harmonic oscillators (normal modes)
$E = (n+1/2)hf$, $n \Rightarrow$ boson statistics

Born-Von Karman (cyclic) boundary conditions in an infinite solid – “travelling wave” solutions

No dissipative processes

No thermal expansion
No temperature dependence of moduli
Isothermal and adiabatic moduli equal

Debye Model

Continuum (isotropic)
Frequency cutoff by requiring 3N modes
Linear dispersion in all branches
DOS α f^2 (and T^3)

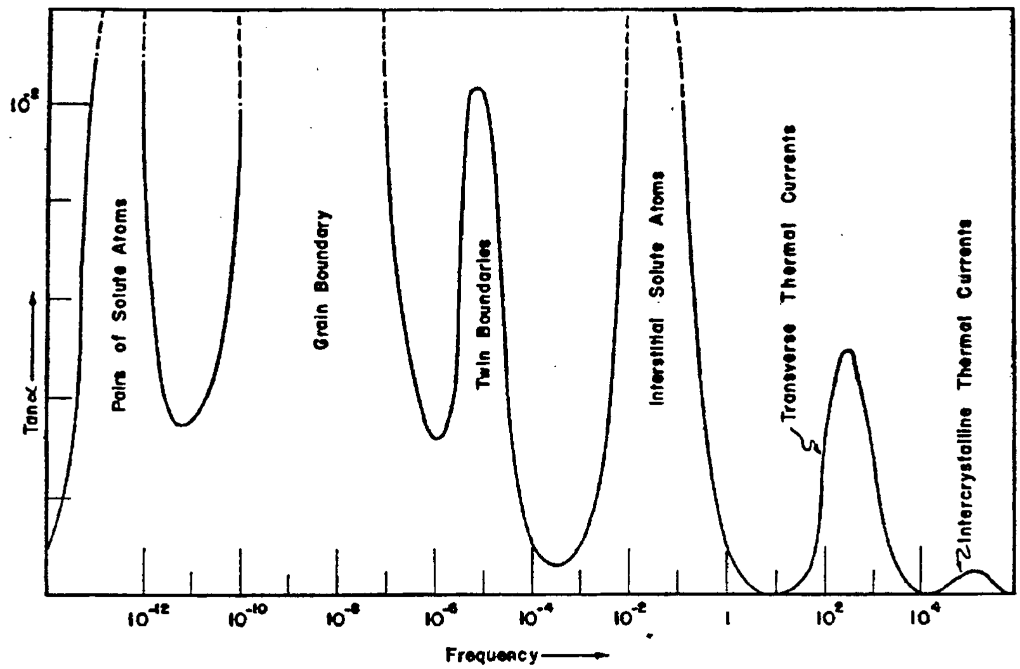

A Typical Relaxation Spectrum

PLOT OF τ^{-1} - ZENER, 1948, LOW TEMPERATURES

RUS HAS A TRICKY TIME HERE, BECAUSE

ω IS GENERALLY HIGH (>> kHz)

WE SCAN ω OVER A WIDE RANGE

SEPARATING OUT CONTRIBUTIONS FROM DISTINCT MODES IS TRICKY BECAUSE OF THE ω VARIATION

BUT, WE ARE IN RANGE OF CERTAIN MOBILE INTERSTITIALS (H) , AND DOMAIN WALLS AND TWIN AND PHASE BOUNDARIES NEAR PHASE TRANSITIONS WHERE THE MOBILITY IS HIGH

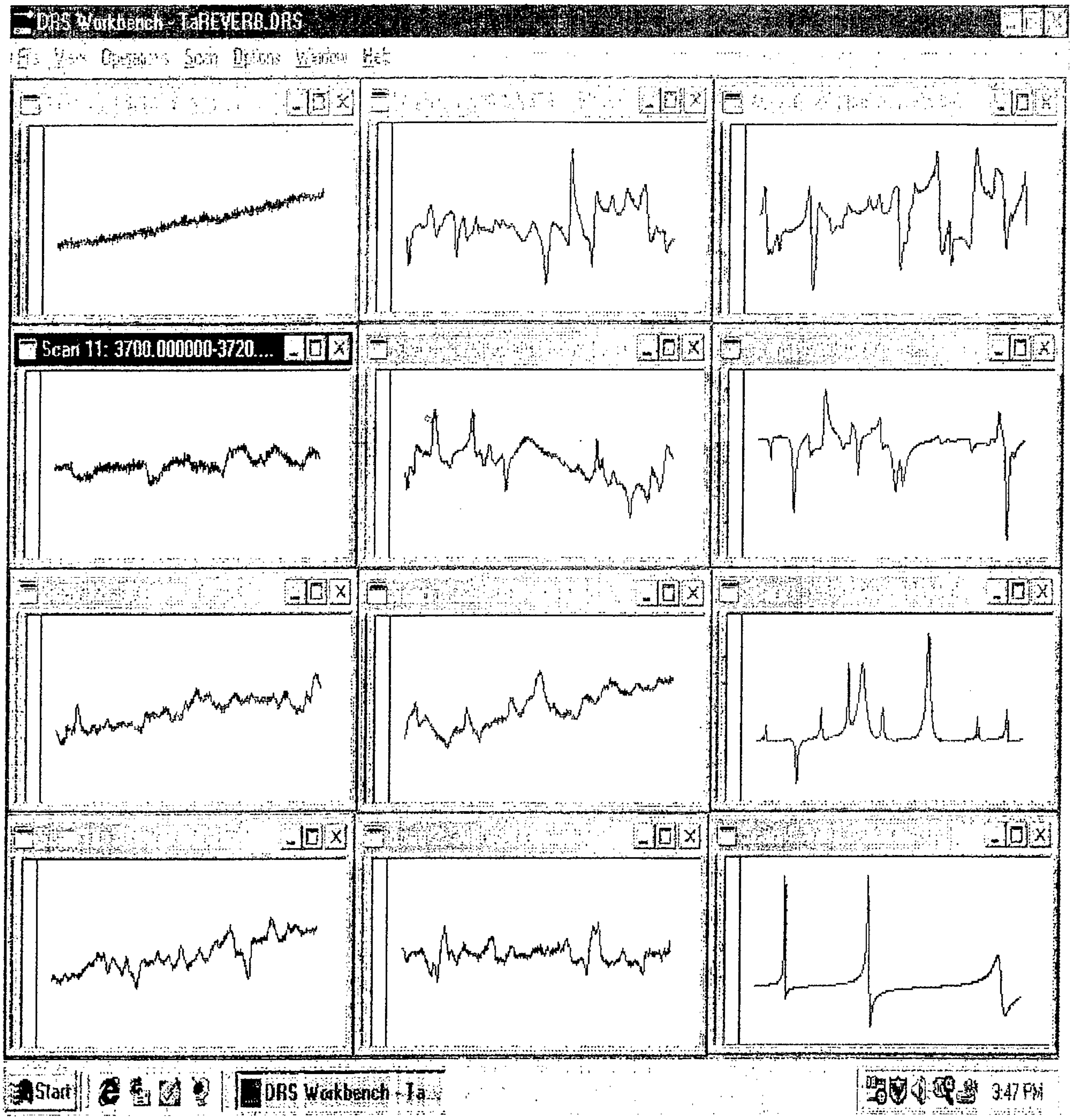

Ta polycrystal data

TR-5

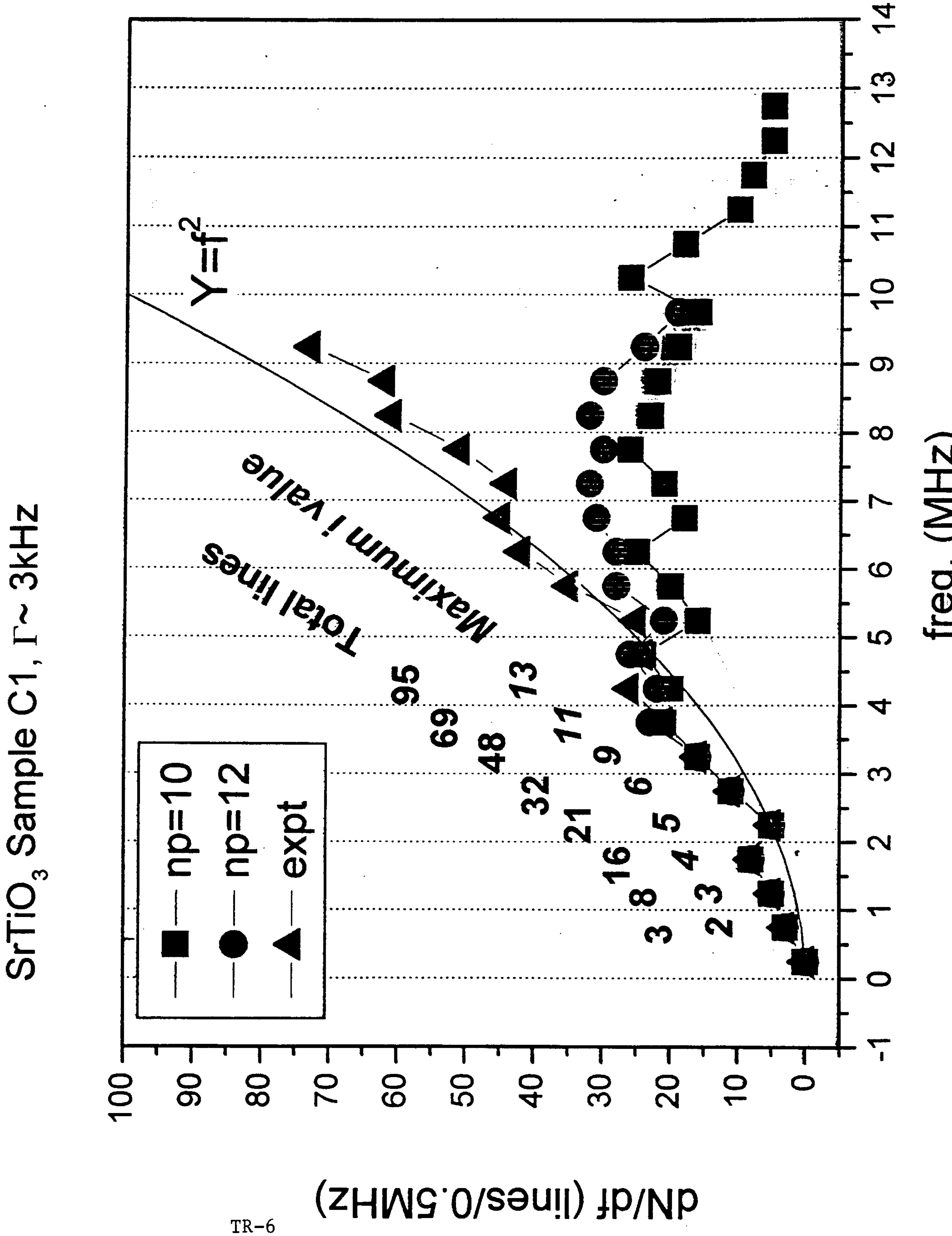

SrTiO3 Sample C1, Γ~ 3kHz
np=10
np=12
expt
Y=f2
Total lines
Maximum i value
3 8 16 21 32 48 69 95
2 3 4 5 6 9 11 13
freq. (MHz)
dN/df (lines/0.5MHz)

TR-6

Specific heat

$$C(T) = \int_0^{\infty} g(\omega) C(\omega, T) d\omega$$

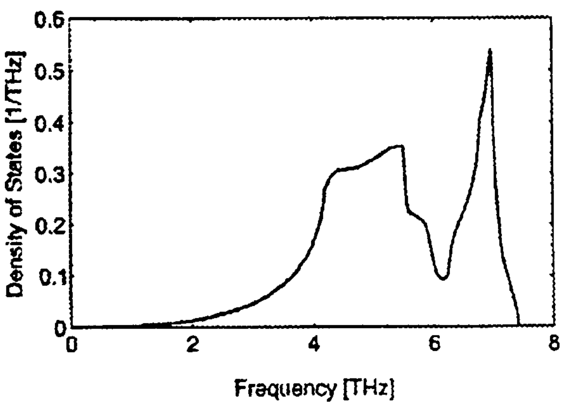

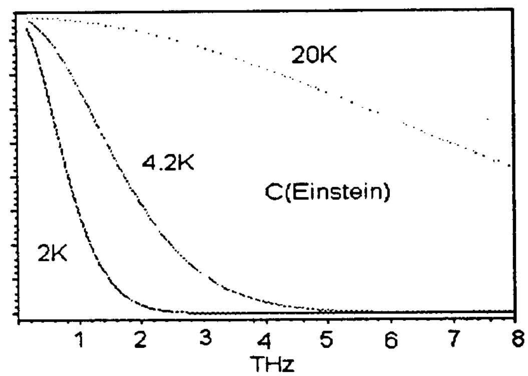

RUS DOS – Relevant for T ~ few μK , otherwise, every material we measure, looks like a Debye solid,

$$g(\omega)\ \alpha\ \omega^2$$

- Don't see optical branches
- Statistics too poor to see anomalies or contributing acoustic branches

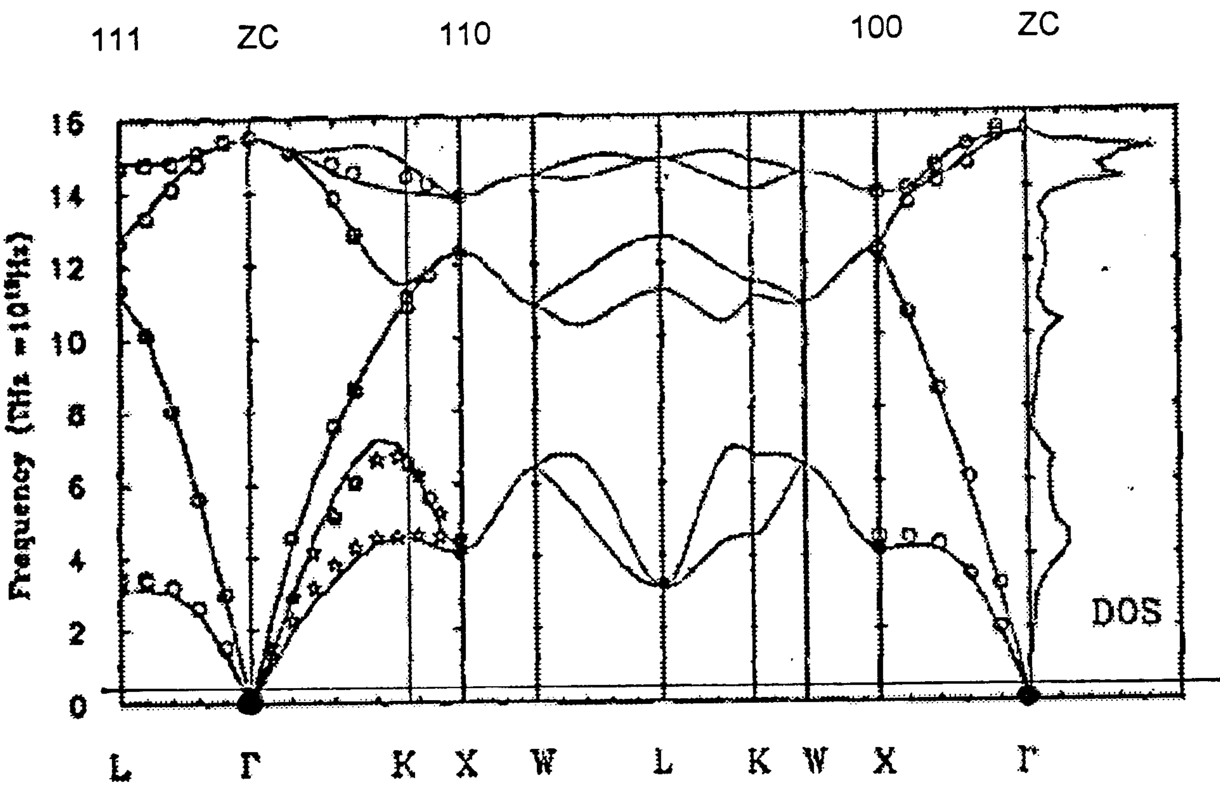

DISPERSION CURVES FOR Si, Ni

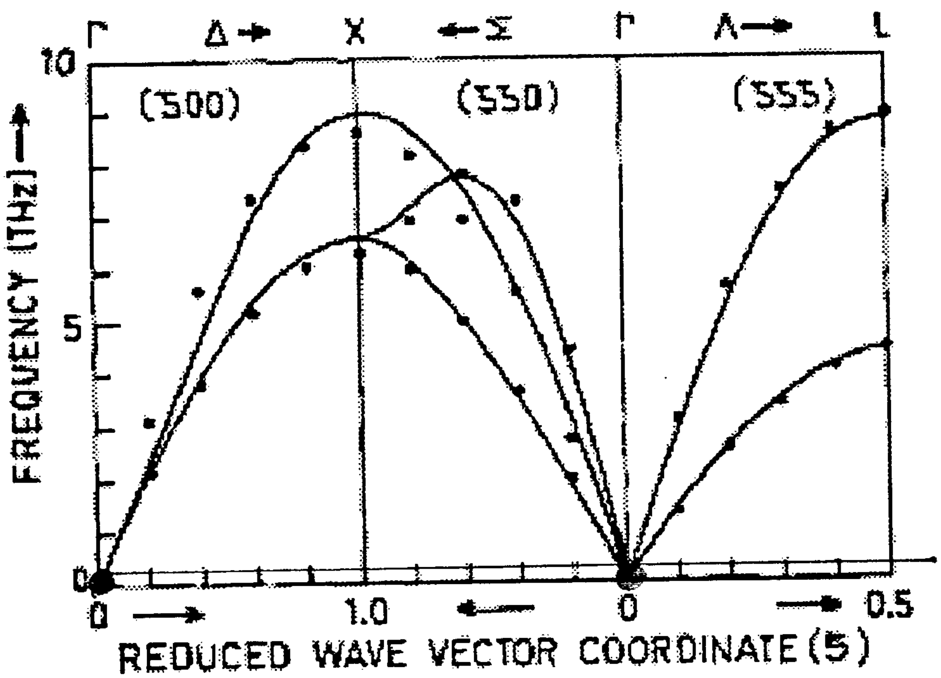

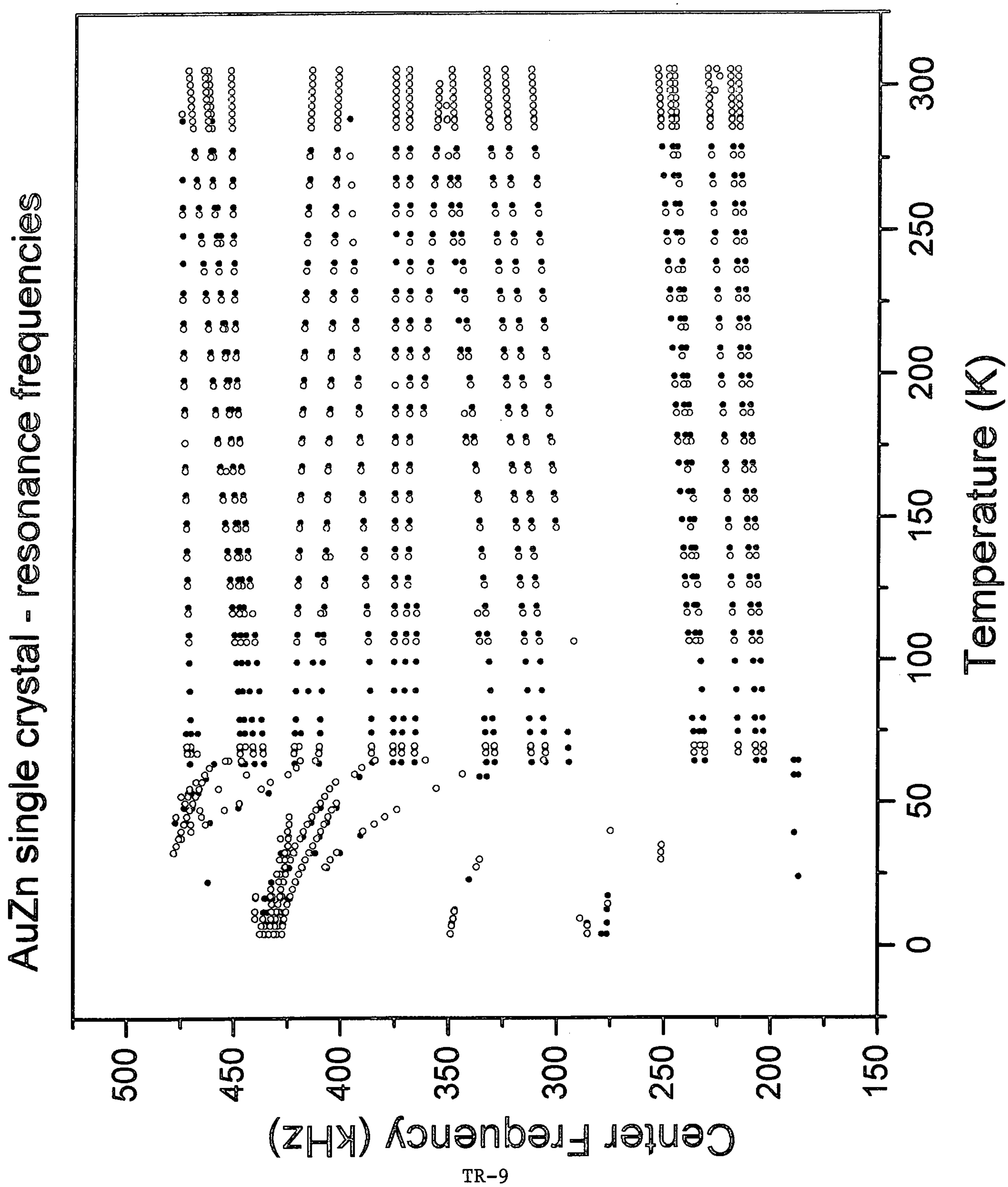
AuZn single crystal - resonance frequencies
Center Frequency (KHz)
Temperature (K)
500
450
400
350
300
250
200
150
0
50
100
150
200
250
300

Applicability of RUS results is only as good as the Debye model.

$\omega = c k$ linear dispersion

c = wavespeed per branch (1 longitudinal, 2 transverse)

Thermodynamic results in terms of $\bar{c}$

$$\frac{3}{\bar{c}^3} = \frac{1}{C_{t_1}} + \frac{1}{C_{t_2}} + \frac{1}{C_l}$$

eg. $\theta_D \propto \omega_D \propto \bar{c}$, Free energy derivatives...

isotropic : $C_{t_1} = C_{t_2}$

cubic + lower symm. : $C_{t_1} \neq C_{t_2}$, and direction dependent

RUS DETERMINES C_t, C_l ... VERY ACCURATELY - PROVIDED WE KNOW HOW MANY BRANCHES (independent C_{ij}'s) THERE ARE:

$$c \propto \sqrt{\frac{C_{ij}}{\rho}}$$

→ GLOBAL SYMMETRY

TR-10

$SrTiO_3$ sample, room temperature, 32 lines

	C11	C33	C23	C12	C44	C66	Bulk	χ^2/nd	RMS
ISO	2.7845				1.2041		1.179	45.39	1.08
ISO*	2.7202				1.2241		1.088		0.098
HEX 1	3.1171	1.2310	1.2310	0.7778	1.1697	1.1697	1.810	25.68	0.87
HEX 2	2.8813	3.0530	0.8137	0.4203	1.2200	1.2305	1.423	8.30	0.35
HEX 3	2.8483	3.0274	0.7780	0.3551	1.2207	1.2466	1.381	3.34	0.24
CUB	3.1692			1.0391	1.2225		1.749	0.75	0.11
TET 1	3.0199	[illegible]	[illegible]	0.8001	1.2303	[illegible]	[illegible]	0.47	0.093
TET 2	3.1538	3.1611	1.0264	1.0171	1.2215	1.2241	1.735	0.92	0.12
TET 3	3.1436	3.1599	1.0214	1.0050	1.2200	1.2302	1.727	0.67	0.10
ORTH	3.0033	2.1977	0.5529	0.6878	1.2321	1.2200	1.356	0.42	0.083

2% chi^2 – increase errors

ISO	1.16				0.42	
HEX 1		18.1	10.85	10.0	0.30	0.5
HEX 2		0.54	2.81	6.84	0.08	0.43
HEX 3		0.39	1.87	5.49	0.06	0.37
CUB	0.28		1.05	0.04		
TET 1	0.49	4.42	[illegible]	1.65	0.04	0.01
TET 2	0.58	0.27	1.56	2.61	0.01	0.09
TET 3	0.72	0.27	1.52	0.53	0.02	0.15
ORTH	0.43	3.93	5.74	1.42	0.08	0.02

"Magic numbers" for RUS fits

Number of lines $<$ np*8
(80 or 96)
(could be <u>much</u> lower depending on c_{ij} and dim.'s)

Number of lines $\geq$ nc*5
(10,15,25,30,45)

rms% $< 0.5\%$ AND all $\Delta c_{ij} \leq 2\%$

rms% changes of $< 20\%$ may not be meaningful

Conclusions:

1. RUS = Debye model

2. Dispersion relations from C_{ij}'s are essential to keep models honest

3. Determining symmetry (# of C_{ij}'s) must be done very carefully

4. It seems we miss some interesting length scales, but sometimes the results of averaging procedures can be enlightening

Future:

Temperature dependence of C_{ij}:

- measurements 4K → 800K
- correlation with thermal expansion
- models for anomalous behavior

Contactless Mode-Selective Resonance Ultrasound Spectroscopy: Electromagnetic Acoustic Resonance

Hirotsugu Ogi[1,2] and Hassel Ledbetter[2]
[1]Osaka University
[2]National Institute of Standards and Technology

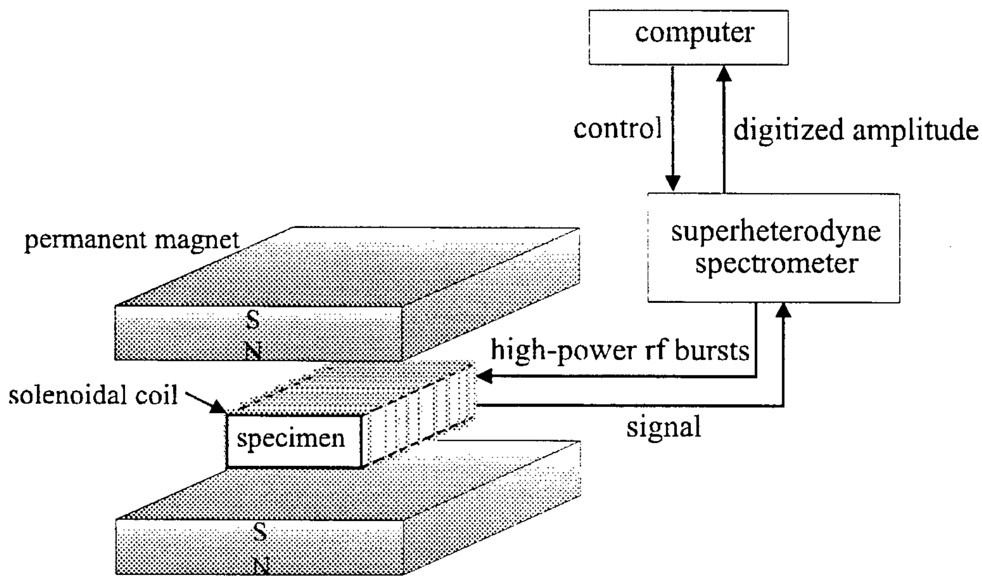

Fig.1 Typical EMAR-measurement setup

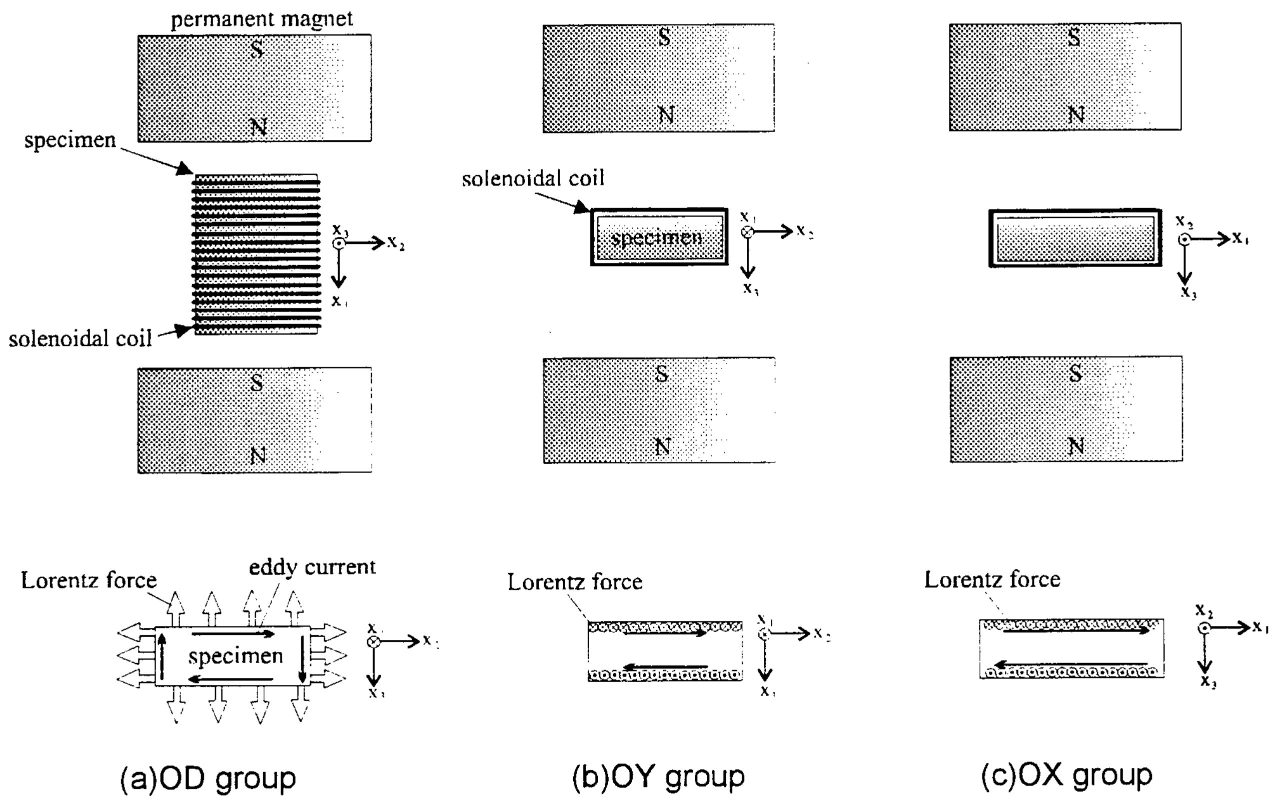

Fig.2 Selection of vibration group with EMAR.

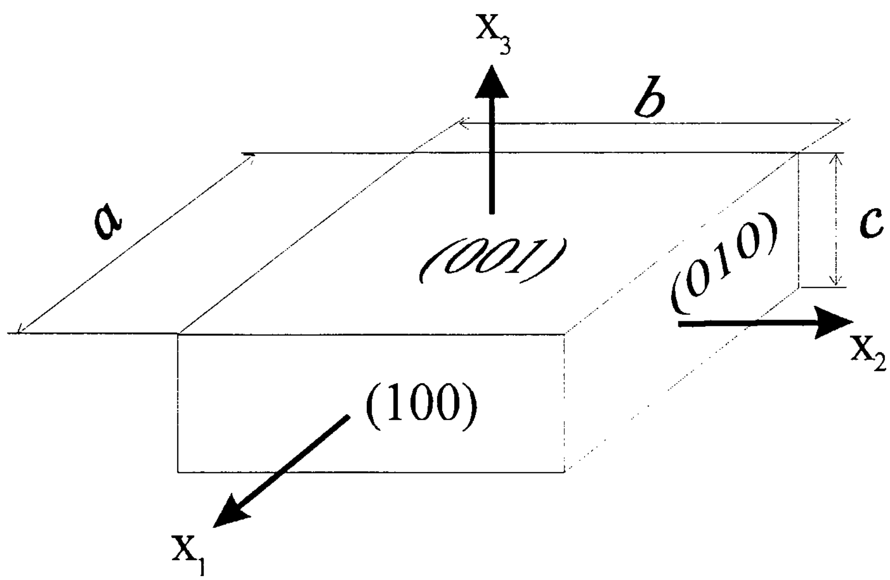

a= 6.195mm, b=6.167 mm, and c=3.404 mm

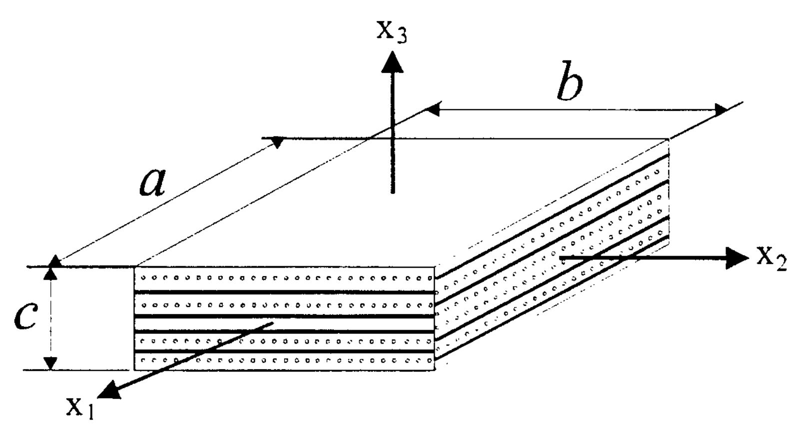

a= 4.977 mm, b=4.015 mm, and c=1.905 mm

Fig. 3 Copper monocrystal (upper) and SiC_f/Ti-6Al-4V crossply composite (bottom).

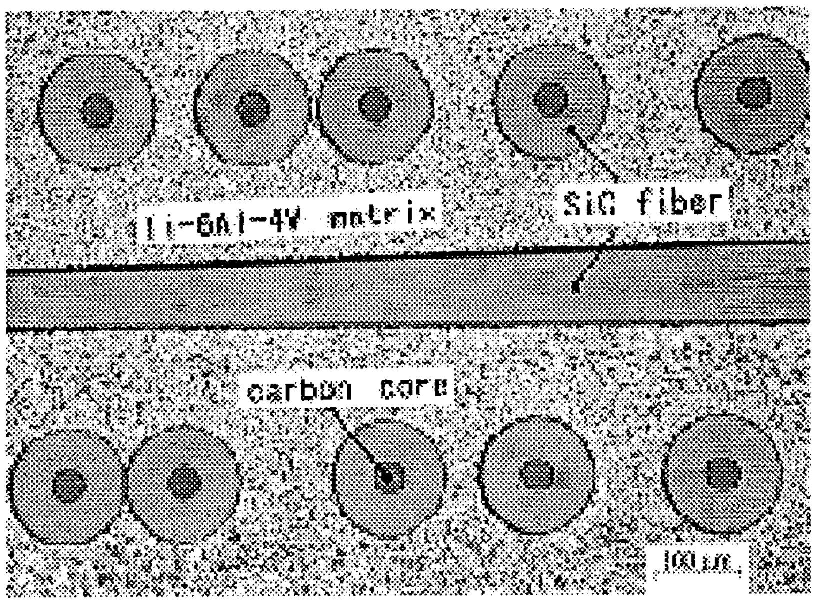

Fig. 4 Microstructure of SiC_f/Ti-6Al-4V crossply composite.

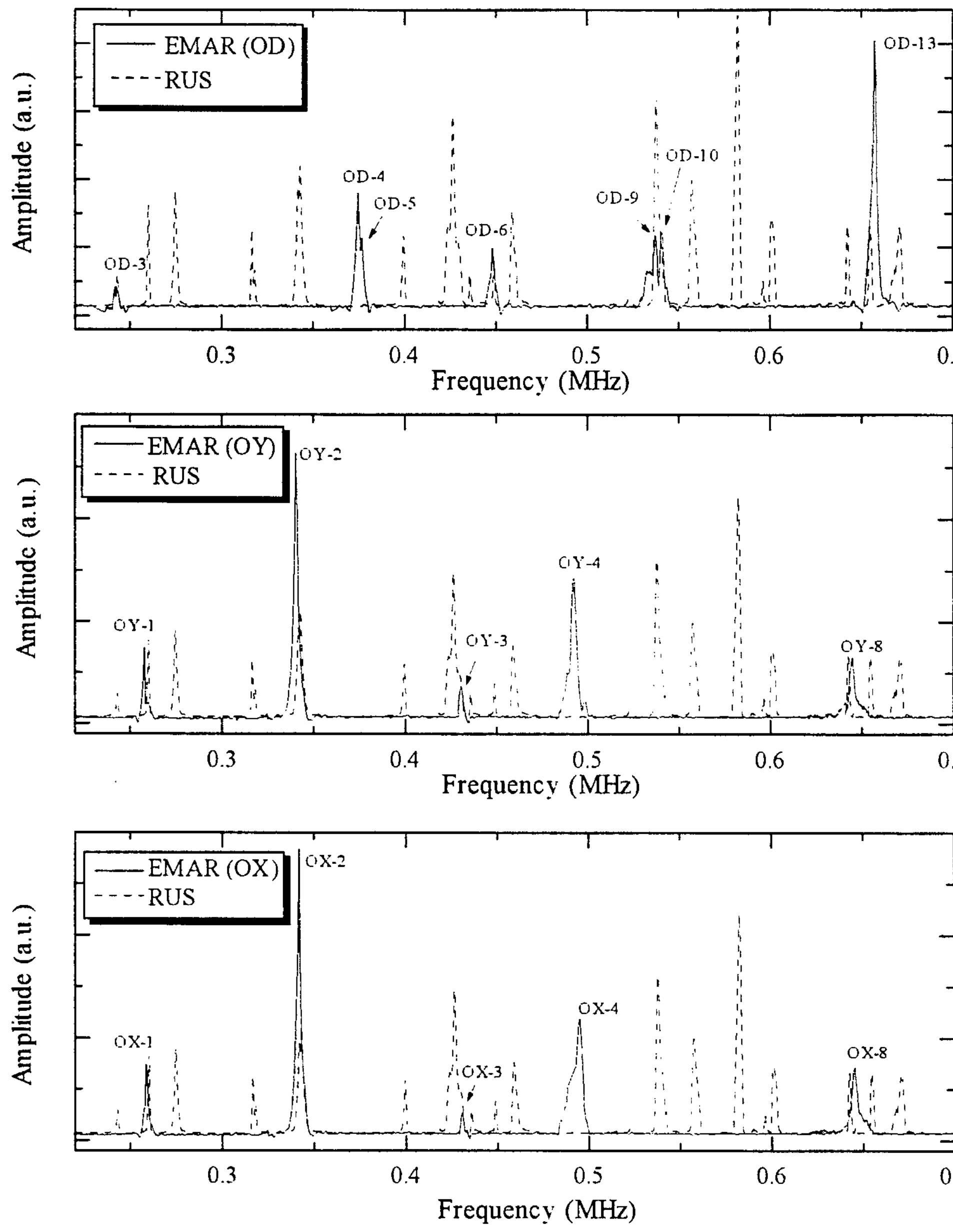

Fig. 5 Resonance spectra for the copper monocrystal measured by RUS and EMAR.

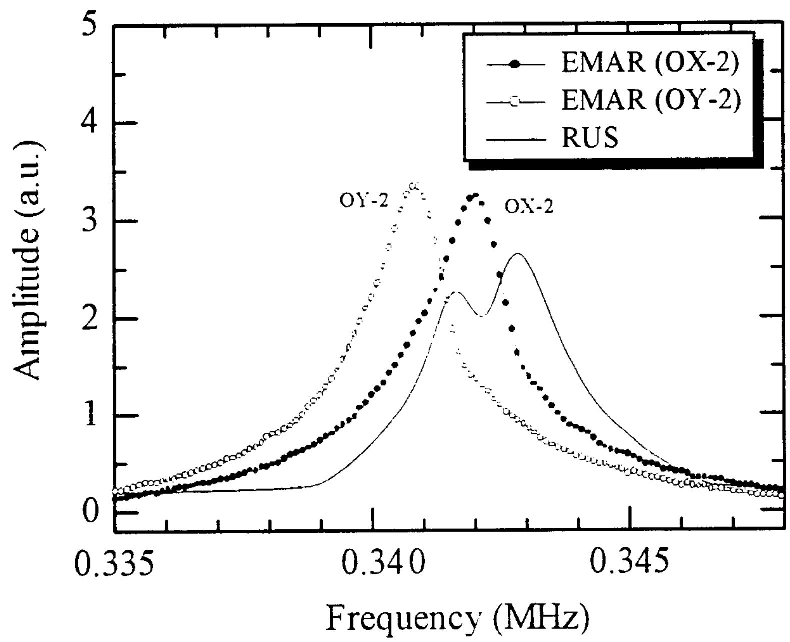

Fig. 6 EMAR and RUS spectra for the copper monocrystal.

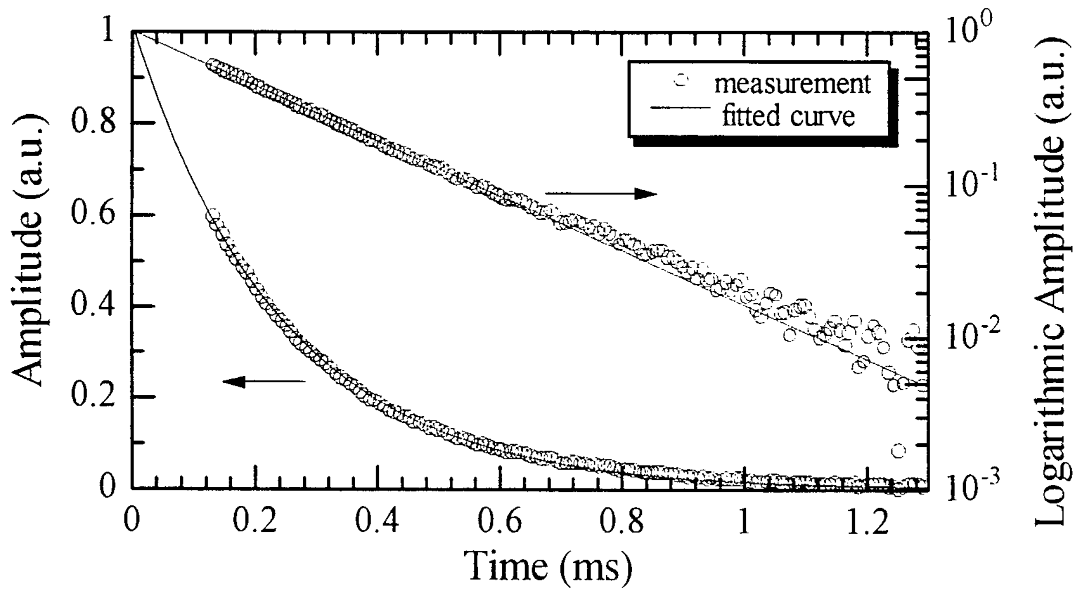

Fig. 7 Amplitude decay and fitted exponential curve for internal friction (copper monocrystal).

Table I Elastic constants and internal friction of a copper monocrystal determined by EMAR and RUS.

	C_{ij}(GPa)				Q_{ij}^{-1} (10^{-3})	
	EMAR	RUS	Ref. 1	Ref. 2	EMAR	RUS
C_{11}	167	168.7	169.7	168.4	1.14	1.74
C_{12}	120.9	121.6	122.6	121.4	0.3	1.34
C_{44}	74.64	75.46	74.49	75.4	2.59	2.46
$B=(C_{11}+2C_{12})/3$	136.2	137.3	137.3	137.1	0.64	1.5
$C'=(C_{11}-C_{12})/2$	23.05	23.52	23.35	23.5	3.34	2.8
$C_{110.110}=(C_{11}+C_{12}+2C_{44})/2$	218.6	220.6	220.6	220.3	1.4	1.87
$C_{111.111}=(C_{11}+2C_{12}+4C_{44})/3$	235.7	237.9	237.6	237.7	1.47	1.9
$C_{111.arb}=(C_{11}-C_{12}+C_{44})/3$	40.25	40.84	40.54	40.8	2.88	2.59
C_L	199.6	201.6	-	-	1.34	1.84
G	47.54	48.22	-	-	2.83	2.57
E	127.8	129.5	-	-	2.6	2.46
ν	0.3437	0.3428	-	-	-	-

1. H. Ledbetter and S. Kim, Personal communication, unpublished.
2. R. Hearmon, Adv. Phys., 5, 323 (1956).

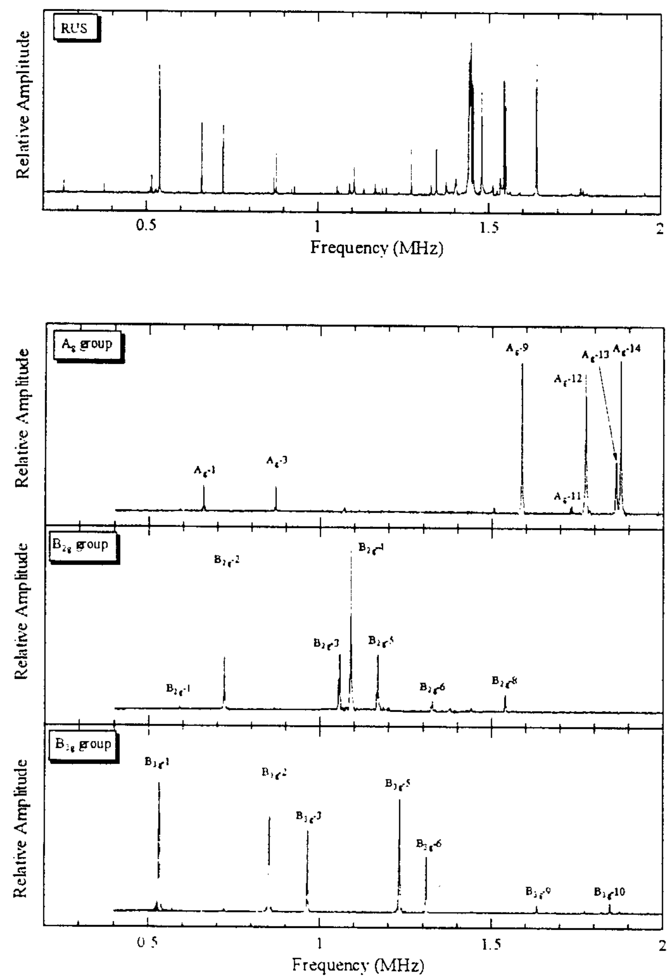

Fig. 8 Resonance spectra of SiC_f/Ti-6Al-4V crossply composite measured by EMAR and RUS methods.

Table II Elastic constants (GPa) and internal friction of SiC_f/Ti-6Al-4V crossply composite measured by EMAR, RUS, and pulse-echo methods.

	EMAR	RUS	pulse echo	EMAR	EMAR*	Q^{-1}_{ij} (10^{-4})
C_{11}	225.4	230.4	–	221.7	222.1	7.79
C_{33}	191.6	185.8	188	182.6	183.3	15.6
C_{44}	54.58	54.98	53.7	54.6	54.63	9.33
C_{66}	51.00	51.73	–	53.02	52.08	6.33
C_{12}	80.82	85.14	–	74.2	74.36	16.1
C_{13}	79.16	80.9	–	71.29	71.65	23.7
E_{11}	180.6	182.3	–	182.7	183.1	3.54
E_{33}	149.7	142.1	–	146.8	147.3	9.59
B	124.5	126.7	–	117.7	118.1	15.2

* Determined from OD and OY vibration groups.

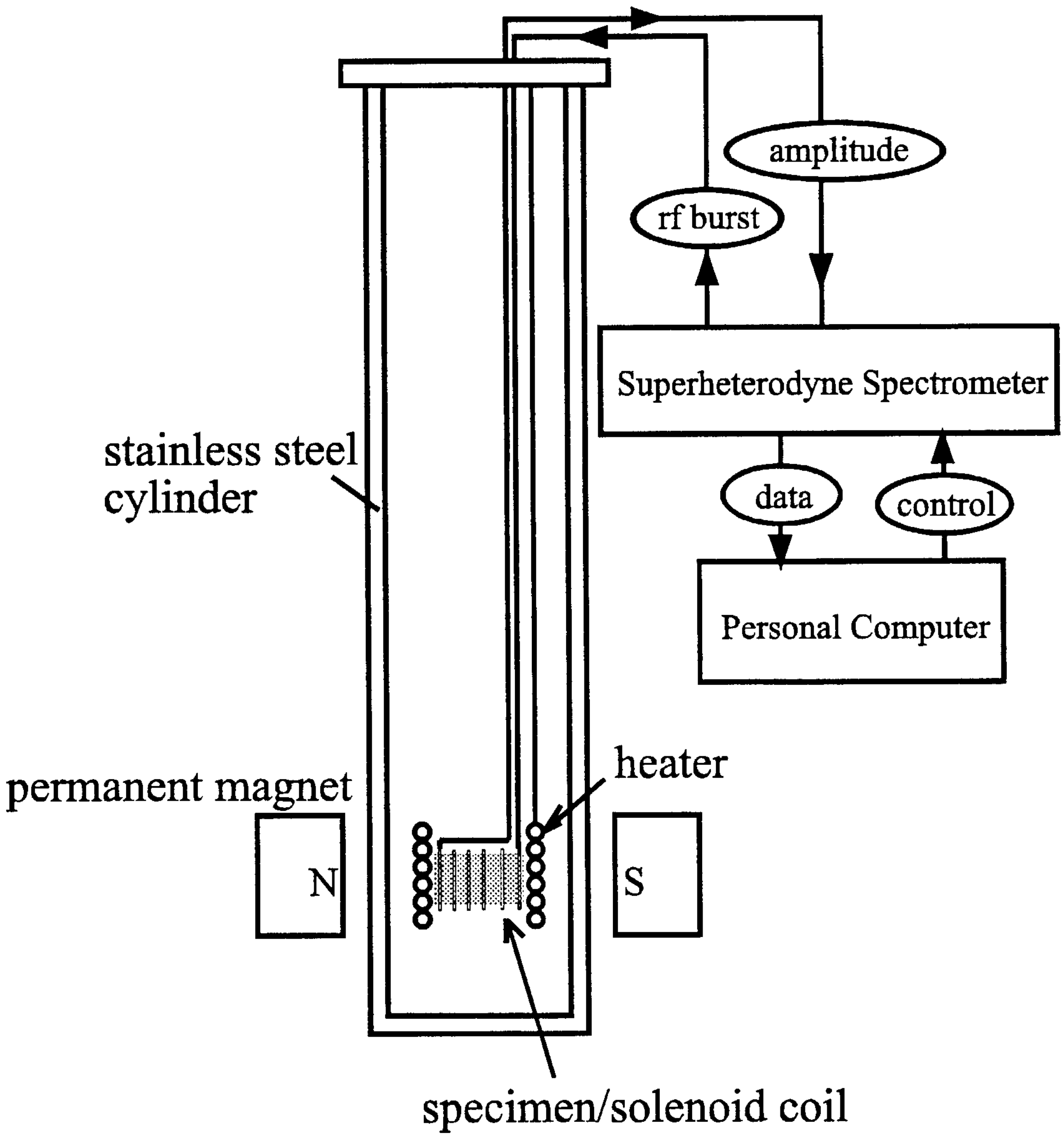

Fig. 9 EMAR measurement setup at elevated temperatures.

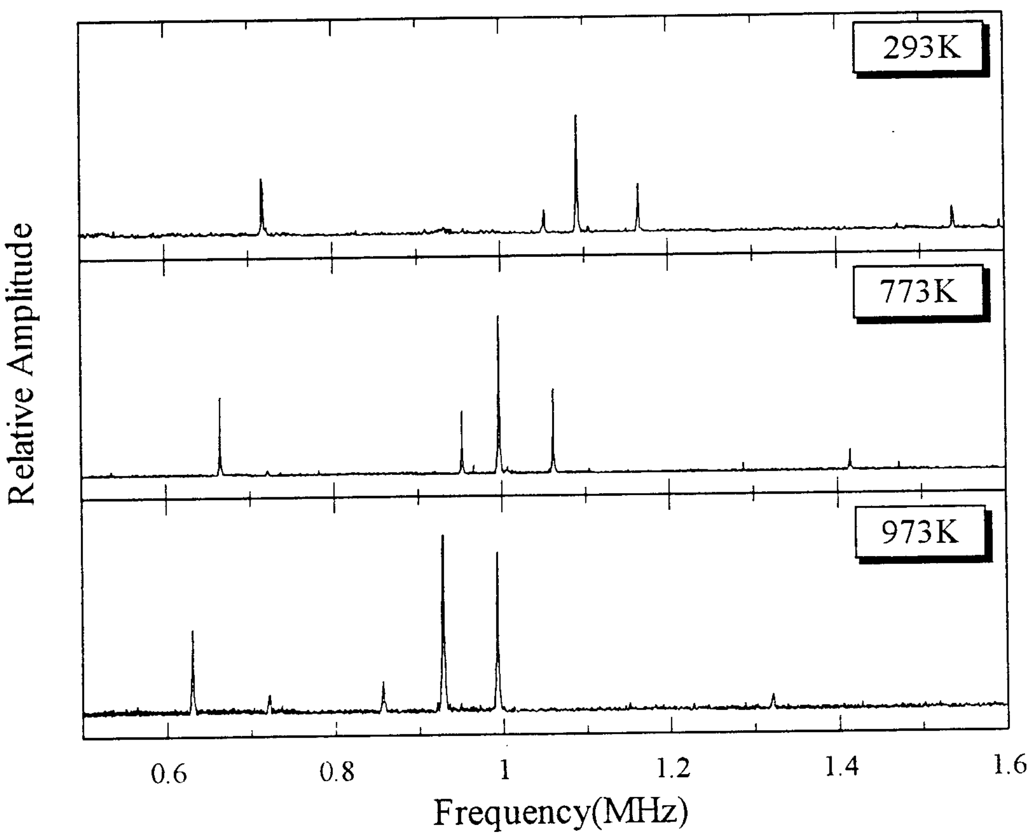

Fig. 10 EMAR spectra of OY group at various temperatures for SiC_f/Ti-6Al-4V crossply composite.

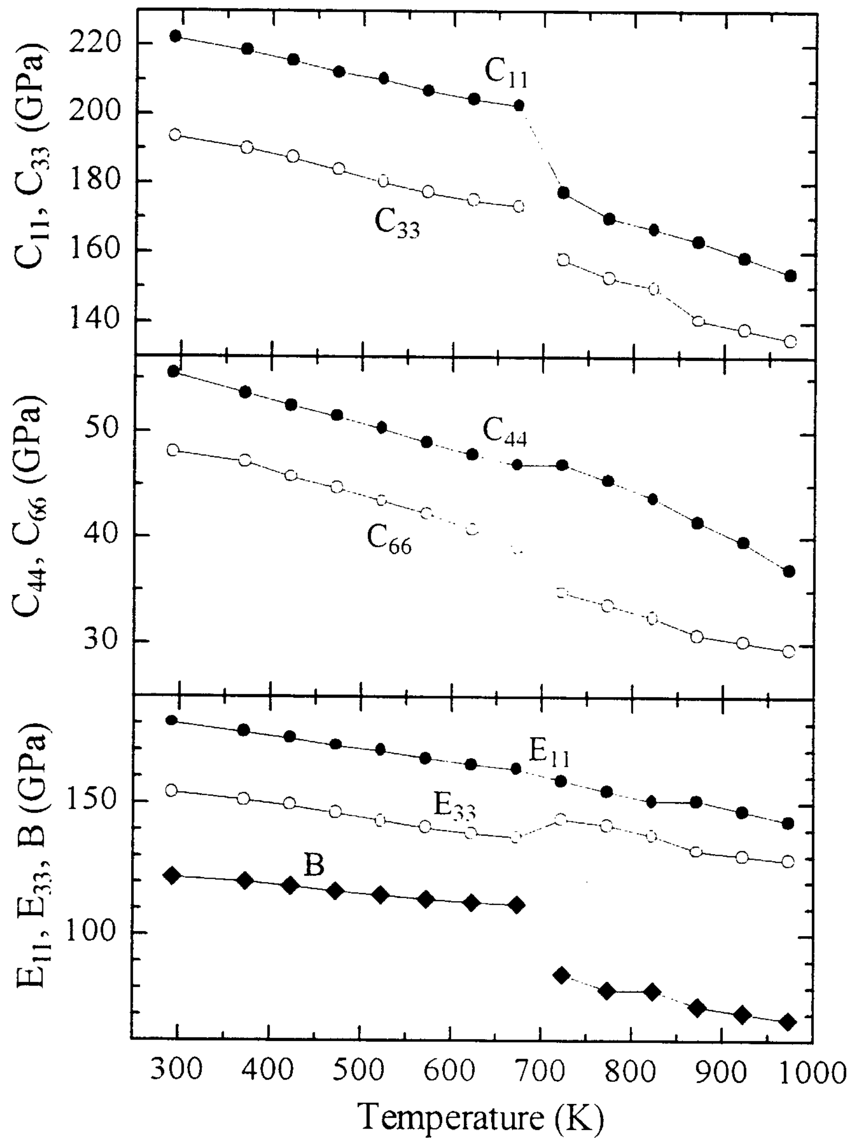

Fig. 11 Temperature dependence of elastic constants of SiC_f/Ti-6Al-4V crossply composite.

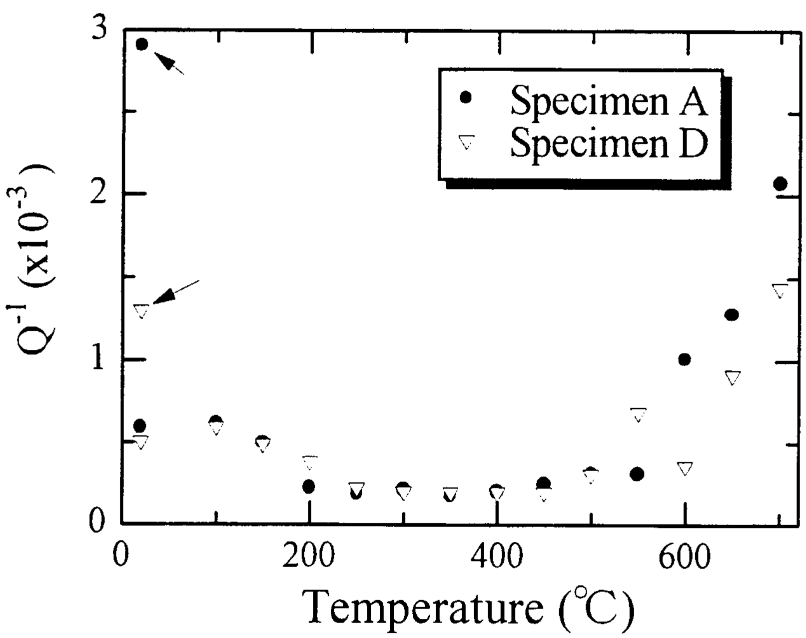

Fig. 12 Temperature dependence of internal friction of a OY mode of SiC_f/Ti-6Al-4V crossply composite. Arrows indicate internal friction after cooling down to room temperature.

Elastic Coefficients and Internal Friction Of Silicon Monocrystal Spheres

Hassel Ledbetter
NIST, Boulder, Colorado

Monocrystal silicon

.low impurity content
.low dislocation density
.used in international standards efforts
    .silicon mole
    .kilogram
    .Avogadro's number

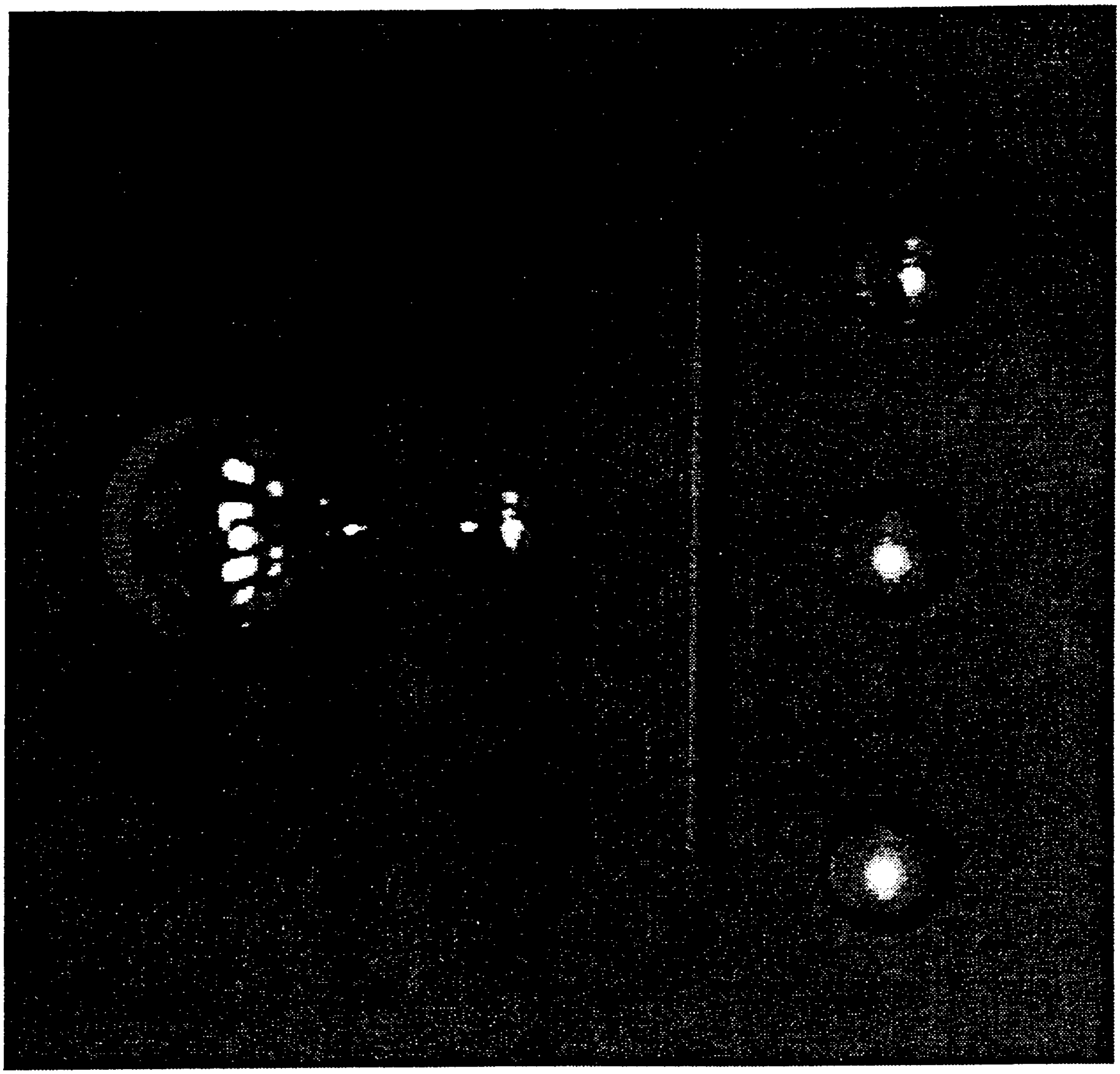

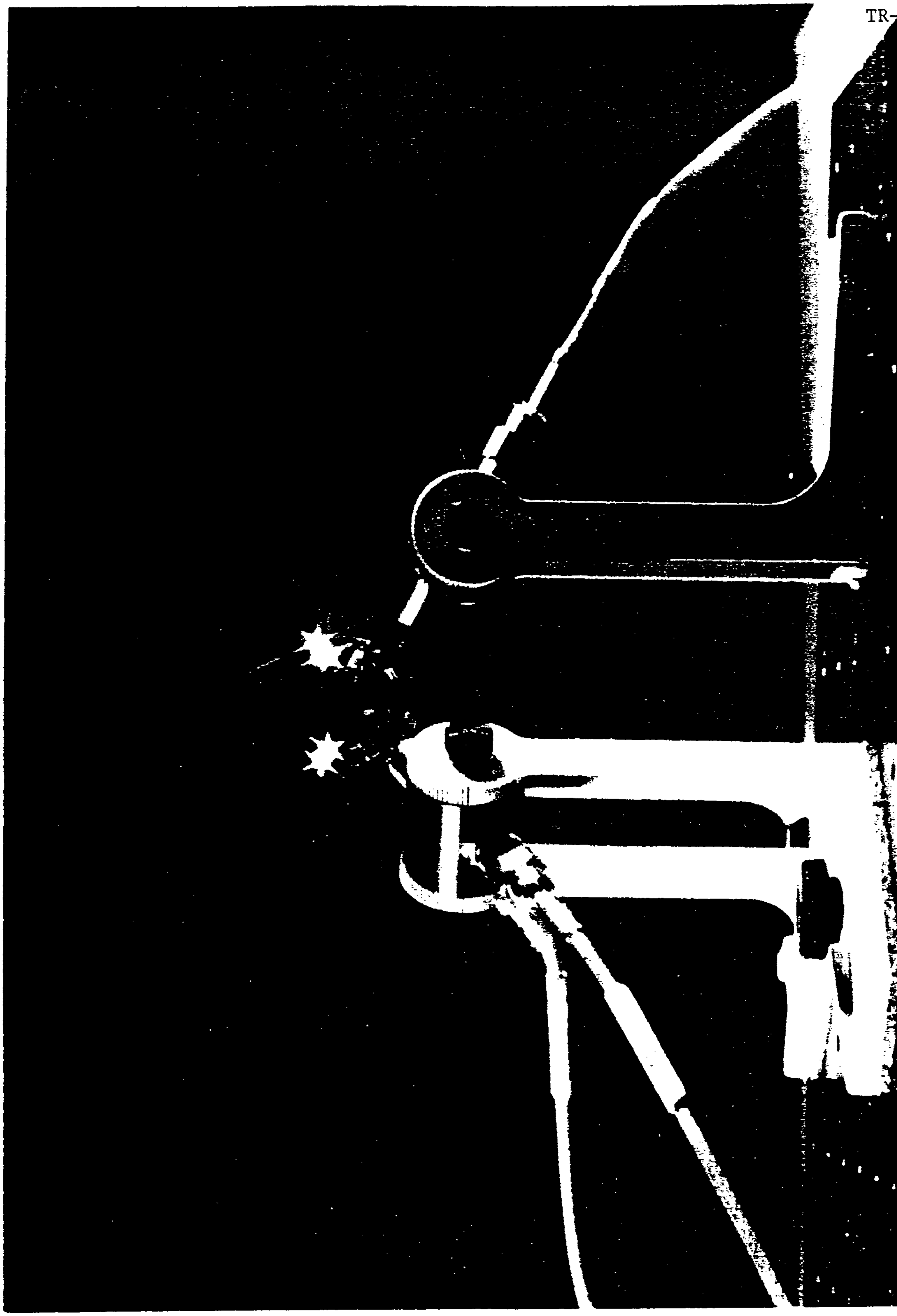

Specimen T2

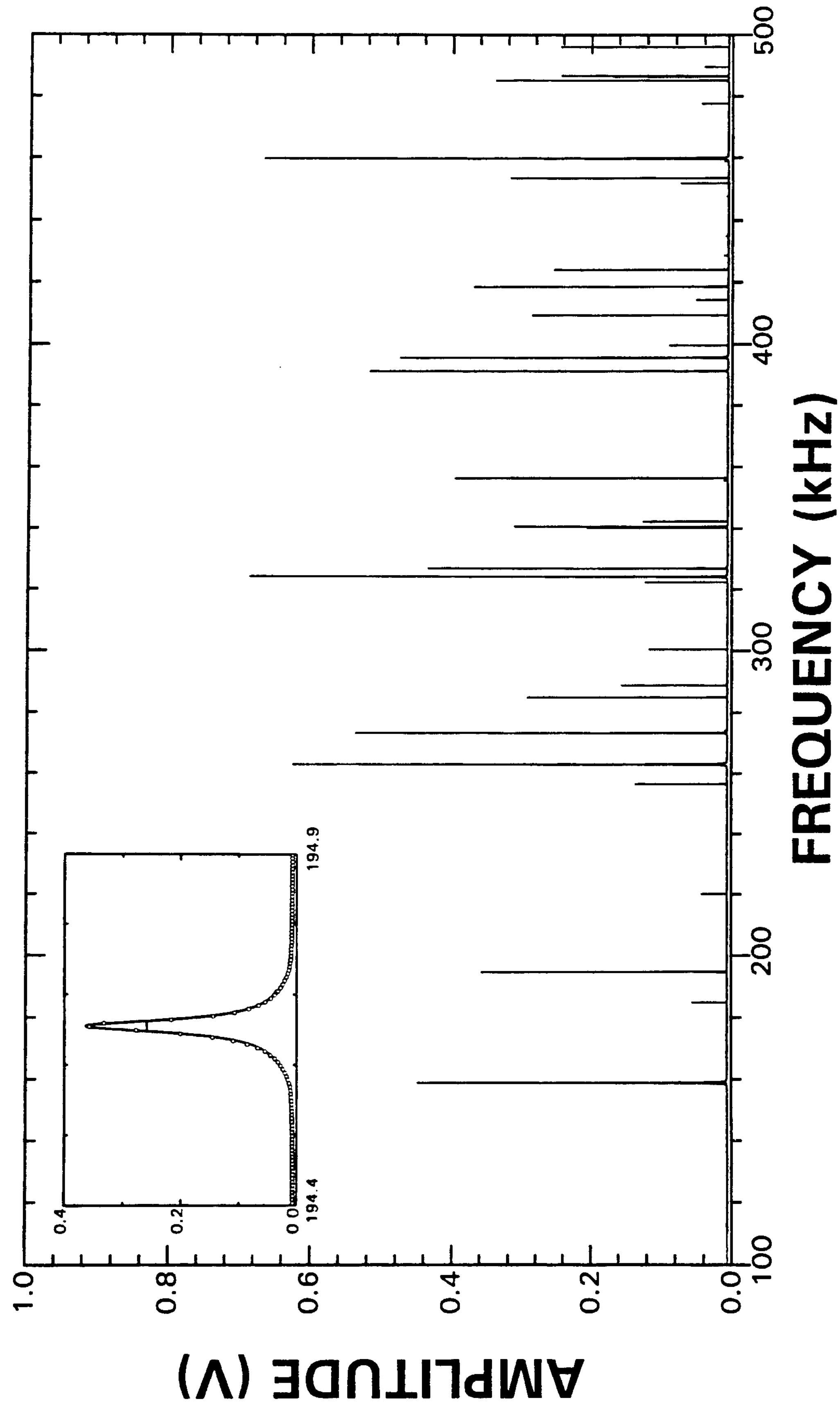
AMPLITUDE (V)
1.0
0.8
0.6
0.4
0.2
0.0
FREQUENCY (kHz)
100
200
300
400
500
0.4
0.2
0.0
194.4
194.9

Si elastic-stiffness coefficients

	K1	K2	K3	T1	T2
T (K)	294.8	294.8	294.8	298.4	299.3
ρ (g/cm^3)	2.33275	2.33292	2.33219	2.32903	2.32999
C_{11} (GPa)	165.73 ±0.03	165.73 ±0.03	165.69 ±0.03	165.58 ±0.05	165.67 ±0.02
C_{12} (GPa)	63.917 ±0.03	63.919 ±0.04	63.914 ±0.03	63.840 ±0.04	63.924 ±0.03
C_{44} (GPa)	79.596 ±0.008	79.579 ±0.008	79.584 ±0.008	79.550 ±0.02	79.577 ±0.008
C' (GPa)	50.906	50.905	50.890	50.868	50.875
$C_{110,110}$ (GPa) = $(C_{11}+C_{12}+2C_{44})/2$	194.42	194.40	194.39	194.26	194.33
$C_{111,111}$ (GPa) = $(C_{11}+2C_{12}+4C_{44})/3$	203.98	203.96	203.95	203.82	203.94
$C_{111,110}$ (GPa) = $(C_{11}-C_{12}+C_{44})/3$	60.469	60.463	60.455	60.429	60.442
B (GPa)	97.854	97.856	97.841	97.752	97.840
G (GPa)	66.604	66.595	66.589	66.561	66.578
E (GPa)	162.86	162.84	162.83	162.74	162.81
C_L (GPa)	186.66	186.65	186.63	186.50	186.61
ν	0.22260	0.22261	0.22265	0.22249	0.22270
rms (%)	0.021	0.023	0.019	0.026	0.016

Source: S. Kim, H. Ledbetter, NIST—Boulder.

26 MAY 1999

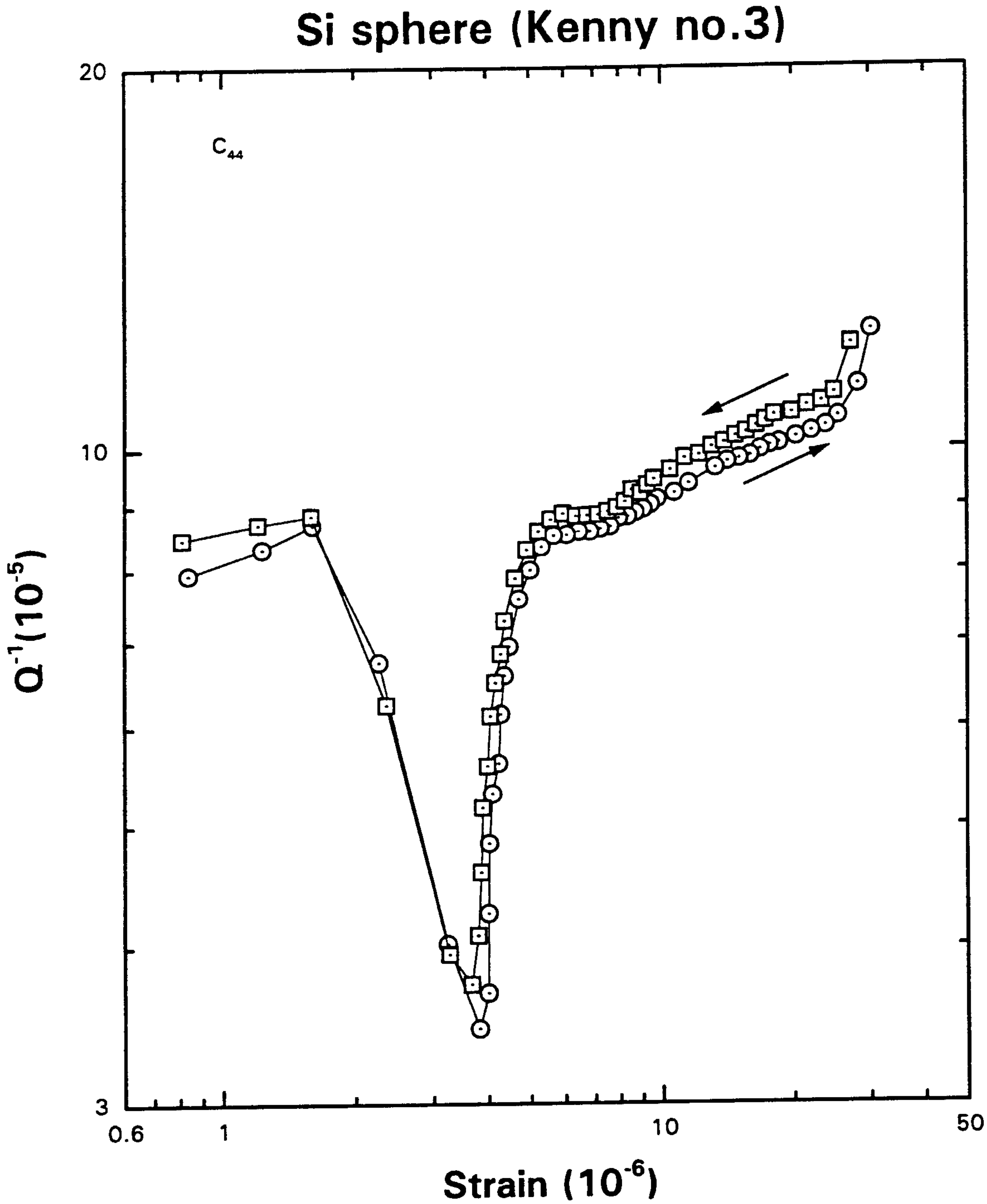

19 MAR 1999
Sikenny3.c44.lqe

From the Koehler–Granato–Lücke stretched-vibrating-string model, we have for low frequencies (in modified form) :

$$Q^{-1} = \frac{576\Omega(1 - \nu)^2 \Lambda L^4 kT\omega}{\pi^3 \rho v_t^3 a^4} .$$

Here Ω denotes an orientation factor, ν is Poisson's ratio, Λ dislocation density, L dislocation-loop length, k Boltzmann's constant, T temperature, ω circular frequency, ρ mass density, v_t shear-wave sound velocity, and a unit-cell dimension.

Granato-Lücke model

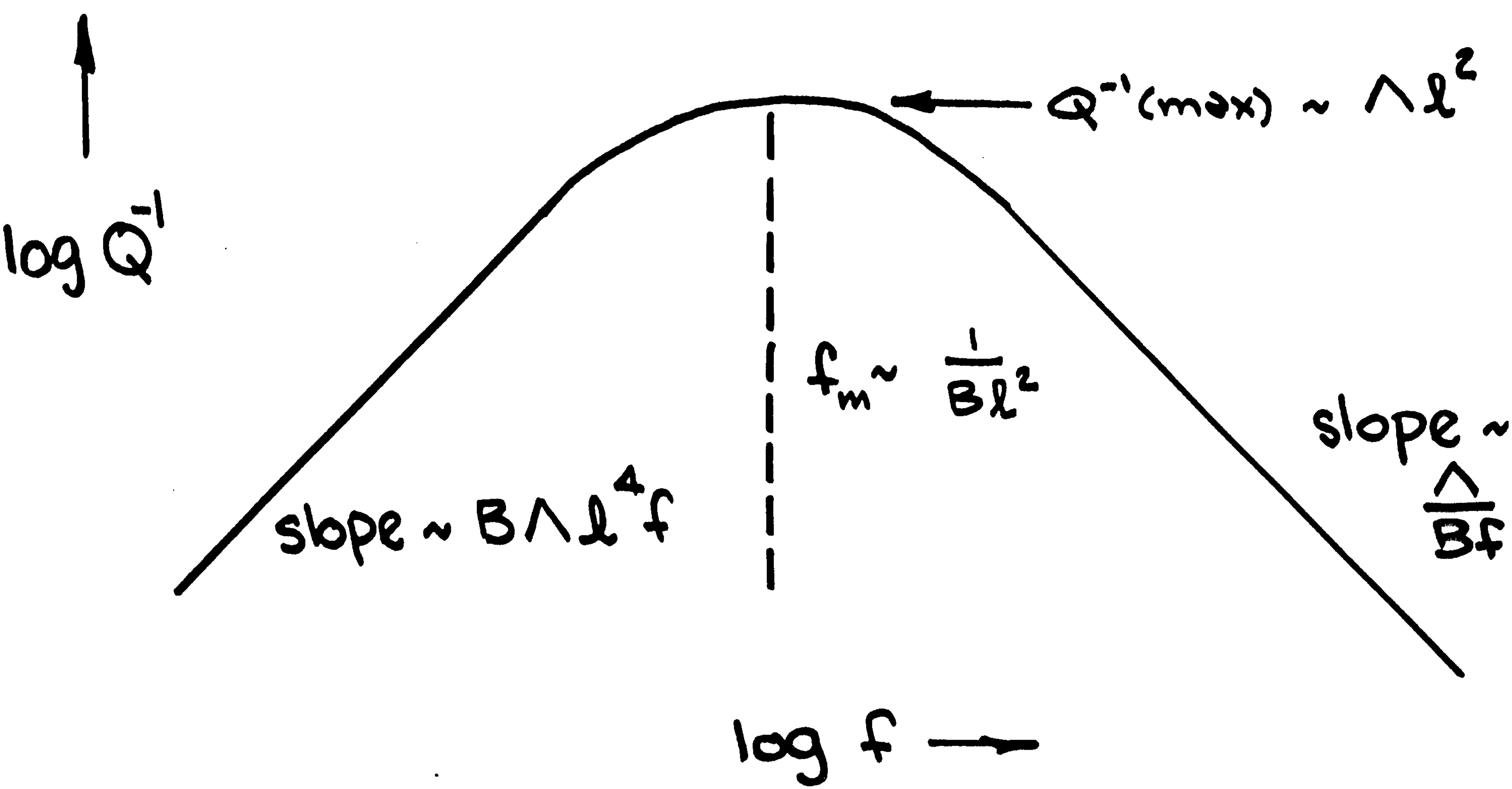

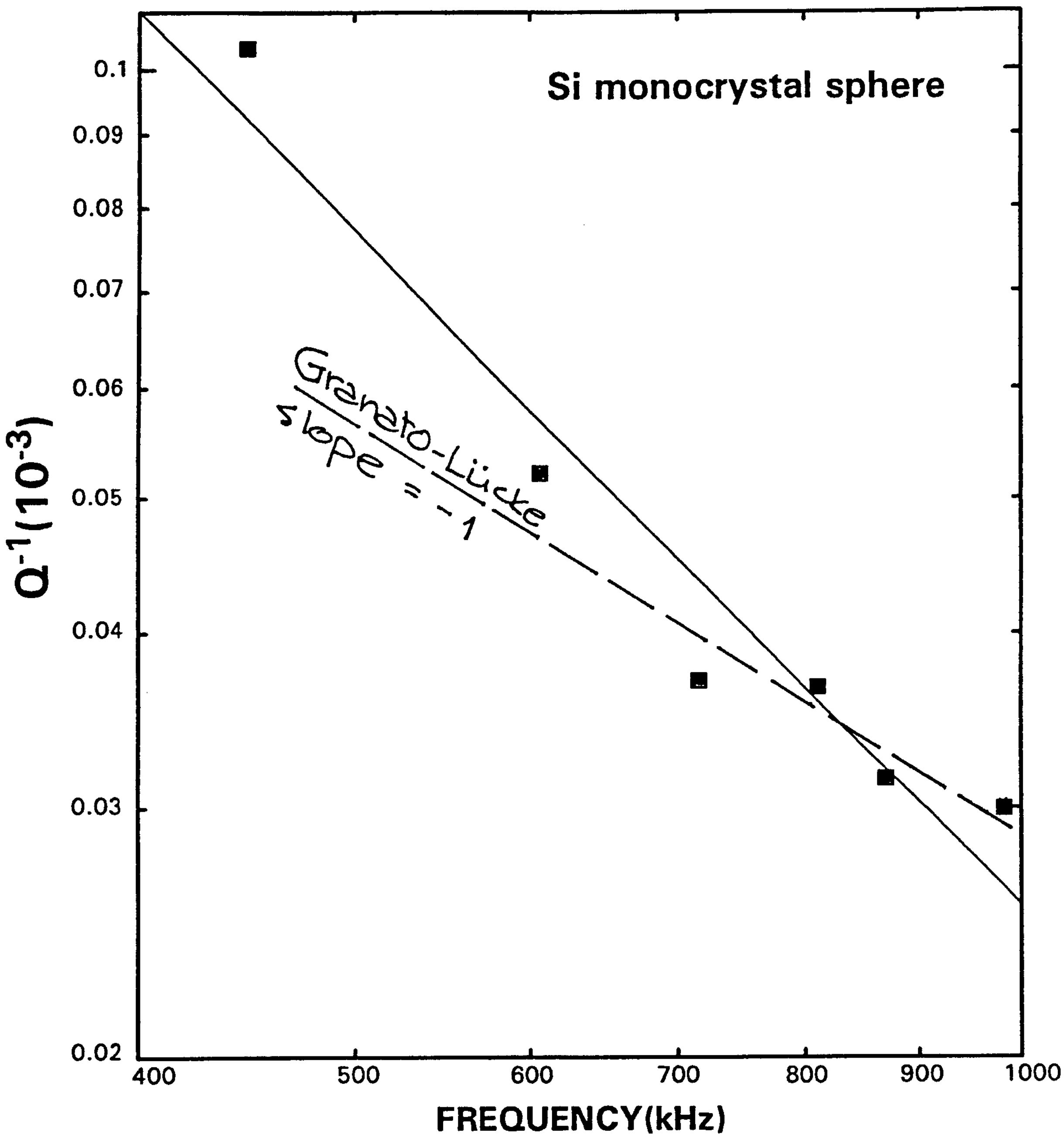

Y = 3.188- 1.593 X

7 Oct 1996

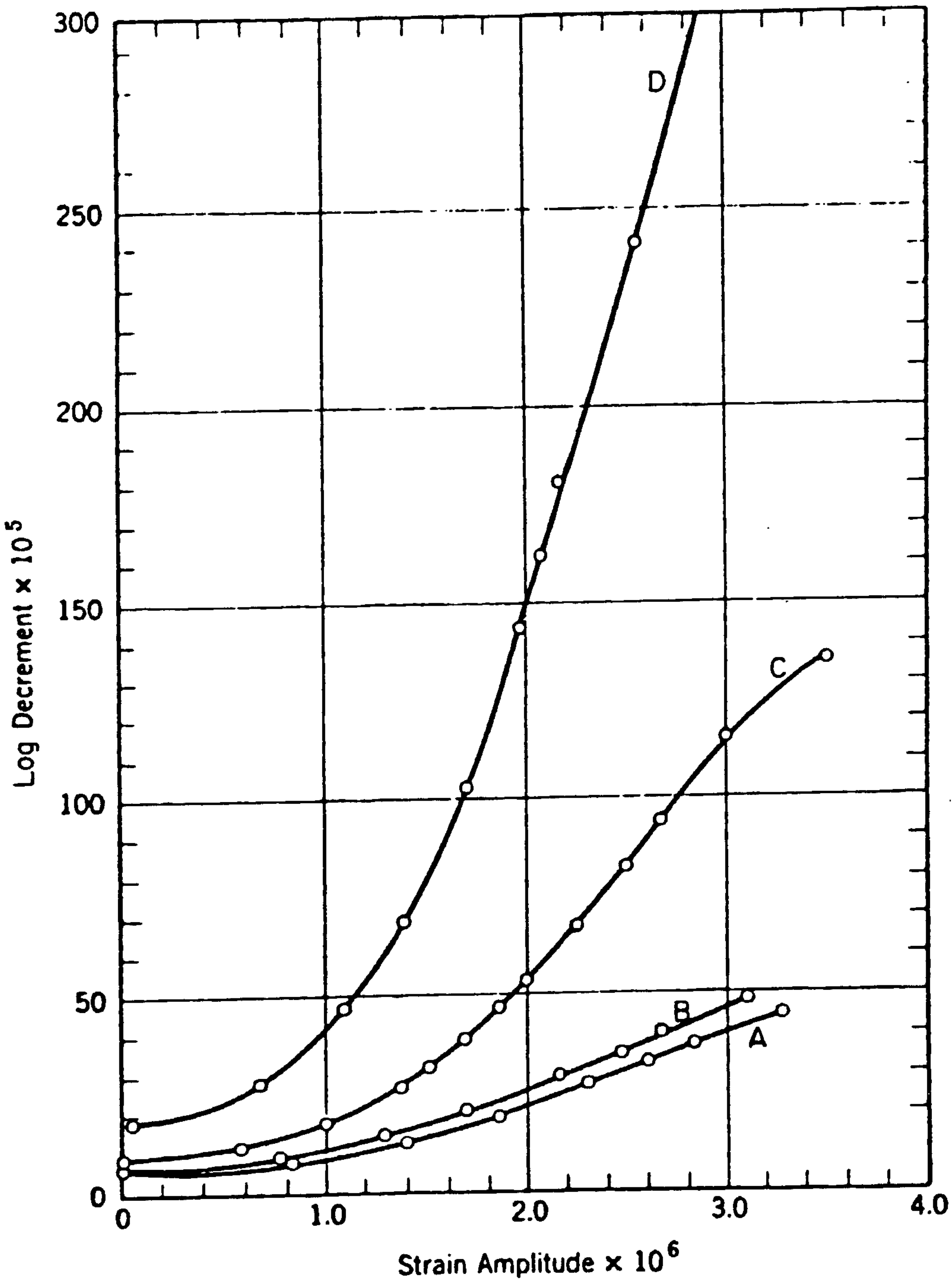

FIG. 14-1. Internal friction as a function of strain amplitude for an undeformed copper crystal (curve A) and after application of stresses of 60, 120, and 150 psi, respectively (curves B, C, and D). Measurements in longitudinal vibration at about 30 kHz. (From Read, 1941.)

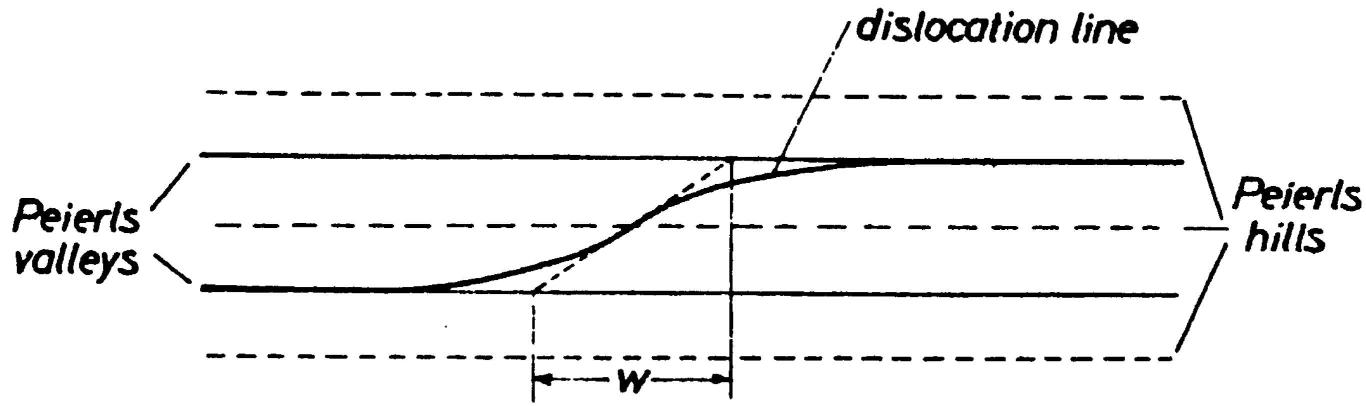

FIG. 3. Kink in a dislocation line at the transition from one Peierls valley tc neighboring valley. w = kink width.

Seeger, Schiller (1966)

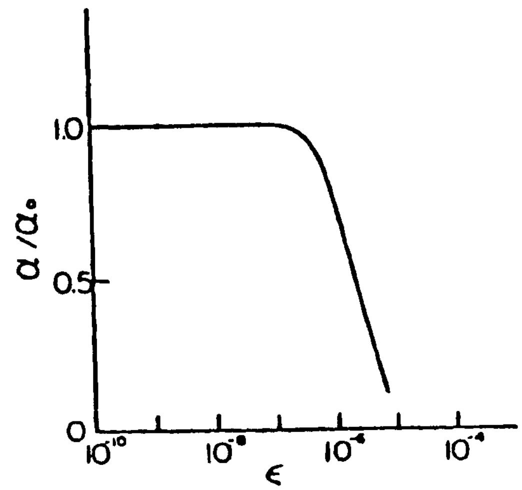

FIG. 4. The ratio of the ultrasonic attenuation α at finite strain amplitude to the attenuation α_0 at infinitely small strain amplitude, when $l=2d_0=2\times10^{-5}$ cm and $\omega=2\pi10^5\ \mathrm{sec}^{-1}$.

Suzuki, Elbaum (1964)

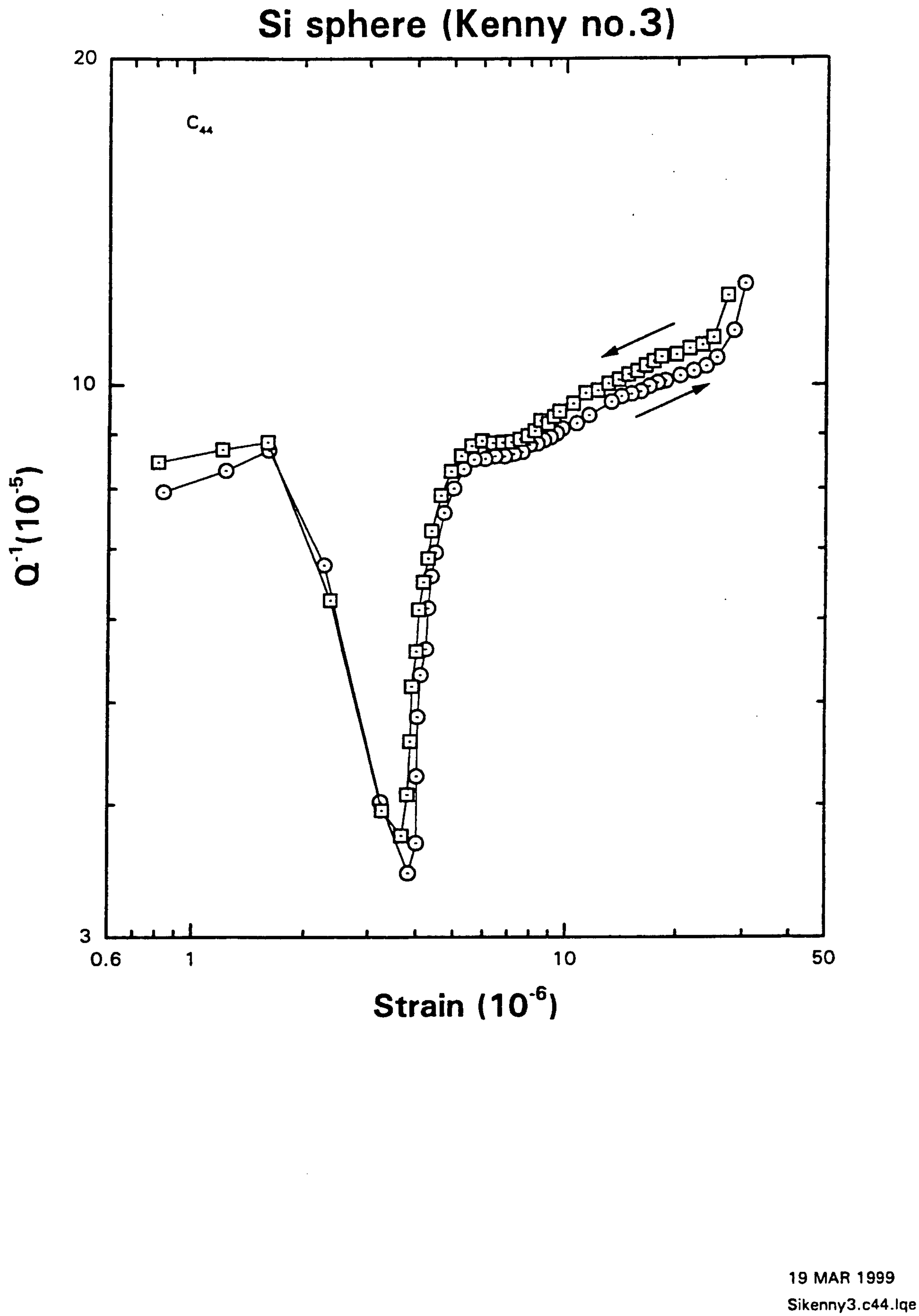
Si sphere (Kenny no.3)
C_{44}
20
10
3
$Q^{-1}(10^{-5})$
0.6
1
10
50
Strain (10^{-6})
19 MAR 1999
Sikenny3.c44.lqe

CONCLUSIONS

1. Within 1 in 1000, new-silicon C_{ij} agree with old-silicon C_{ij}.
2. At low strains, dislocation kinks contribute most of Q^{-1}.
3. At high strains, Koehler-Granato-Lücke depinned string-model dislocations contribute most to Q^{-1}.

Elastic Constants and Internal Friction of Quartz and Langasite

Ming Lei*
Dynamic Resonance Systems, Powell, Wyoming

Hassel Ledbetter
National Institute of Standards and Technology, Boulder, Colorado

Resonance Workshop, Oxford, Mississippi, June 1999

*Now at Lucent, Denver

	Langasite	**Quartz**
Phase transform.	-----	573°C
Q^{-1} (10^{-5})**	17.3	12.6
ϵ_{11}	168	39
ϵ_{33}	460	41
e_{11} (C/m^2)	–0.43	–0.173
e_{14} (C/m^2)	0.11	0.04
k^2	4.2	2.5

***Equivalent designations: P321, D_3^2, hP9.**

****First torsional mode of a cylinder.**

Table 1. Langasite and Quartz: basic properties

	Langasite	Quartz
Formula	$La_3Ga_5SiO_{14}$	SiO_2
Mass density (g/cm^3)	5.744	2.6500
Point (space) group	Trigonal 32 (150)*	Trigonal 32 (150)
Atoms/cell	23	9
C_{11} (GPa)	186.1	87.05
C_{33} (GPa)	259.8	106.9
V_{11} (cm/μs)	0.5692	0.5731
V_{33} (cm/μs)	0.6725	0.6328

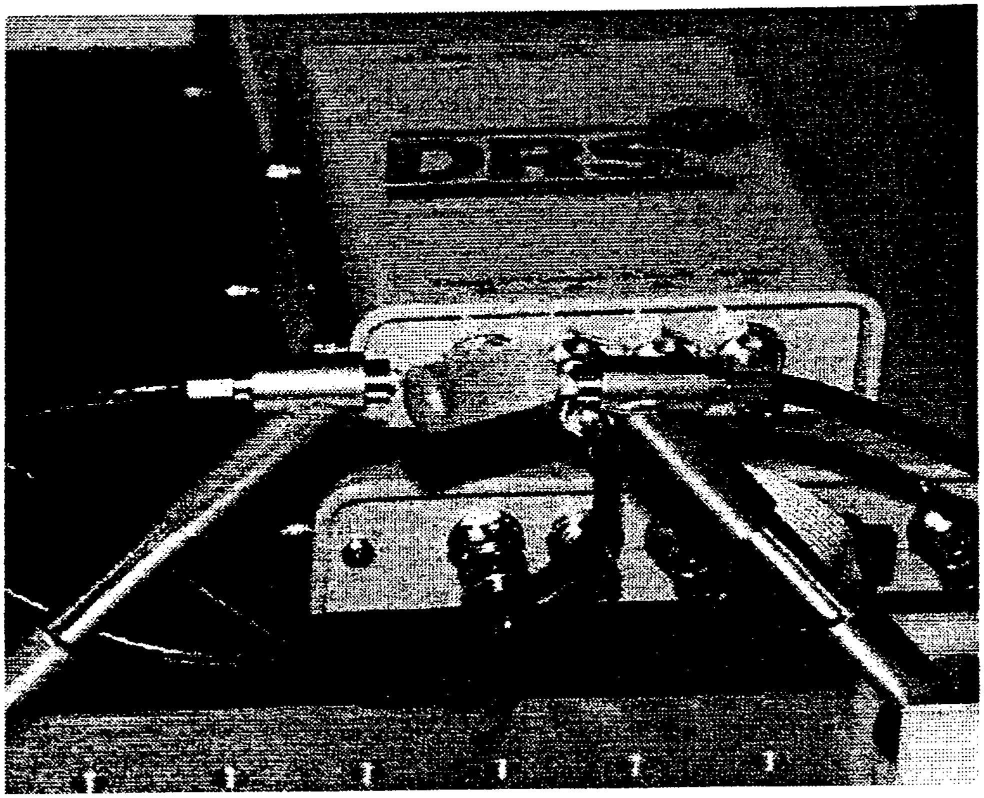
DRS

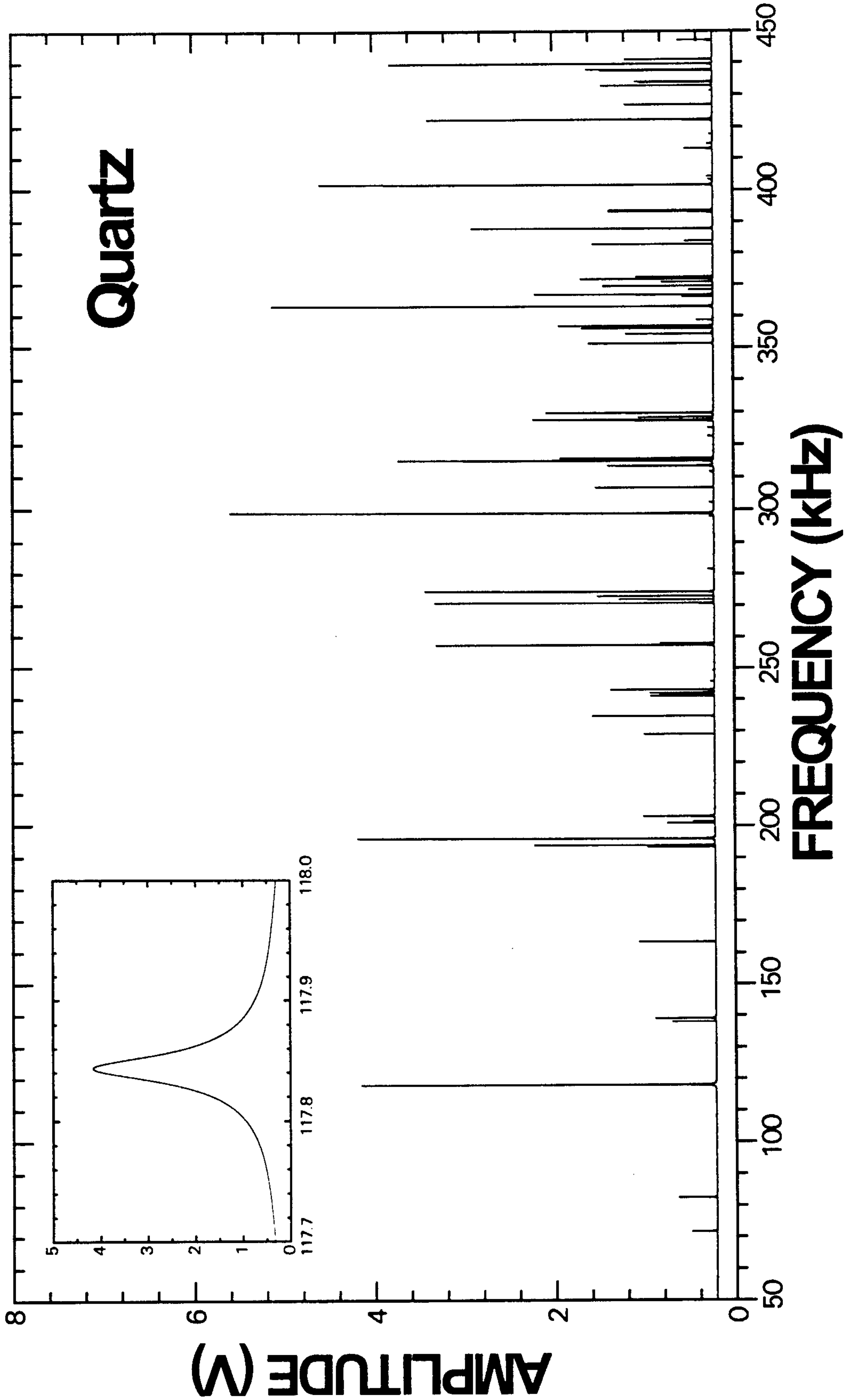
Quartz
FREQUENCY (kHz)
AMPLITUDE (V)
0
2
4
6
8
50
100
150
200
250
300
350
400
450
117.7
117.8
117.9
118.0
0
1
2
3
4
5

Quartz elastic-stiffness coefficients

	Present	Ohno	McSkimin
ρ (g/cm^3)	2.6496	2.648	2.6485
C_{11} (GPa)	87.10	88.1	86.8
C_{33} (GPa)	106.1	104.7	105.75
C_{44} (GPa)	58.26	58.6	58.20
C_{66} (GPa)	40.17	40.25	39.88
C_{12} (GPa)	6.76	8.1	7.04
C_{13} (GPa)	12.17	12.0	11.91
C_{14} (GPa)	-18.07	-18.1	-18.04

26 May 1999

Quartz and Langasite elastic-stiffness coefficients

	Quartz		Langasite	
	C_{ij} (GPa)	$Q_{ij}^{-1}(10^{-3})$	C_{ij} (GPa)	$Q_{ij}^{-1}(10^{-3})$
ρ (g/cm^3)	2.650		5.744	
C_{11}	87.10	-0.09	186.1	0.18
C_{33}	106.1	0.66	259.8	0.27
C_{44}	58.26	-0.07	53.87	0.07
C_{66}	40.17	-0.17	42.68	0.03
C_{12}	6.76		100.7	
C_{13}	12.17		93.50	
C_{14}	-18.07		14.08	
rms (%)	0.19		0.26	
C_L (GPa)	100.7	0.11	202.4	0.22
B (GPa)	37.80	0.41	133.0	0.31
G (GPa)	47.18	-0.07	52.00	0.05
E (GPa)	99.94	0.07	138.0	0.08
ν	0.0593		0.3271	

21 June 1999

$$\left| C_{ijkl} + \left[\frac{e_{rij} q_r e_{skl} q_s}{\kappa_{mn} q_m q_n} \right] - \rho v^2 \delta_{ijkl} \right| = 0$$

24 May 1999
File: LGS.F

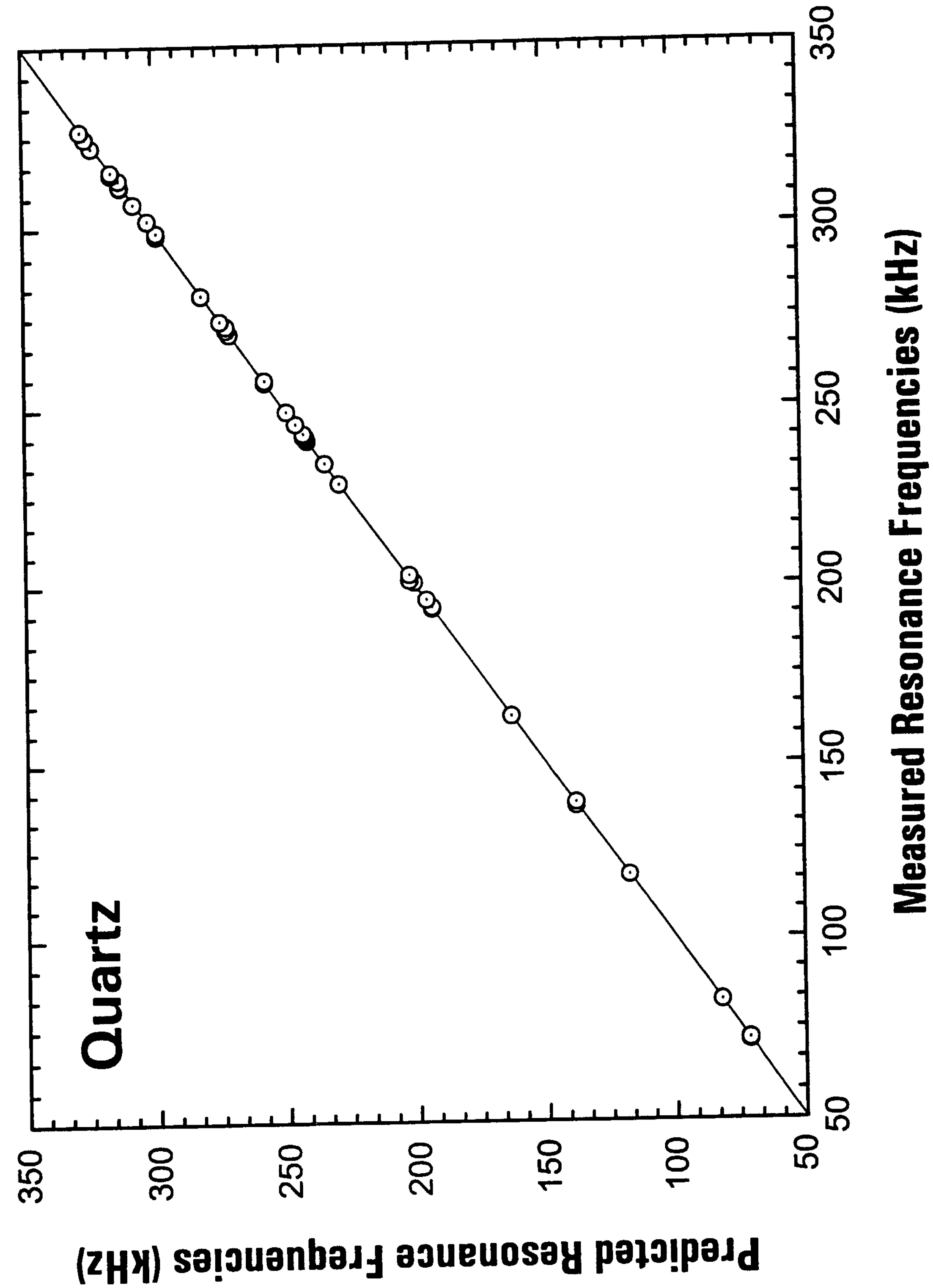

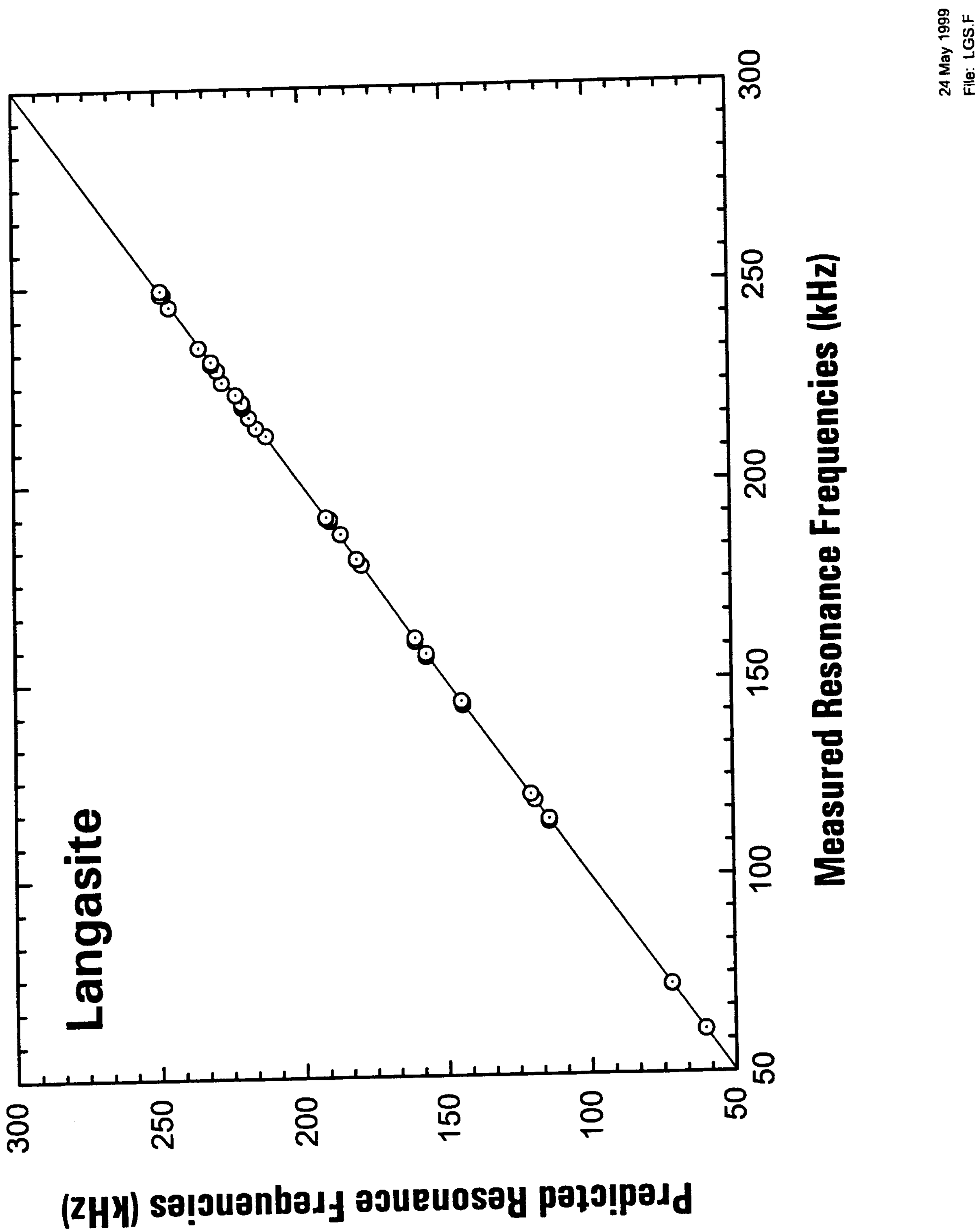
Langasite
Measured Resonance Frequencies (kHz)
Predicted Resonance Frequencies (kHz)
50
100
150
200
250
300
24 May 1999
File: LGS.F

Elastic vs. Piezoelectric Analyses

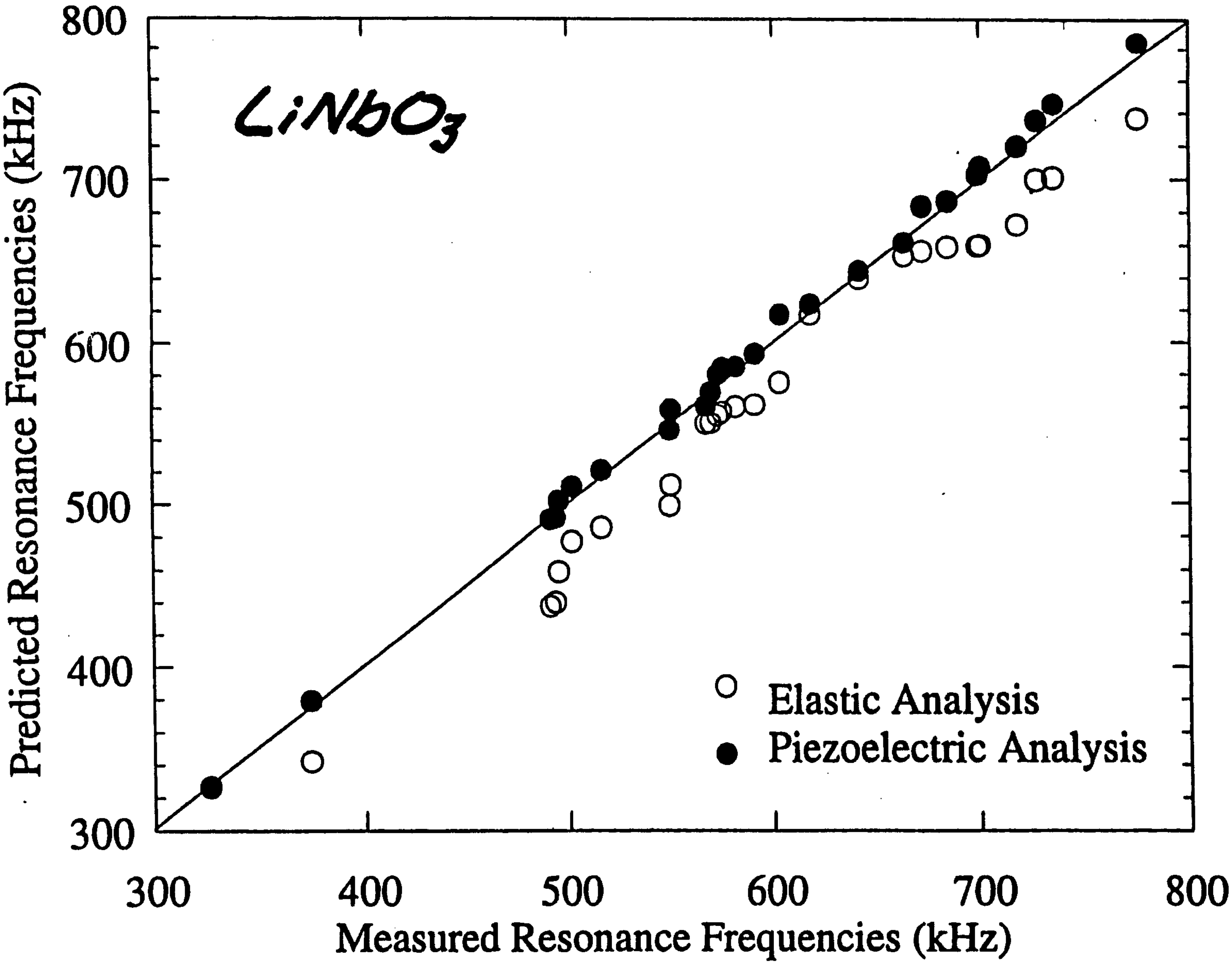

Plans

1. Q_{ij}^{-1} both quartz and langasite.

2. Relationships between Q_{mech} and Q_{elec}.

3. From mechanical spectrum, determine e_{ijk}, especially for $LiNbO_3$.

RUS STUDIES OF CRYPTO-CLATHRATES:

PERFECT CRYSTALS WITH THE ELASTIC PROPERTIES OF GLASSES

Veerle Keppens

K. U. Leuven

and

NCPA, University of Mississippi

Collaborators

ORNL:

B.C. Sales

D. Mandrus

B. C. Chakoumakos

KUL:

C. Laermans

LANL:

A. Migliori

T. Darling

glasses vs. crystals

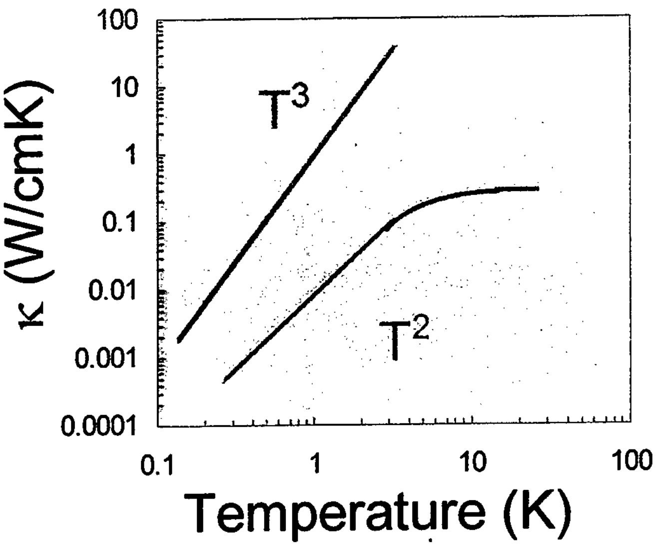

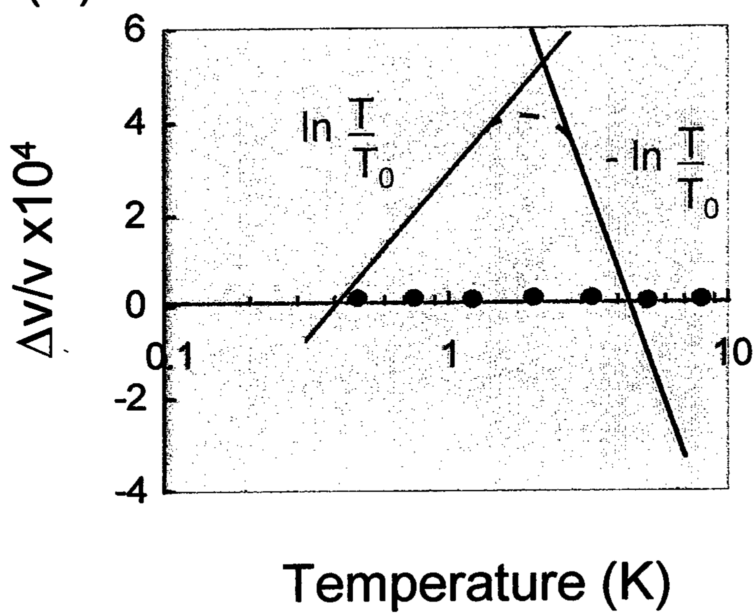

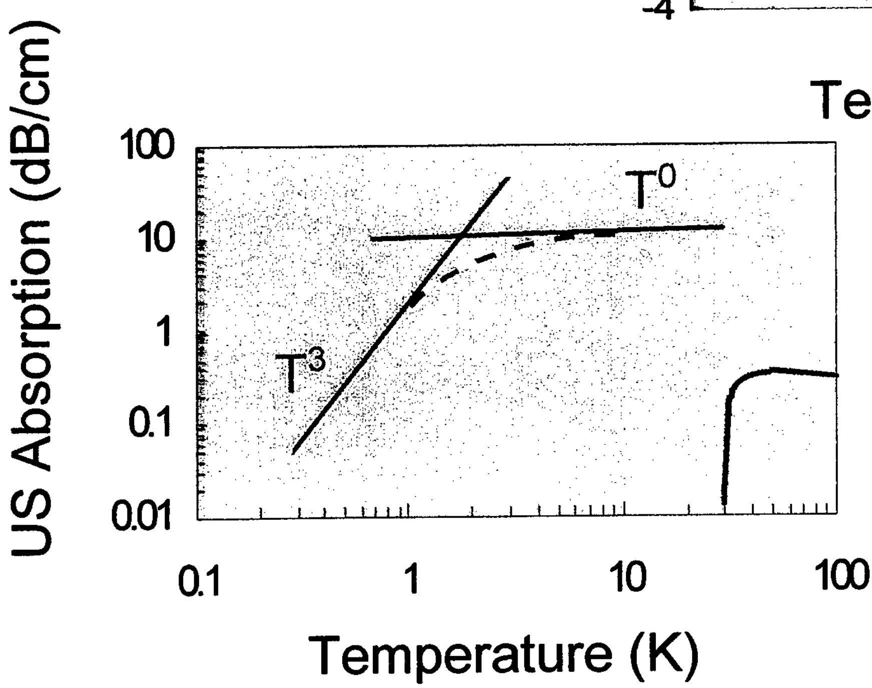

Filled skutterudites: RM_4X_{12}

R=Sr, Ba, La, Ce, Pr, Nd, Eu,Gd, U, Th

M=Ru, Fe, Os

X=P, As, Sb

R-atoms "rattle" in atomic cage

→ reduce $\kappa_{lattice}$

excellent example of "electron-crystal phonon glass"

→ New class of thermoelectric materials

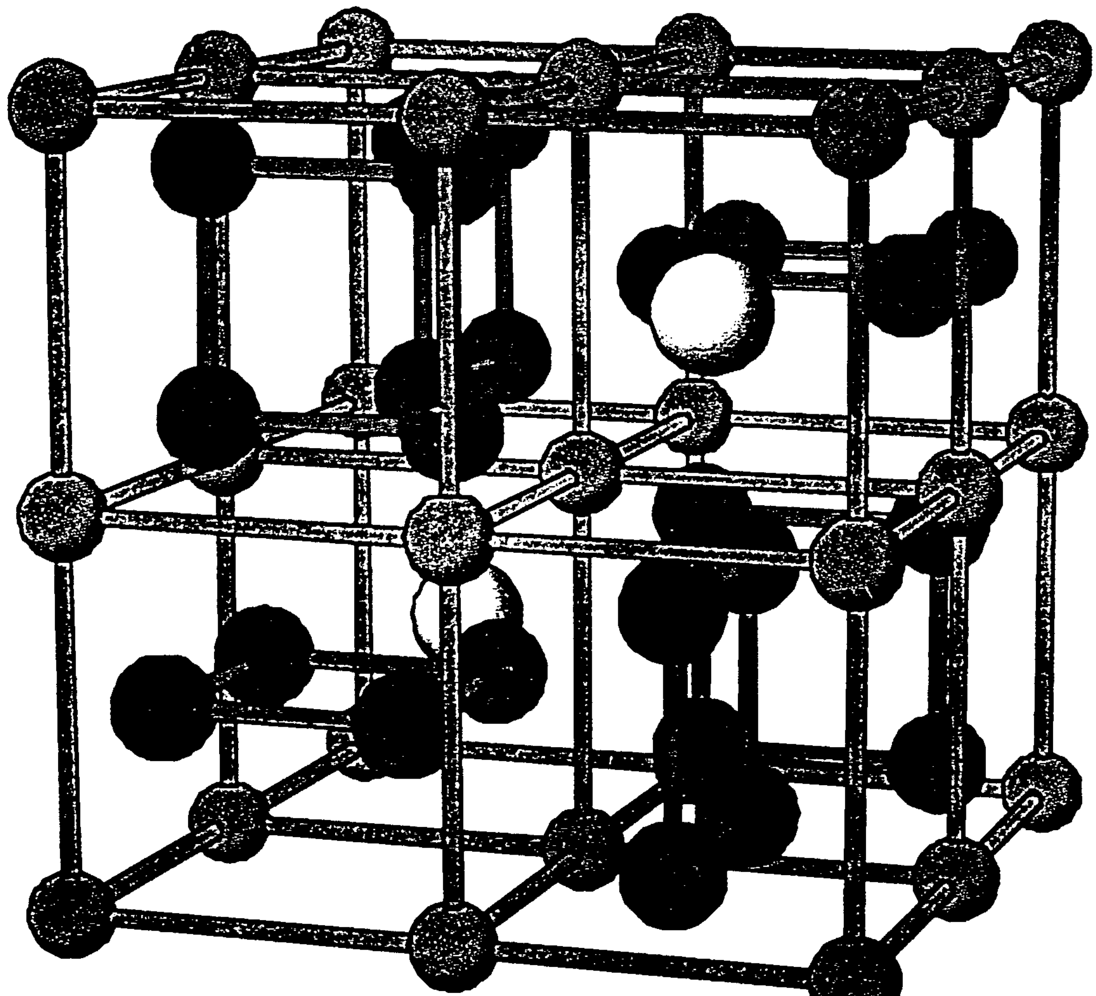

TR-5

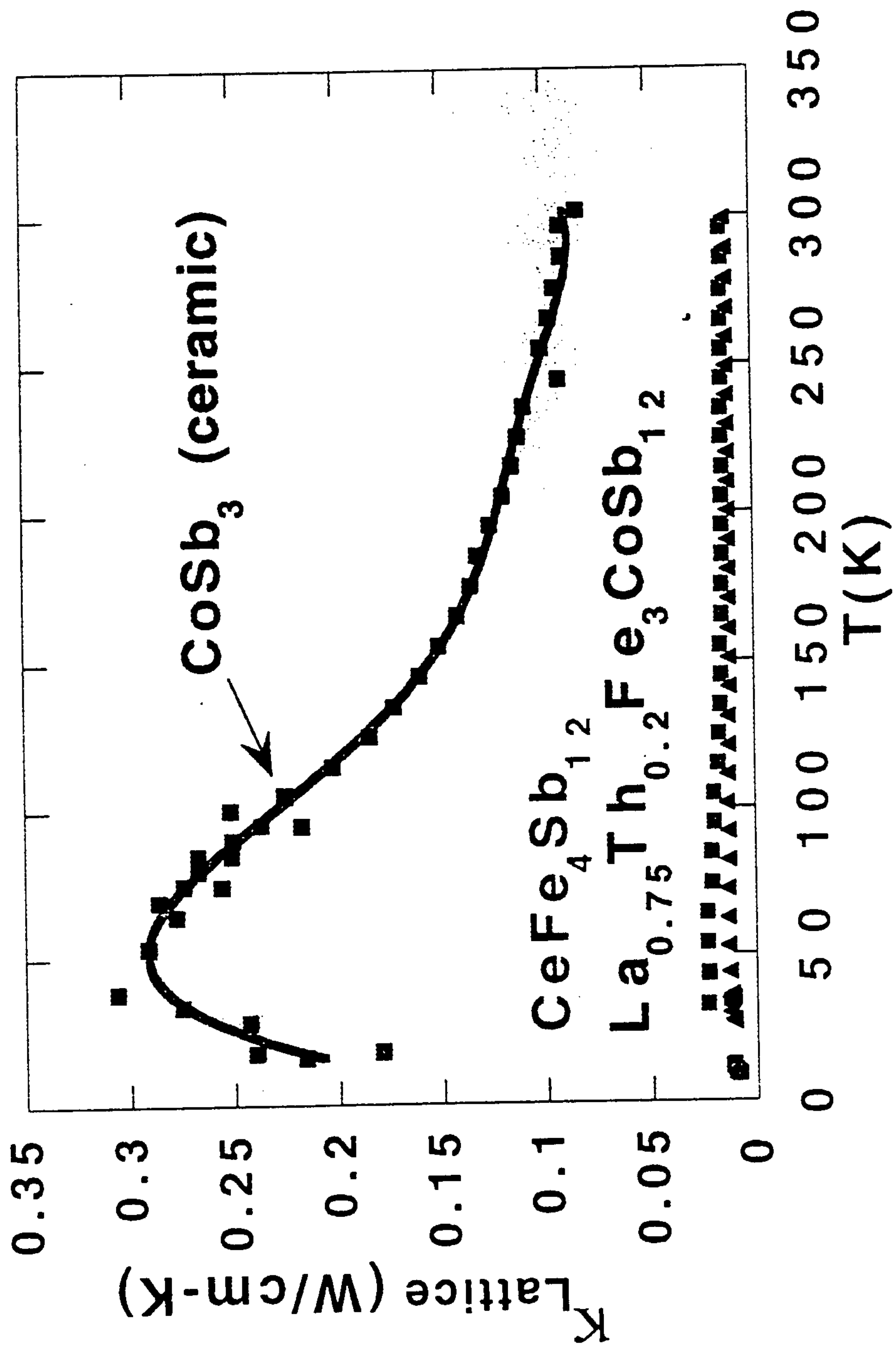

CoSb3 (ceramic)
CeFe4Sb12
La0.75Th0.2Fe3CoSb12
κLattice (W/cm-K)
T(K)
0
0.05
0.1
0.15
0.2
0.25
0.3
0.35
0
50
100
150
200
250
300
350

Clathrates: X_8E_{46}

X = Na, K, Rb, Cs, Sr, Ba
E = Si, Ge, Sn, Al, Ga

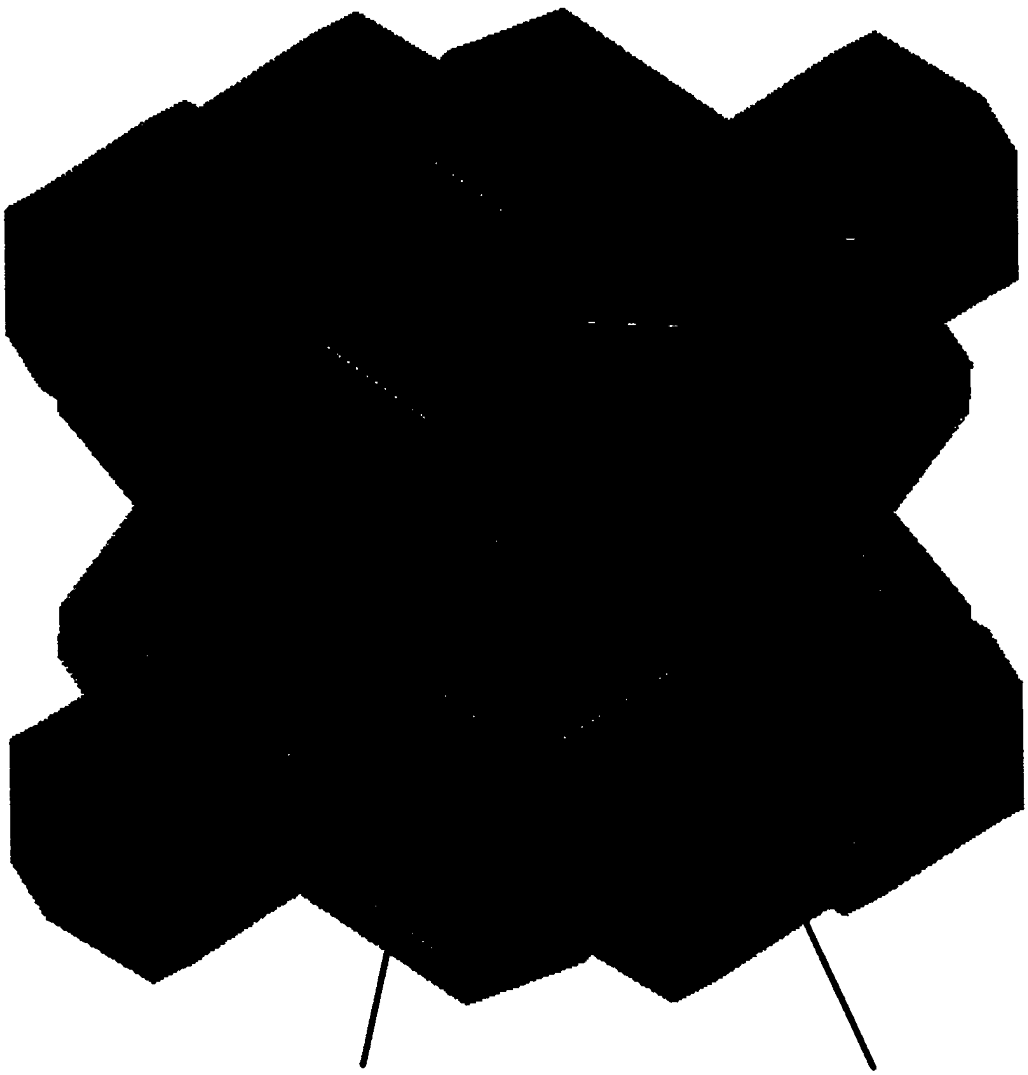

J. L. Cohn, G. S. Nolas, V. Fessatidis,
T. H. Metcalf, and G.S. Slack,
PRL 82, 779 (1999)

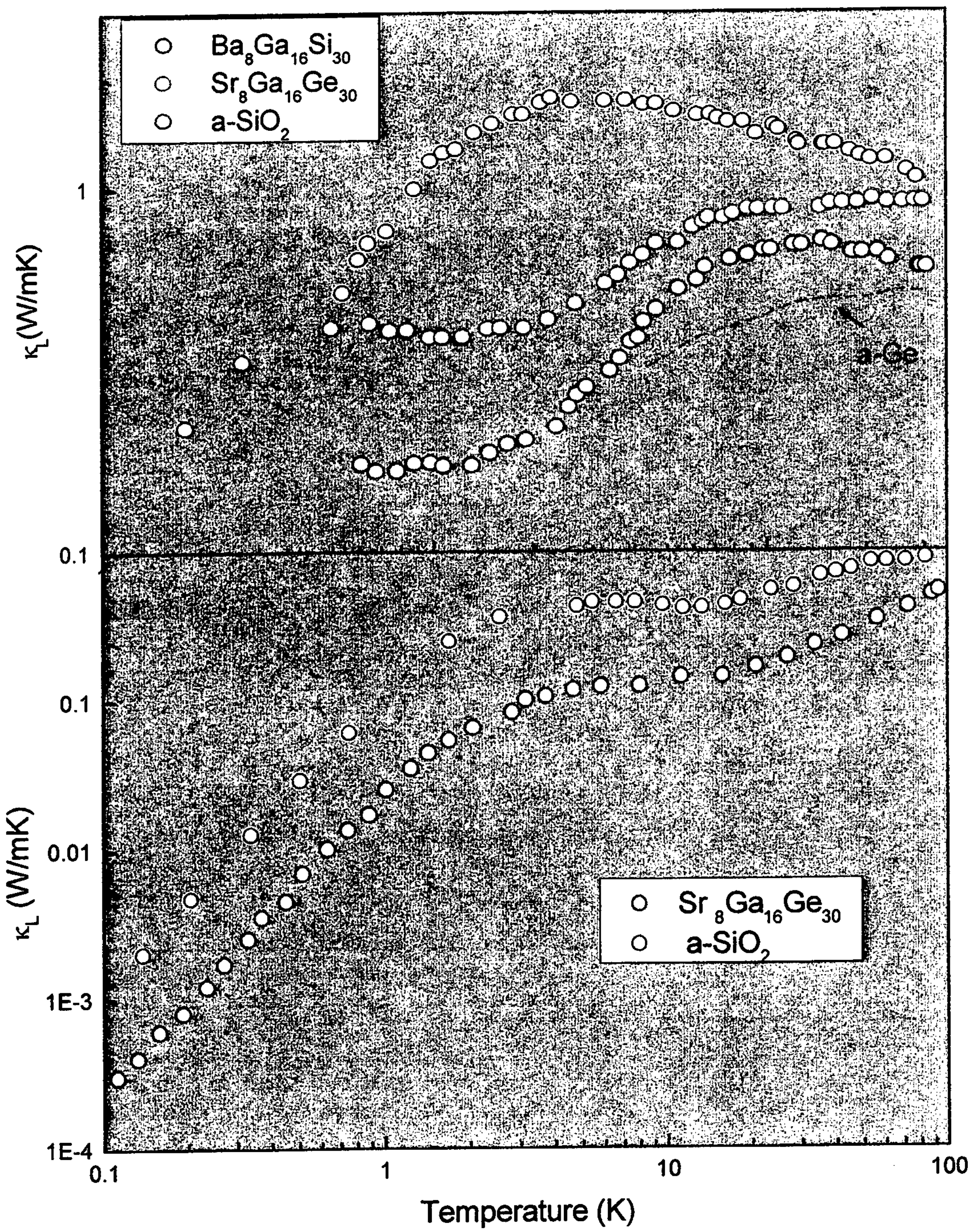

ELASTIC PROPERTIES OF CRYPTO-CLATHRATES:

RUS on filled and unfilled skutterudite antimonides:

$CoSb_3$

$La_{0.75}Fe_3CoSb_{12}$

polycrystalline $\longrightarrow$ c_{11} and c_{44}

T: 5 - 300 K

US absorption (pulse-echo) on Ge-clathrates:

$Sr_8Ga_{12}Ge_{30}$

single crystal

T: 0.4 - 30 K

$CoSb_3$

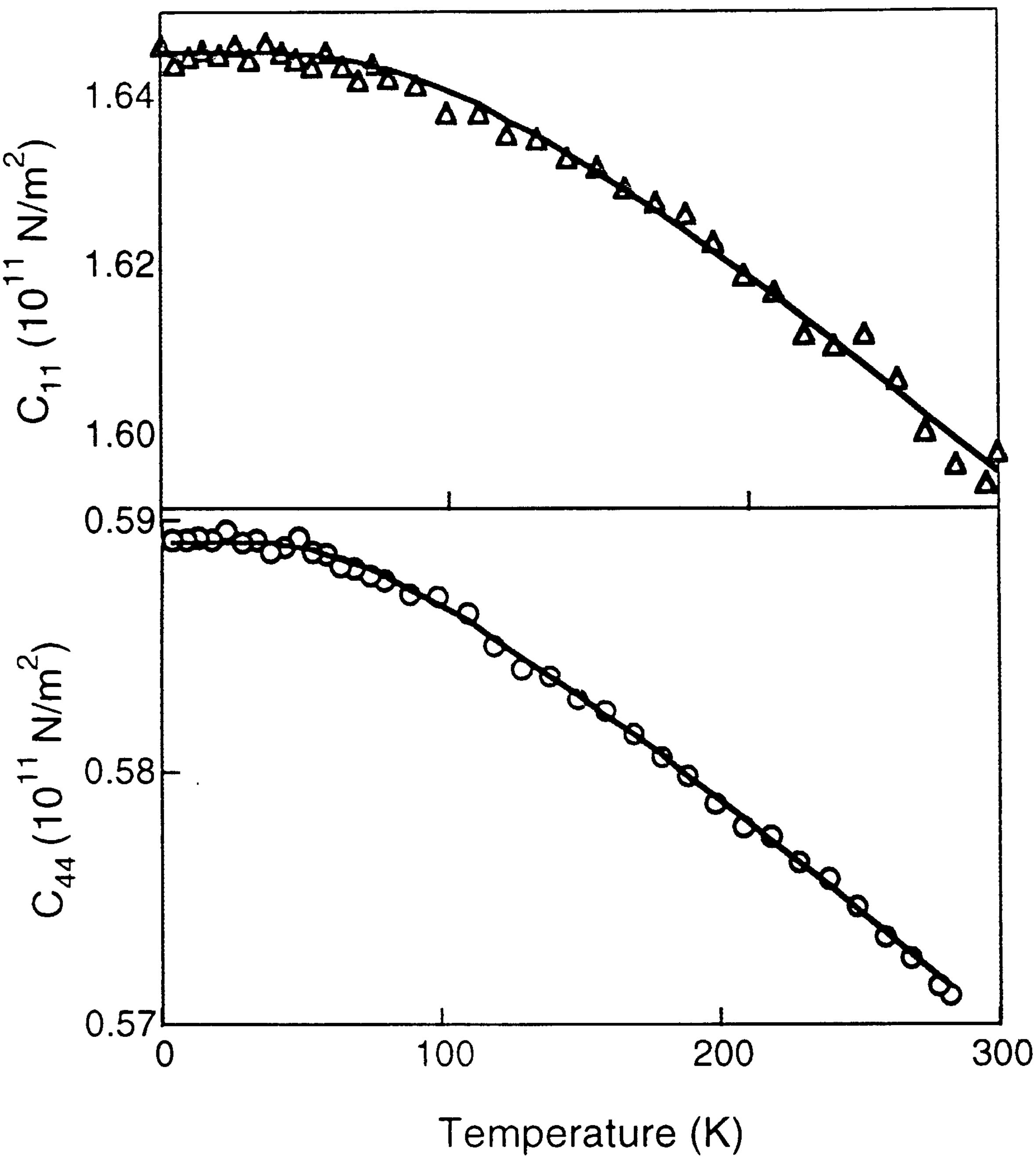

Varshni-behavior: $c_{ij} = c_{ij}^{0} - s / (e^{(t/T)} - 1)$

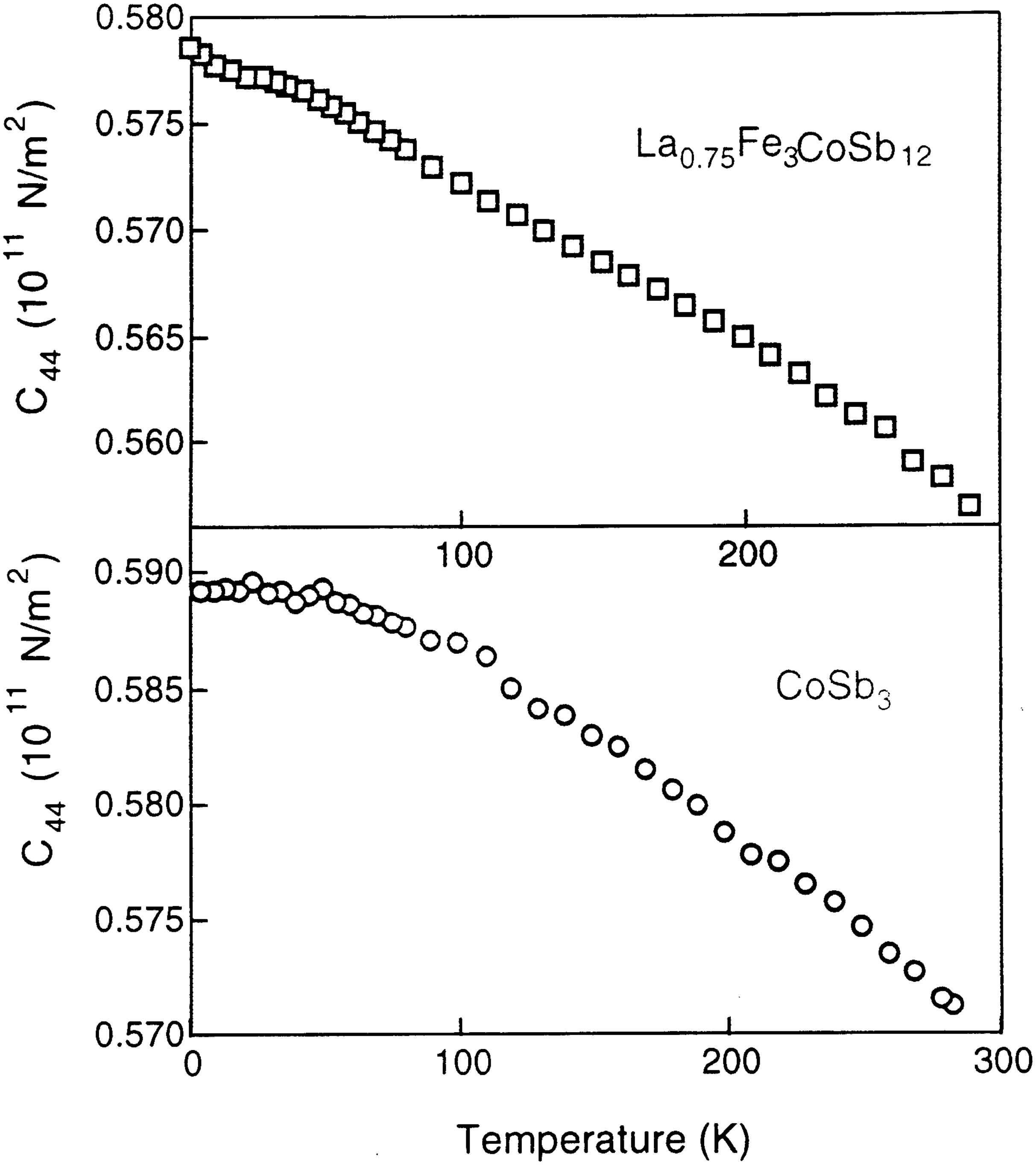

0.580
0.575
0.570
0.565
0.560
C_{44} (10^{11} N/m^2)
$La_{0.75}Fe_3CoSb_{12}$
100
200
0.590
0.585
0.580
0.575
0.570
C_{44} (10^{11} N/m^2)
$CoSb_3$
0
100
200
300
Temperature (K)

elastic constants for two-level system

$c = \partial^2 F / d\varepsilon^2$ $\quad$ $F = -N_A k_B T \ln(1+e^{-\Delta/T})$

$\Delta = \Delta_0 + A\varepsilon$

$La_{0.75}Fe_3CoSb_{12}$:

$c =$ c (background)

+ c (TLS #1, $\Delta_{01} = 50$ K)

+ c (TLS #2, $\Delta_{02} = 200$ K)

c (background) = Varshni-fit for unfilled sample

$La_{0.75}Fe_3CoSb_{12}$

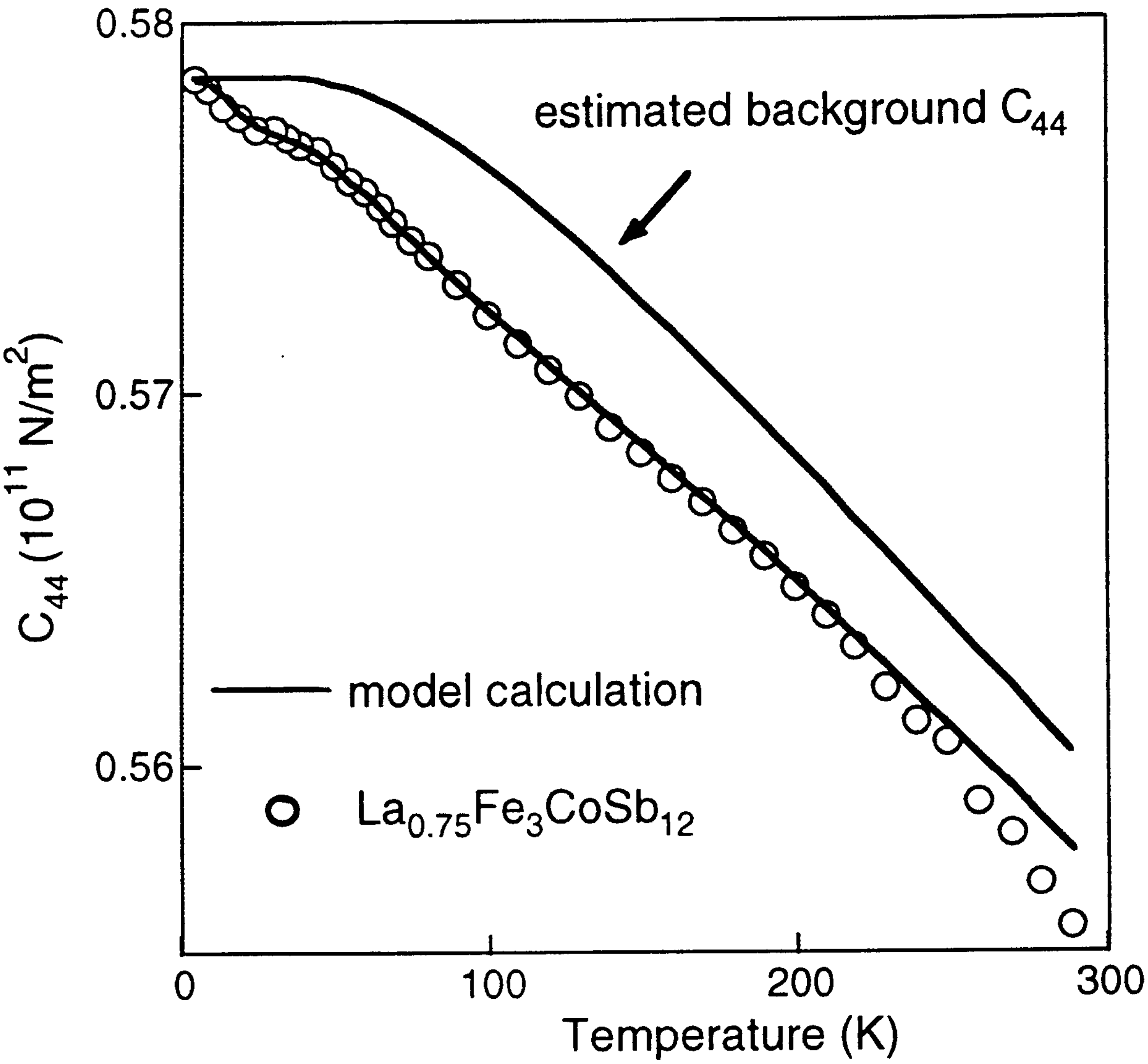

$$c_{44}(\text{model}) = c_{44}(\text{background})$$
$$+ c_{44}(\text{TLS \#1}, \Delta_{01} = 50\text{ K})$$
$$+ c_{44}(\text{TLS \#2}, \Delta_{02} = 200\text{ K})$$

Keppens et al., Nature 395, 876 (1998)

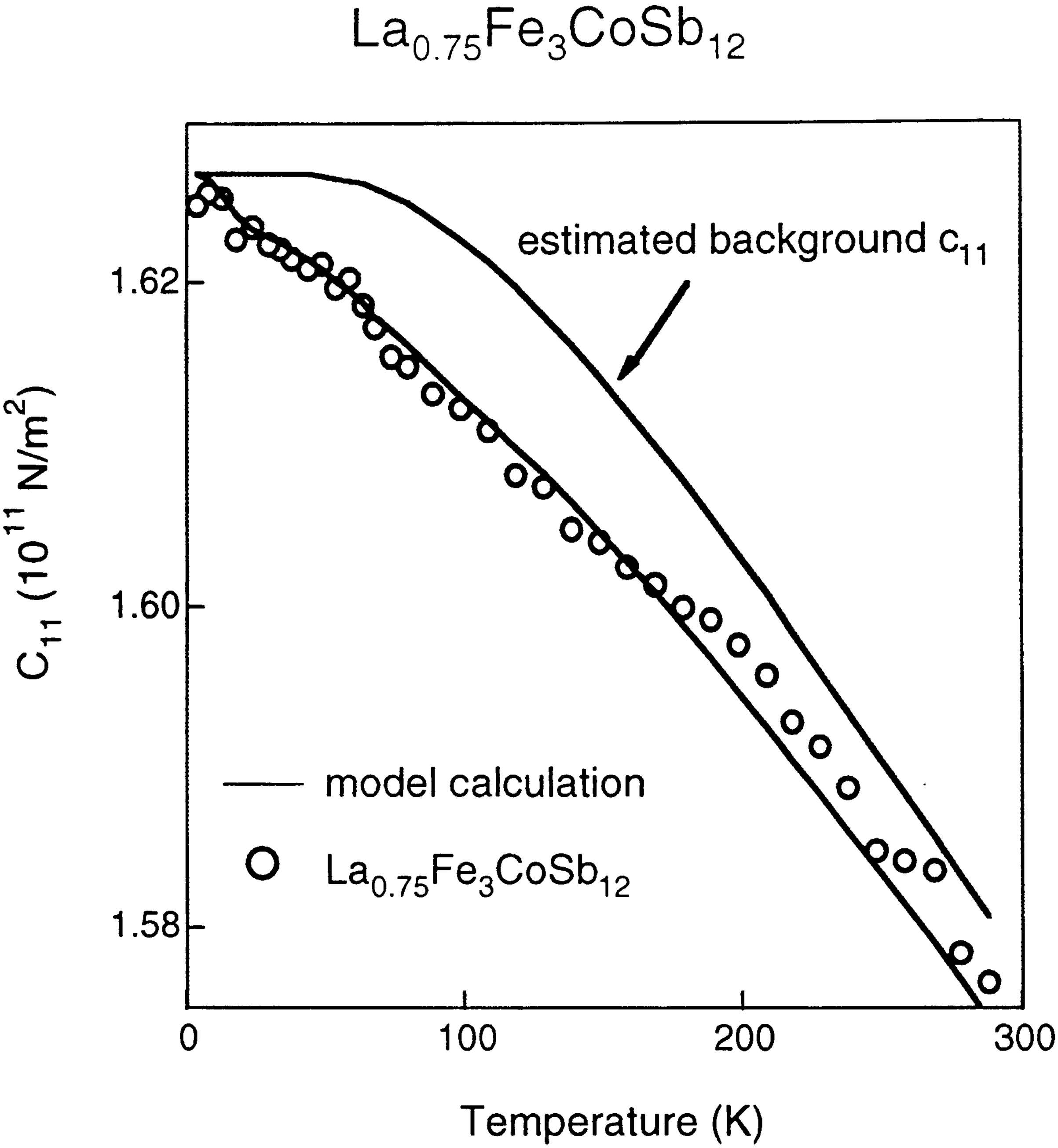

$$c_{11}(\text{model}) = c_{11}(\text{background}) + c_{11}(\text{TLS \#1}, \Delta_{01}= 50\text{ K}) + c_{11}(\text{TLS \#2}, \Delta_{02}= 200\text{ K})$$

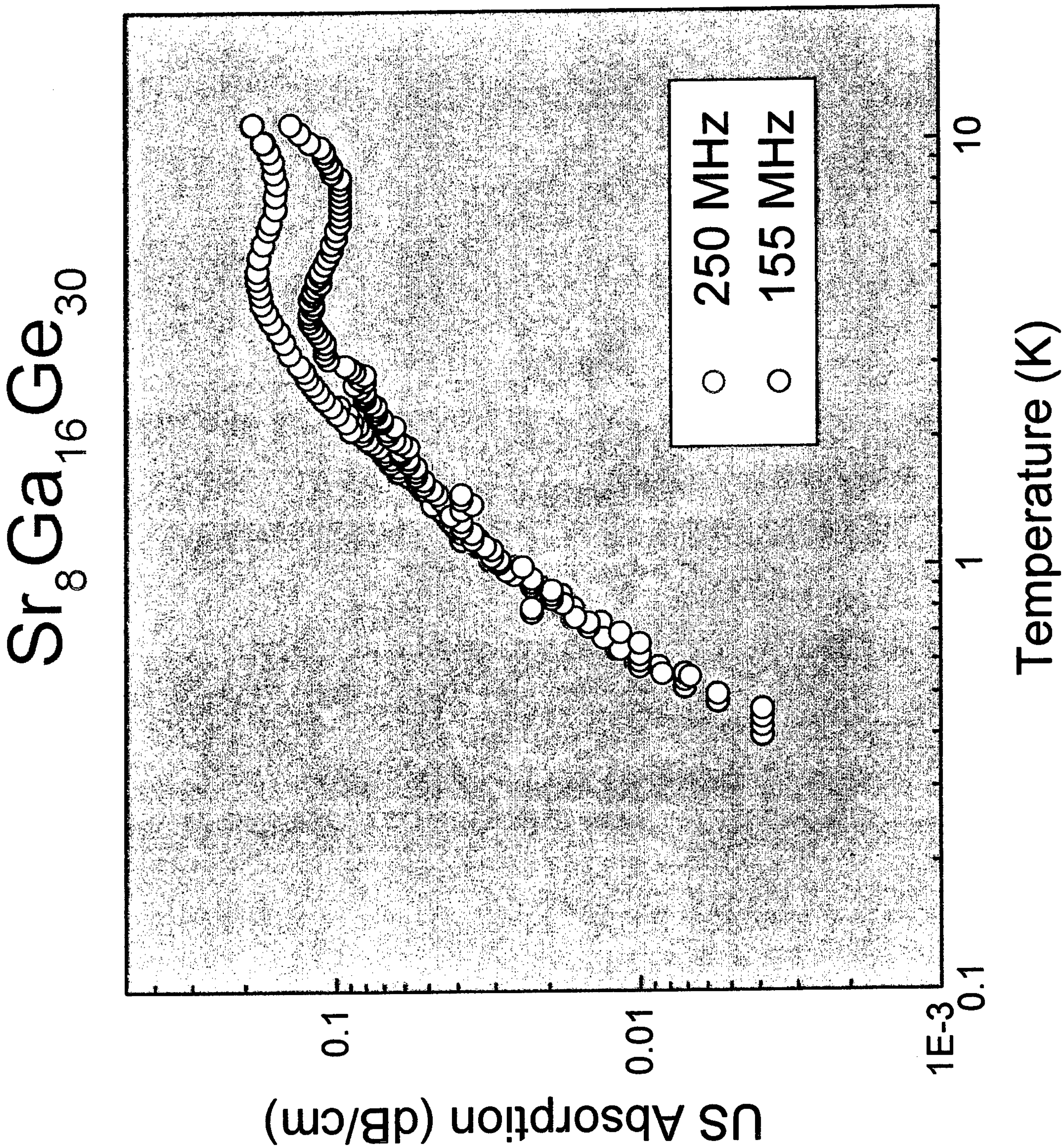
Sr8Ga16Ge30
250 MHz
155 MHz
US Absorption (dB/cm)
Temperature (K)
0.1
0.01
1E-3
1
10

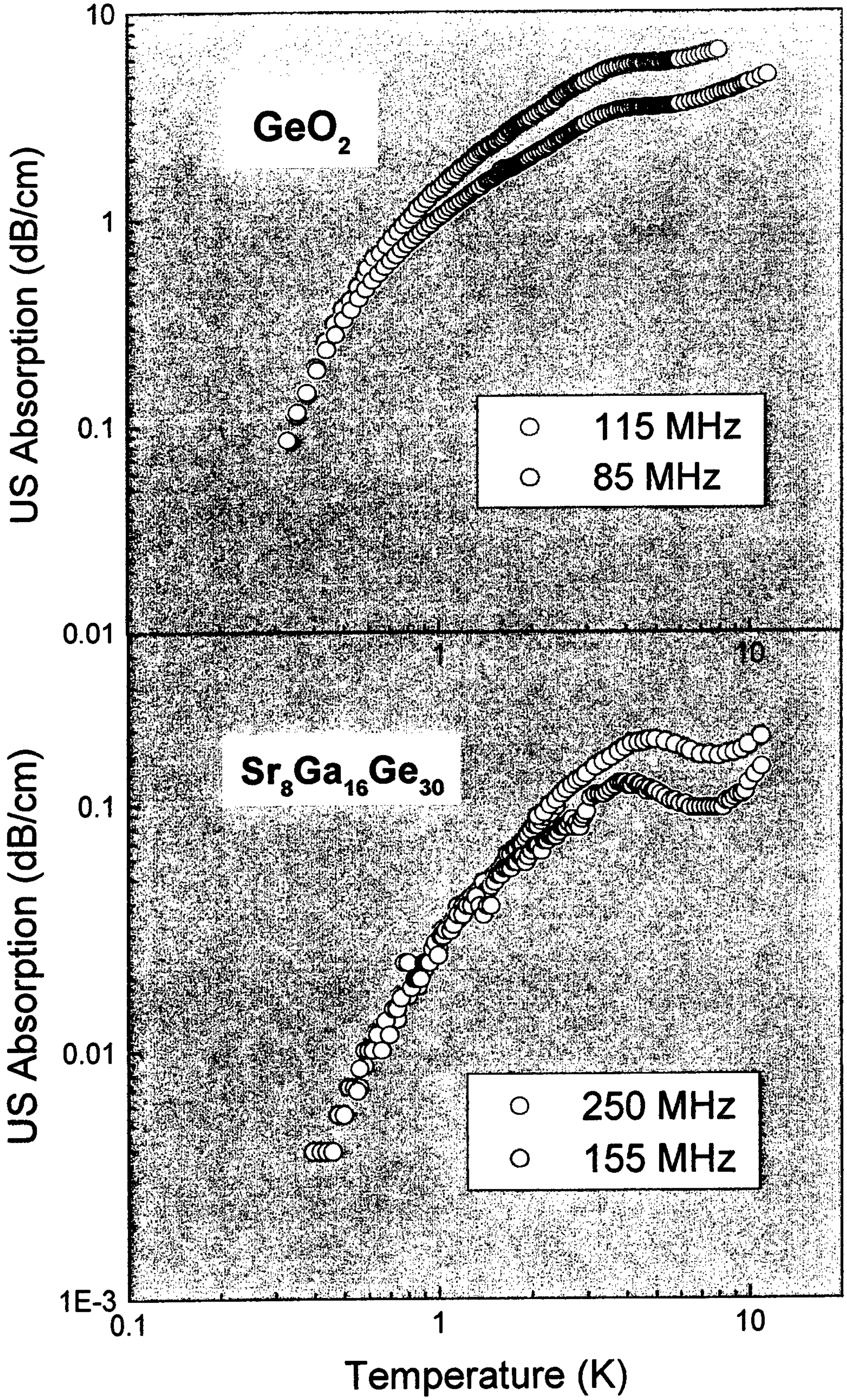

GeO2
115 MHz
85 MHz
Sr8Ga16Ge30
250 MHz
155 MHz
US Absorption (dB/cm)
US Absorption (dB/cm)
Temperature (K)
10
1
0.1
0.01
1E-3
0.1
1
10

Tunneling states

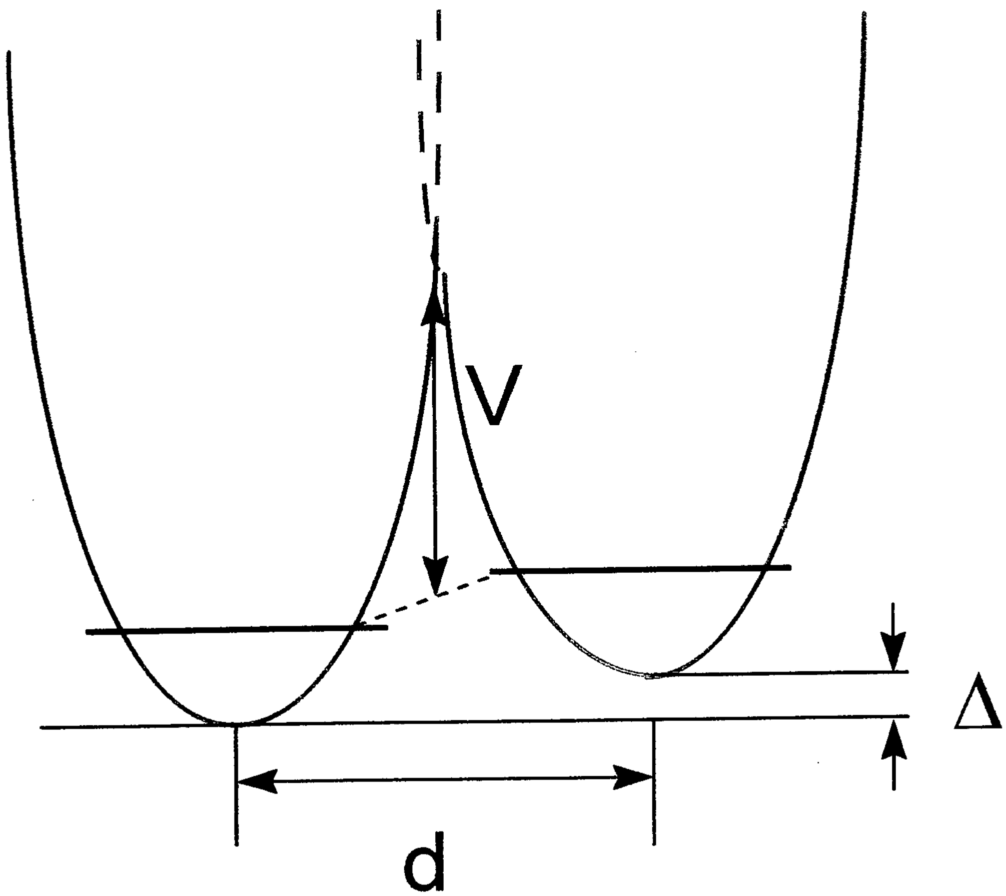

Δ: asymmetry

Δ_0: energy-overlap

→ broad and uniformly distributed

CONCLUSIONS - FUTURE WORK

2 *local modes* in filled skutterudites

tunneling states in Ge-clathrates

→ *perfect crystals* with glasslike elastic properties

<u>future work:</u>

RUS study of Ge-clathrate

US attenuation of skutterudites

Comparison of radiation and scattering mechanisms for objects having Rayleigh wave velocities greater than or smaller than the speed of sound in the surrounding water

Philip L. Marston
Florian J. Blonigen
Brian T. Hefner
Karen Gipson*
Scot F. Morse**
Dept. of Physics
Washington State University
Pullman, WA 99164-2814

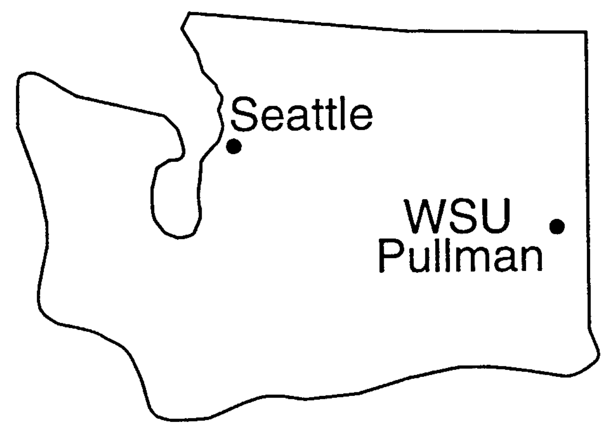

Supported by the Office of Naval Research.

*Physics Department, University of Puget Sound, 1500 North Warner, Tacoma, WA 98416

**Physical Acoustics Branch, Code 7136, Naval Research Laboratory, 4555 Overlook Ave., SW, Washington, DC 20375

- Fluid loading mechanisms for metallic objects in water: review and recent progress (Morse, Gipson, Blonigen).
- Reflection from plastics, fluid loading, and the subsonic Rayleigh wave.
- Novel backscattering enhancements for plastic (and rubber) objects in water (Blonigen, Hefner).

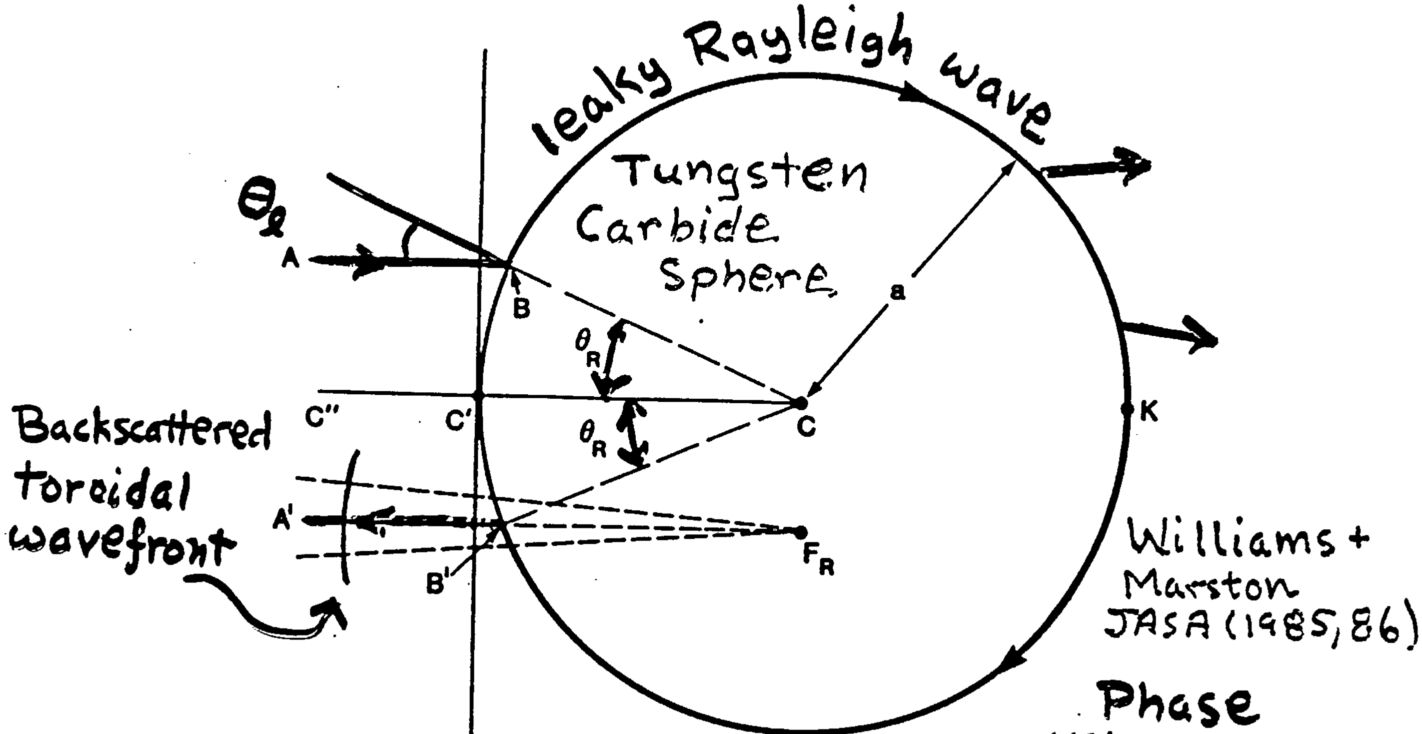

Angle of incidence for coupling to leaky wave of type ℓ $\Big\}$ $\theta_\ell = \sin\left(\frac{c}{c_\ell}\right)$, Phase velocity of surface wave $c_\ell > c$

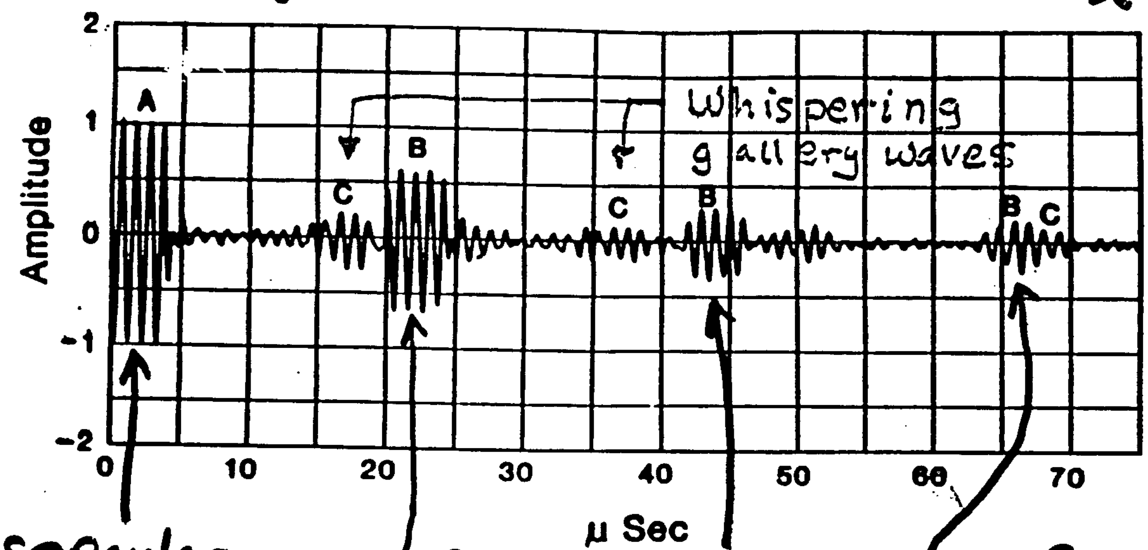

Back-scattering of a tone burst with ka=49

specular reflection

Rayleigh wave echoes

$m=0$ $m=1$ $m=2$ $\Big\}$ Circumnavigation index m

$$\boxed{ka = \left(\frac{2\pi}{\lambda \text{ in Water}}\right)\left(\begin{matrix}\text{sphere}\\ \text{radius}\end{matrix}\right) = \left(\frac{\omega_{burst}}{c}\right) a}$$

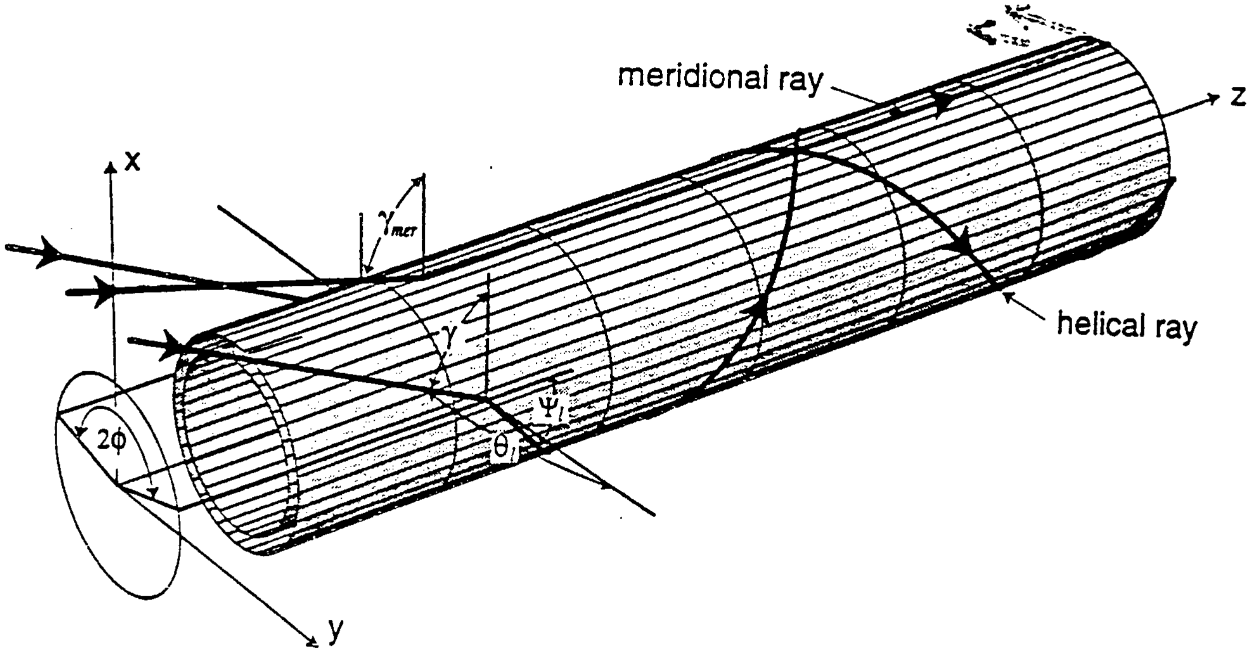
meridional ray
z
x
γ_{mer}
γ
Ψ_i
θ_i
2ϕ
helical ray
y

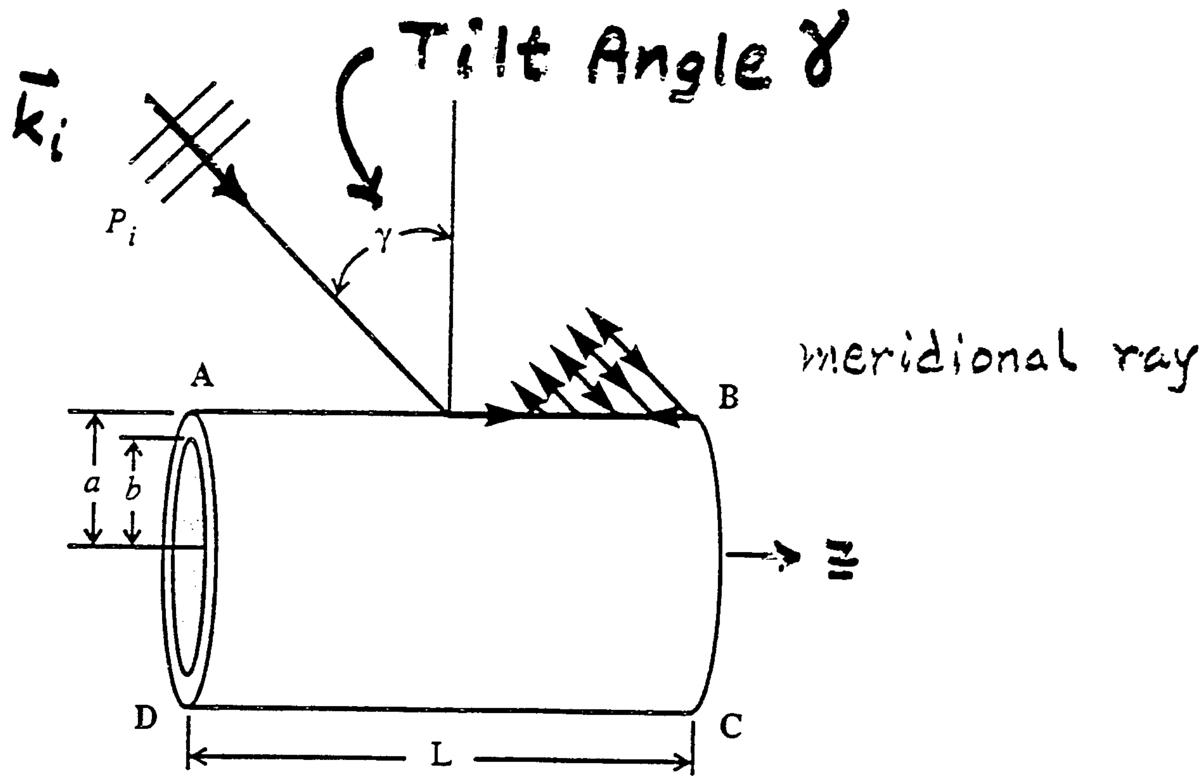
Tilt Angle γ
$\vec{k}_i$
P_i
γ
meridional ray
A
B
a
b
z
D
C
L

TR-3

Morse, Marston & Kaduchak JASA (1998)

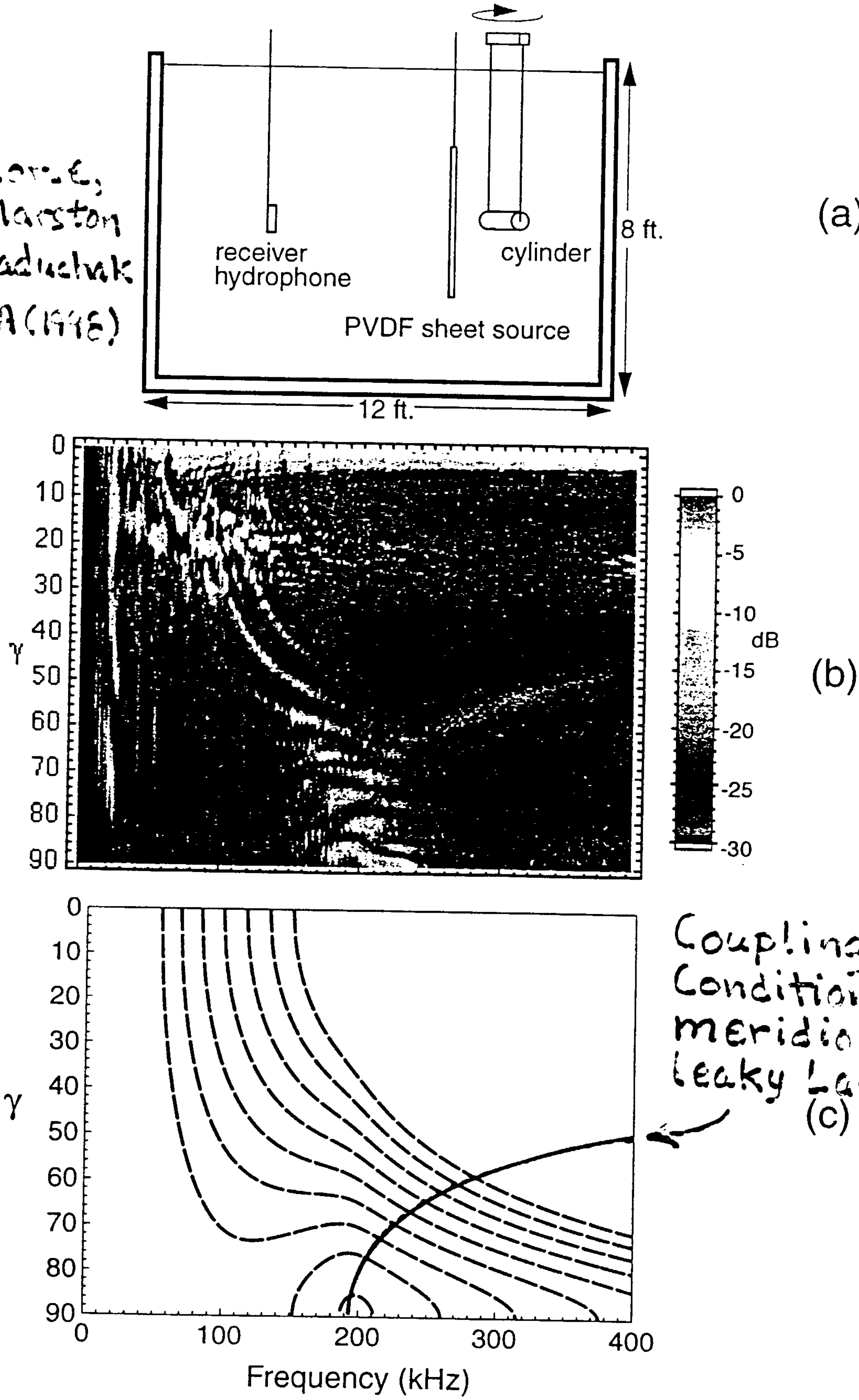

Coupling Condition for meridional a_0 leaky Lamb wave

n = shell thickness   a = radius   h/a = 0.076

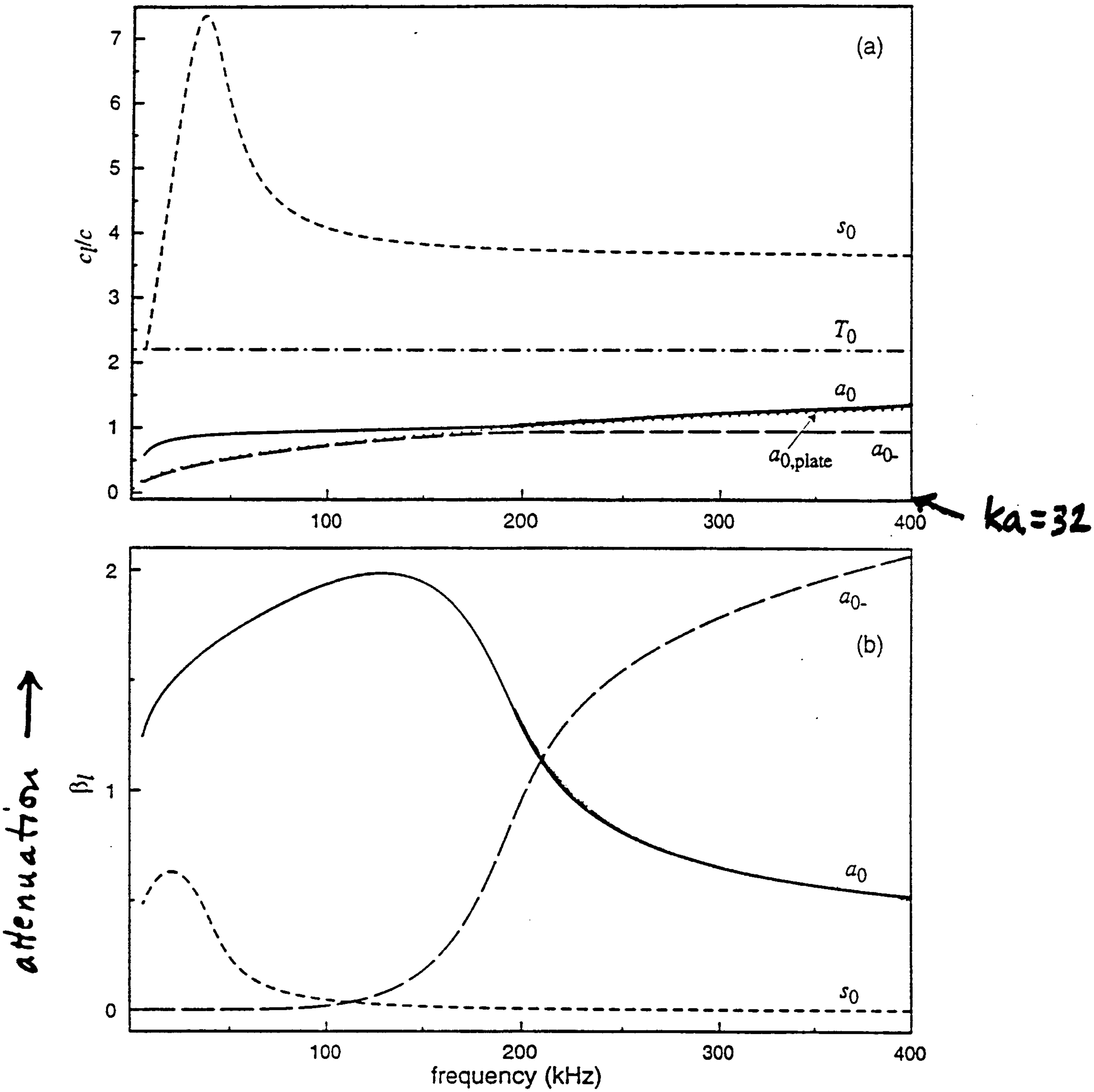

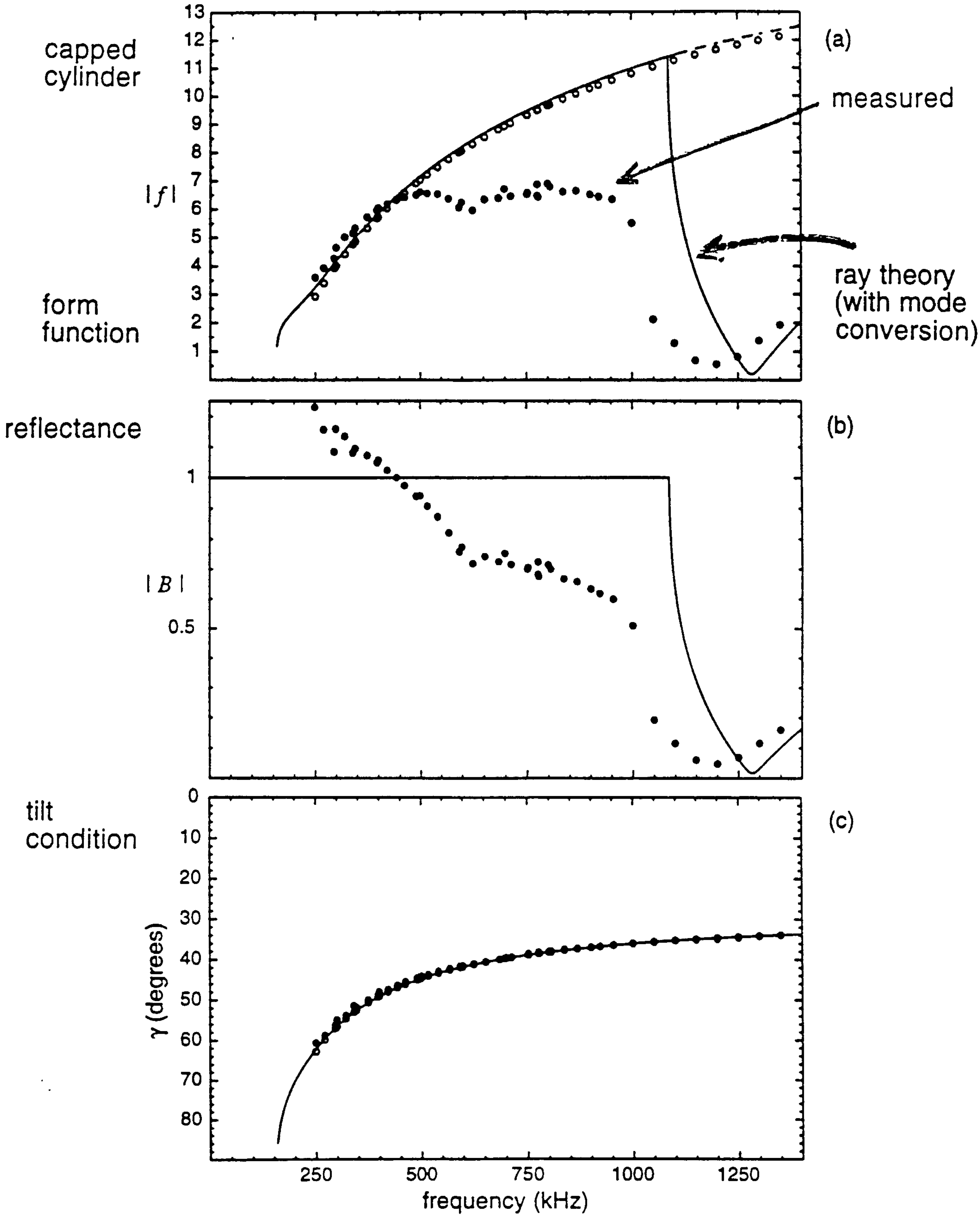

capped
cylinder
form
function
|f|
13
12
11
10
9
8
7
6
5
4
3
2
1
(a)
measured
ray theory
(with mode
conversion)
reflectance
|B|
1
0.5
(b)
tilt
condition
γ (degrees)
0
10
20
30
40
50
60
70
80
(c)
250
500
750
1000
1250
frequency (kHz)

TR-6

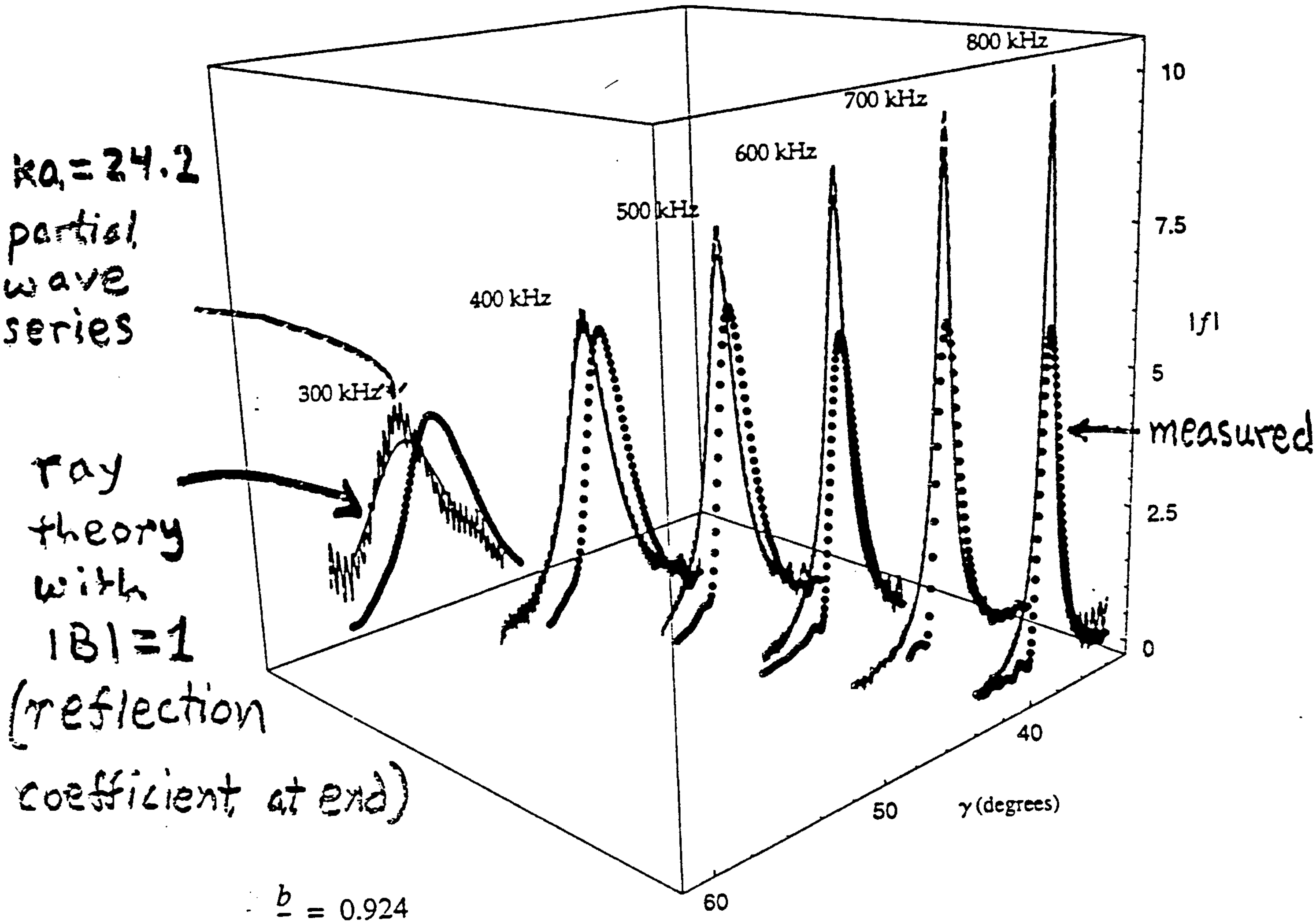

$\frac{b}{a} = 0.924$

For a rigid cylinder, edge diffraction at the end gives $|f| = O(ka)^{-1/2}$

TR-7

Mindlin (1959) Analysis of Plate Modes

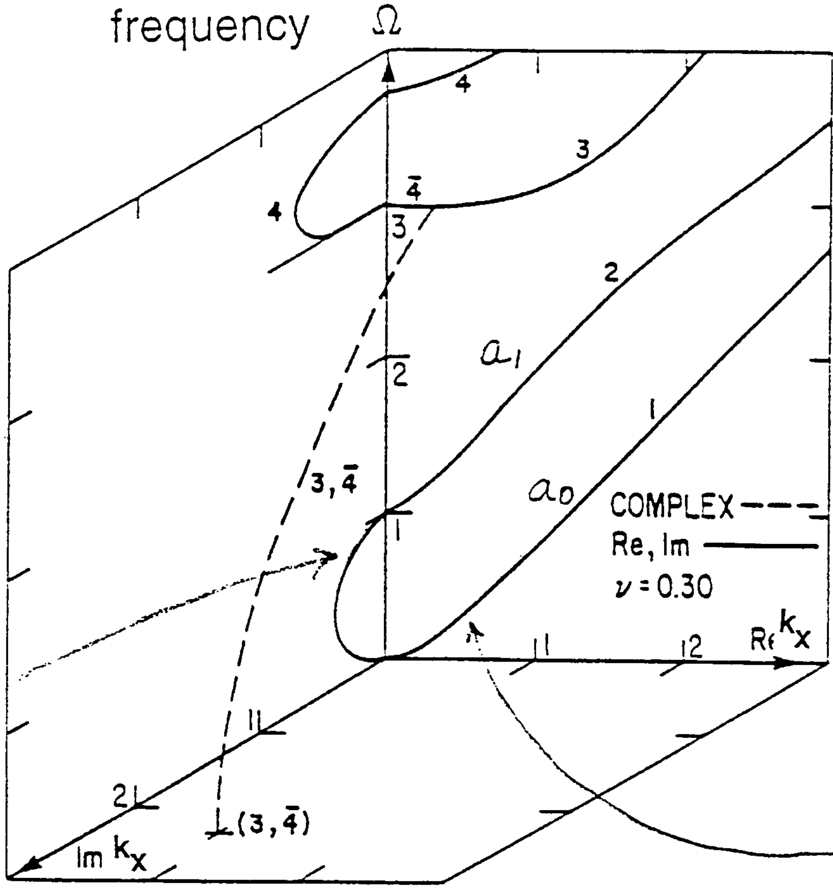

Real, imaginary, and complex segments of branches of an isotropic plate for antisymmetric family of modes. (Source: Courtesy of Dr. P. C. Y. Lee.)

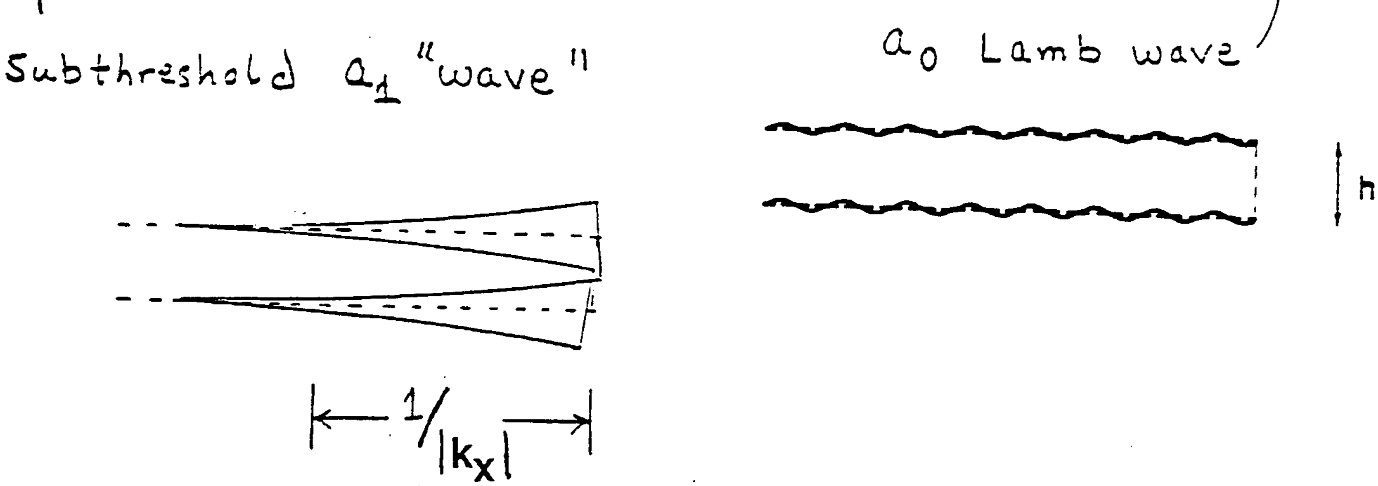

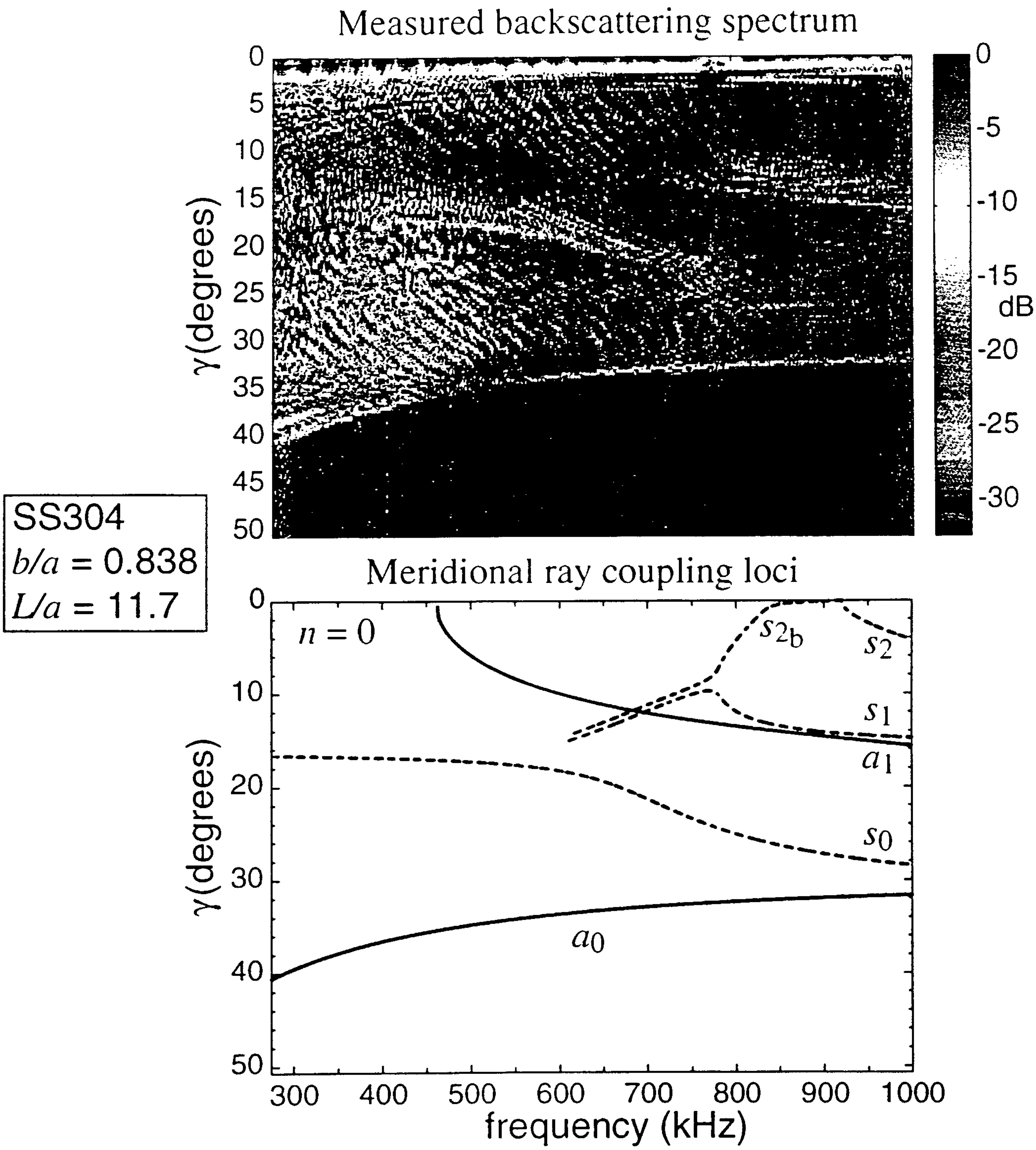

Measured backscattering spectrum
γ(degrees)
dB
SS304
b/a = 0.838
L/a = 11.7
Meridional ray coupling loci
n = 0
s2b
s2
s1
a1
s0
a0
γ(degrees)
frequency (kHz)

Space-Time Approach to Non-Relativistic Quantum Mechanics

R. P. Feynman

Cornell University, Ithaca, New York

(Rev. Mod. Phys. 1948)

Path Integral Formulation of Q.M.

$$\psi(x_{k+1}, t+\epsilon)$$

$$= \int \exp\left[\frac{i}{\hbar}S(x_{k+1}, x_k)\right]\psi(x_k, t)dx_k/A. \quad (18)$$

7. DISCUSSION OF THE WAVE EQUATION

The Classical Limit

This completes the demonstration of the equivalence of the new and old formulations. We should like to include in this section a few remarks about the important equation (18).

This equation gives the development of the wave function during a small time interval. It is easily interpreted physically as the expression of Huygens' principle for matter waves.[*] In geometrical optics the rays in an inhomogeneous medium satisfy Fermat's principle of least *time*. We may state Huygens' principle in wave optics in this way: If the amplitude of the wave is known on a given surface, the amplitude at a near by point can be considered as a sum of contributions from all points of the surface. Each contribution is delayed in phase by an amount proportional to the *time* it would take the light to get from the surface to the point along the ray of least *time* of geometrical optics. We can consider (22) in an analogous manner starting with Hamilton's first principle of least *action* for classical or "geometrical" mechanics. If the amplitude of the wave ψ is known on a given "surface," in particular the "surface" consisting of all x at time t, its value at a particular nearby point at time $t+\epsilon$, is a sum of contributions from all points of the surface at t. Each contribution is delayed in phase by an amount proportional to the *action* it would require to get from the surface to the point along the path of least *action* of classical mechanics.[16]

Fermat's principle

Huygens' principle

TR-10

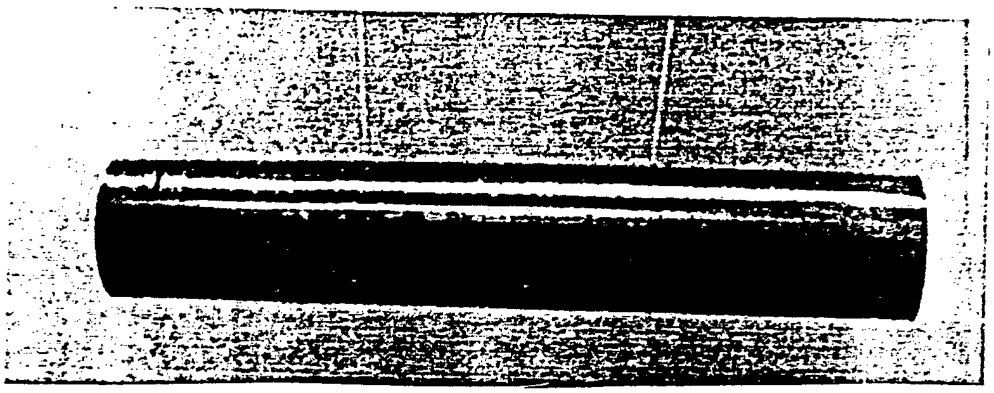

Observed far-field backscattered form function

Karen Gipson
1998 Ph.D. thesis

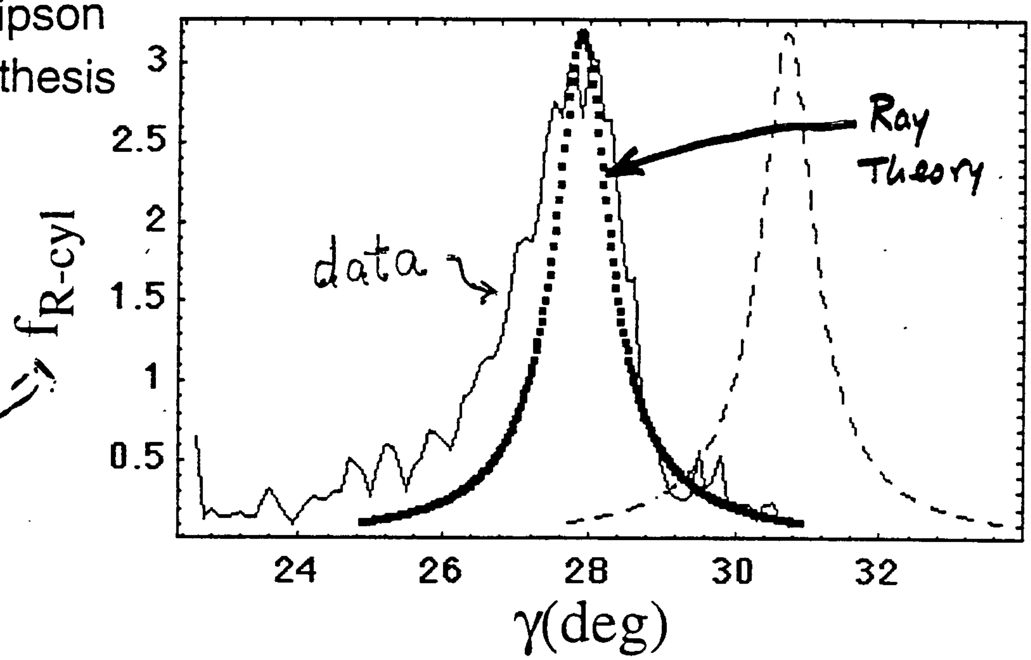

frequency=1.03 MHz

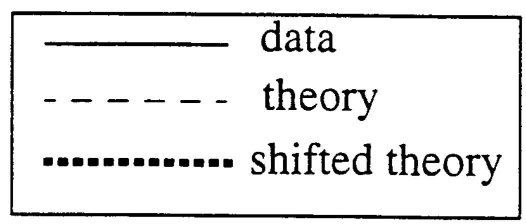

$$P_{sca} = P_{inc} \frac{f_{cyl}\, a}{2r} e^{ikr}$$

frequency	data peak	theory peak	% discrepancy
620 kHz	2.60	3.45	25%
1.03 MHz	3.05	3.20	5%

Fluid Loading Properties Relevant to Scattering:

	c (m/s)	ρ (g/cc)
1. Water	1490	1.0
2. Sandy Sediment (fluid model)	1800	1.8

Elastic Parameters (Solid or Shell "Target"):

	c_R	c_S	c_L	ρ
3. Stainless Steel	2904	3141	5675	7
4. Solid Polymers:				
A. PMMA	1250	1340	2690	1.19
Polystyrene	1075	1150	2400	1.05
B. RTV Rubber	-	-	1080	1.02

What are some mechanisms for enhanced backscattering from TYPE 4(A) or (B) targets with TYPE 1 or 2 loading?

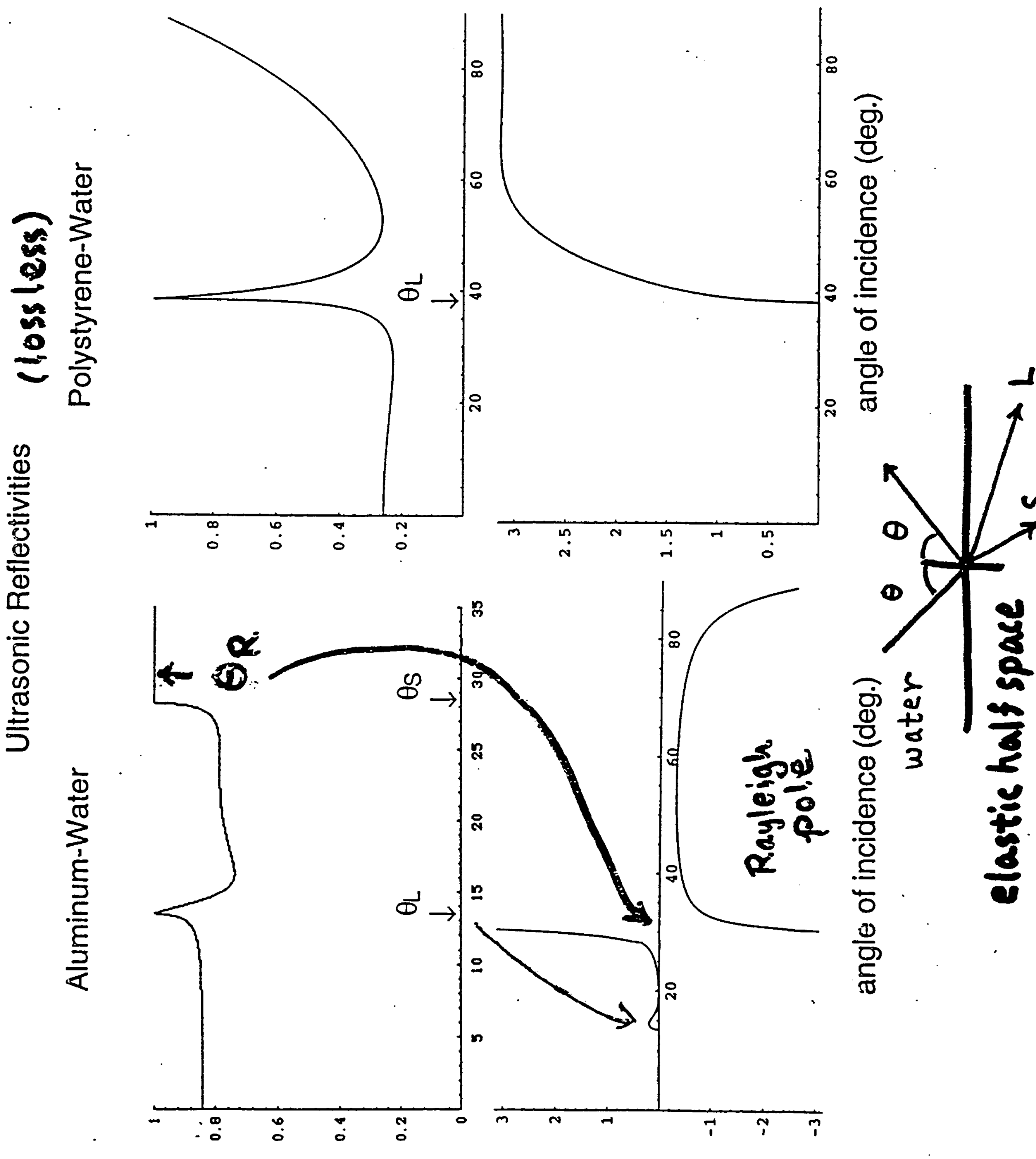

Ultrasonic Reflectivities
(lossless)
Aluminum-Water
Polystyrene-Water
|r|
phase
θ_L
θ_S
θ_R
θ_L
Rayleigh pole
angle of incidence (deg.)
angle of incidence (deg.)
water
elastic half space
θ
θ
L
S

PLASTIC PROPERTIES

GLASS TRANSITION - a second order phase transition from the glassy state to the rubbery state having a negligible shear modulus.

GLASS TRANSITION TEMPERATURE (T_g) - the temperature at which the glass transition occurs in the low frequency limit.

	T_g (C)
PMMA	105
Polystyrene	100

- While the shear wave velocity c_s is relatively dispersive, for $T \approx 20$ C at low ultrasonic frequencies,

  $$\Delta c_S << 0.01\, c_S$$

  for the frequency range in our experiments.

- With $$k_S = (\omega / c_S)(1 + i\delta_S)$$
  $$k_L = (\omega / c_L)(1 + i\delta_L)$$

  $\delta_s << 1$ and $\delta_L << 1$ at low ultrasonic frequencies and do not depend on ω. Example: PMMA $\delta_S \approx 0.0053$

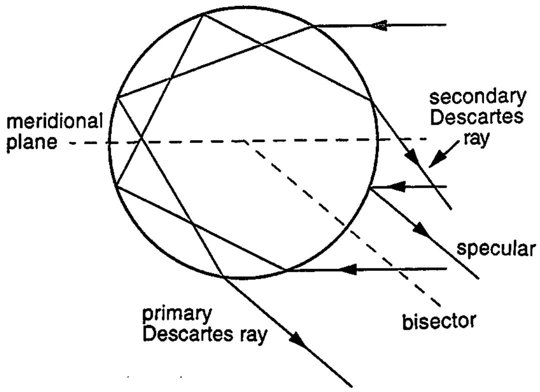

Fig. 4. Primary and secondary Descartes rays projected onto the base plane for a circular ice cylinder with $n = 1.31$ and illuminated at $\gamma = 20°$. As shown for this case in Fig. 3, the Descartes ray scattering angle θ_D for $p = 2$ exceeds θ_D for $p = 3$. The projected specular reflection and bisector of the cylinder are shown from the perspective of a distant observer at the θ_D of the primary rainbow. The meridional plane that contains the cylinder's axis and the incident wave vector is shown. Glare points associated with specular reflection were not as bright as those for the Descartes rays for situations in which the glare points from Descartes rays were visible.

the base plane for the cases of $p = 2$ and 3, which are analogous to primary and secondary rainbows. The filled circle shown is the location of the corresponding ray-optics discontinuity in Fig. 5 of Ref. 8 for the specific case of $\gamma = 45°$. This comparison, as well as laboratory experiments,[15] gives support to this analysis. As the tilt angle increases, the $p = 2$ caustic evolves in such a way that θ_D reaches 180° at a critical tilt angle γ_c given by taking $n' = 2$ in Eq. (1). This corresponds to a merging in the meridional scattering plane of the Airy caustics from both sides of the cylinder (see Appendix A).

For small values of tilt, the evolution of the values of θ_D and the locations of the associated rays are more closely related to the observations of sunlit icicles. Figure 4 shows the locations of the Descartes rays projected onto the base plane for $p = 2$ and 3 as well as the specular ray (which may be assigned the value $p = 0$), which has the same scattering angle as θ_D for the primary rainbow ray. For the tilt angle γ of 20° used in this figure, an observer positioned to view the glare of the primary rainbow ray would be in the shadow zone of the secondary rainbow (see Fig. 3) so that no rays having two internal reflections would be visible. Conversely, an observer positioned to view the glare of the secondary rainbow ray would be in the shadow zone of the primary rainbow.

3. Caustics and Glare Points Created by Sunlit Icicles

Sunlit icicles were observed visually and photographically in Pullman, Wash., during February 1996. Most of the observations and supporting photographs were taken in midmorning with the Sun position calculated to be 20° to 25° above the horizon. With the axis of the icicle approximated as vertical, the corresponding values for γ in the cylinder model range from 20° to 25°. Figures 5(a) and 5(b) show color photographs with the camera focused on the icicle such that the camera is on opposite sides of the me-

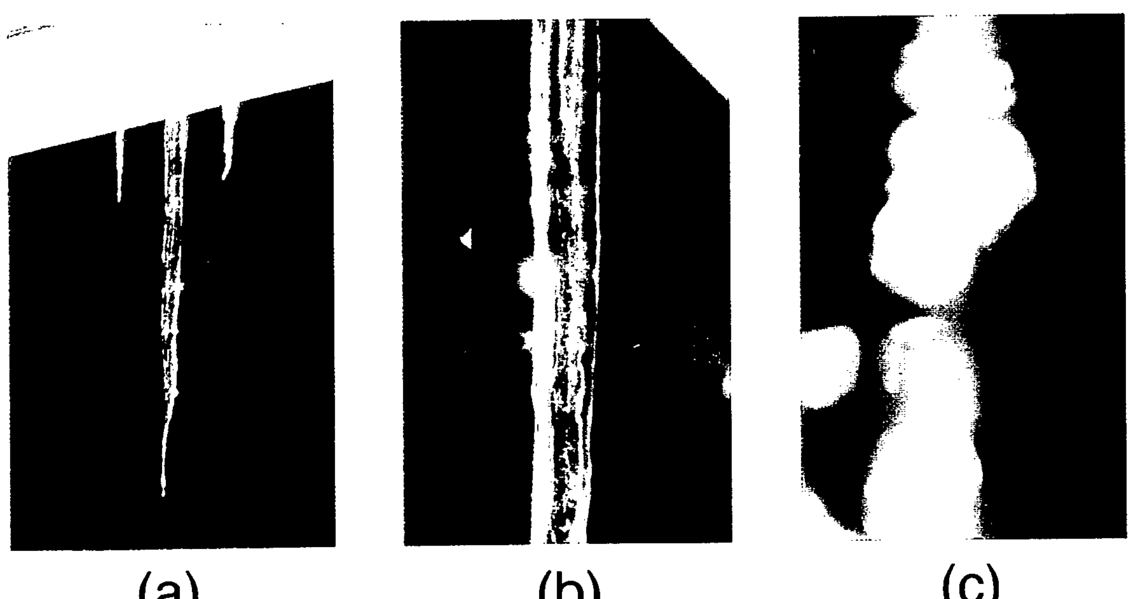

Fig. 5. (a) Descartes glare point for the primary Airy caustic of an icicle is visible as the bright patch on the right-hand side of the icicle near its center. The weak glare point visible on the left-hand side is for a twice-reflected and twice-refracted ray. (b) The same icicle viewed from the other side of the meridional plane shows a line of primary Descartes glare points on its left-hand side with a line of specular glints to the right of an imaginary center line (shown as the cylinder's bisector in Fig. 4). The lower of the two very bright glare points has a green hue. (c) Perspective as in (b) but with the camera's focal plane conjugate to the far-field scattering. The glare points are now out of focus, and some of the Descartes glare points appear to be associated with colored regions.

ridian formed by $\mathbf{k}_i$ and the cylinder's axis. Glare points evident in these photographs were also easily observed by eye. The causes of the glare points were identified when the head of the observer moved and by comparisons with ray diagrams as shown in Fig. 4. Note that Fig. 4 is drawn for the perspective shown in Fig. 5(b) such that the Descartes ray appears on the left whereas a glint from external specular reflection appears on the right-hand side of the bisector. Corresponding features can be identified in Fig. 5(b). The lowest bright glare point has a green hue.

The glare points (or point) from the two-chord ray in Fig. 5(b) disappeared when θ was reduced below a value that was interpreted to be θ_D because the transition appeared to be associated with the Descartes ray. In support of this interpretation, the glare was observed to be especially bright at this Airy transition when compared with the glare of the specular reflection. Furthermore, observations with a camera defocused, so the focal plane was conjugate to the far-field scattering, manifested the color sequence of the rainbow in the defocused image of some two-chord glare points but not for the specularly reflected glint. (This viewing method displays the angular dependence of the scattered light. Other examples of out-of-focus viewing are discussed on pp. 231–234 of Ref. 7.) Figure 5(c) is a far-field image for the camera perspective as in Fig. 5(b) and Fig. 4. Vertical colored bands apparently associated with the Airy caustic of the primary rainbow rays are visible slightly below the center of the photograph, with the red side (and the corresponding shadow region of the caustic) appearing on the right-hand side of the bands. It was confirmed with a diagram based on elementary lens theory that the shadow side in the defocused photograph [Fig. 5(c)] agreed with predictions in which the illuminating rays correspond to the primary rainbow rays of the icicle. The limited extent of the colored bands in Fig. 5(c) appears to be the result of vignetting due to the lens aperture. With the observer in the two-ray region of the primary rainbow, it was difficult to resolve the distinct glints of the associated rays (labeled 1 and 2 in Fig. 2); however, that may be more a deficiency of the observer's vision (the author's) than of the actual optical phenomenon.

Although it was not feasible to measure θ_D for natural icicles, some information about relative positions of Descartes angles is available because glare points that have the expected properties of a secondary or $p = 3$ Descartes ray were occasionally visible by careful positioning of the observer. Such a glare point is visible on the left-hand side of the icicle in Fig. 5(a). This glare point is slightly below a primary Descartes ray glare point visible on the right-hand side. Although Fig. 4 shows that the primary and the secondary glare points, if visible, should be on opposite sides of a cylinder, the recording of both glare points with a single camera position merits some discussion. This is because inspection of Figs. 3 and 4 shows that the secondary rainbow lies in the shadow region of the primary rainbow of a cylinder except for small values of γ, namely, $\gamma < 4.9°$ for $n = 1.31$. The simultaneous observation of the primary and the secondary glare points as in Fig. 5(a) may be indicative of deviations from a circular cross section or a cylindrical shape, both of which are visible in Fig. 5 and from direct inspection of the icicle. It is noteworthy here that the vertical spread of the glints from the $p = 2$ ray also indicates deviations from a cylindrical shape, since it is to be expected that, for perfect cylinders, the vertically displaced glare points would spread vertically and merge into vertical lines.

Although Fig. 5 and the observations described are based on an icicle that has a diameter of approximately 1 cm, the qualitative features of the primary Descartes ray were confirmed with observations based on clusters of smaller icicles in December 1996.

4. Discussion and Conclusions

The observations summarized in Section 3 show that rays within icicles can produce bright glare points that have the expected properties of primary and secondary Descartes (or rainbow) rays. The observations were first made with the unaided eye and are supplemented by color photographs, as shown in Fig. 5. The observations were made without the aid of a polarizer and with solar illumination unobscured by clouds.

A model was presented for how the projected scattering angle for primary and secondary Descartes rays varies with the tilt angle γ of the illumination relative to the axis of the icicle for the situation in which the icicle has the shape of a circular cylinder. This model neglects the taper and the shape variations of real icicles. For a sufficiently small value of γ, corresponding to nearly horizontal illumination, the model suggests that a sufficiently distant observer could lie within the two-ray region of both the primary and the secondary caustics. The observations were made with γ only somewhat larger than the crossover value (predicted to be at or near 4.9°) so that the apparent simultaneous observation of primary and secondary rainbow glare points in Fig. 5(a) may be due to deviations from the simplified shape assumed.

The above-mentioned model also predicts that at a critical value of tilt γ_c (predicted to be at 60.75° for ice) the primary rainbow Descartes rays from both sides of the cylinder merge in the meridional plane. The expression for γ_c, Eq. (A3), may be derived either with the Bravais effective refractive index, Eq. (1), or from a direct calculation of the appropriate principal curvature of the refracted internal wave front in the meridional plane, Eq. (A5). Although it is not currently known whether the caustic-merging transition (CMT) is observable for naturally sunlit icicles, if it is observable for icicles, the transition glare point should be very bright. This consequence of the enhanced focusing is discussed in Appendix A. The merging and the general brightness enhancement of the two-chord glare point were both confirmed by the viewing of a long tilted polished glass rod illuminated with light from a distant slide projector. Unfortunately, conditions favorable for such observations

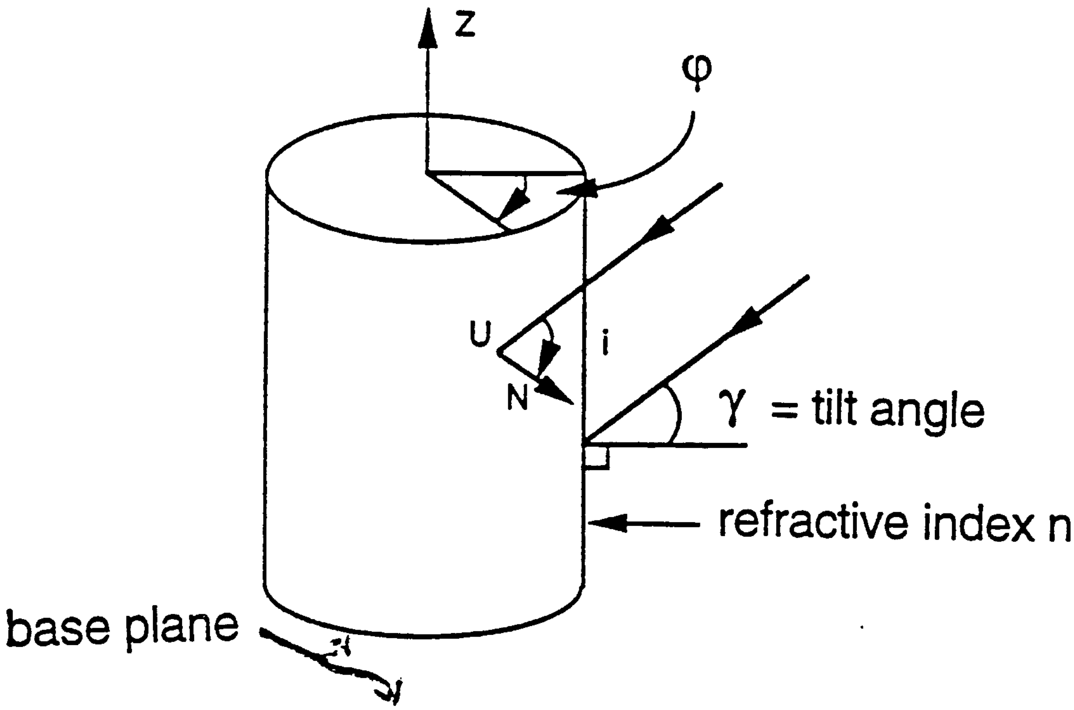

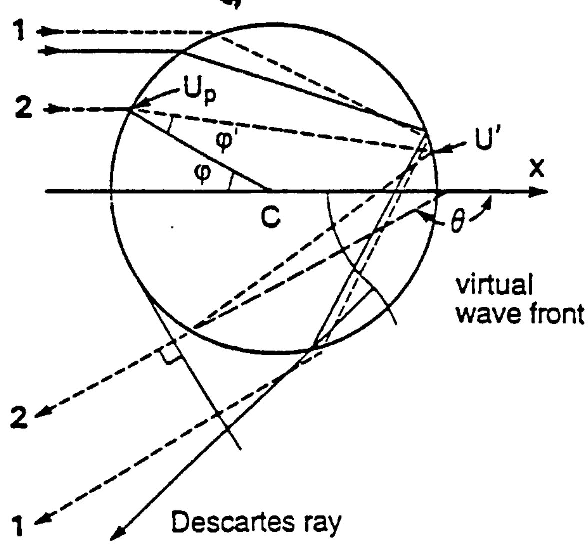

The projection is like rays through a cylinder at normal incidence having a refractive index of

$$n'(\gamma) = \frac{\sqrt{n^2 - \sin^2\gamma}}{\cos\gamma}$$

(Bravais law of refraction of skew rays)

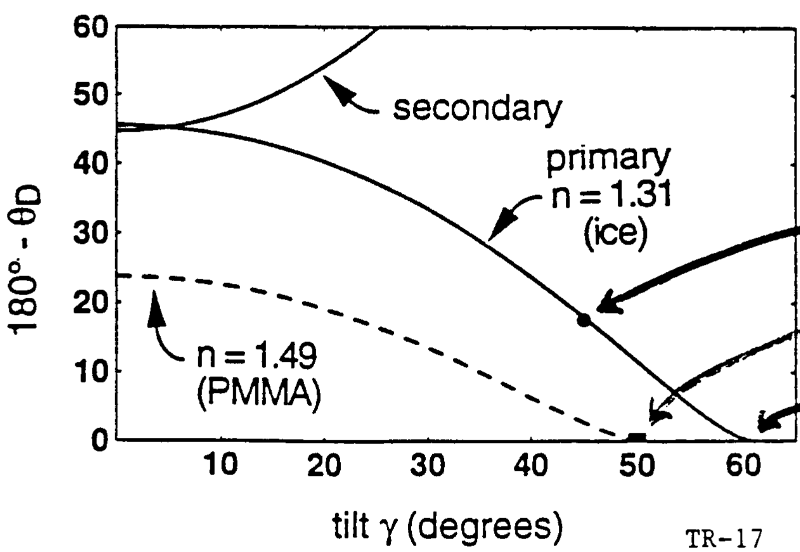

halo simulation
Takano + Tanaka (1980)

C. Mount (data)

γ_c

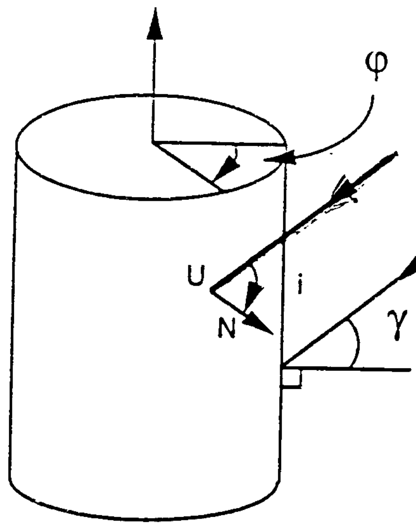

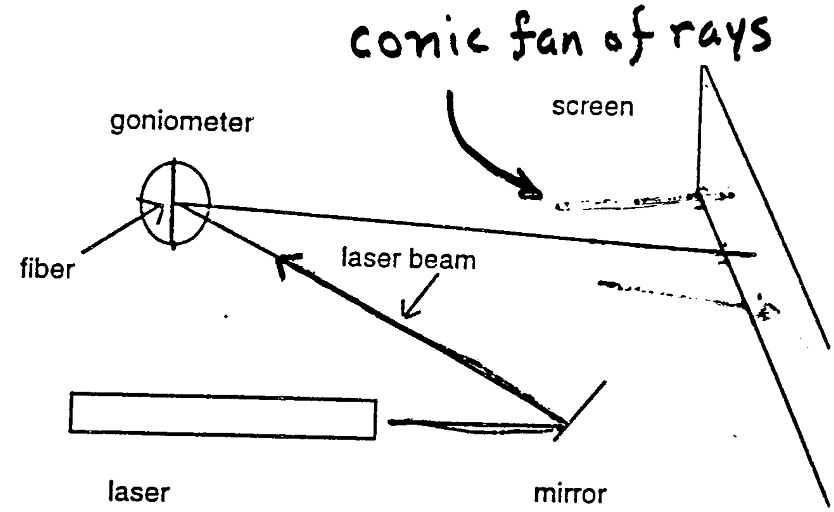

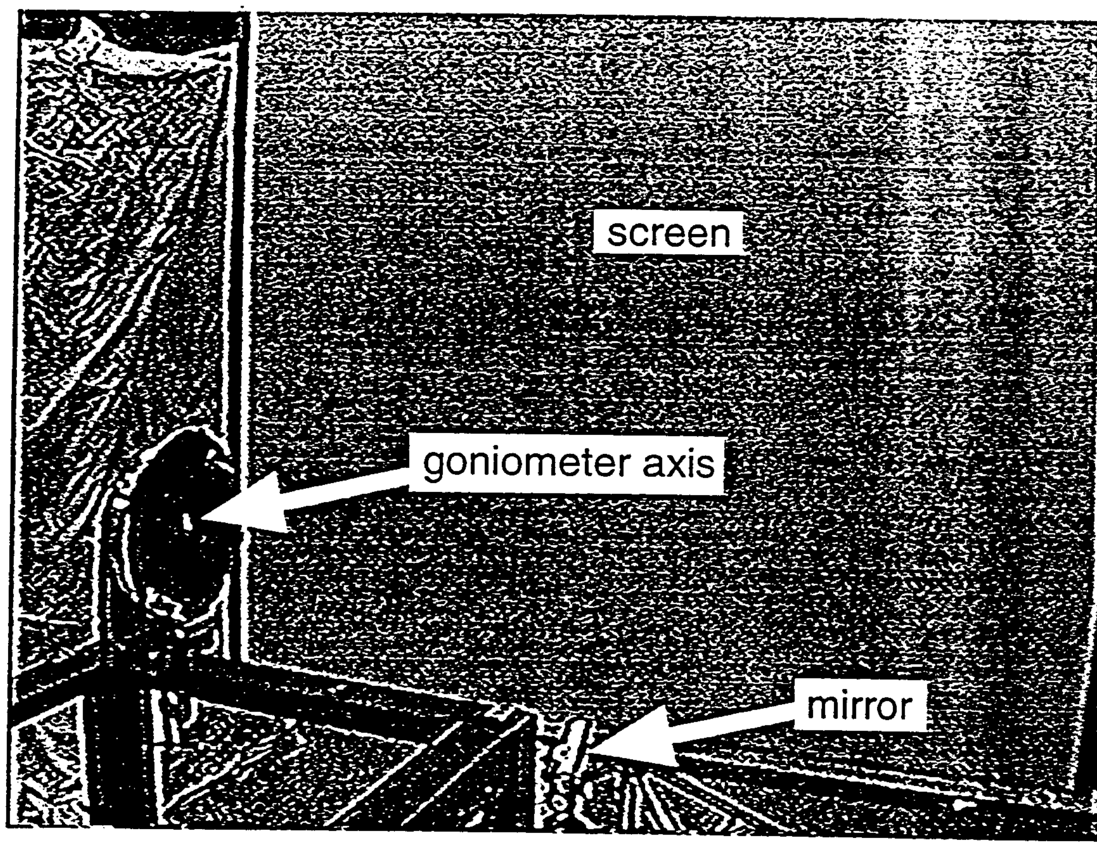

Scattering observations for tilted transparent fibers: evolution of Airy caustics with cylinder tilt and the caustic merging transition

Catherine M. Mount, David B. Thiessen, and Philip L. Marston APPLIED OPTICS / Vol. 37, No. 9 20 March 1998

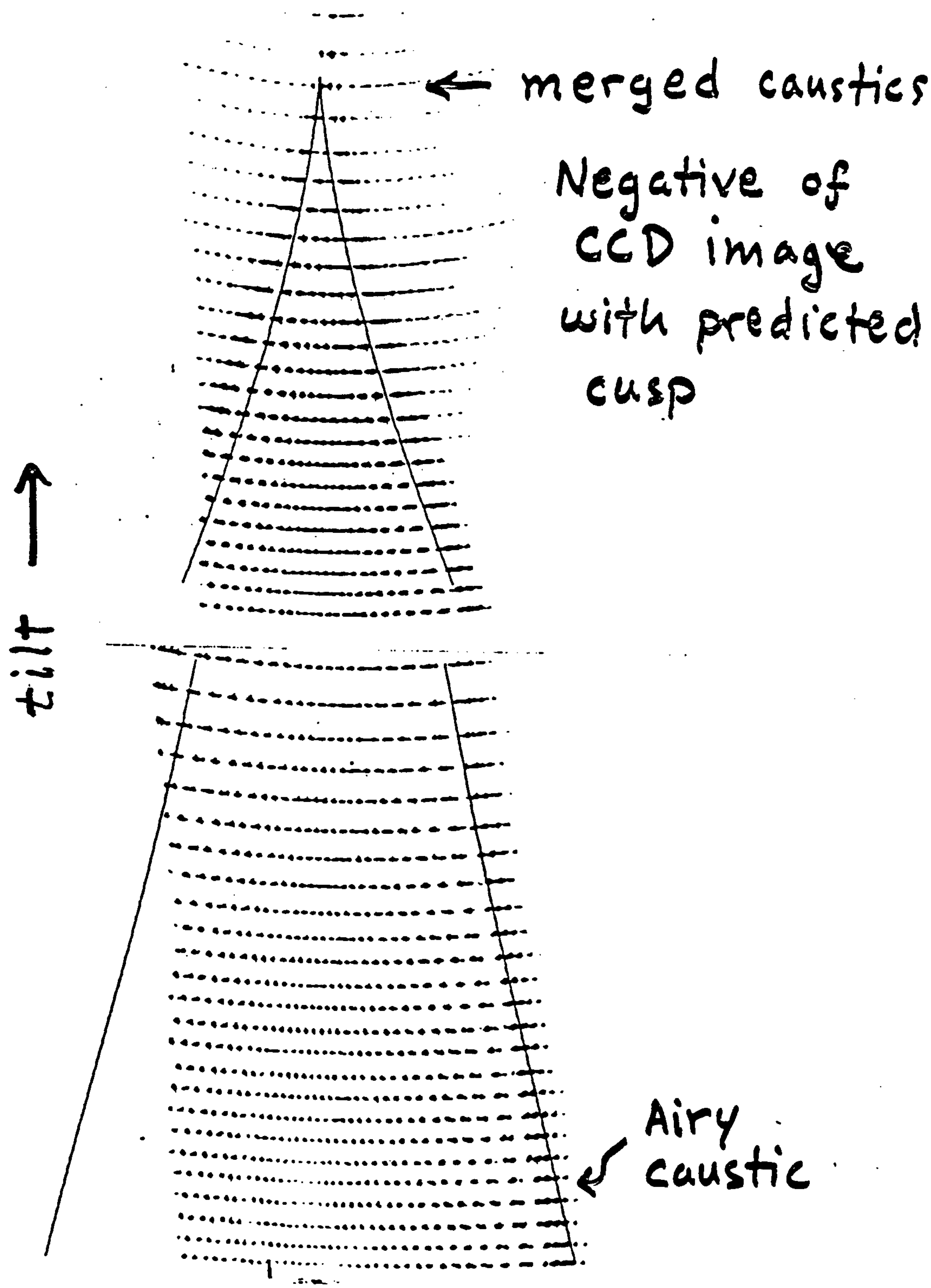
merged caustics
Negative of CCD image with predicted cusp
tilt
Airy caustic

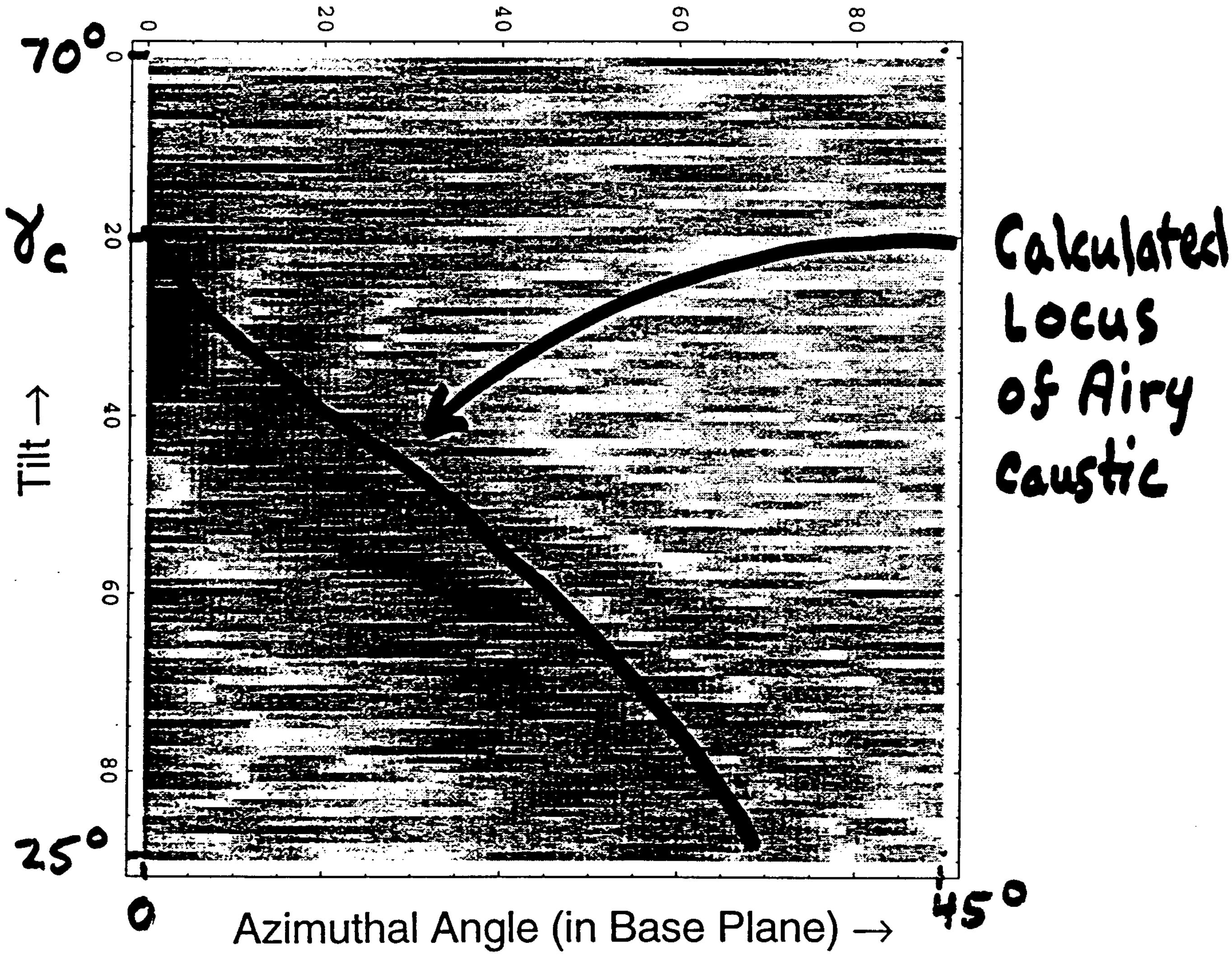

Calculated for infinite polystyrene (elastic) cylinder in water for sound with ka = 50.

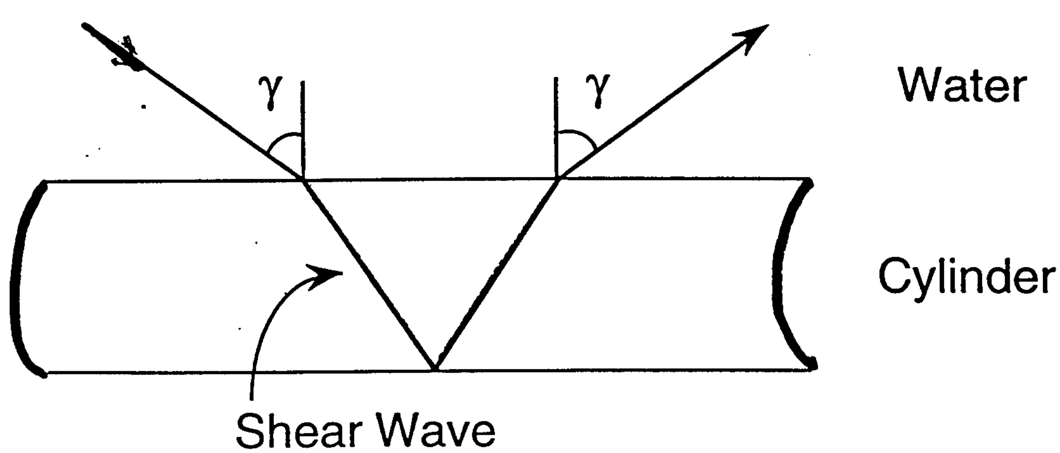

TR-20

In the Meridional Plane...

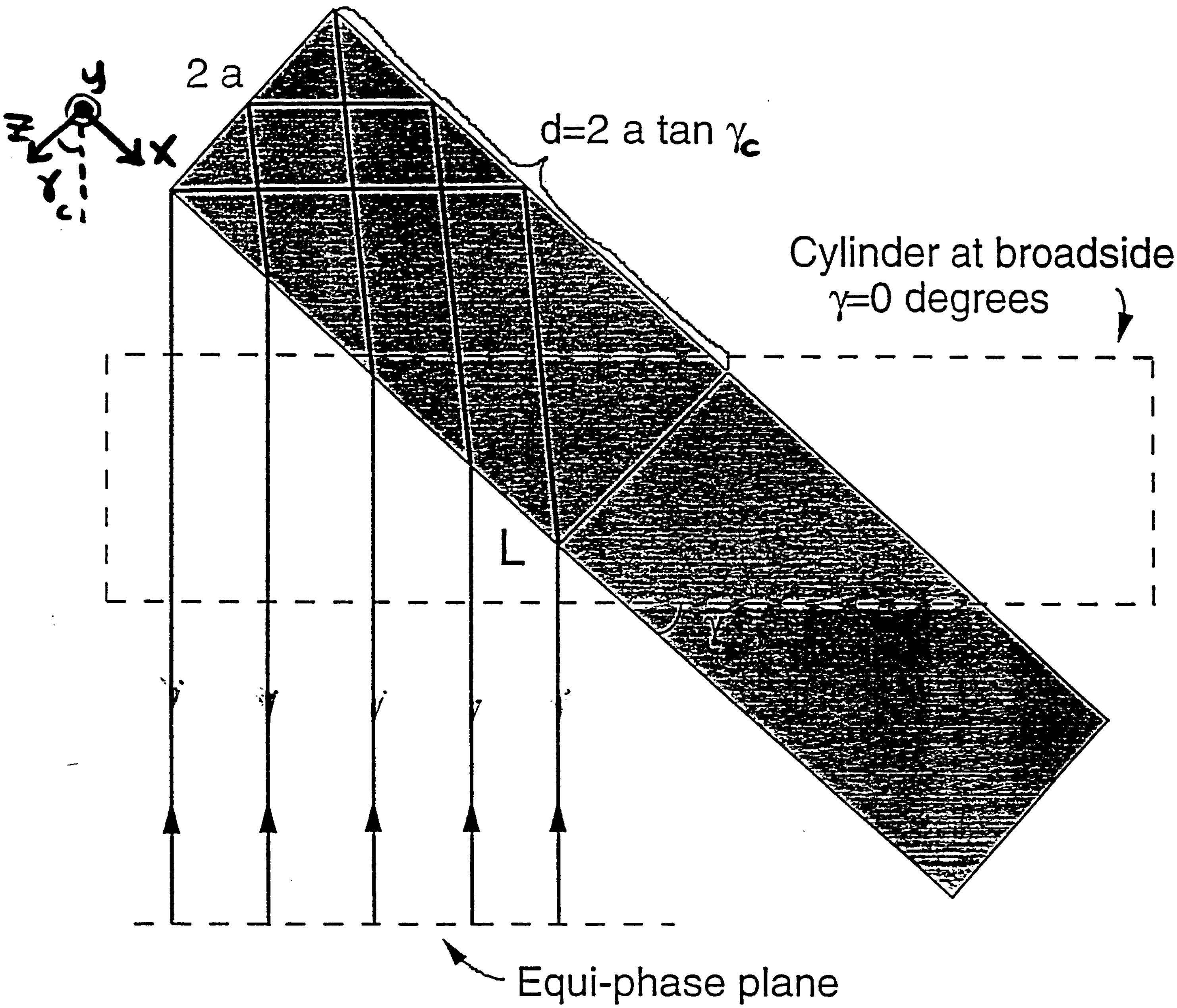

$$W(x, y=0) = x \sin\gamma \quad (0 < x < d)$$

New Backscattering Enhancement Mechanisms for Solid Polymer Targets

1. For filled targets (such as solid cylinders): "New" transmitted rays for generating flat scattered wavefronts.

Examples: Subsonic shear waves (PMMA or Polystyrene)
Subsonic longitudinal waves (RTV)

Geometry: Tilted bluntly truncated cylinder

Caustic merging transition at critical tilt:

$$\gamma_c = \arccos\left[\left(\left(N^2 - 1\right)/3\right)^{1/2}\right], \; N > 1,$$

Refractive Index $N = c/c_T$ or c/c_L

Marston, Applied Optics **37**, 1551-1556 (1998)
Blonigen and Marston, JASA (abstract) **102**, 3088 (1997)

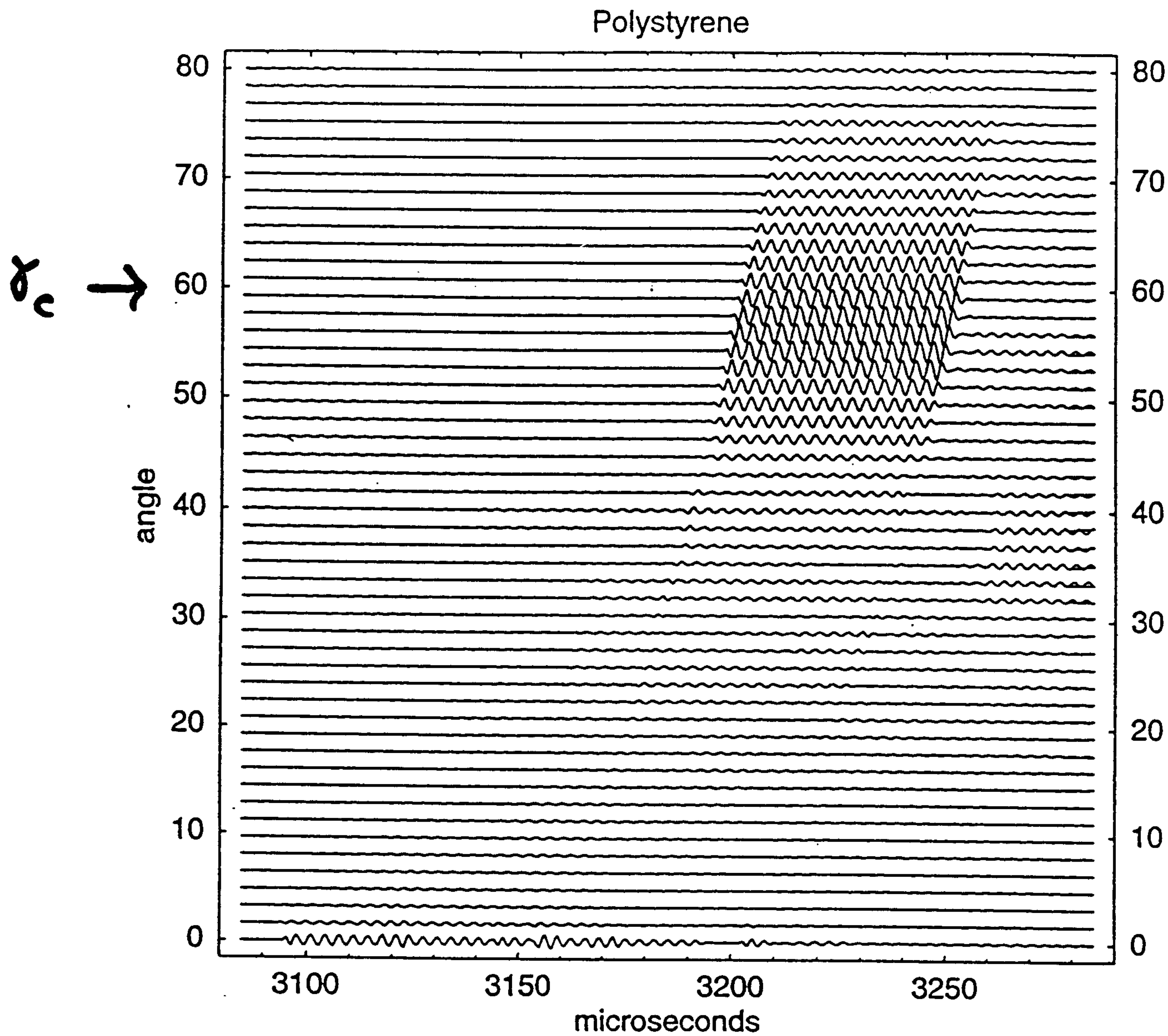

$ka = 20.5$

300 kHz

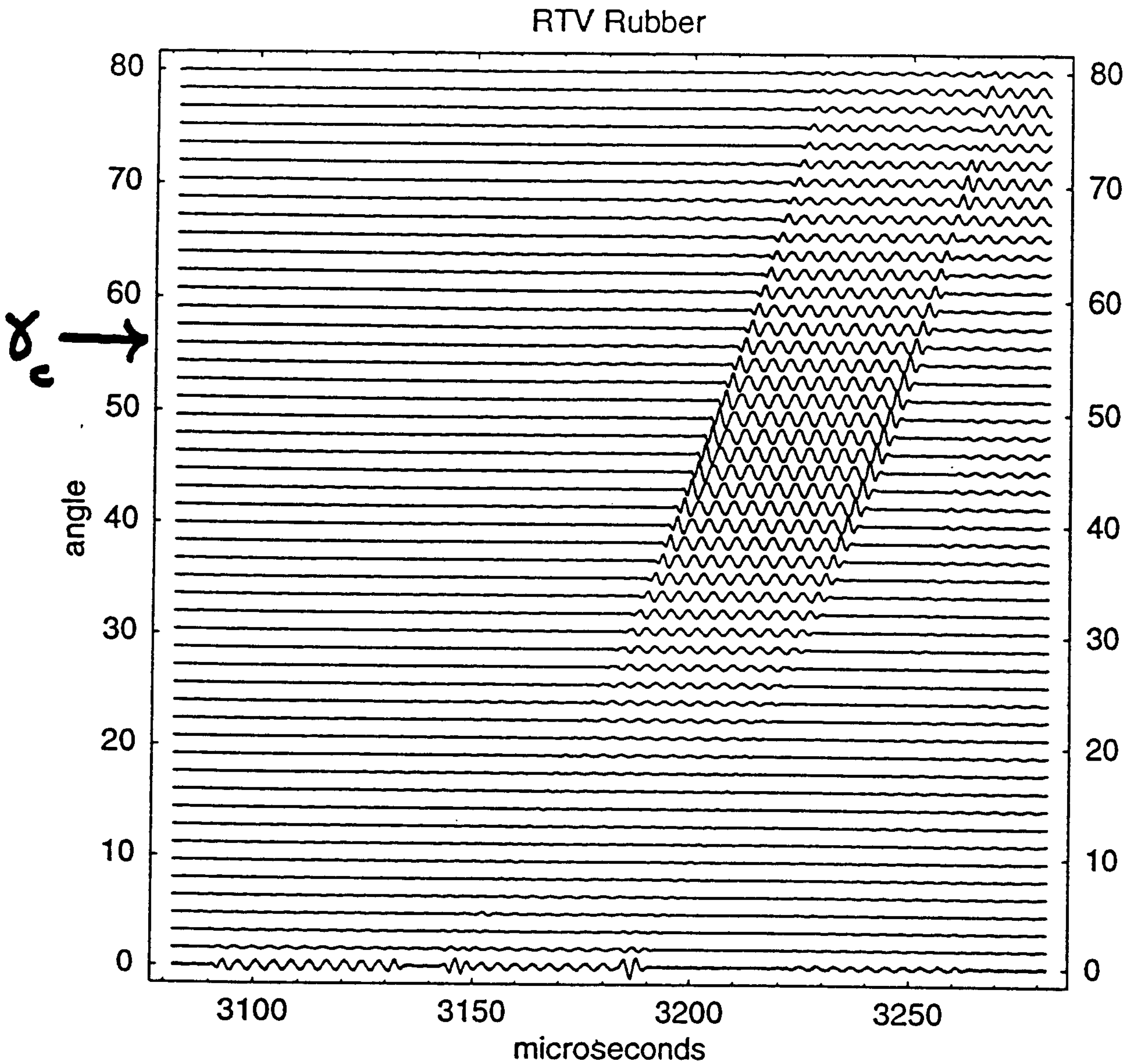

$ka = 14.3$ 250 kHz

TR-24

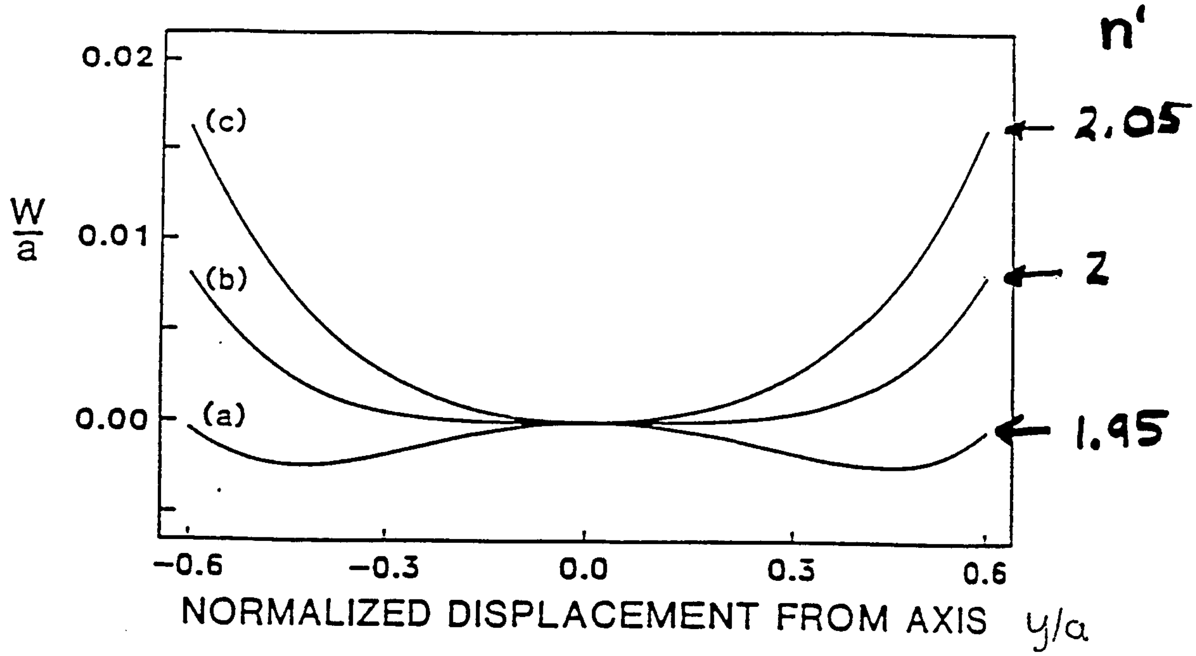

$$W(x=0,y) = a_4 y^4 - a_2 y^2$$

For $n' \approx 2$ $\Big\}$ $\quad a_2 = \dfrac{1}{2\alpha} \approx \dfrac{(2-n')}{a n'}$; $\quad a_4 \approx \dfrac{2}{a^3 n'^3 (2+n')}$

$$\Rightarrow W(0,y) = y^4 / 16 a^3$$

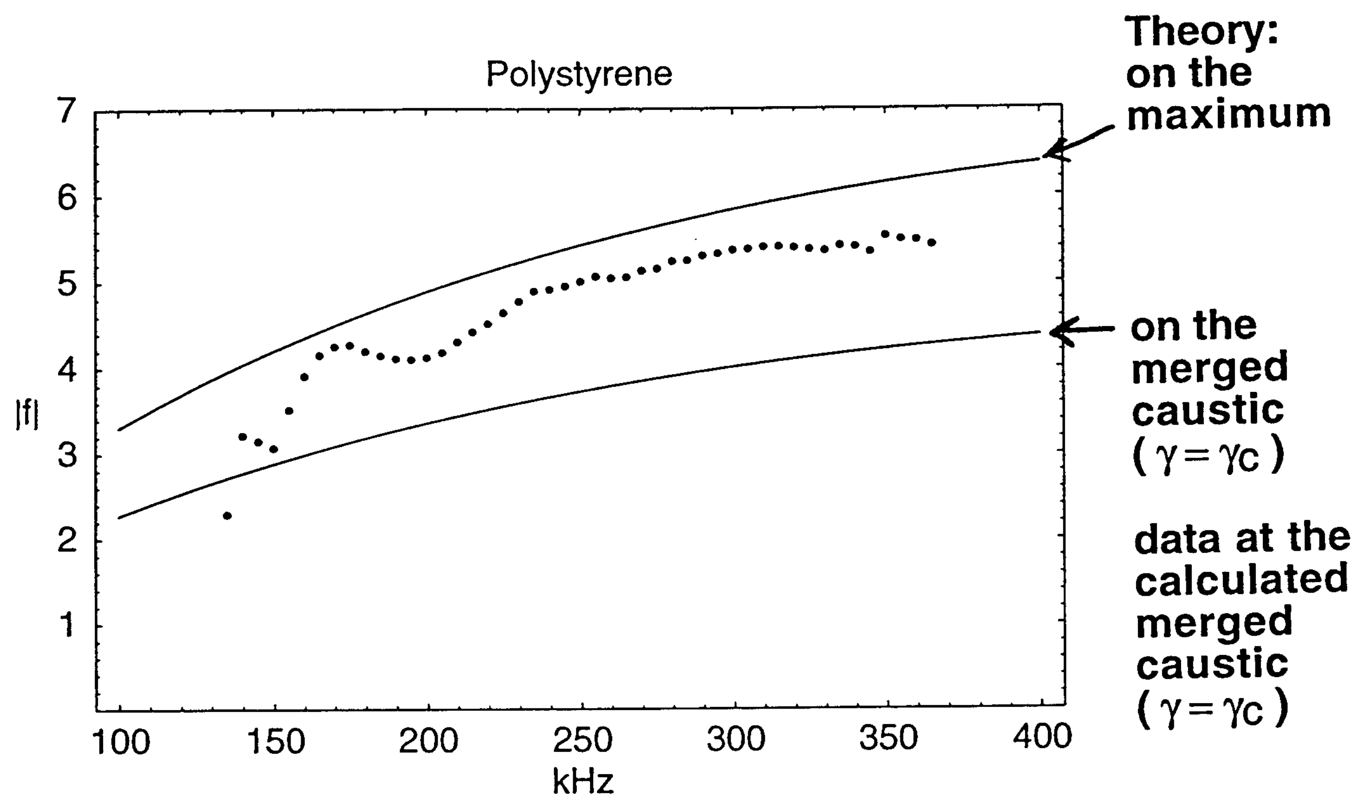

Polystyrene
7
6
5
4
3
2
1
|f|
100
150
200
250
300
350
400
kHz
Theory:
on the
maximum
on the
merged
caustic
($\gamma = \gamma_c$)
data at the
calculated
merged
caustic
($\gamma = \gamma_c$)

Pearcey Function

$$P_{\pm}(w_1, w_2) = \int_{-\infty}^{\infty} ds \, \exp[\pm i(s^4 + w_2 s^2 + w_1 s)]$$

$$P_{\pm}(0,0) = \frac{1}{2}\Gamma(\tfrac{1}{4})\, e^{\pm i\frac{\pi}{8}}$$

Backscattered Pressure:

$$P = P_i \frac{a}{2r} f e^{ikr}$$

where f = form function

hard sphere: $|f| = 1$

tilted cylinder: On the caustic $w_1 = w_2 = 0$,

$$|f| = \frac{2}{\pi}\Gamma(\tfrac{1}{4})|B| \, (ka)^{3/4} \sin\gamma_c / (\cos\gamma_c)^{1/2}$$

Pearcey Function

$$P_{\pm}(w_2, w_1) = \int_{-\infty}^{\infty} \exp[\pm i(s^4 + w_2 s^2 + w_1 s)]\, ds$$

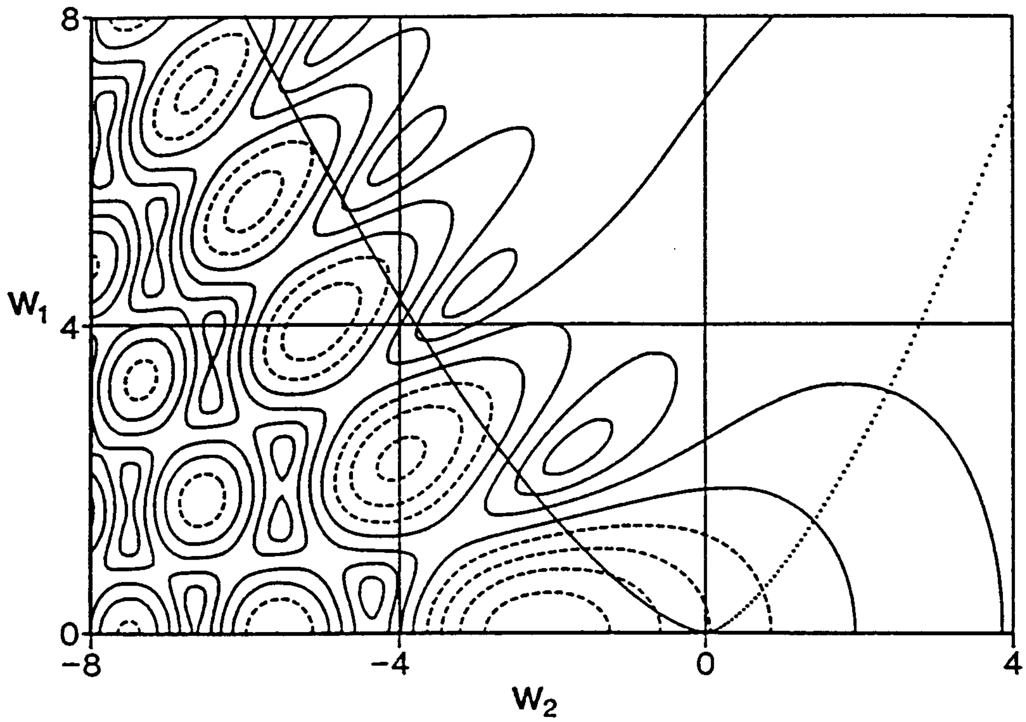

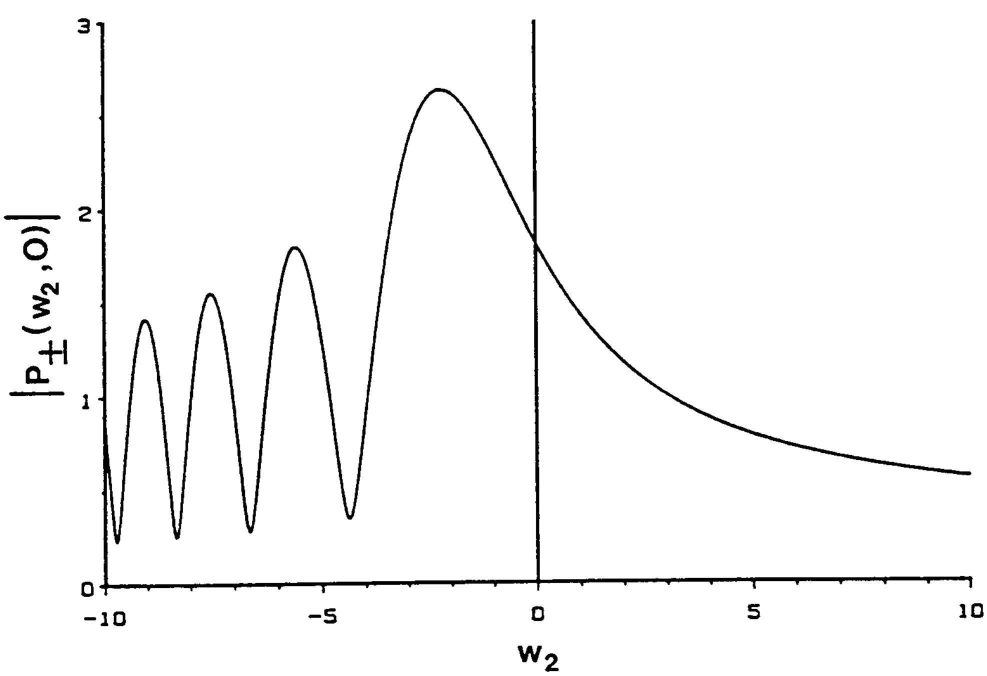

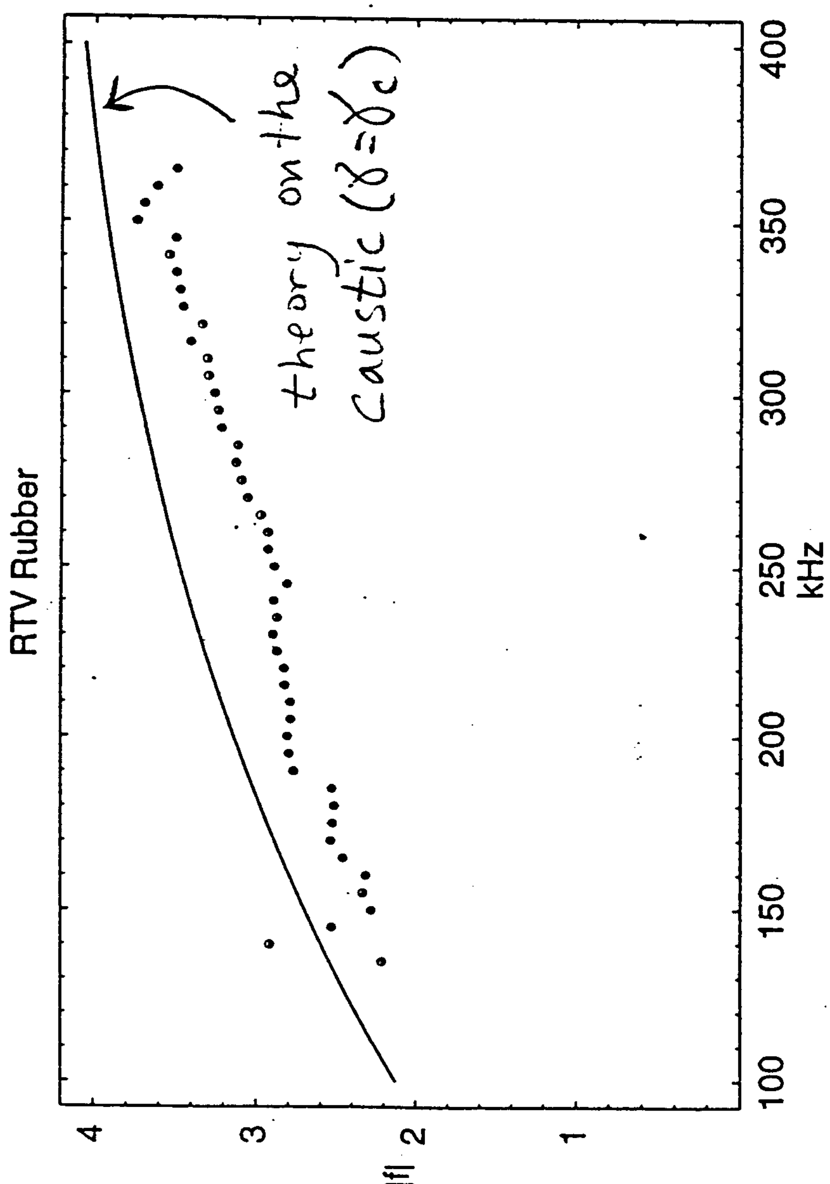
RTV Rubber
theory on the caustic (γ=γ_c)
kHz
|f|
100
150
200
250
300
350
400
1
2
3
4

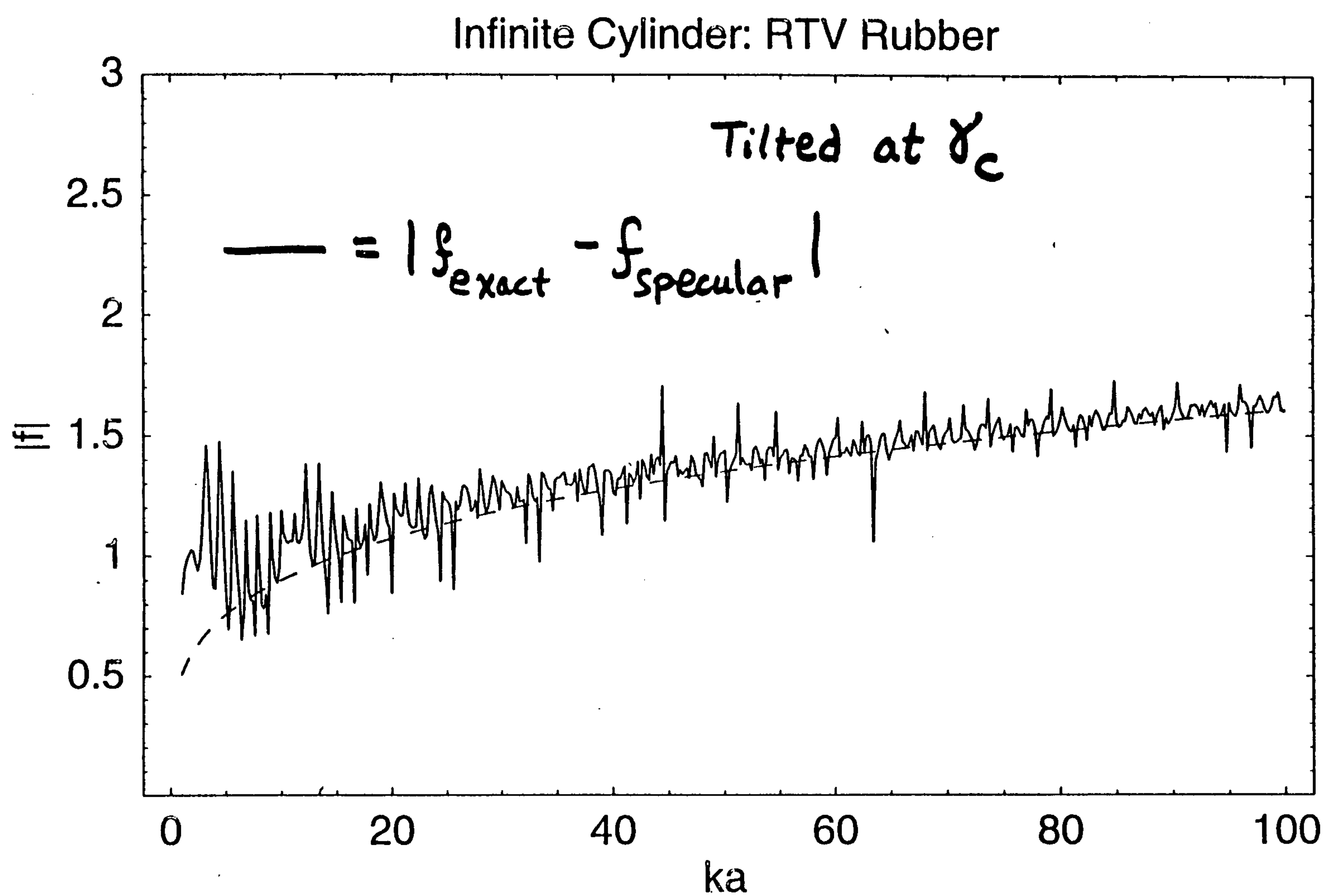

$$|p_{2d}| = p_i \sqrt{\frac{a}{2r_\perp}}\, |f|$$

- - - - Ray theory: $|f_{ray}| = \dfrac{2|B|}{\sqrt{\pi}} (ka \cos\gamma_c)^{1/4} |P_-(0,0)|$

→ 1. Coincidence frequency of a_0 Lamb wave and tunneling model: [Zhang, Sun, & Marston (1992), Kaduchak & M(1993), M & Sun (1995) JASA]

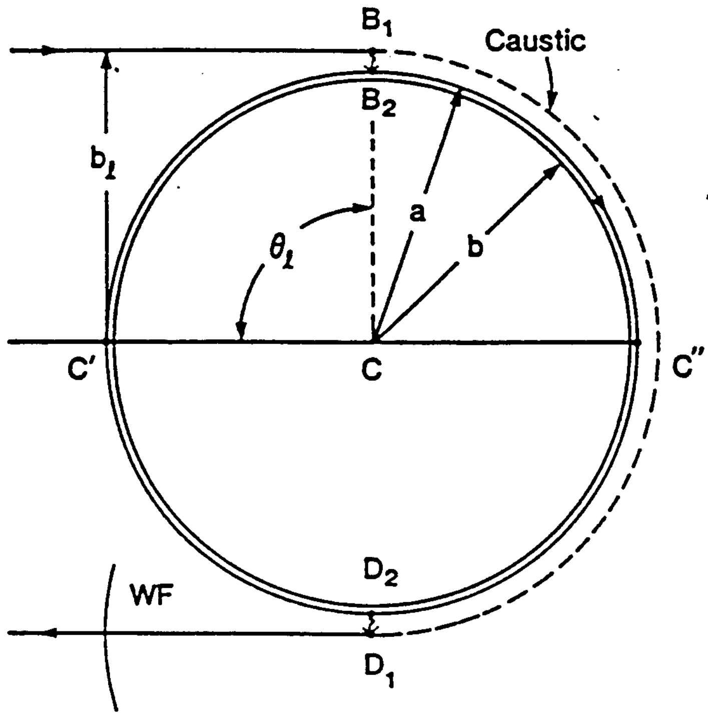

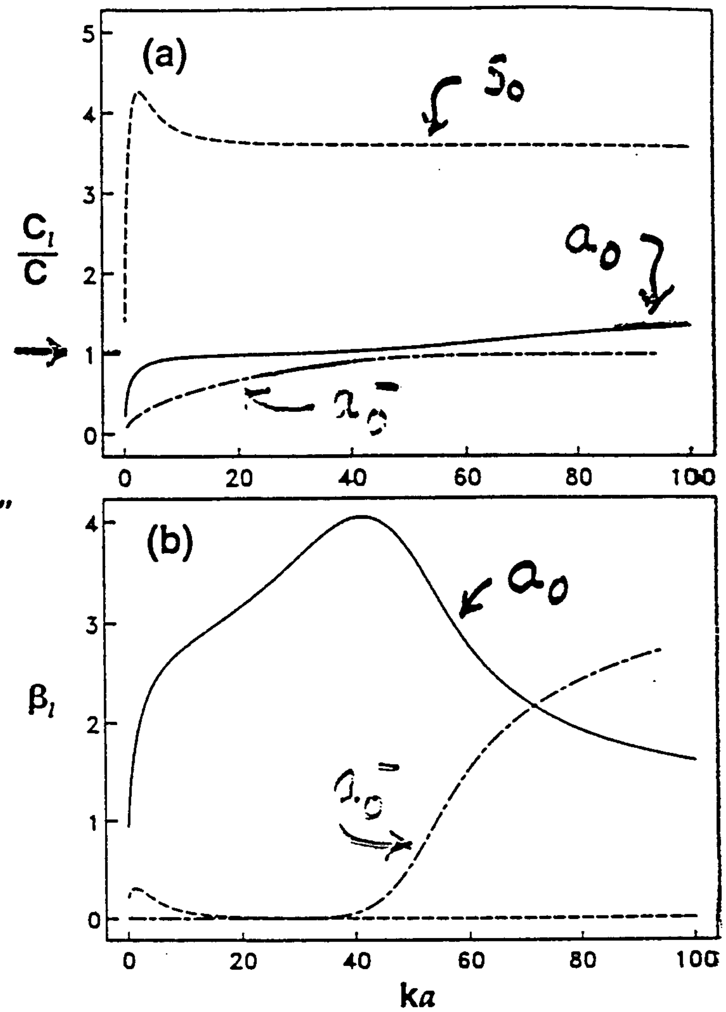

New Backscattering Enhancement Mechanisms for Solid Polymer Targets

2. Tunneling enhancements for "new" subsonic waves

- Example: Rayleigh wave on PMMA or Polystyrene becomes subsonic with respect to water or sediment loading.
- Ray Theory: Same as Zhang, Sun, & Marston (1992) but with Rayleigh wave parameters and attenuation.
- Experimental confirmation for solid spheres: B. T. Hefner.

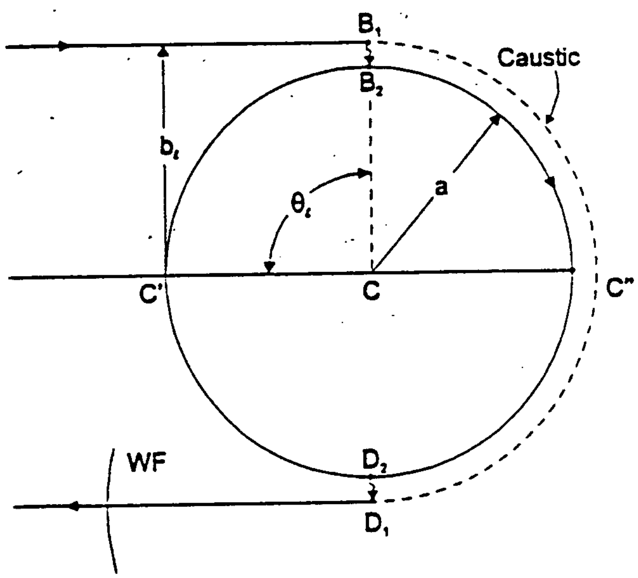

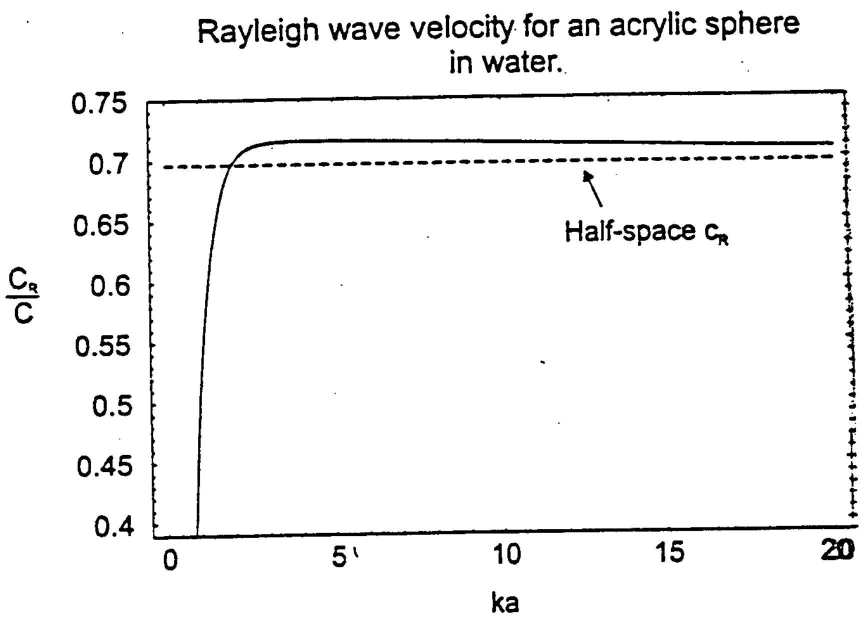

3. New coincidence frequency and backwards wave enhancements for shells.

Summary

- Quantitative leaky ray theory has been confirmed for meridional ray backscattering enhancements for truncated steel shells and solid cylinders (Morse and Gipson).
- In addition to leakage by supersonic a_0 waves, reflection from the end of a shell near a mode threshold causes radiation due to the collective motion of a cut-off a_1 wave (Morse).
- Plastic targets in water or sediment require rethinking of enhancement mechanisms.
- For blunt tilted solid cylinders of polystyrene and RTV a backscattering enhancement due to the merging of farfield caustics of transmitted rays has been observed (Blonigen).
- PMMA spheres were observed to give a backscattering enhancement due to tunneling to a subsonic Rayleigh wave (Hefner).
- We modeled the resulting Rayleigh wave resonance scattering by extending previous ray-tunneling models of subsonic a_0 waves on steel shells [Zhang, Sun, & Marston JASA (1992)].

Subsonic Rayleigh wave resonances on solid polymer spheres in water and backscattering enhancements associated with tunneling: experiments, models, and the relative significance of material and radiation damping

Brian T. Hefner
and
Philip L. Marston
Dept. of Physics
Washington State University
Pullman, WA 99164-2814

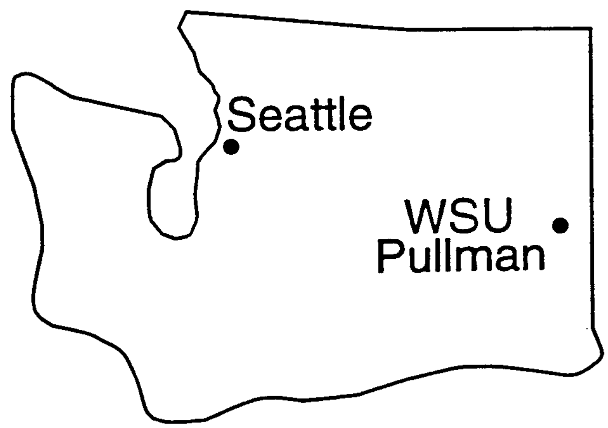

Supported by the Office of Naval Research.

TR-1

Backscattering from solid spheres

Material properties:

	Longitudinal velocity (mm/μs)	Shear velocity (mm/μs)	Rayleigh velocity (mm/μs)	Density (g/mm^3)
Stainless Steel	5.675	3.141	2.903	7.57
Acrylic (PMMA)	**2.690**	**1.340**	**1.250**	**1.19**
Water	1.479			1.00

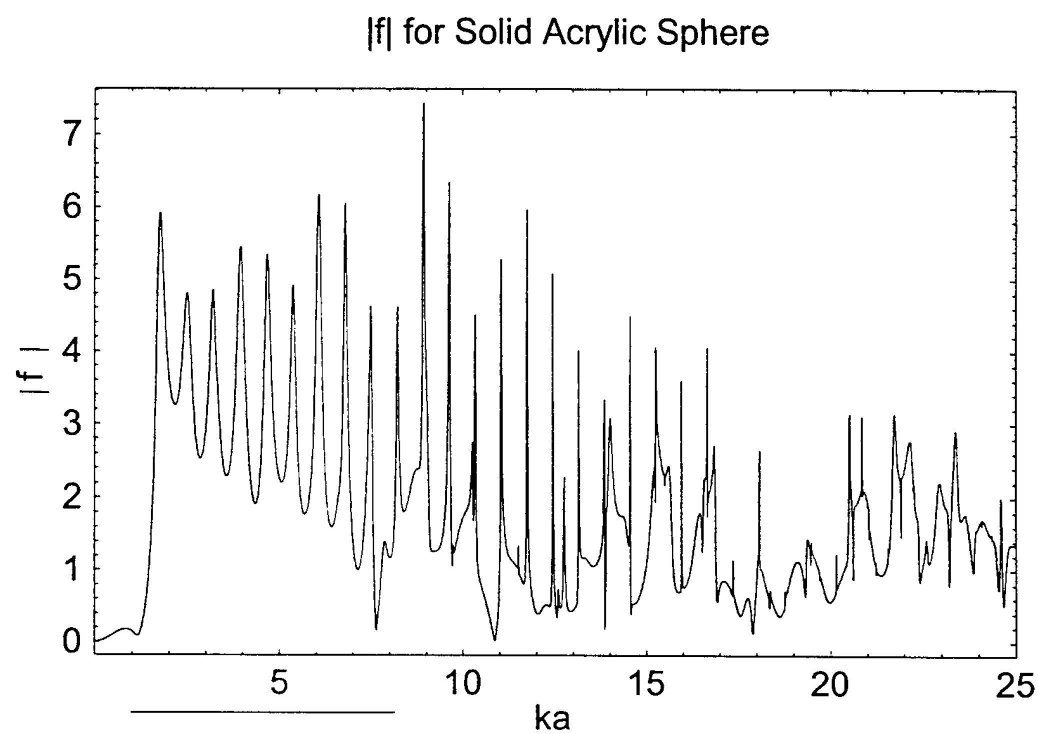

Low frequency enhancement associated with subsonic Rayleigh wave resonances.

Enhancement is absent from |f| for steel.

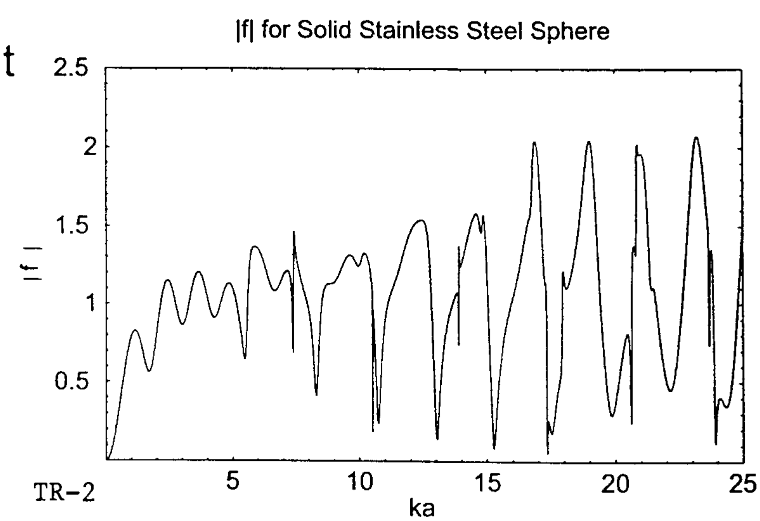

Coupling of incident field to subsonic Rayleigh wave:

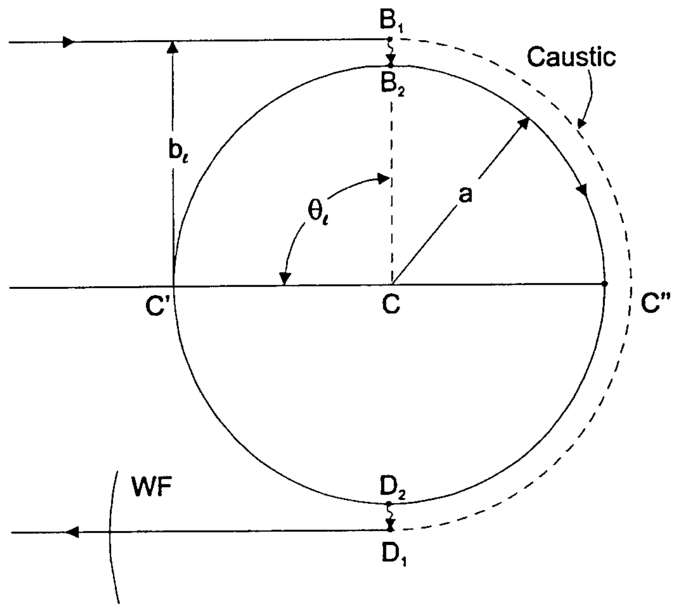

Partial wave series (PWS) solution :

$$p_{sca} = p_{inc}(a/2r) f\, e^{i(kr-\omega t)} \qquad f^{PWS} = \frac{2}{ika}\sum_{n=0}^{\infty}(-1)^n(2n+1)\frac{B_n(ka)}{D_n(ka)}$$

Sommerfeld Watson Transform (SWT):

$$D_{\nu_l}(x) = 0$$

$$\nu_l = \alpha_l + i\beta_l$$

$$\frac{c_l}{c} = \frac{x}{\alpha_l + \frac{1}{2}}$$

c_l : phase velocity for the l th surface wave

β_l : damping coefficient

Rayleigh wave contribution:

$$f_{mR} = -G_R \exp[-\pi\beta_R - 2\pi m\beta_R + i(\eta_R - m\pi + 2\pi m x\, c/c_R)]$$

$$f_R = \sum_{m=0}^{\infty} f_{mR} = \frac{-G_R \exp(-\pi\beta_R + i\eta_R)}{[1+\exp(-2\pi\beta_R + i2\pi x\, c/c_R)]}$$

$$|G_R| \approx 8\pi\beta_R c/c_R \qquad \eta_R = \pi kac/c_R$$

Incorporating material absorption into the backscattering formulations.

Assume both longitudinal and shear wave velocities have linear absorptions

$$k_L \Rightarrow k_L(1+i\alpha_L)$$
$$k_S \Rightarrow k_S(1+i\alpha_S)$$

For Acrylic: $\alpha_L = 0.0034$, $\alpha_S = 0.0053$

In the exact |f|-

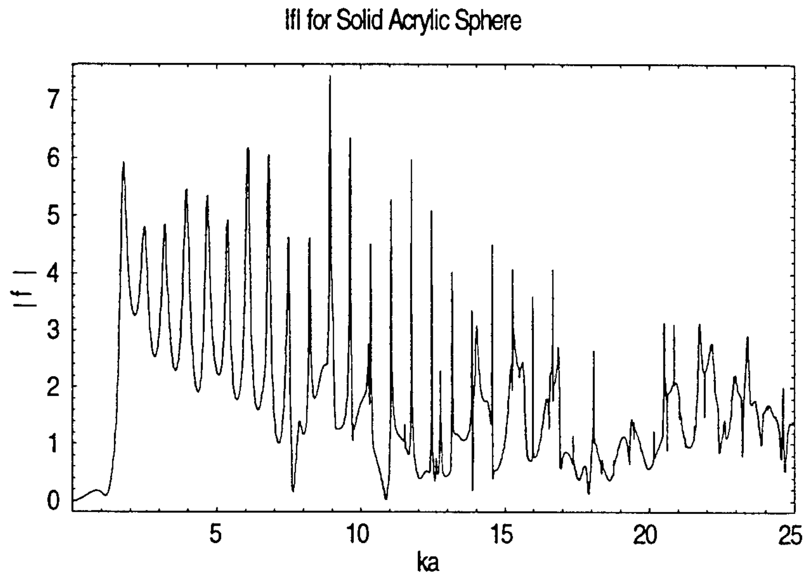

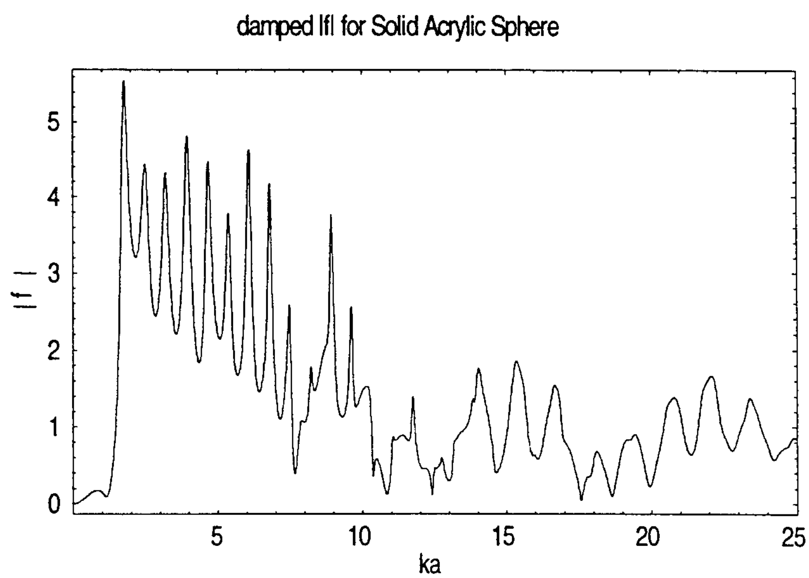

TR-4

10-cycle tone burst backscattered from acrylic sphere.

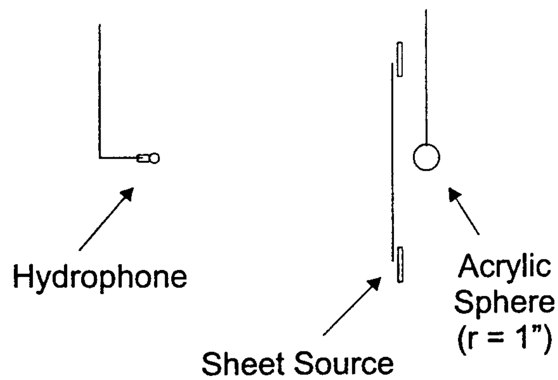

For calculated resonance at 15.9 kHz

Measured: Q = 9.31

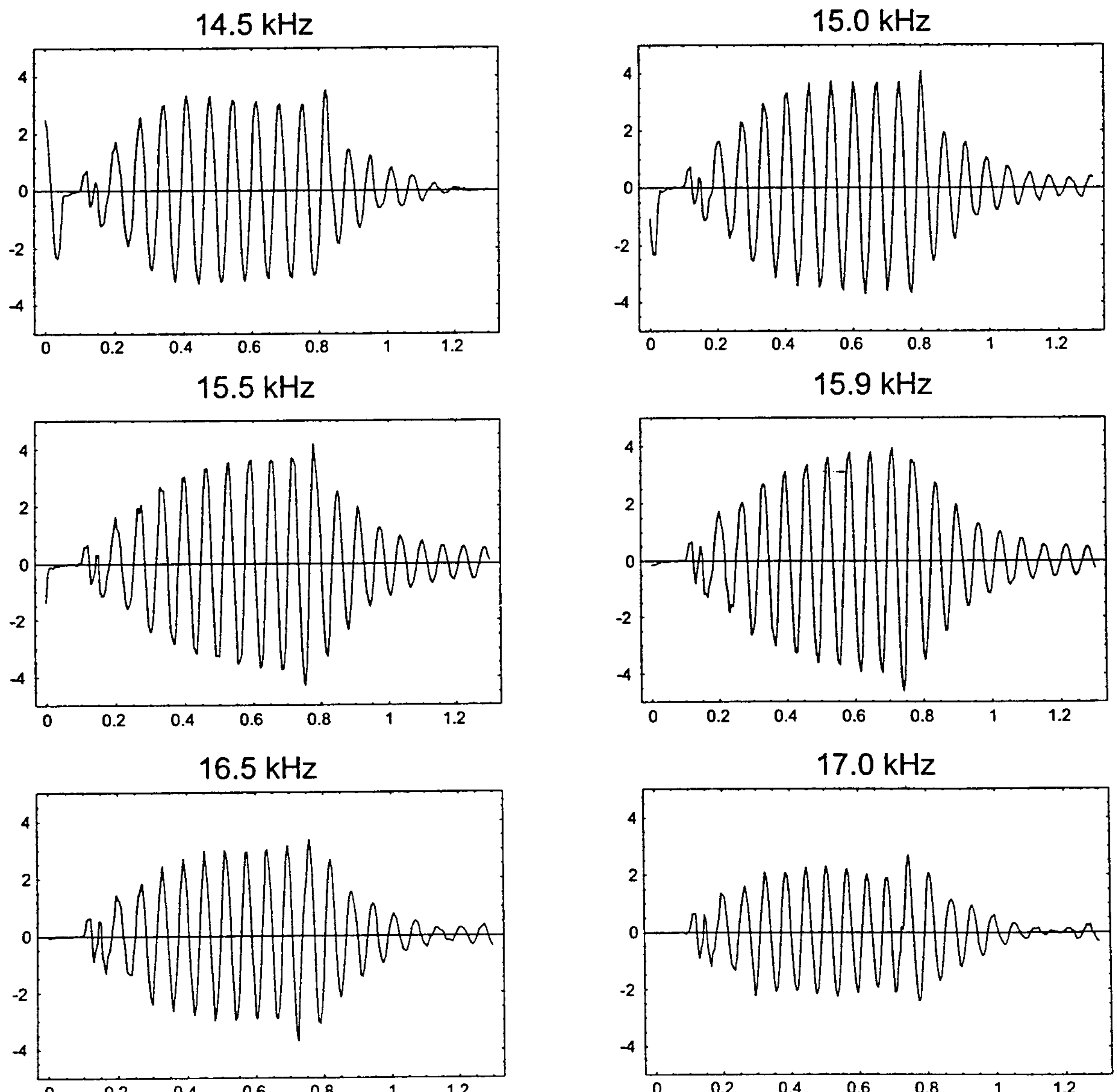

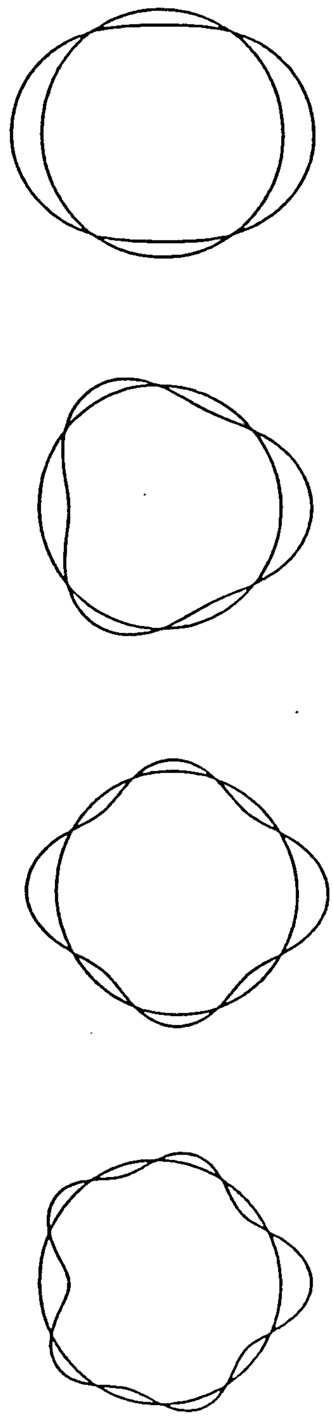

TR-6

Absorption in the approximate Rayleigh wave contribution.

$|G_R| \approx 8\pi\beta_R c / c_R$ depends on the radiation damping parameter, β_R

In the remaining expression for f_{ml}, the damping parameter must include both radiation damping and material absorption.

The equation $D_{\nu_R}(x) = 0$ is then solved with the complex longitudinal and shear wavenumbers to yield $\nu'_R = \alpha'_R + i\beta'_R$ and

$$f_R = \sum_{m=0}^{\infty} f_{mR} = -G_R \frac{\exp(-\pi\beta'_R + i\eta_R)}{[1 - \exp(-2\pi\beta'_R + i2\pi x\, c/c_R)]}$$

Possible to approximate α'_R and β'_R by using results for fluid-loaded PMMA half space:

$$k'_R = k_R(1 + i\gamma_R) \quad \Rightarrow \gamma_R = 0.00149$$

Using this value and the values calculated for the sphere without material absorption:

$$\alpha'_{R(approx)} \approx \alpha_R$$

$$\nu'_{R(approx)} \approx \alpha_R\left(1 + i\left(\frac{\beta_R}{\alpha_R} + \gamma_R\right)\right) \qquad \beta'_{R(approx)} \approx \beta_R + \gamma_R\left(\frac{x}{c_R / c} - \frac{1}{2}\right)$$

Rayleigh wave velocity for an acrylic sphere in water.

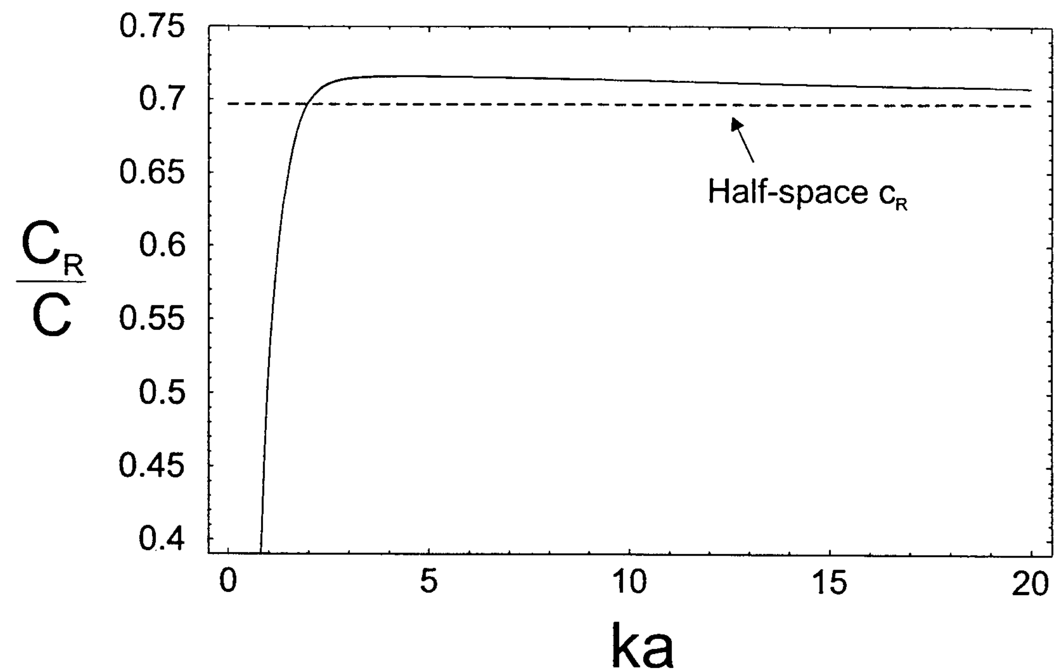

Rayleigh wave damping for an acrylic sphere in water.

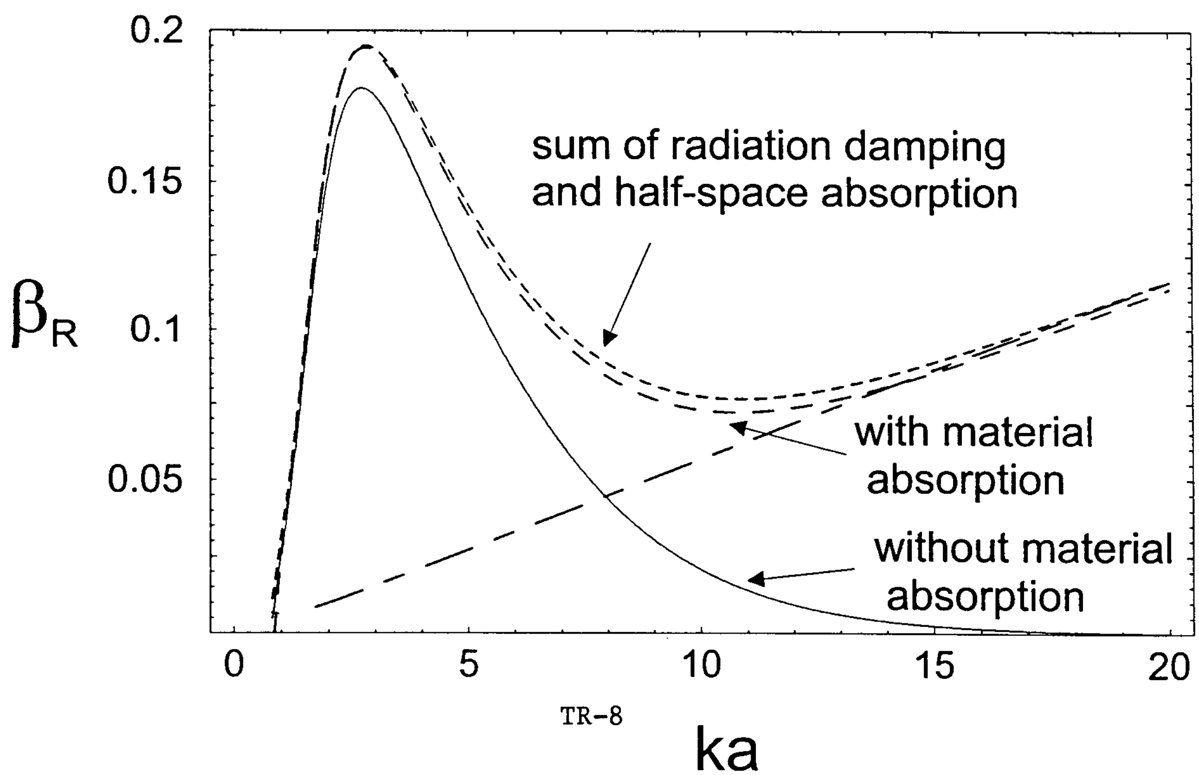

TR-8

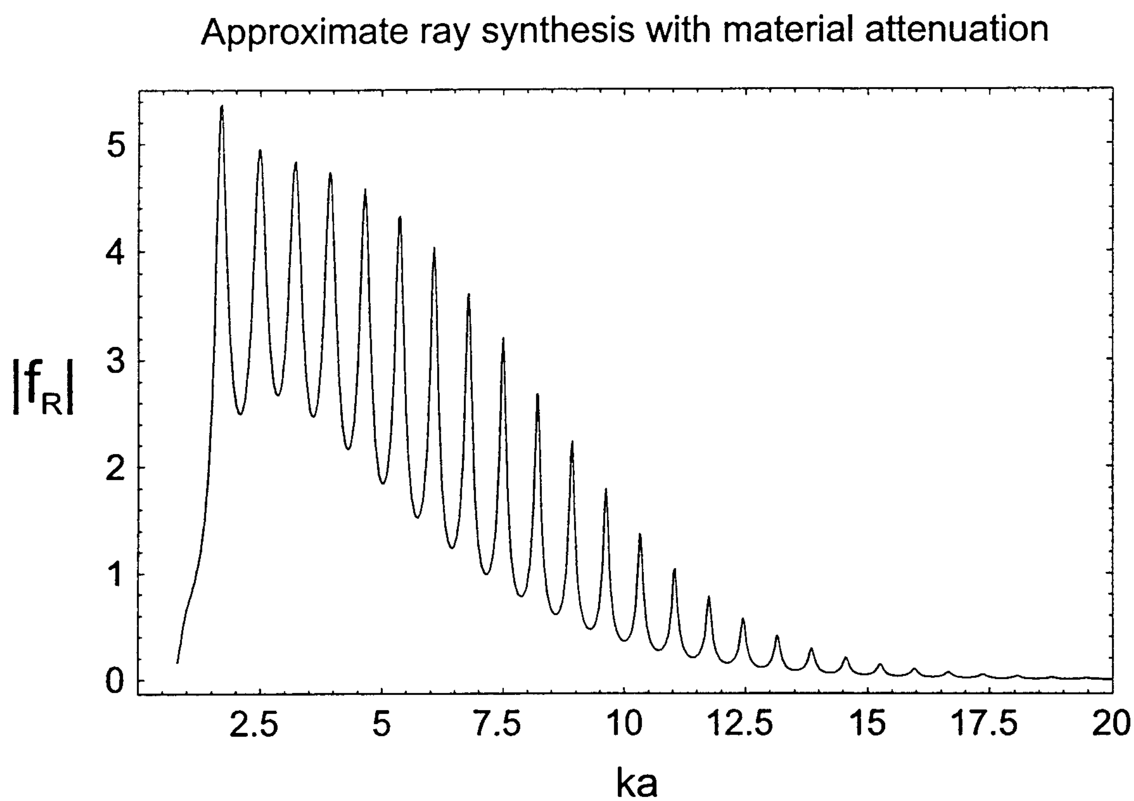
Approximate ray synthesis with material attenuation
|fR|
0
1
2
3
4
5
2.5
5
7.5
10
12.5
15
17.5
20
ka

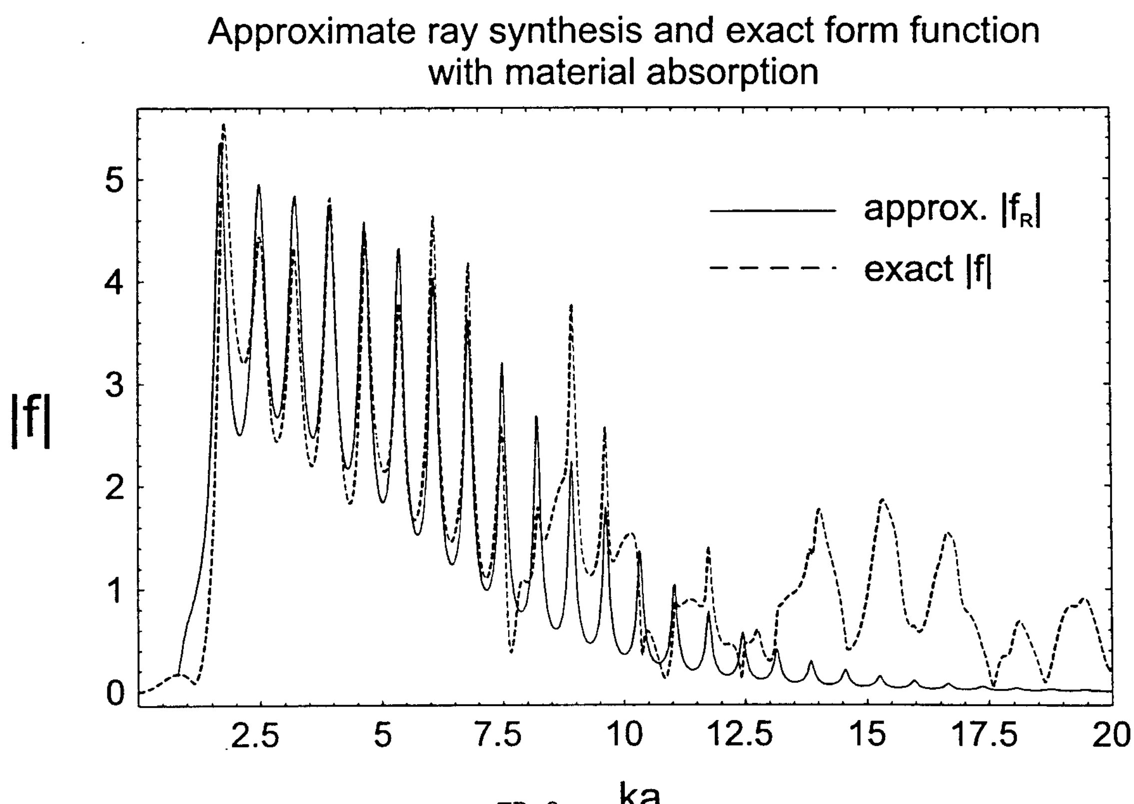
Approximate ray synthesis and exact form function
with material absorption
approx. |fR|
exact |f|
|f|
0
1
2
3
4
5
2.5
5
7.5
10
12.5
15
17.5
20
ka

Measurements of form function for acrylic sphere.

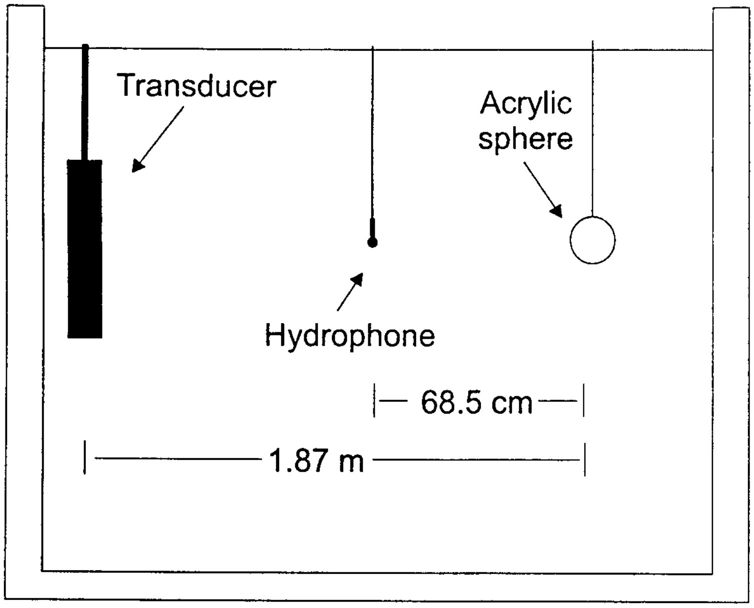

30-cycle tone bursts from a 3-1 composite transducer.

The response was normalized by measuring the signal when the hydrophone was placed at the sphere location.

Data taken for two spheres in the frequency range 30 - 60 khz

▲ a = 1.27 cm

♦ a = 2.54 cm

Comparison of mesured and calculated |f|

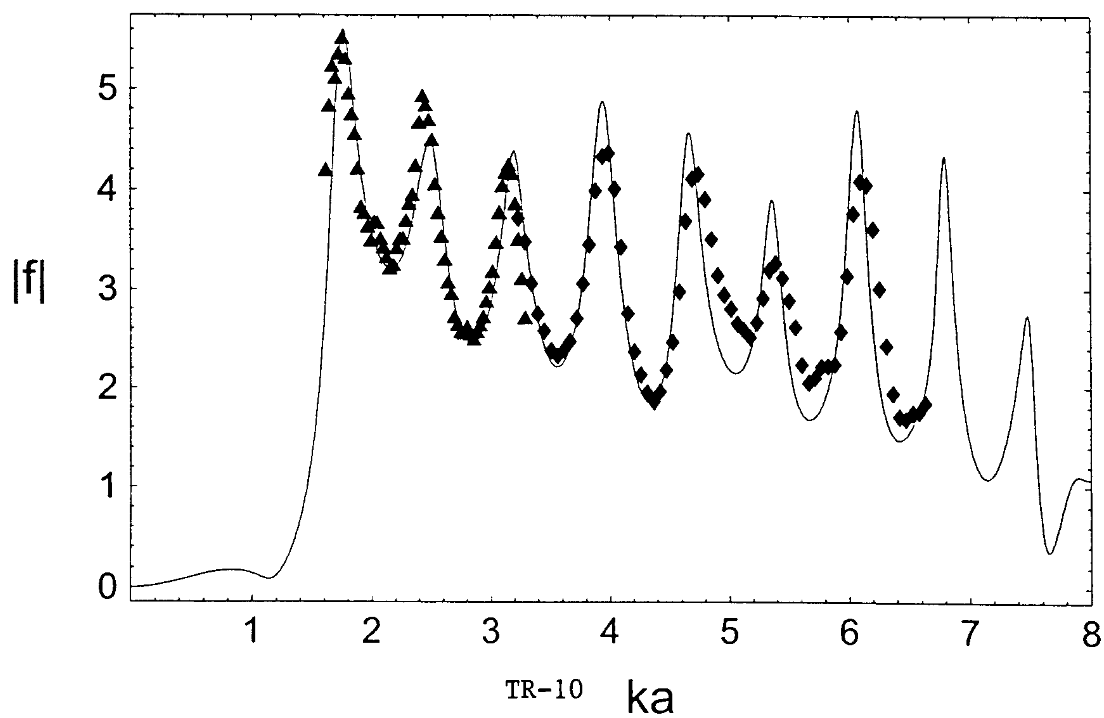

TR-10

Calculation of quality factors for Rayleigh wave resonances of a fluid-loaded PMMA sphere.

Quality factors of resonances can be calculated from decay rate of echo amplitudes (L. R. Dragonette, et. al. 1996)

$$\text{mth echo} \quad \rightarrow \quad A_m \approx B \exp\left(-T\beta_R \, c_{gR}/c\right)$$

$$T \equiv (ct - R)/a$$

$$Q \approx ka/(2\beta_R \, c_{gR}/c)$$

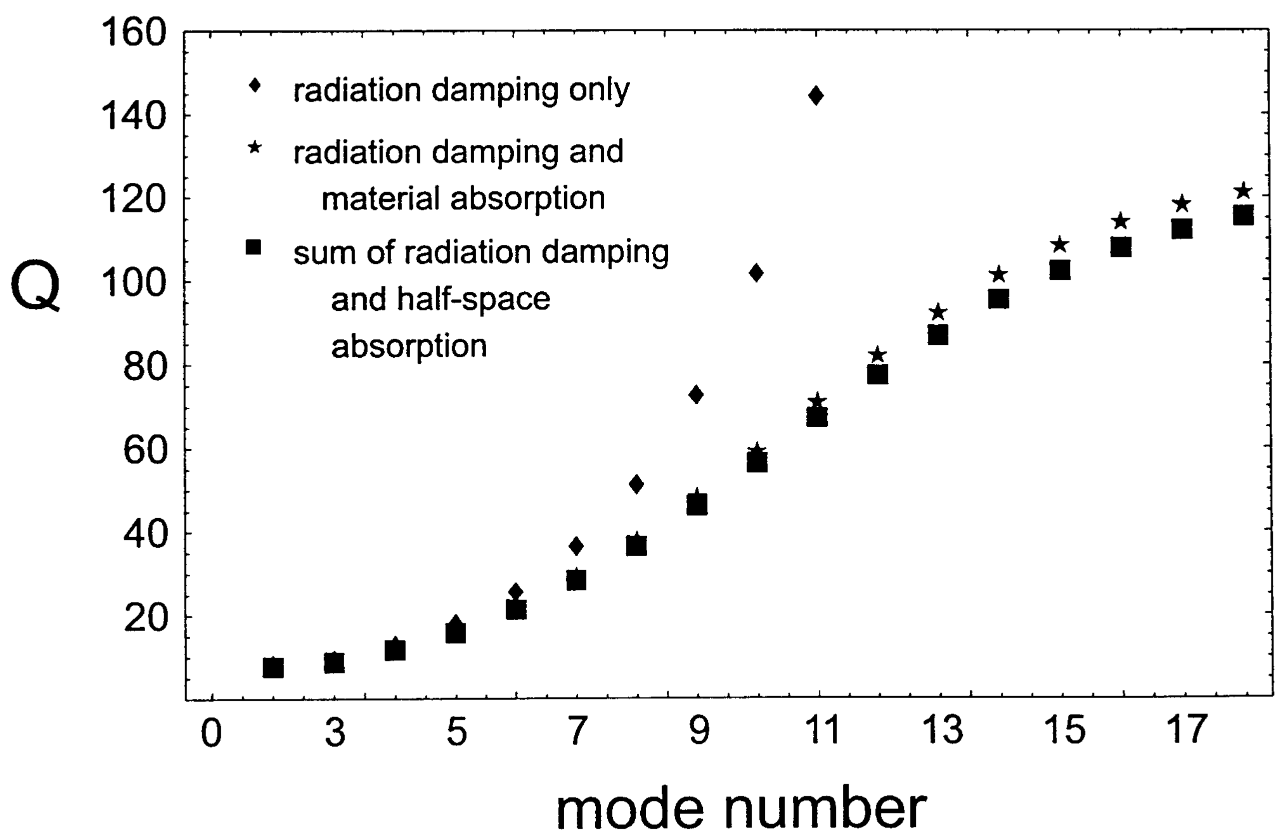

Target Strength for PMMA spheres.

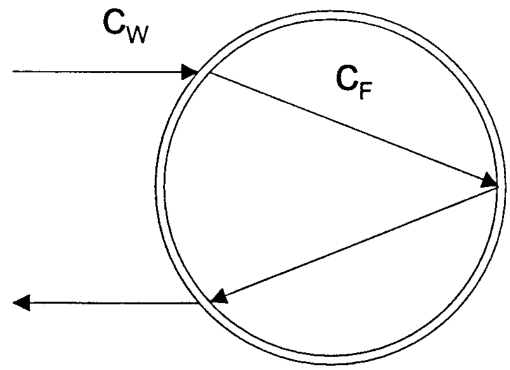

Thin fluid-filled shells typically used as passive sonar targets.

Glory scattering

$c_w < c_F$

CFC's have typically been used as filler fluid however alternatives are now required due ban on CFC's. (G. Kaduchak and C. M. Loeffler, 1998)

For a PMMA sphere at largest resonance

$(ka = 1.73)$

$$\mathrm{TS} = 20\log\left(|f|\frac{1.73c}{4\pi R_{ref} F}\right)$$

$a(m) = 407/F(Hz)$
$R_{ref} = 1\ m$
$|f| = 5.63$

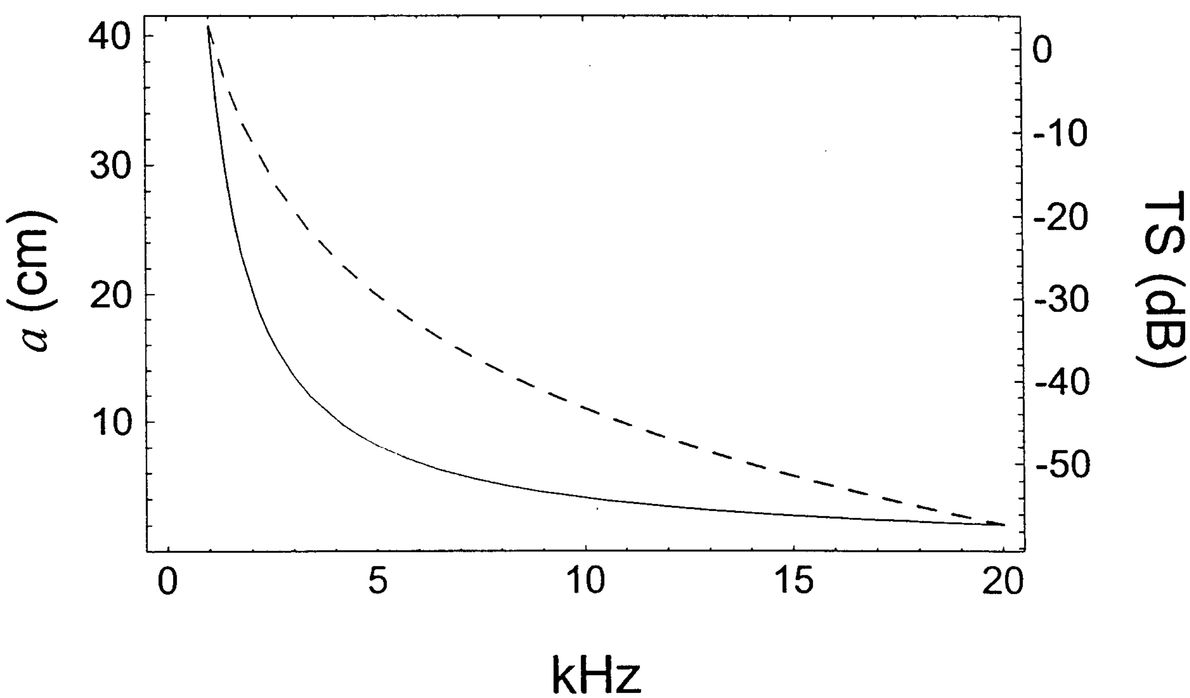

Lamb waves on an acrylic plate.

Phase velocities for 2mm thick acrylic plate
without fluid-loading

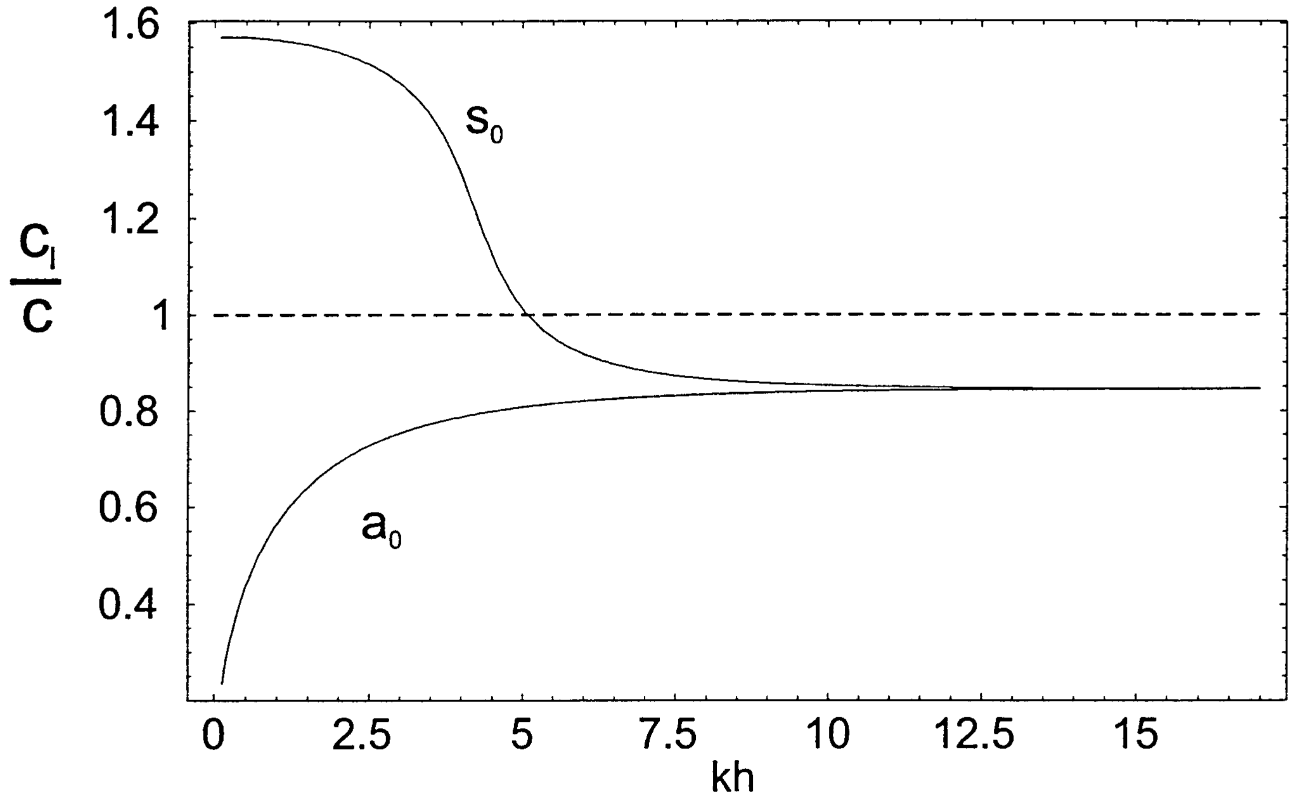

Characteristic equation for symmetric waves on a plate immersed in water.

$$\text{Vacuum term} \quad \left[\left(\xi^2+\beta^2\right)^2 \cosh(\alpha h/2)\sinh(\beta h/2) - 4\xi^2\alpha\beta\cosh(\beta h/2)\sinh(\alpha h/2)\right] +$$

$$\text{Fluid-loading} \quad \left[\frac{\rho c^2}{\rho_e c_s{}^2}\frac{\eta^2-\xi^2}{\eta}\alpha\left(\beta^2-\xi^2\right)\sinh(\beta h/2)\sinh(\alpha h/2)\right] = 0$$

Two properties of acrylic which significantly affect the fluid-loaded Lamb wave spectrum:

1) $c_R < c_W$

2) $\rho_E \sim \rho_W$

Phase velocities for 1.44 mm thick SS304 plate

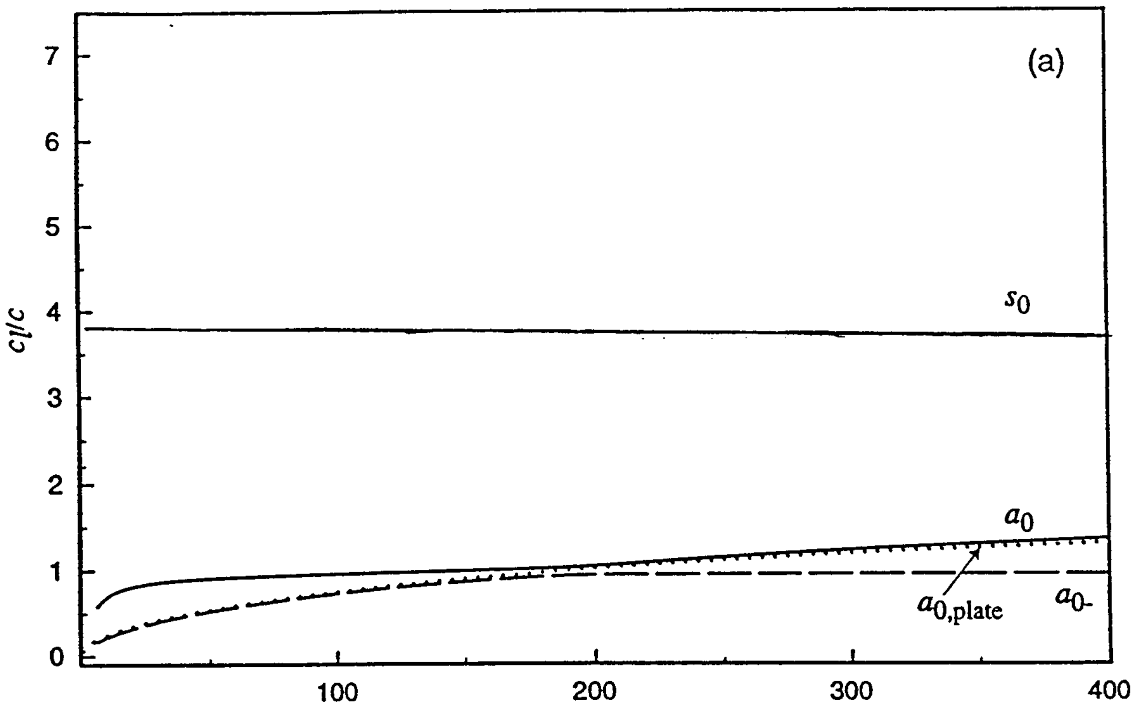

kHz

Phase velocities for fluid-loaded acrylic plate

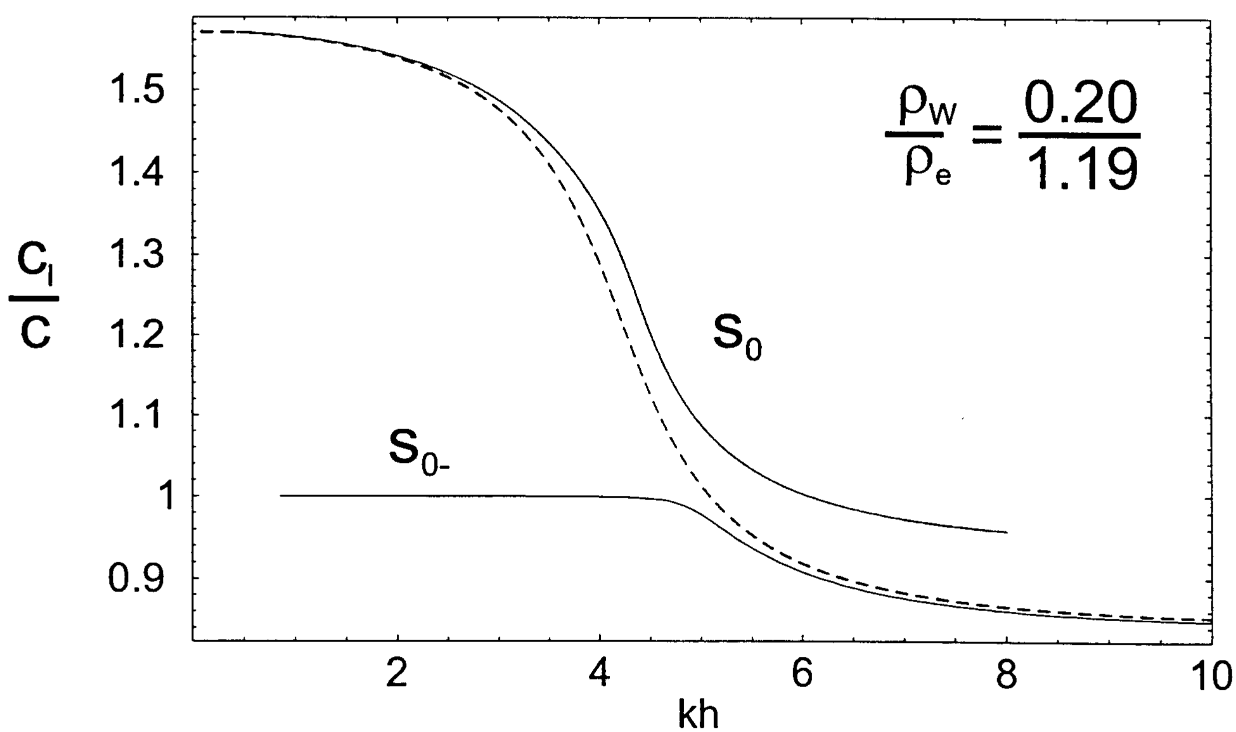

TR-14

For Acrylic: $\frac{\rho}{\rho_e} = \frac{1.00}{1.19} = 0.84$

For Stainless Steel: $\frac{\rho}{\rho_e} = \frac{1.00}{7.57} = 0.13$

For large density ratios, fluid-loading is no longer a small perturbation to Lamb wave spectrum.

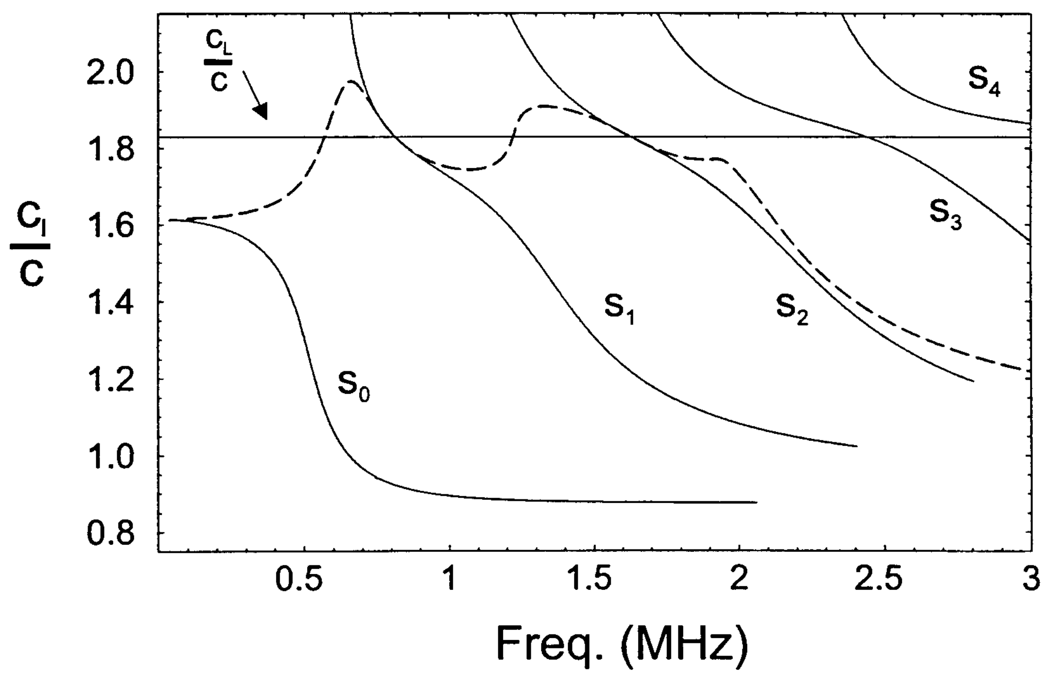

As ρ_W/ρ_E increases, the Lamb wave spectrum transitions to a plate with mixed boundary conditions.

S.I. Rokhlin et.al., J. Acoust. Am. **85**(3), March 1989

A. Freedman, J. Acoust. Am. **99**(6), June 1996

Surface waves on a 5% acrylic shell

Phase velocities for an empty fluid-loaded acrylic shell

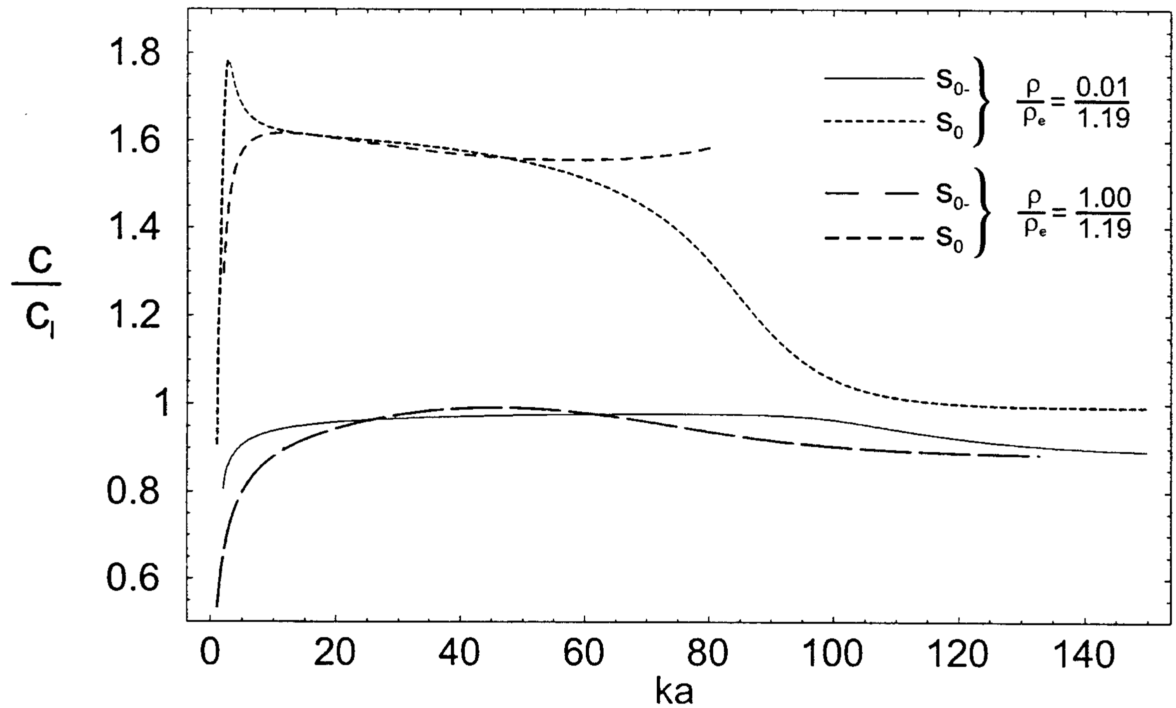

Damping parameters for an empty fluid-loaded acrylic shell

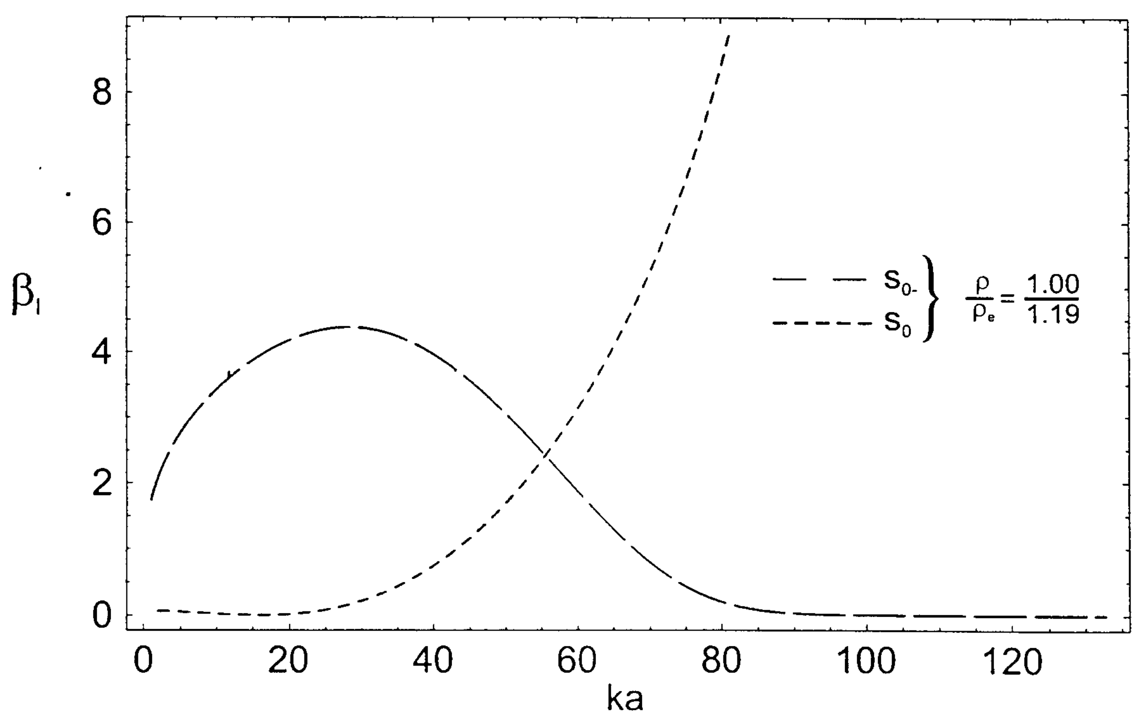

Backscattering form function for 5% acrylic shell with material absorption.

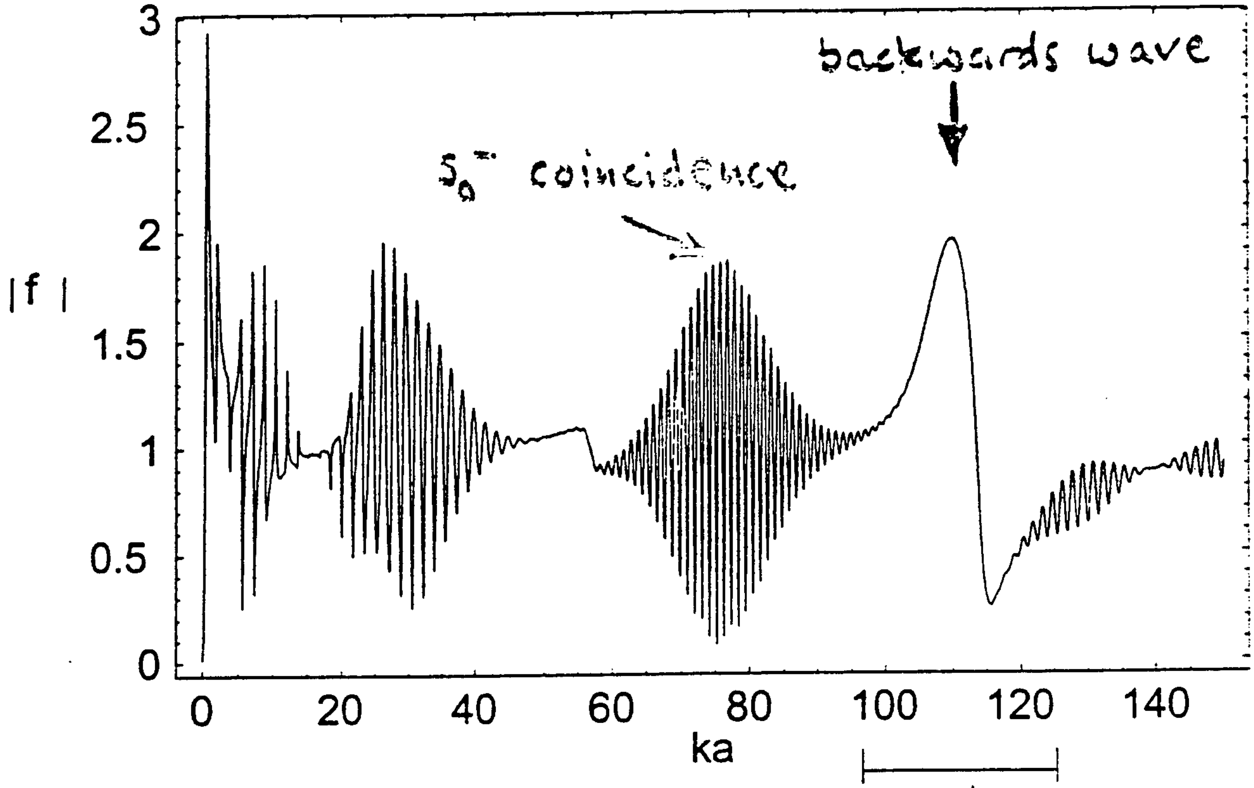

Possible backwards wave enhancement

This type of enhancement was previously observed in SS304 shells.

G. Kaduchak et. al., J. Acoust. Am. **96** (6), 1994

|f| for 7.5% SS304 shell

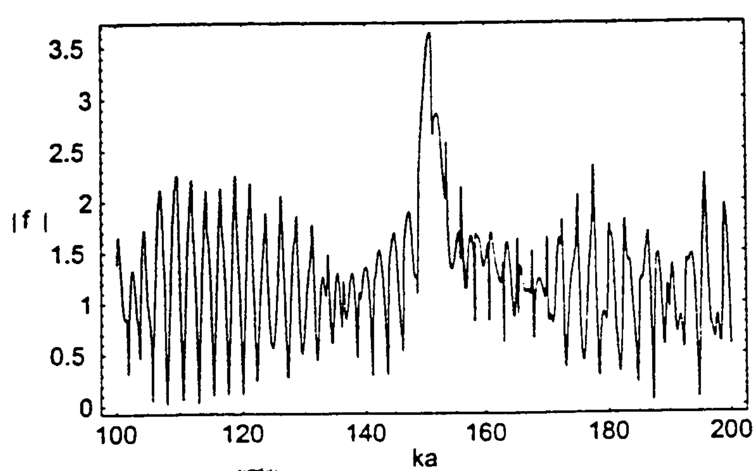

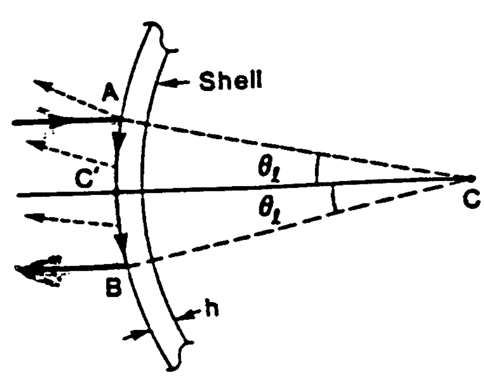

Summary

- PMMA spheres were observed to give a backscattering enhancement due to tunneling to a subsonic Rayleigh wave.

- We have modeled the resulting Rayleigh wave resonance scattering by extending the previous ray-tunneling models of subsonic a_0 waves on steel shells [Zhang, Sun, & Marston JASA (1992)].

- Radiation damping and intrinsic material absorption are similar in magnitude and are additive.

Computational study for shells:

- Because the Rayleigh wave velocity is subsonic, there are two branches associated with the lowest symmetric mode, the s_0 and s_{0-} waves which give rise to associated backscattering enhancements.

- Although the intrinsic material absorption may suppress enhancements associated with waves which travel around the shell, it may be possible to detect enhancements associated with a backwards wave on the shell.

Remote Ultrasonic Classification of Fluids using Acoustic Resonance Characteristics of the Container

Dipen N. Sinha, Gregory Kaduchak and Michael J. Keleher

Los Alamos National Laboratory

Electronic and Electrochemical Materials and Devices Group

Noninvasive Identification of CW Agents

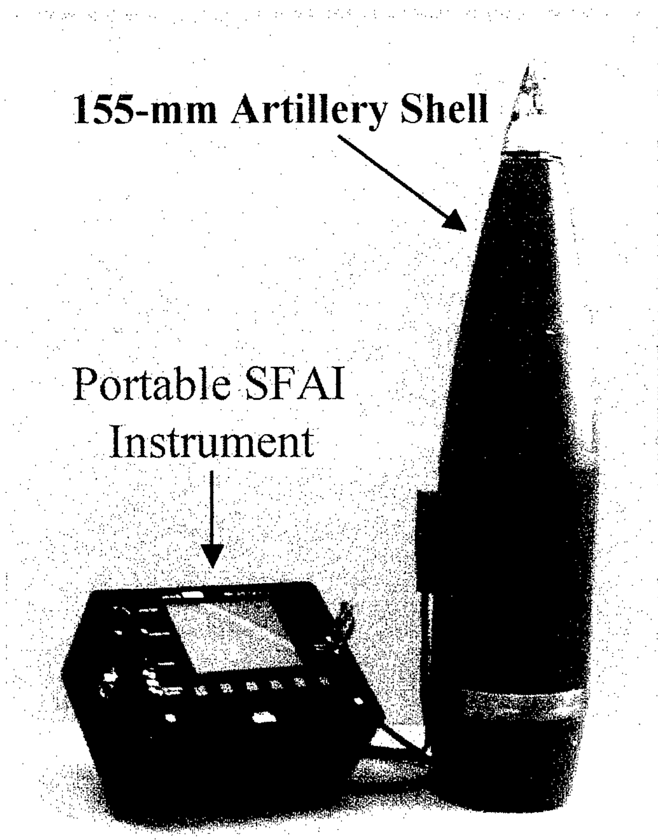

SFAI Measurements of CW Agent Physical Properties

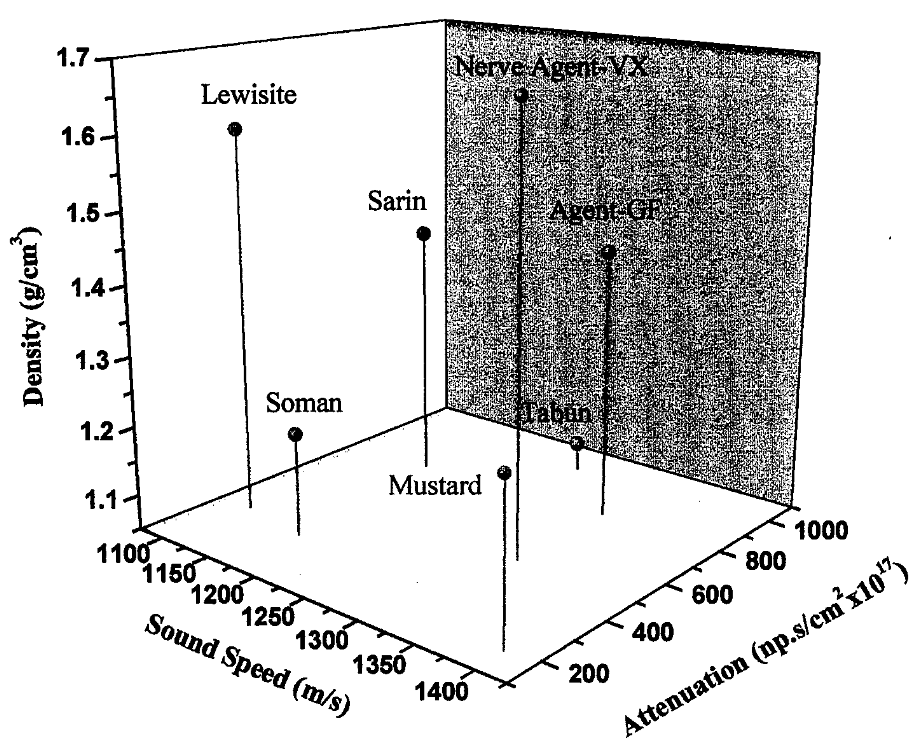

Remote Classification of Fluids

Why needed:

Determining information on contents of containers in hazardous situation (leaking toxic vapors, radioactivity, etc.,) or inaccessible areas.

Where:

- Waste storage facilities (Rocky Flats, WIPP)
- Law enforcement
- Chemical weapons compliance monitoring
- Chemical and other industry
- Firefighters, HAZMAT

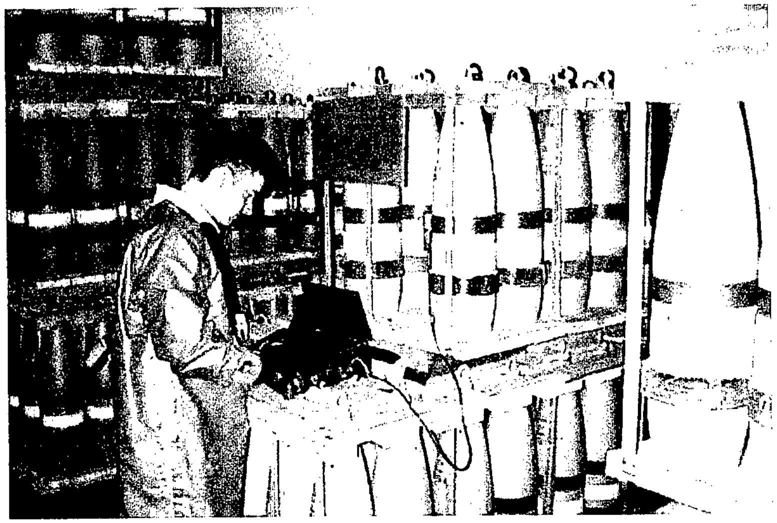

Noninvasive Identification of Chemical Agents using Ultrasonic Interferometry

- Identification is based on physical properties of chemicals
- Requires physical contact between transducer and item being tested
- Need a technique that does not require operator to be exposed to hazardous situation (e.g., chemical vapor, radioactive, etc.,)

TR-4

Nonlinear Sound Propagation in Air

Direction of
sound propagation

Compression ⟶ Warmer ⟶ *Faster*

Source

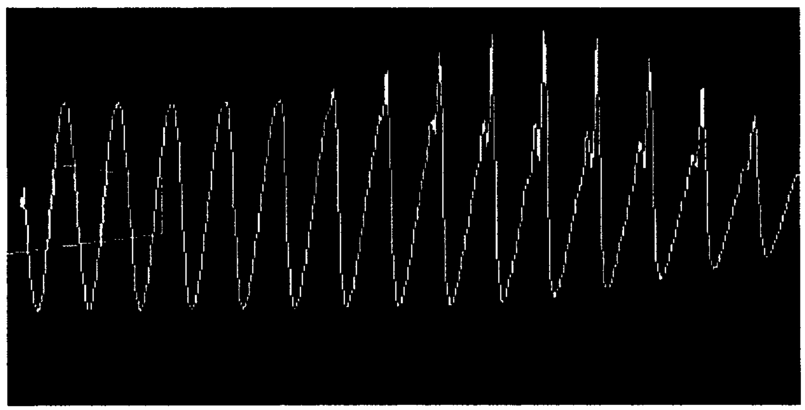

Rarefaction ⟶ Cooler ⟶ ***Slower***

For high intensity sound waves, the waves start to distort as they travel, generating harmonics, 'self-demodulation', rectification, and shocks.

(Figure: Courtesy of F. Joseph Pompei, MIT Media Lab)

Remote Excitation of Vibration

How?

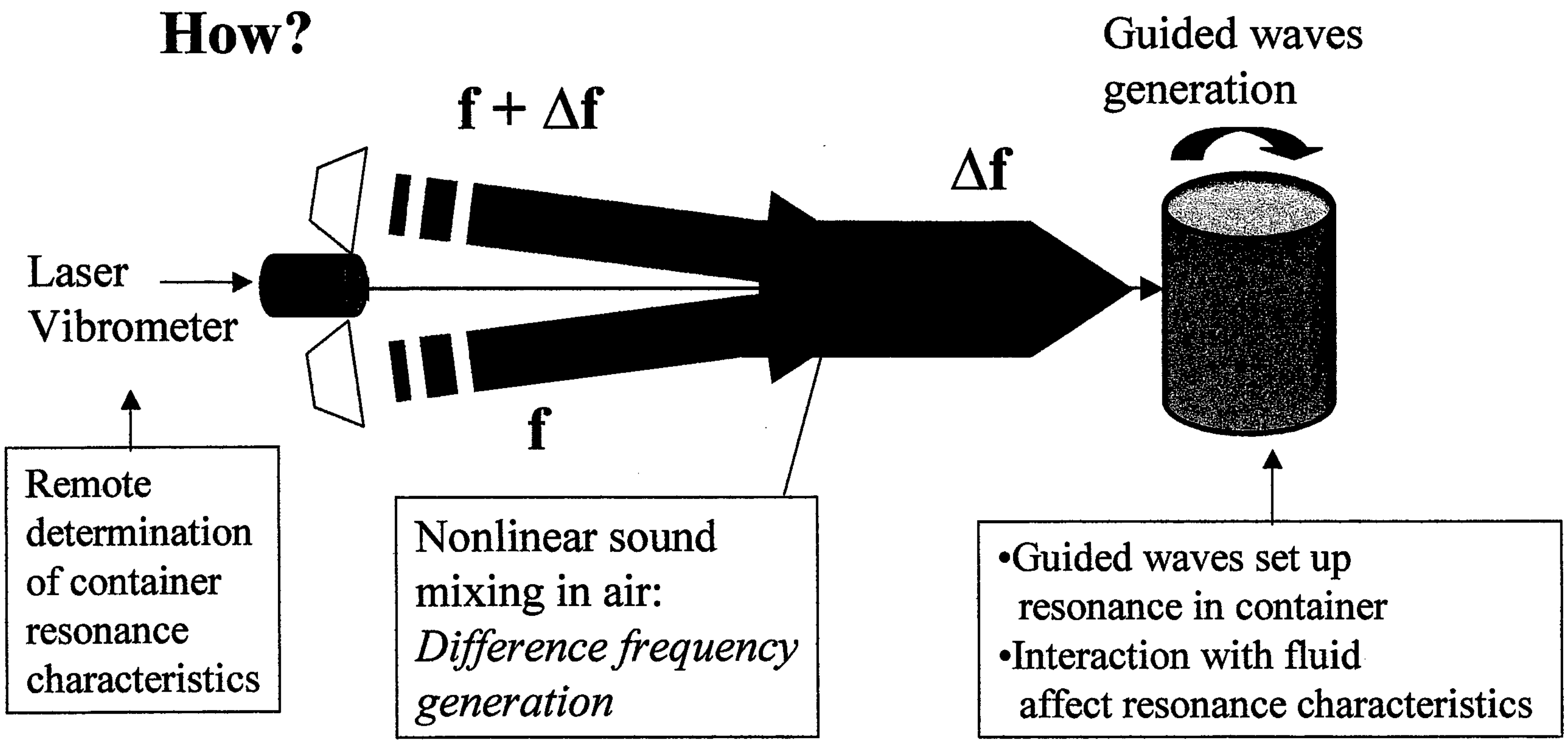

Remote Classification of Fluids

How?

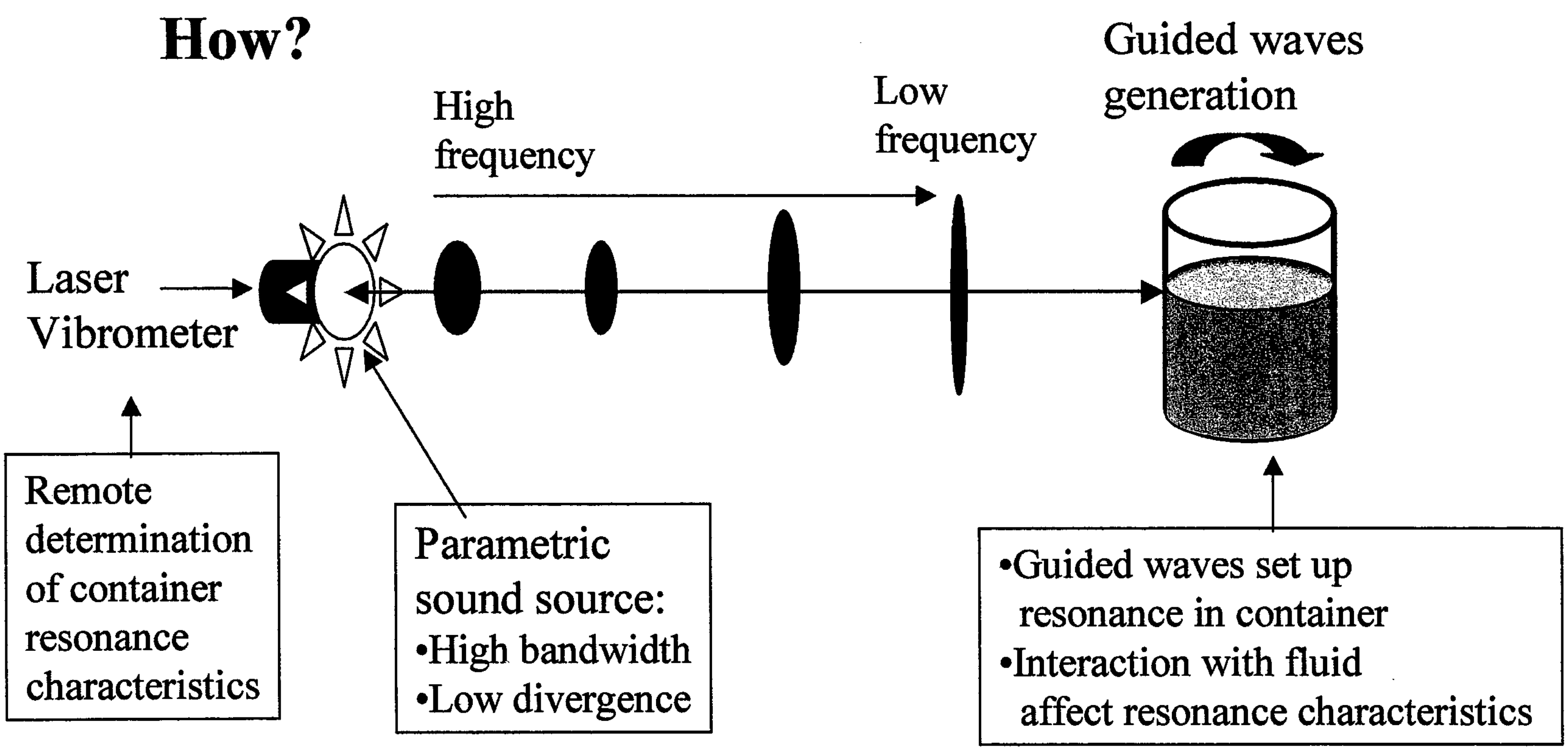

Parametric Array

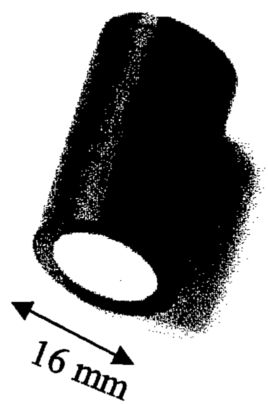

AIRMAR
AT200

Q ~ 25
Beamwidth ~7°

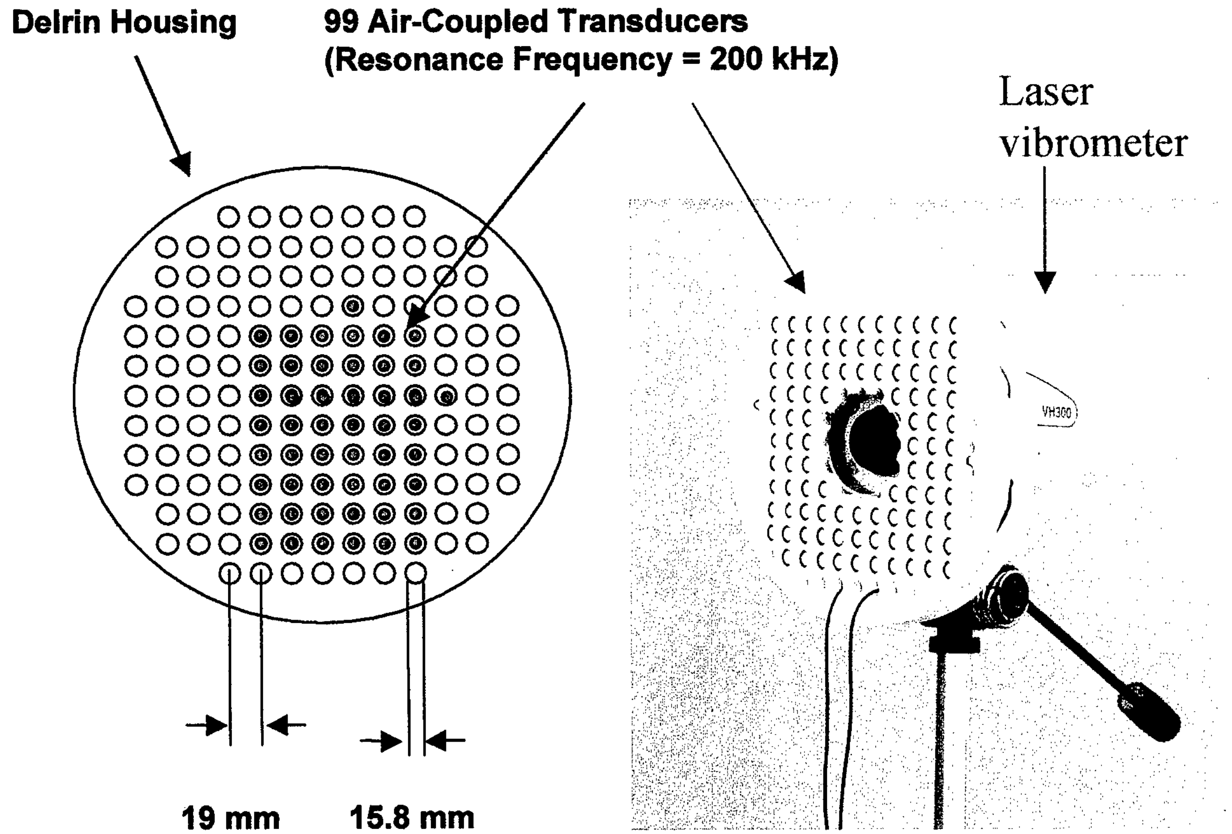

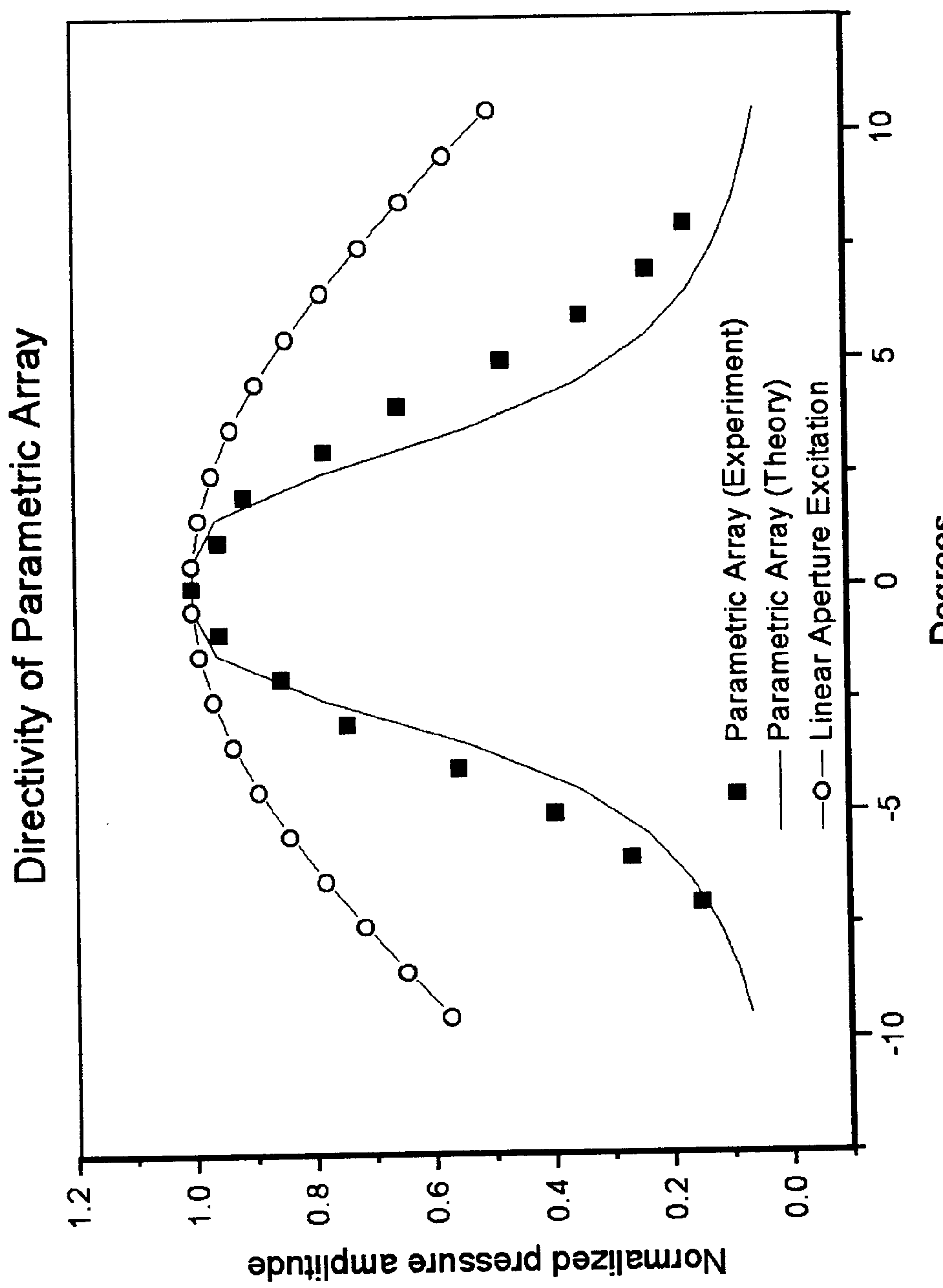
Directivity of Parametric Array
Parametric Array (Experiment)
Parametric Array (Theory)
Linear Aperture Excitation
Degrees
-10
-5
0
5
10
Normalized pressure amplitude
0.0
0.2
0.4
0.6
0.8
1.0
1.2

Experimental Configuration

AM Modulated Beam

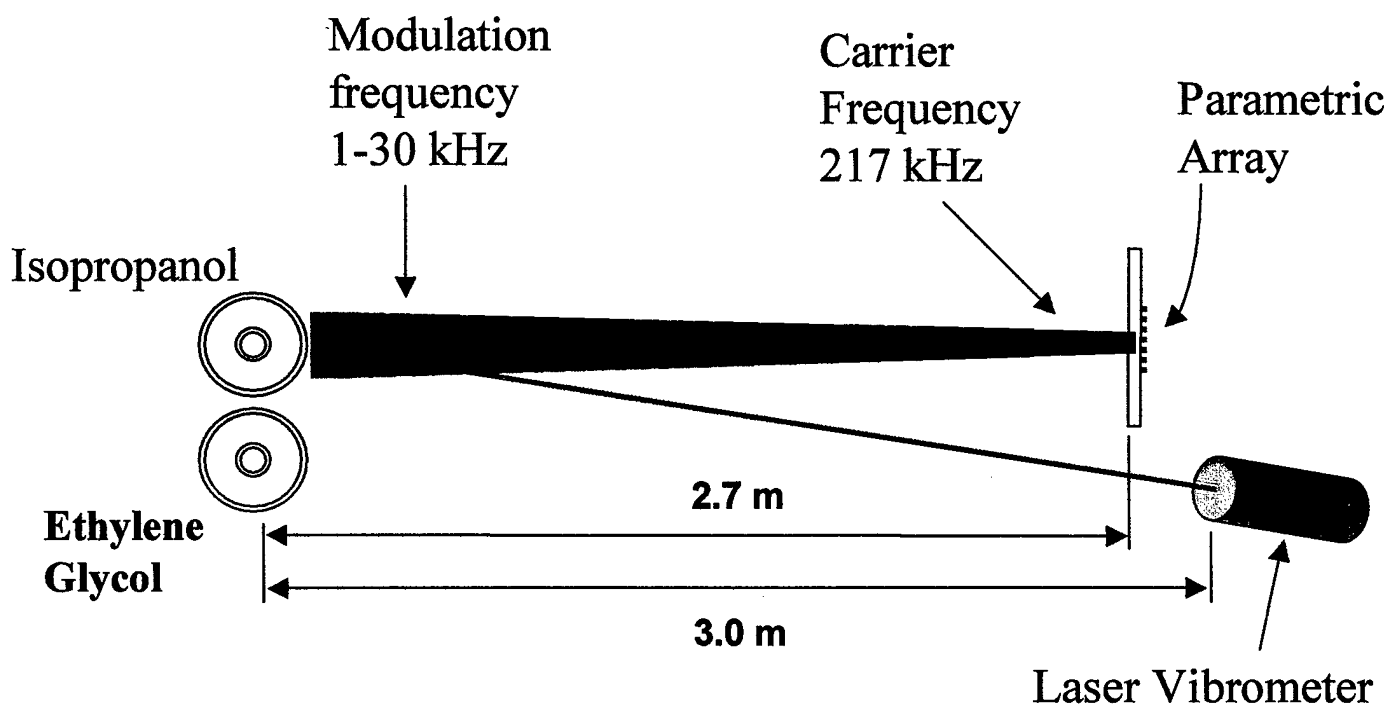

Instrument Setup

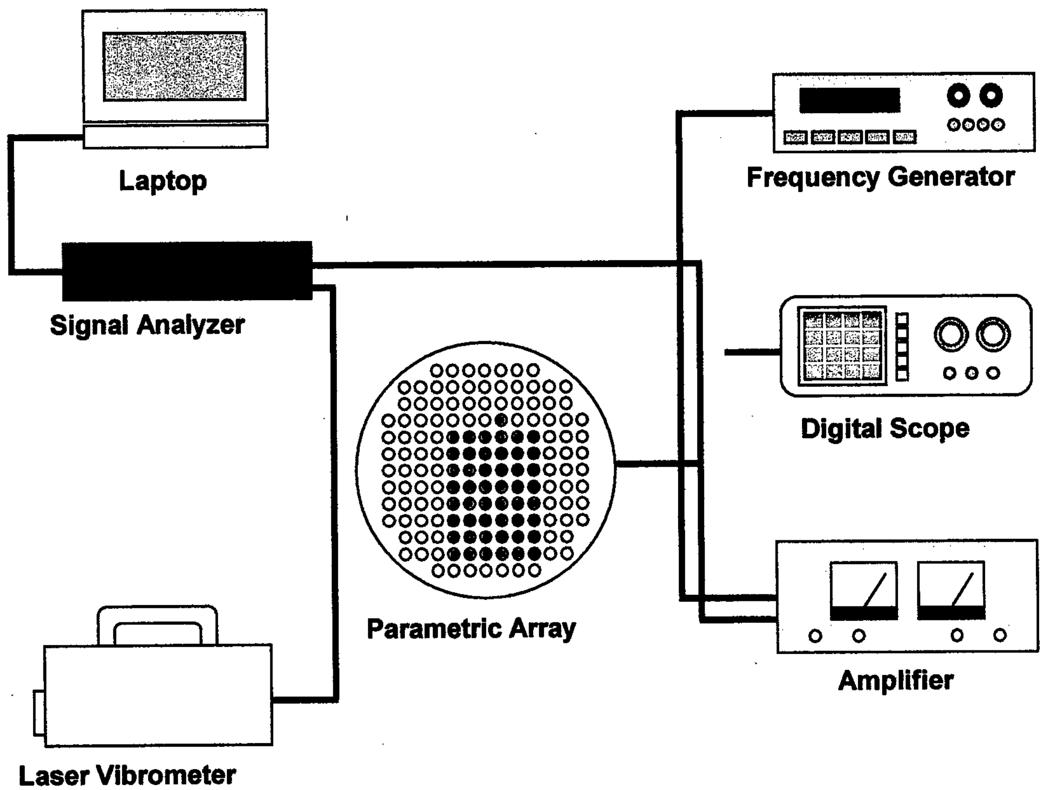

Ultrasonic Remote Assay of Munitions

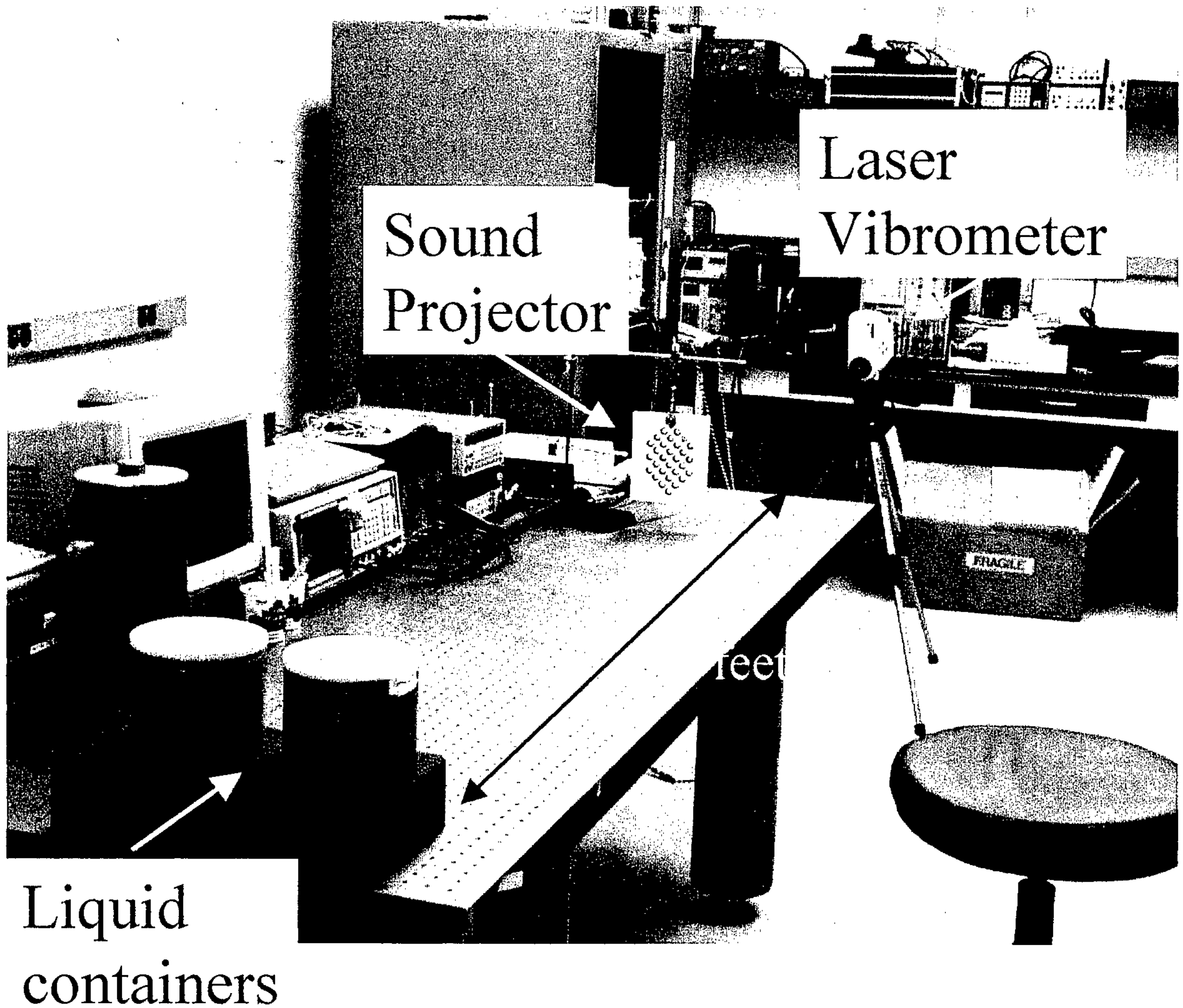

Liquid-filled Steel Containers

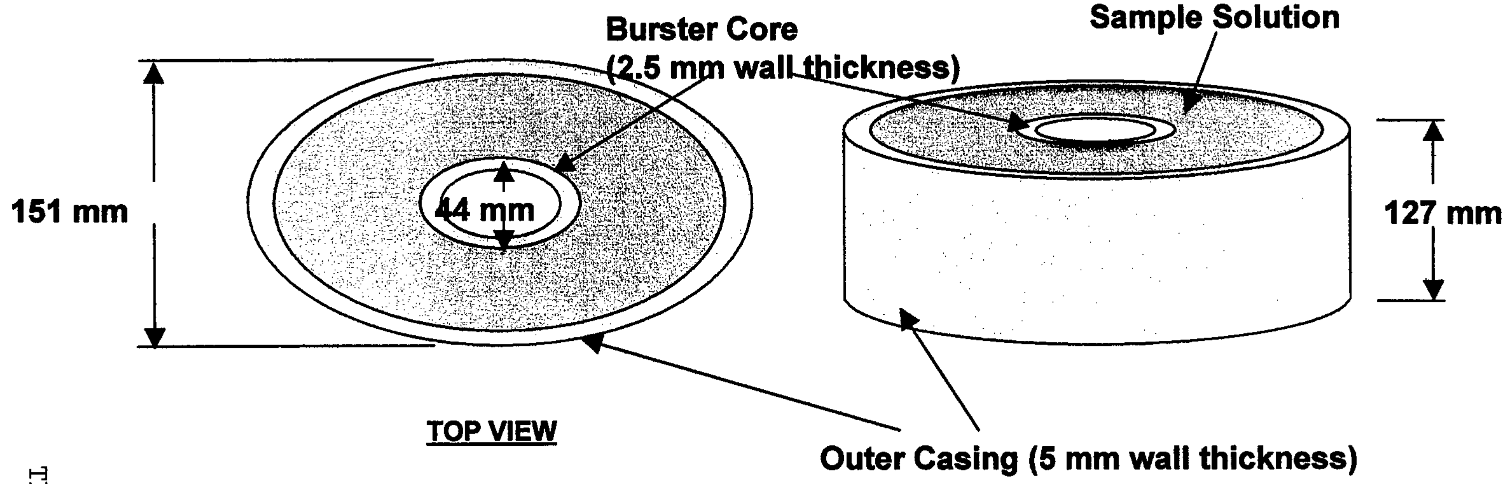

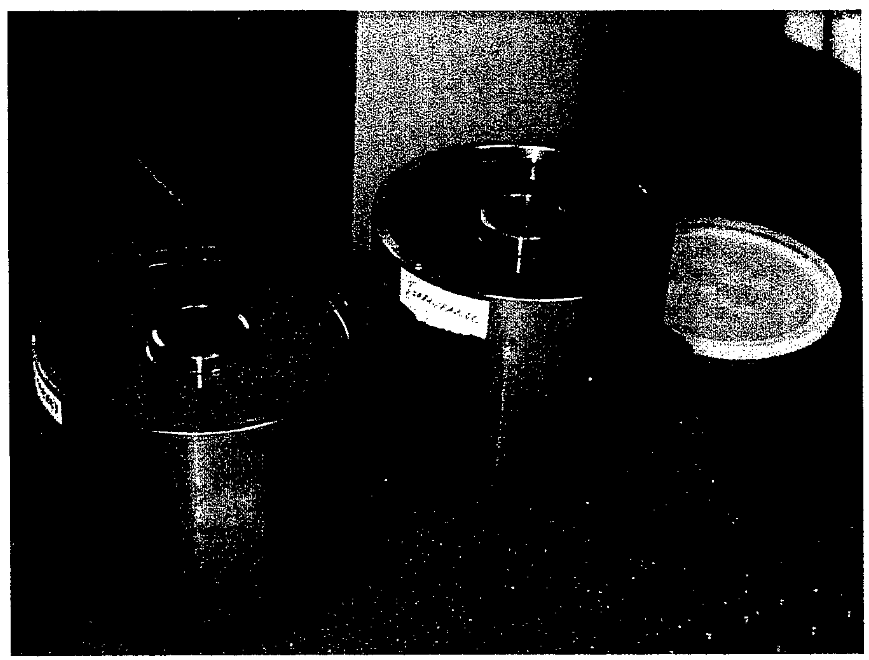

Guided waves

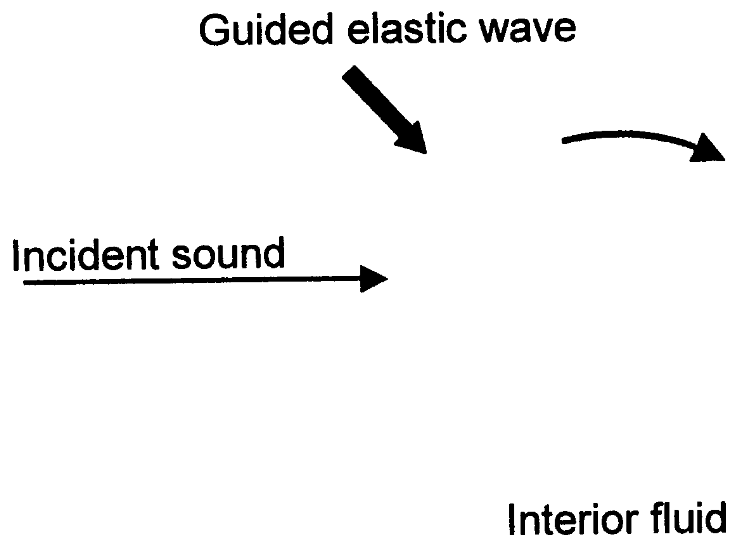

Resonance occurs at $f_{res} = n\,\lambda_{gw}$

<u>Guided wave properties may be used to determine:</u>

- interior fluid sound speed
- interior fluid density
- interior fluid attenuation
- shell diameter
- shell thickness or material composition

Calculated Phase Velocity and Radiation Damping for a_o Lamb Wave

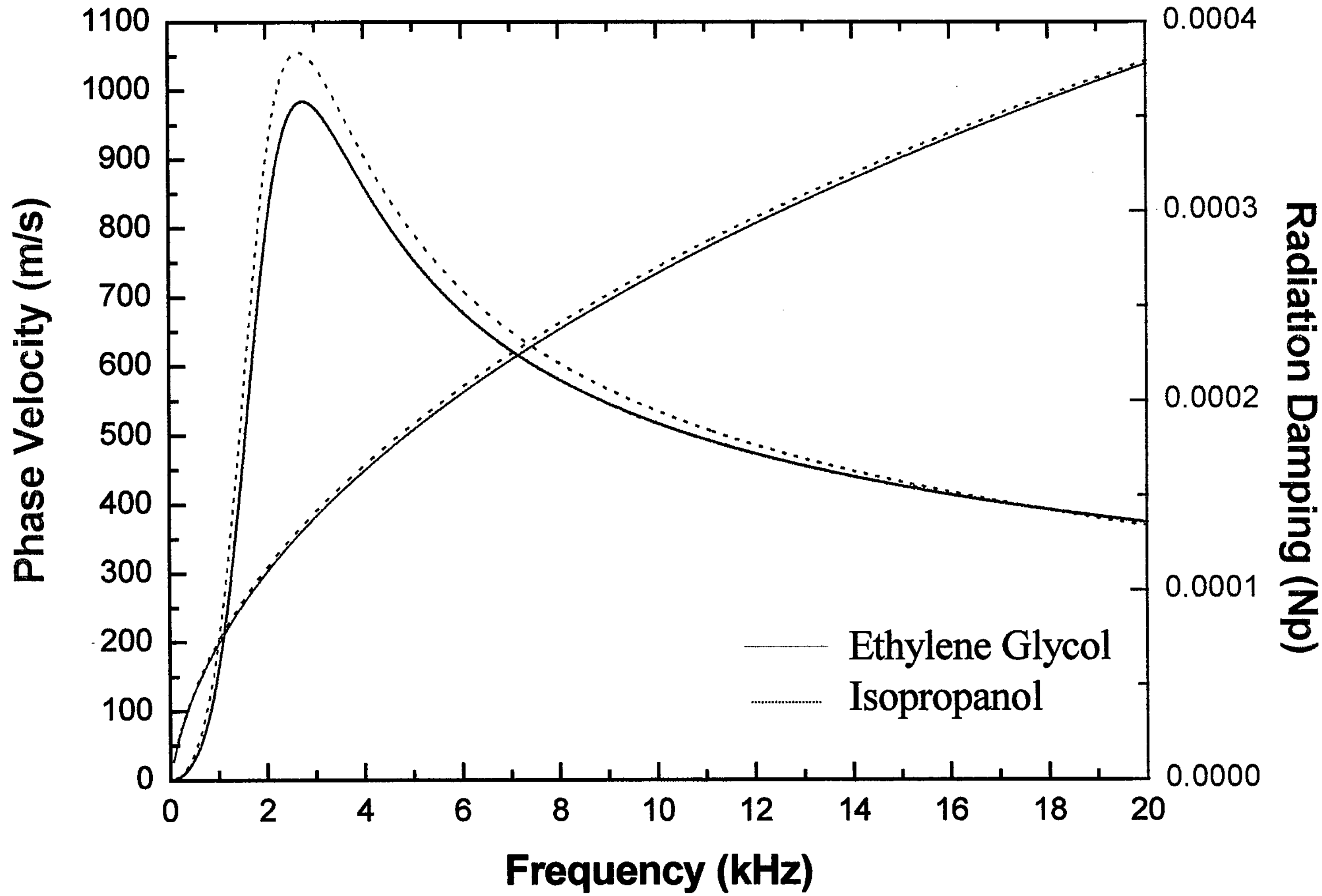

Calculated Phase Velocity Difference

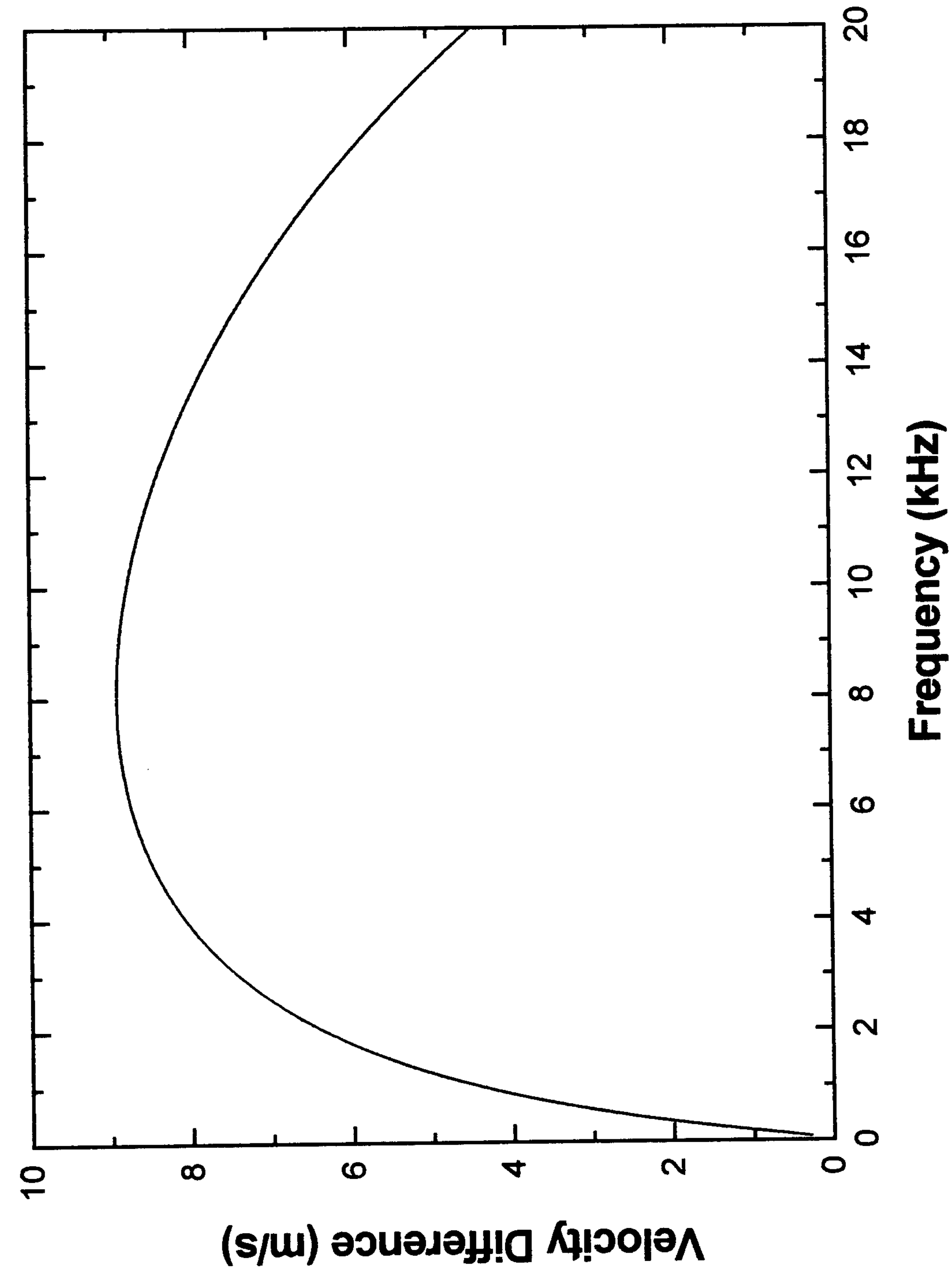

Resonance Spectrum of Two Liquid-filled Steel Containers

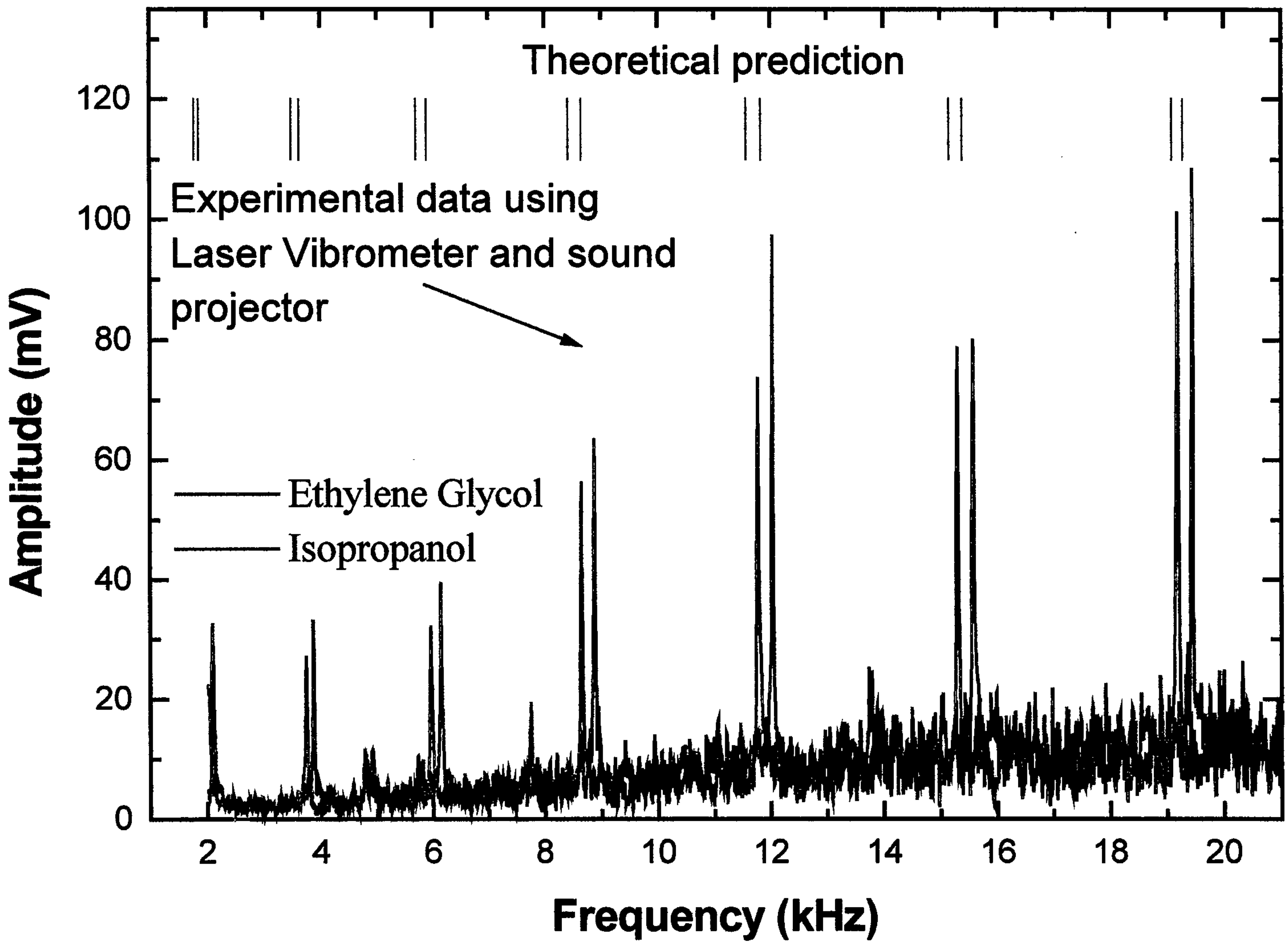

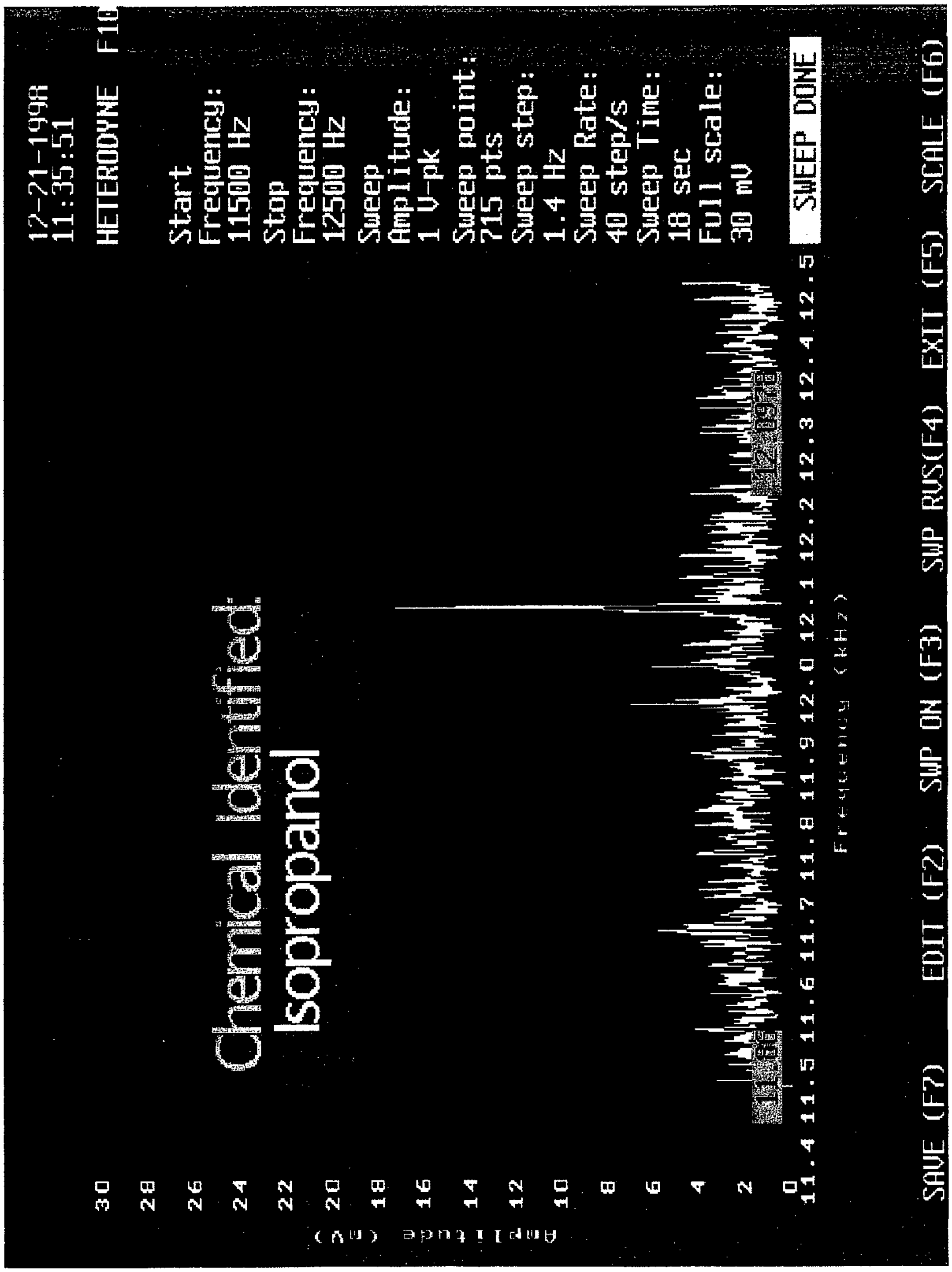
12-21-1998
11:35:51
HETERODYNE F10
Start
Frequency:
11500 Hz
Stop
Frequency:
12500 Hz
Sweep
Amplitude:
1 V-pk
Sweep point:
715 pts
Sweep step:
1.4 Hz
Sweep Rate:
40 step/s
Sweep Time:
18 sec
Full scale:
30 mV
SWEEP DONE
Chemical Identified:
Isopropanol
Amplitude (mV)
30 28 26 24 22 20 18 16 14 12 10 8 6 4 2 0
11.4 11.5 11.6 11.7 11.8 11.9 12.0 12.1 12.2 12.3 12.4 12.5
Frequency (kHz)
SAVE (F7) EDIT (F2) SWP ON (F3) SWP RVS(F4) EXIT (F5) SCALE (F6)

TR-18

Liquid Level Determination

AM Modulated Beam

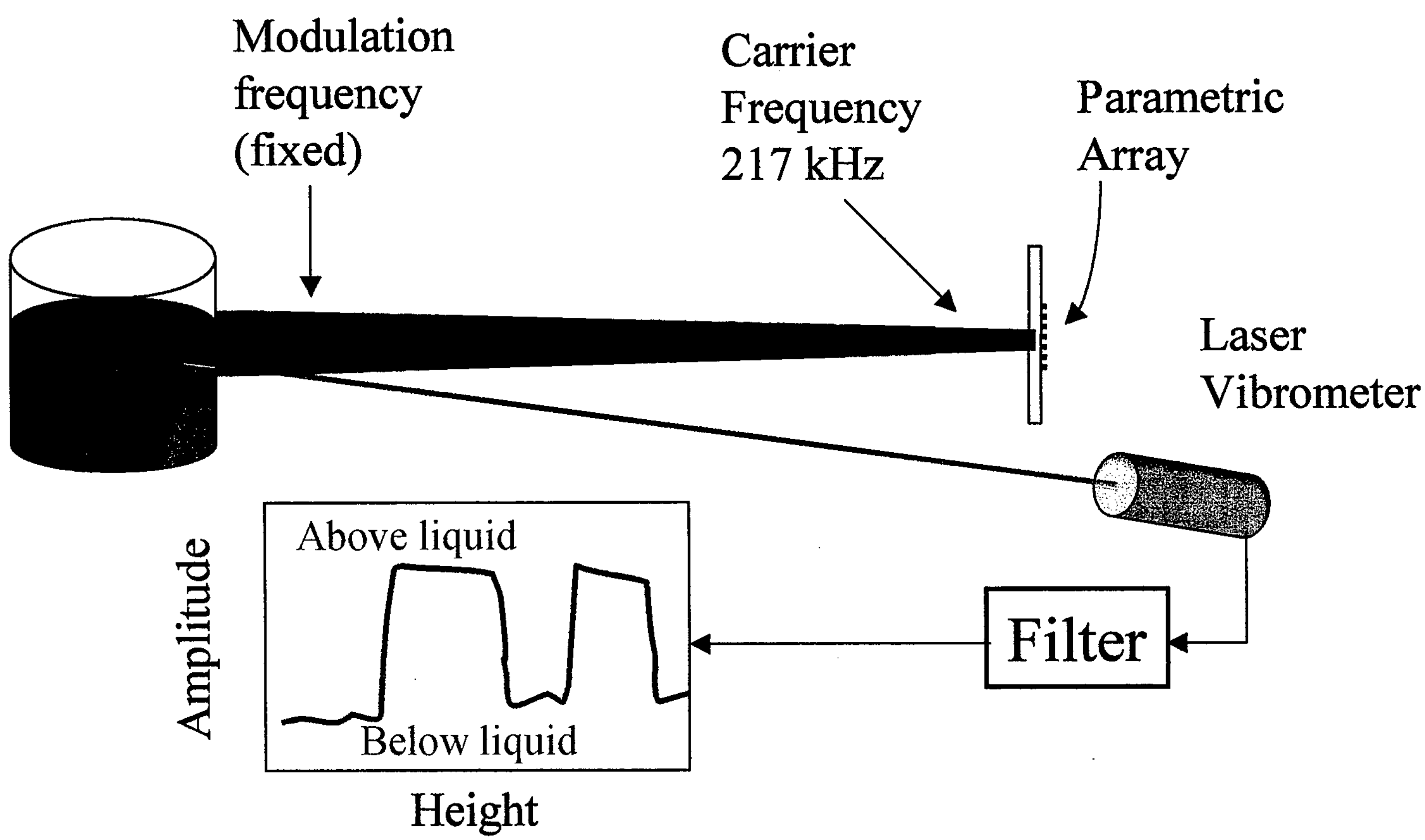

CONCLUSIONS

- It is possible to excite guided waves in liquid-filled containers remotely using a parametric sound source
- A simple and inexpensive parametric source in air is demonstrated
- Guided wave-liquid interaction can be used to determine liquid physical property for liquid identification
- It is possible to monitor liquid level remotely
- It is also possible to determine wall integrity
- This remote monitoring approach has many applications

Acoustic Gas Resonators for Measurements of Thermophysical Properties and Thermometry

James B. Mehl

Resonance Meeting, 1999
University of Mississippi

University of Delaware

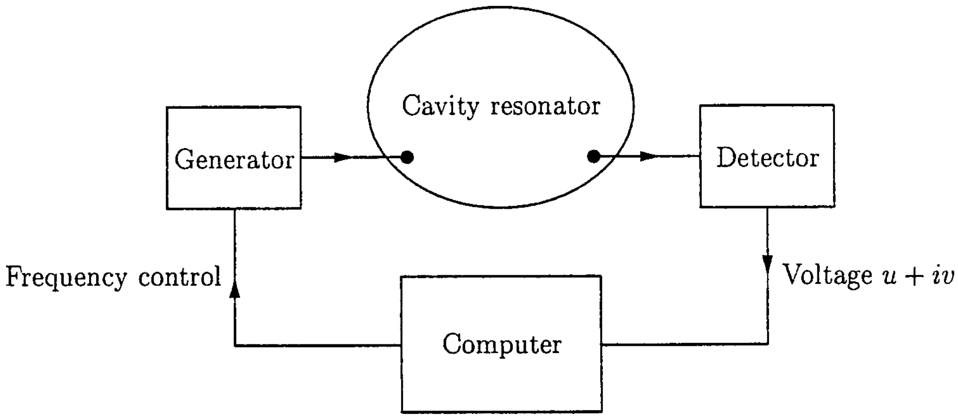
Cavity resonator
Generator
Detector
Frequency control
Voltage $u + iv$
Computer

$|u + iv|$ vs. f

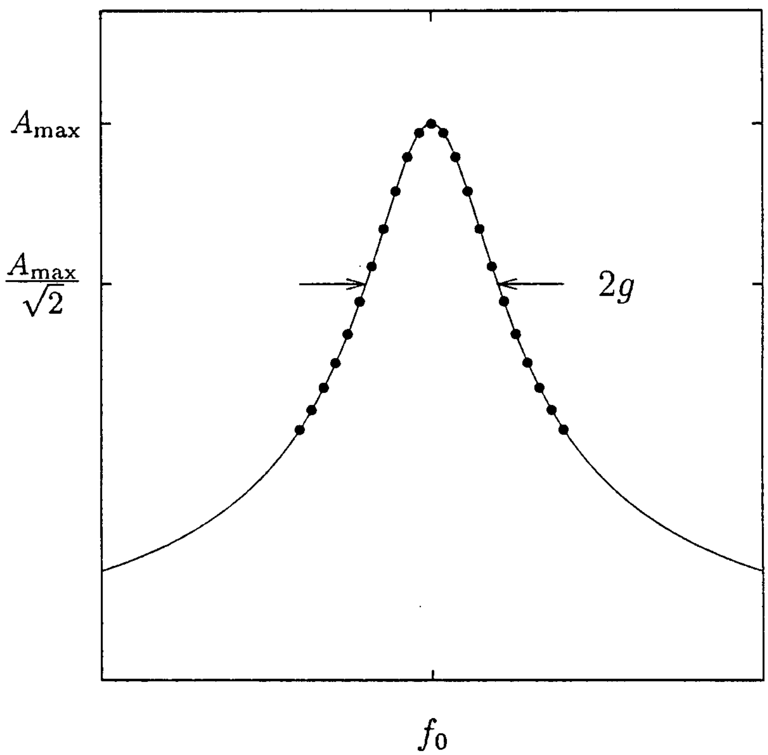
$A_{\max}$
$\frac{A_{\max}}{\sqrt{2}}$
$2g$
f_0

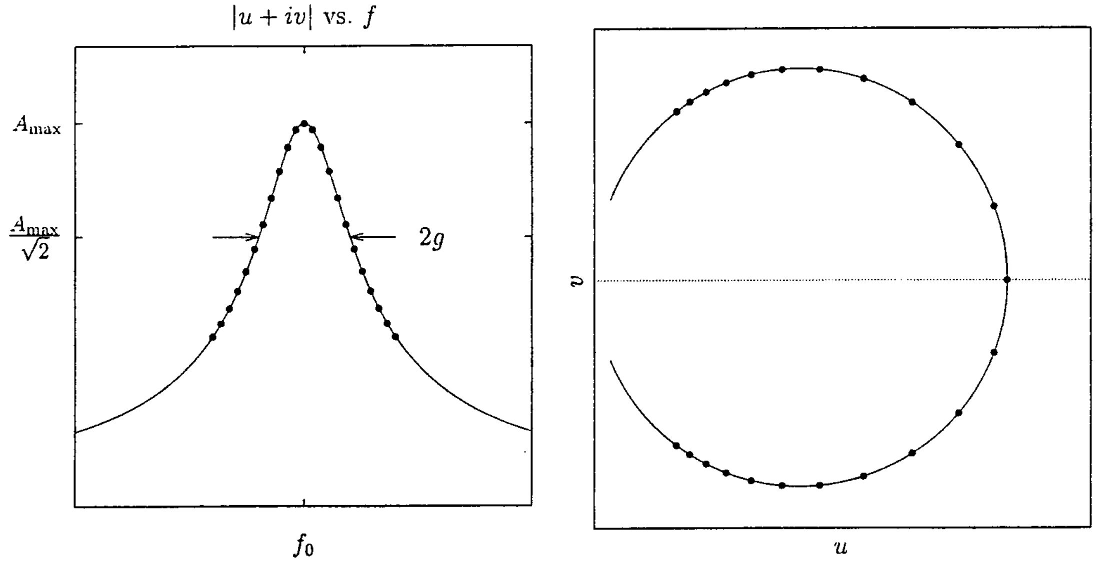

Acoustic pressure at point $\mathbf{r}$ in an enclosure, with source S at point $\mathbf{r}'$ [Morse-Ingard (9.5.14)]:

$$p = \frac{i\rho\omega S}{V} \sum_N \frac{\Psi_N(\mathbf{r})\Psi_N(\mathbf{r}')}{\Lambda_N(k^2 - K_N^2)}$$

Signal detected:

$$u + iv = \sum_N \frac{if\mathbf{A}_N)}{f^2 - F_N^2}$$

For a single mode of interest:

$$u + iv = \frac{if\mathbf{A})}{f^2 - (f_0 + ig)^2} + \mathbf{B} + \mathbf{C}(f - \tilde{f}) + = \ldots$$

Fit: Pick $\mathbf{F}$, $\mathbf{A}$, $\mathbf{B}$, ... to minimize

$$\sum \left[(u_i - u(f_i))^2 + (v_i - v(f_i))^2 \right]$$

Interesting parameters: $\mathbf{F} = f_0 + ig$.

$$u + iv = \frac{i\mathbf{A}f}{f^2 - \mathbf{F}^2} + \text{background}$$

Insert extra factor of f in numerator:

$$f = \mathbf{F} + (f - \mathbf{F}) = \mathbf{F} + \Delta f$$

Then

$$\begin{aligned} u + iv &= \frac{i\mathbf{A}f\mathbf{F}}{f^2 - \mathbf{F}^2} + \frac{i\mathbf{A}f\Delta f}{(f + \mathbf{F})\Delta f} + \text{background} \\ &= \frac{i\mathbf{A}'f}{f^2 - \mathbf{F}^2} + \frac{i\mathbf{A}\left(1 + \frac{\Delta f}{\mathbf{F}}\right)}{1 + \frac{\Delta f}{2\mathbf{F}}} + \text{background} \\ &= \frac{i\mathbf{A}'f}{f^2 - \mathbf{F}^2} + \text{modified background} \end{aligned}$$

Similar relations will handle, *e.g.*

$$\mathbf{A}(f) = \mathbf{A}(\mathbf{F}) + \frac{d\mathbf{A}}{df}\Delta f + \ldots$$

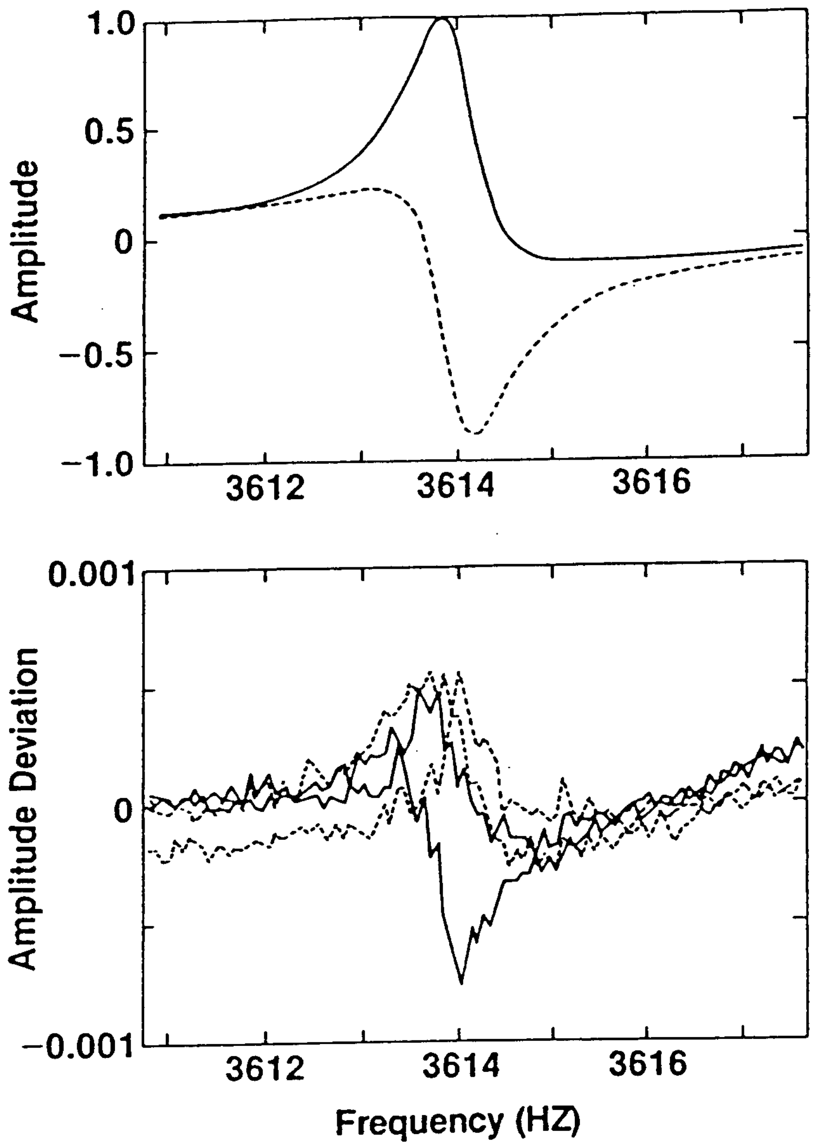

FIG. 4. Top: In-phase (solid curve) and quadrature (dashed curve) voltages from the detector as a function of frequency near the (0,2) resonance in argon at 0.4032 MPa and 296.309 K. Bottom: Measured voltages minus calculated voltages [Eq. (75)] with the fitted parameters $f_{02} = 3613.9970$ Hz, $g_{02} = 0.4275$ Hz, $A = 0.7535 - 0.5831i$, $B = 0.0048 + 0.0068i$, and $C = 0.0001 + 0.0001i$. Data were taken at intervals of 0.07 Hz, first from the lowest to the highest frequency and then back to the lowest frequency. Separate deviation plots for the upward and downward frequency sweeps show the effects of drifts in the lock-in amplifier.

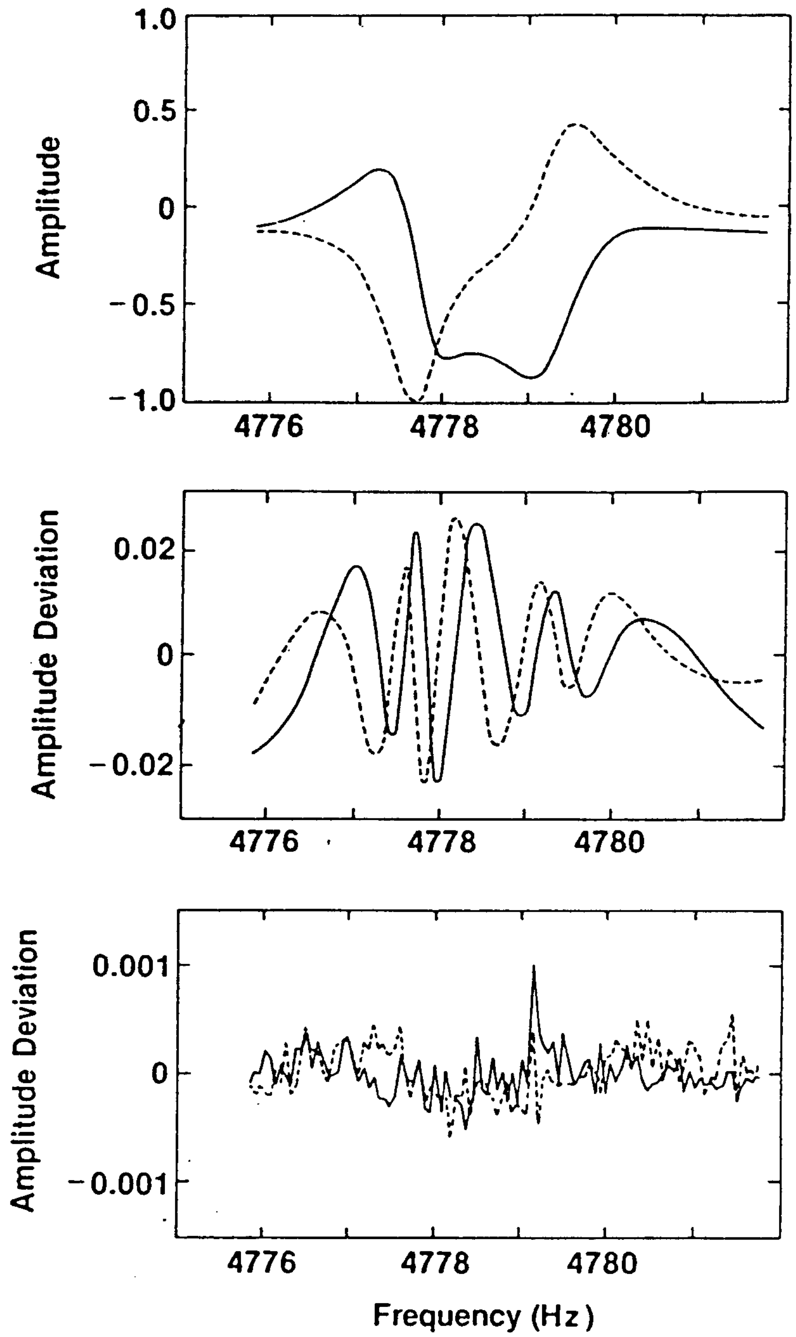

FIG. 5. Top: In-phase (solid curve) and quadrature (dashed curve) voltages from the detector as a function of frequency near the (1,2) resonance in argon at 0.4032 MPa and 296.309 K. Middle: Measured voltages minus two-resonance trial function. Note that the deviations are systematic although the trial function has twelve parameters [eight parameters specify resonances at 4777.63 and 4779.38 Hz, and four specify the constant and linear background terms in Eq. (75)]. Bottom: Measured voltages minus fitted function. The fitted function has sixteen parameters [twelve parameters specify resonances at 4777.693, 4777.903, and 4779.351 Hz with half-widths of 0.550, 0.546, and 0.555 Hz. The remaining four parameters specify B and C in Eq. (75)]. TR-5

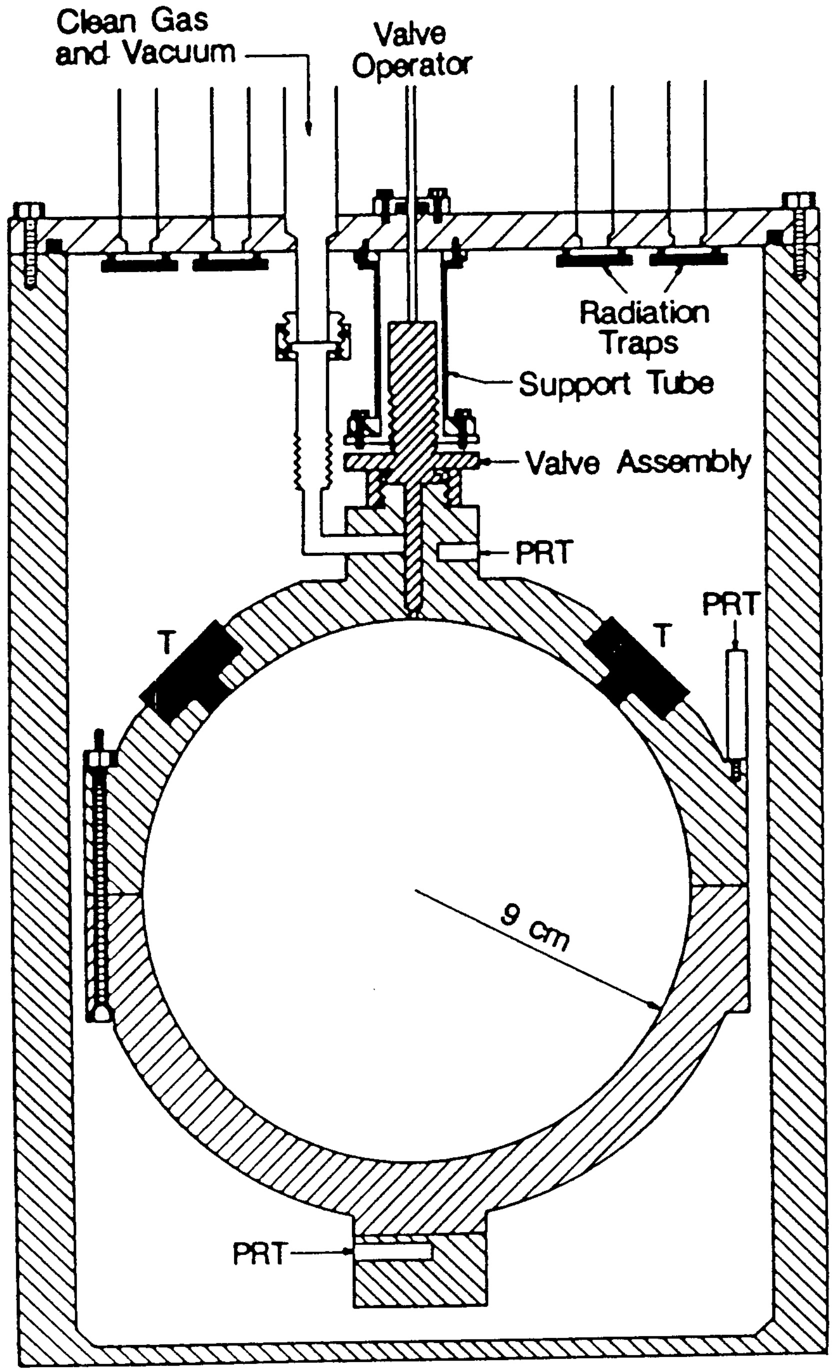

Figure 5. Cross-section of resonator and pressure vessel. The transducer assemblies are indicated by "T," and the locations of the capsule thermometers are indicated by "PRT."

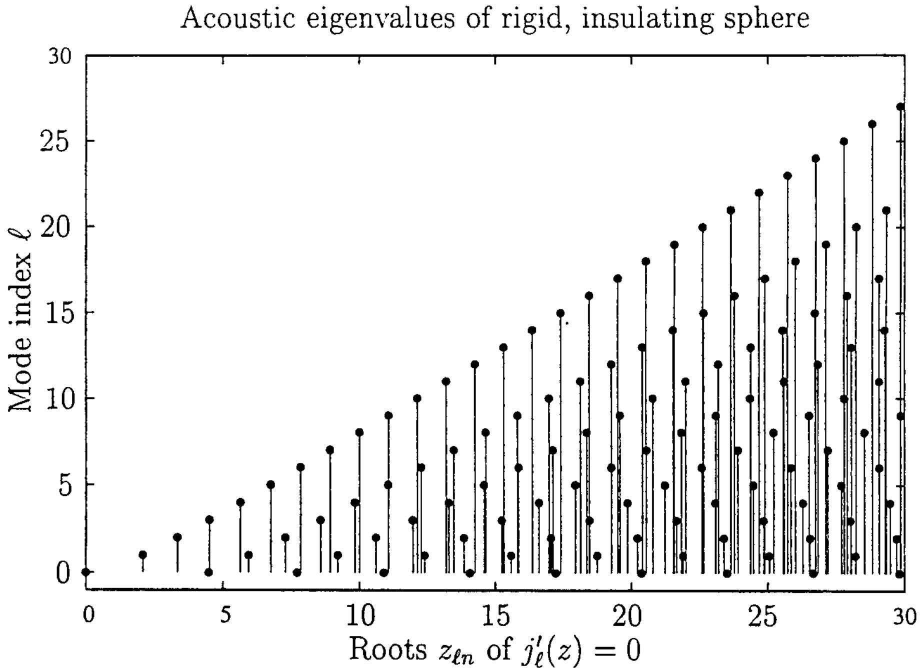

A gas filled, acoustic resonator with rigid, thermally insulating walls, has acoustic resonances at the frequencies

$$f_{\ell n} = \frac{z_{\ell n} c}{2\pi a} \approx (0.577 \text{ kHz}) z_{\ell n},$$

where the numerical value is for argon at room temperature ($c \approx 322\text{m/s}$) in the 8.89 cm-SS spherical resonator. The acoustic pressure in the sphere is proportional to

$$j_\ell(z_{\ell n} r/a) Y_{\ell n}(\theta, \phi).$$

The modes are $(2\ell + 1)$-fold degenerate for perfect spherical geometry.

Theory of spherical acoustic resonator

Temperature, pressure, particle velocity fields
PDEs (Kirchhoff 1868)
Navier Stokes: longitudinal
Navier Stokes: transverse
Fourier: Heat flow
Conservation of mass
Conservation of energy

4th order PDE in temperature
Prediction: two wave modes
Δp, ΔT, particle velocity, $\propto e^{i\omega t}$
acoustic mode ($k_p \approx u/\omega$)
thermal mode ($k_t \approx (1-i)/\delta_t$)

Boundary conditions at gas-shell boundary:
velocity of gas = velocity of shell
heat flow continuous
temperature continuous (hydrodynamic region)

Shell motion:
Classical elastodynamic theory exactly soluble
for isotropic, isolated, spherical shell

Complete problem:
Exactly soluble for spherical geometry

TR-8

Acoustic experiment

1. Measure resonance frequencies f_{lnm} and half-widths g_{lmn}
2. Correct for
   (a) thermal boundary layer
   (b) viscous boundary layer (non-radial modes)
   (c) shell motion
   (d) imperfect geometry
3. Results:

$$f_{lnm} = \frac{uz_{ln}}{2\pi a} + \Delta f_t + +\Delta f_v + \Delta f_{\text{sh}} + \Delta f_{\text{geom}}$$

$$g_{lmn} = g_t + g_v + g_{\text{bulk}}$$

Thermal and viscous boundary layer effects

$$\frac{\Delta f_t + i g_t}{f} = -\frac{\gamma - 1}{2} \frac{\delta_t}{a} \frac{1}{1 - l(l+1)/z_{ln}^2}$$

$$\frac{\Delta f_v + i g_v}{f} = -\frac{\gamma - 1}{2} \frac{\delta_v}{a} \frac{l(l+1)}{1 - l(l+1)/z_{ln}^2}$$

$$\delta_t = \sqrt{\frac{D_t}{\pi f}}; \quad \delta_v = \sqrt{\frac{D_v}{\pi f}}$$

Boundary shape perturbation:

$$r = a\left[1 - \epsilon\mathcal{F}(\theta, \phi)\right]$$

$\epsilon =$ deformation parameter.

For deformations that conserve the volume:

$$\left(\frac{\Delta f}{f}\right)_{0n}^{\text{geom}} = O(\epsilon^2)$$

$$\left(\frac{\Delta f}{f}\right)_{\ell n}^{\text{geom}} = O(\epsilon)$$

For nonradial acoustic and electromagnetic modes:

Average over $2\ell + 1$ components of a multiplet.

$$\left\langle\frac{\Delta f}{f}\right\rangle_{\ell n} \text{geom} = O(\epsilon^2)$$

Shell admittance function

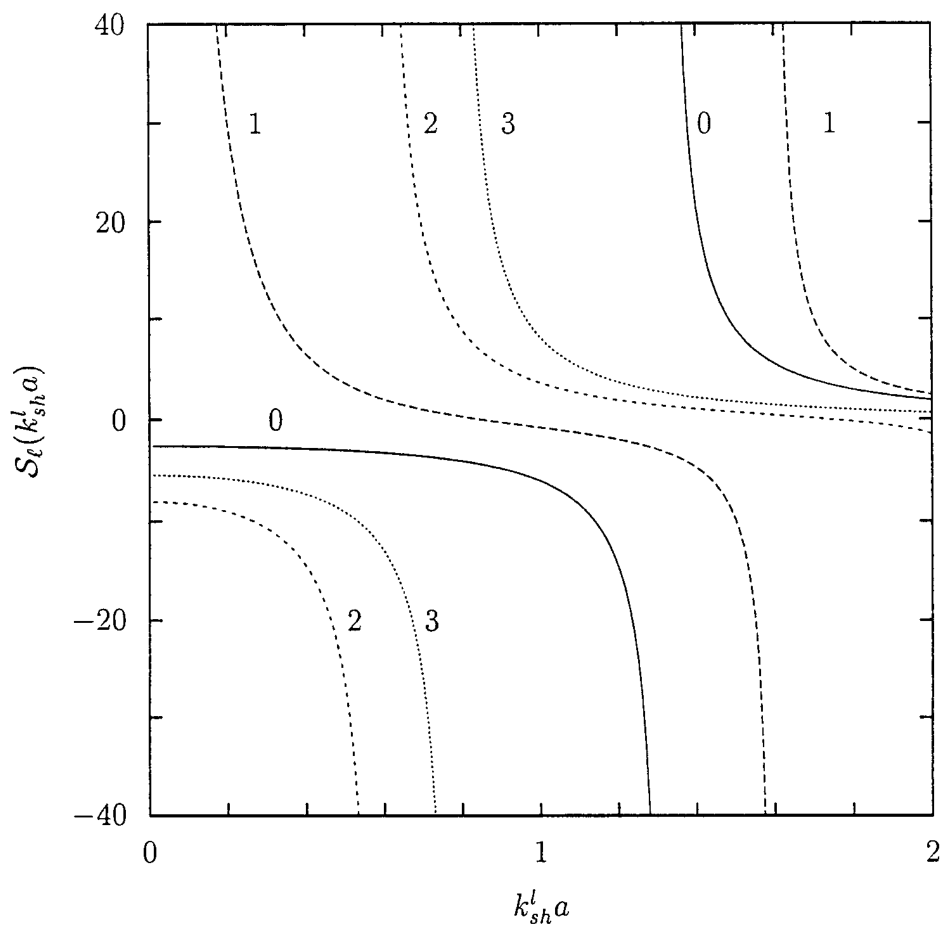

Shell admittance function for the stainless-steel resonator with $a = 8.89$ cm and $b/a = 1.215$ (a = inner radius, b = outer radius). The curves are labeled with the mode index ℓ, for acoustic pressures proportional to $P_\ell(\cos\theta)$. The fractional frequency perturbation due to shell motion is

$$\left(\frac{\Delta f}{f}\right)_{\ell n} \approx \frac{\rho_g c_g^2}{\rho_s c_{s,l}^2} \frac{S_\ell(k^l_{sh}a)}{1 - \ell(\ell+1)/z^2_{\ell n}}.$$

Here $k^l_{sh} = \omega/c_{sh,l}$, with $c_{sh,l}$ the longitudinal speed of sound in the shell.

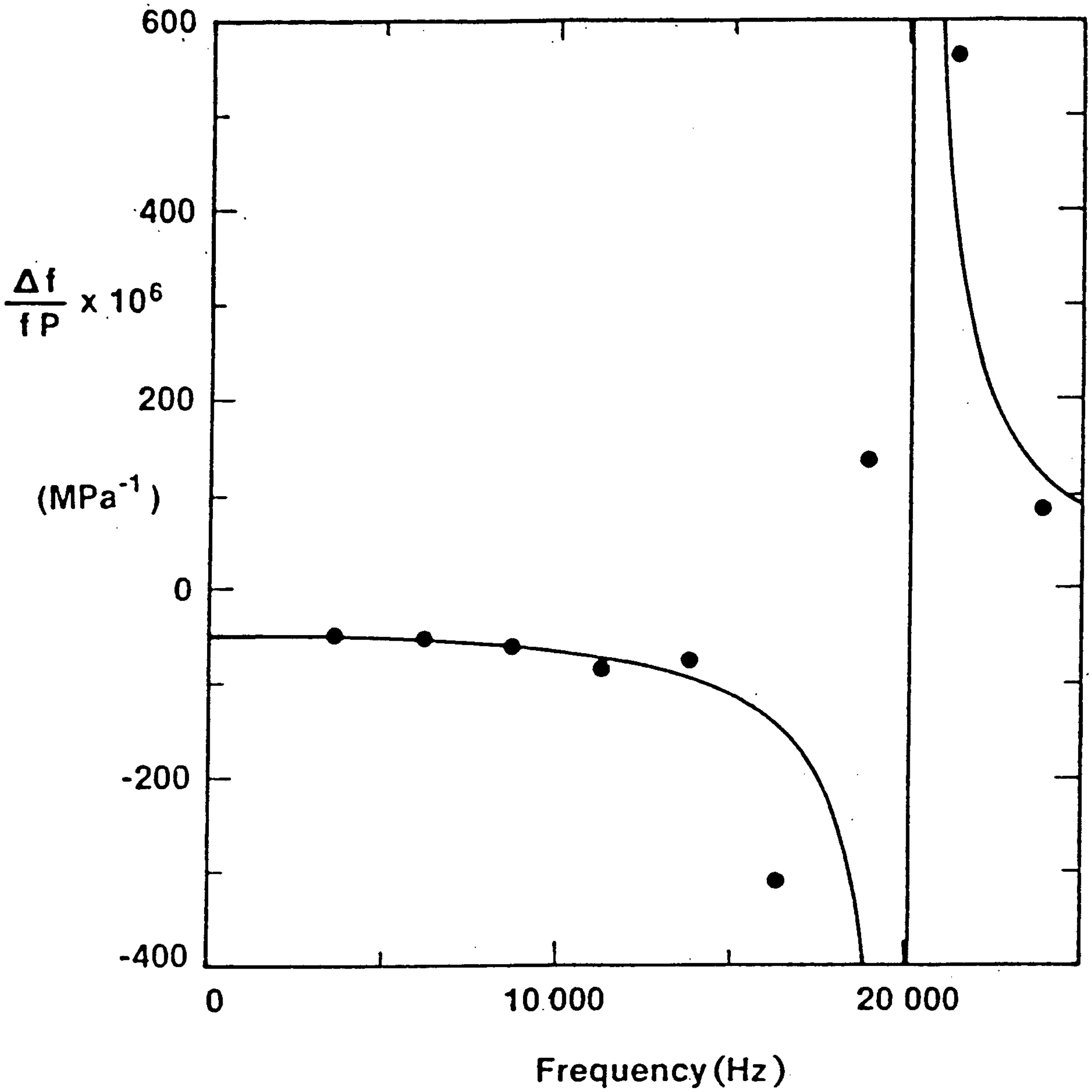

FIG. 11. Response of the shell to radially symmetric excitation as a function of frequency. The points are the average slopes of the curves in Fig. 9. The curve is calculated for an isotropic seamless shell using the theory of elasticity and the elastic constants tabulated for aluminum (see Table V). The idealized shell has a breathing resonance near 20.2 kHz.

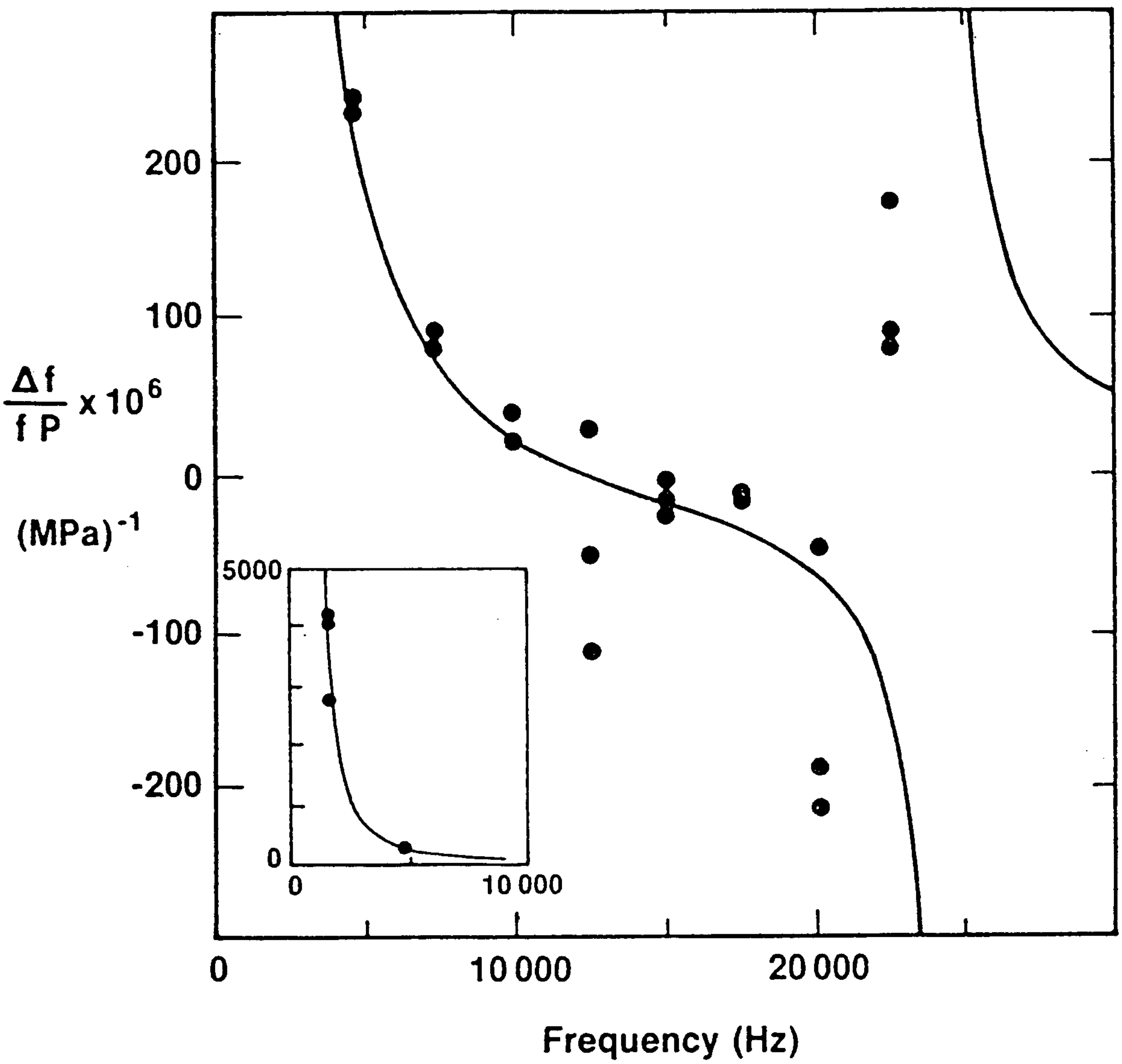

FIG. 12. Elastic response of the shell to excitation with symmetry of $Y_{1m}(\theta,\phi)$ as a function of frequency. The points are the average slopes of curves such as those shown in Fig. 10. The curve is calculated for an isotropic, seamless shell using the theory of elasticity and the elastic constants tabulated for aluminum. The idealized shell has Y_{1m} resonances at 0 and 24.5 kHz.

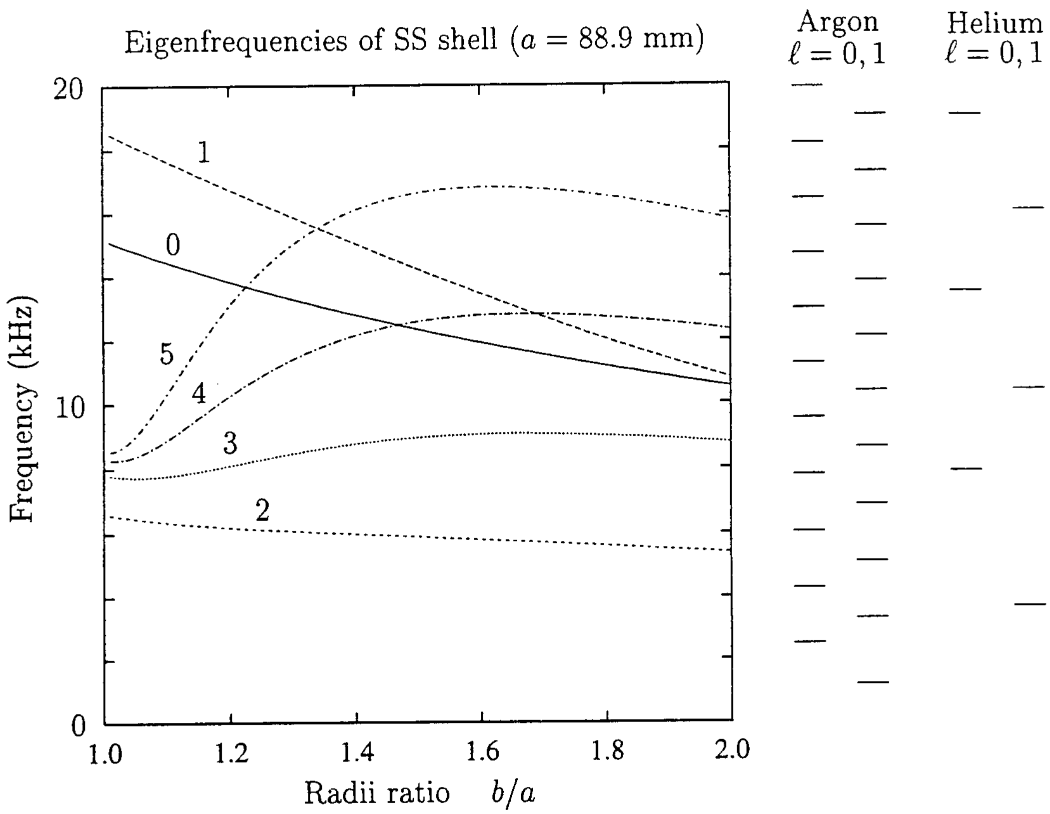

Eigenfrequencies of SS shell ($a = 88.9$ mm)
Argon
$\ell = 0, 1$
Helium
$\ell = 0, 1$
20
10
0
1.0
1.2
1.4
1.6
1.8
2.0
Frequency (kHz)
Radii ratio b/a
0
1
2
3
4
5

TR-14

Sampled Continuous Wave measurement on single crystals of YBCO and BSCCO.

Debashis Dasgupta
Jeff Feller

Carsten Hucho
Moises Levy
Bimal K Sarma

Resonance Meeting, 1999
Univ. of Mississippi

Graduate School, UW-Milwaukee
Physics Department, UW-Milwaukee
Office of Naval Research

Small size of HTSC single crystals.
(typically ~ 1000 X 800 X 200 microns)

Objective:

Develop an ultrasonic technique for investigating properties of these small HTSC crystals.

➡ Sampled CW Technique

2

OUTLINE

Type-II Superconductors

- Essentials (Magnetic phase diagram)
- Flux lines and Pinning sites

Description of Sampled CW Setup

Experimental Results On YBCO

- Untwinned Crystal
- Twinned Crystal
- ➡ Susceptibility Results (Twinned)

Experimental Results on BSCCO

Conclusions

Future

3

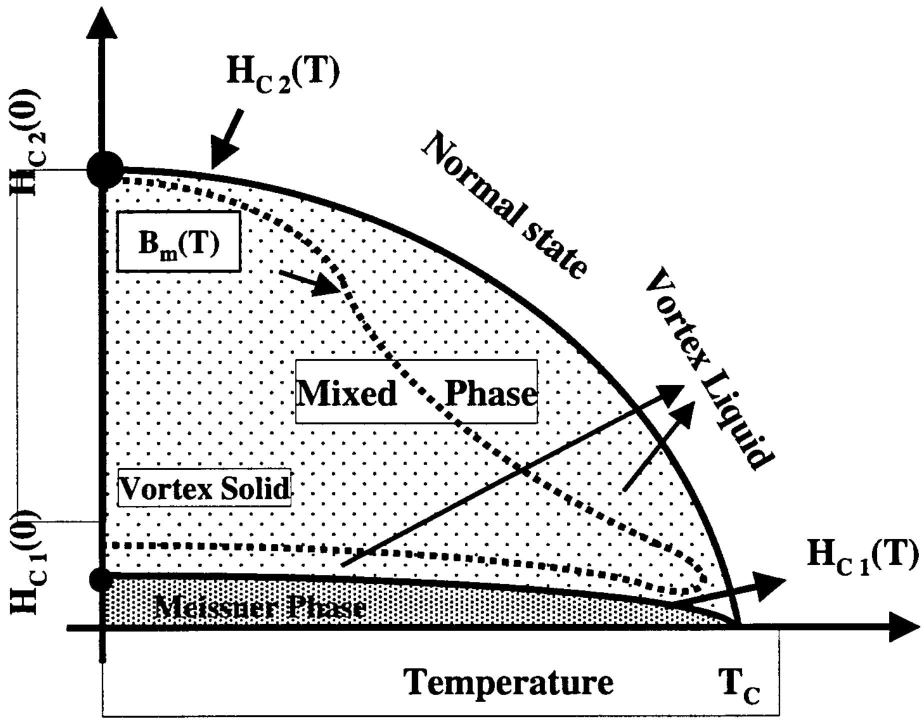

A schematic of complex magnetic phase diagram of a Type-II superconductor. Some of the regimes shown are magnified for clarity.

4

Forces acting on flux lines:

1) Repulsive Force

$$F/L = J_2 \times \Phi_1$$

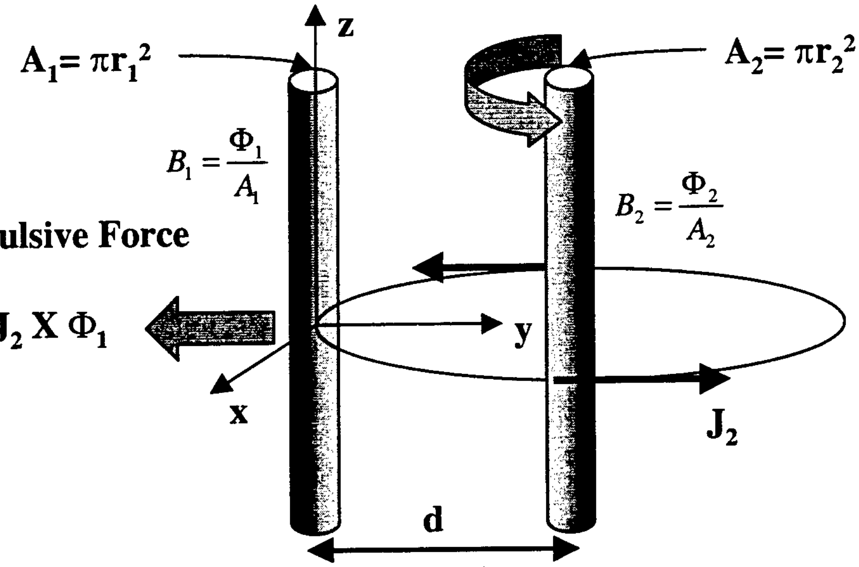

2) Lorentz Force

$$F = J \times B$$

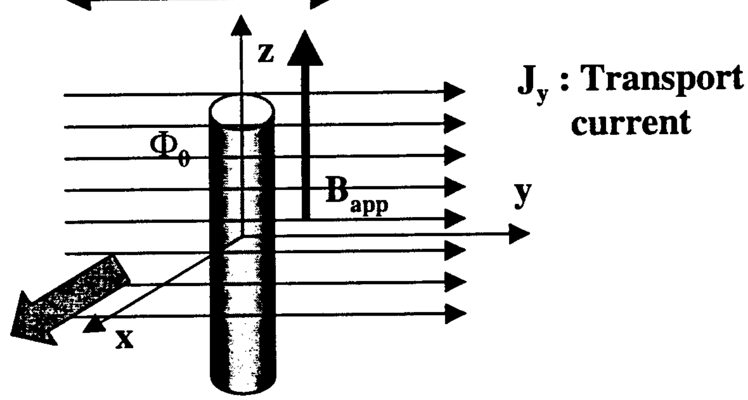

3) Magnus Force

$$F_M \sim - v_\phi \times \Phi_0$$

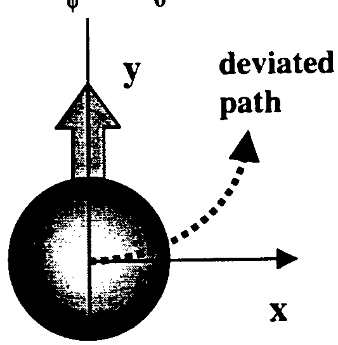

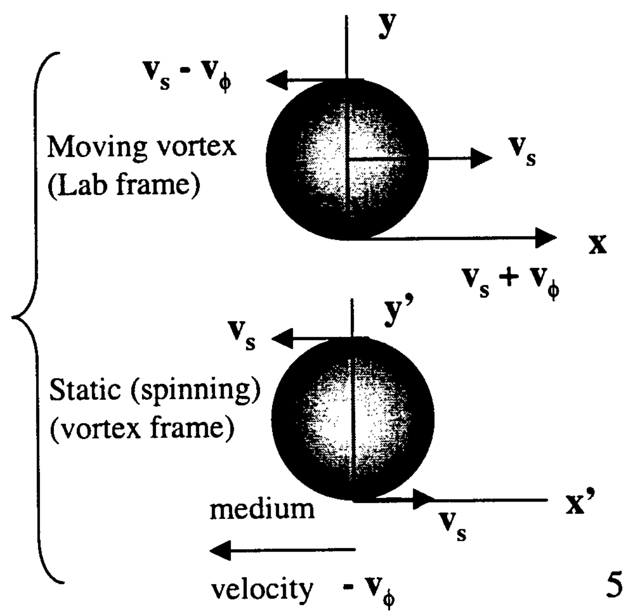

5

Pinning sources for flux lines

<u>Point defects</u>
- Oxygen Vacancies
- Electron Irradiation induced point defects

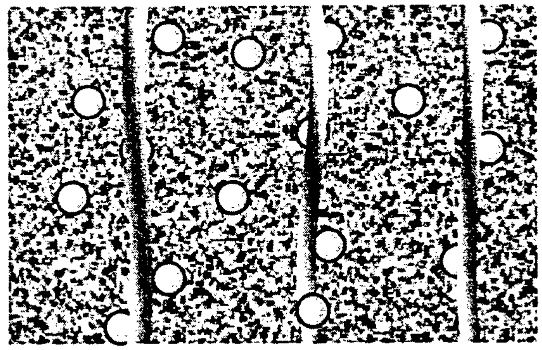

<u>Line Defects</u>

- Heavy ion irradiation induced columnar tracks

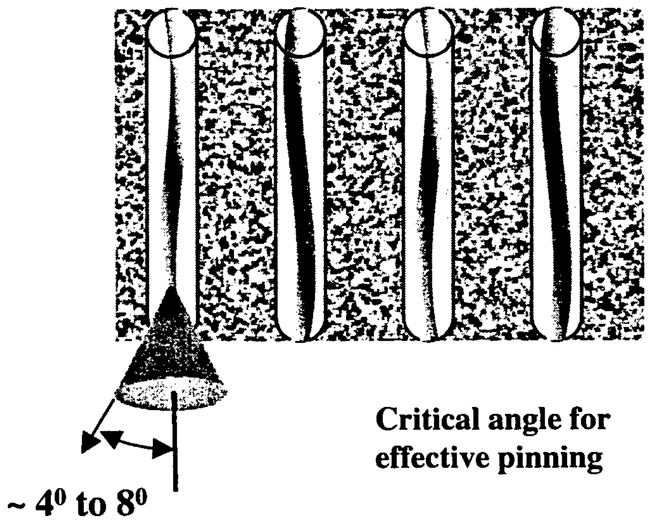

<u>Planar Defects</u>

- Twin Boundaries
- Layered Structure

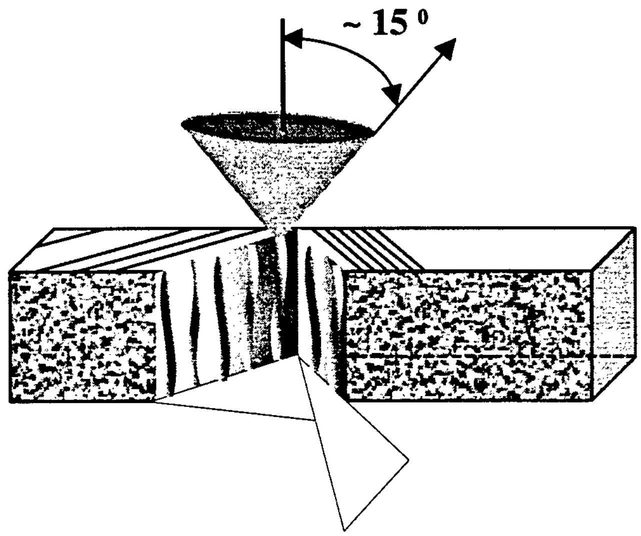

6

Continuous Wave Technique

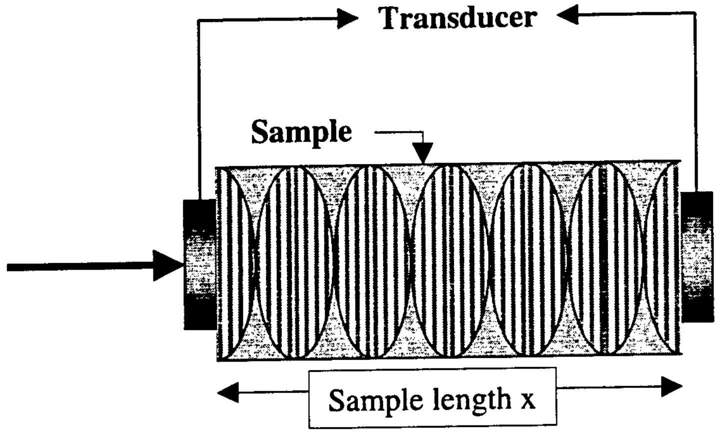

• **Setup standing wave resonances**

$$Q_m = \frac{\omega_m}{\Delta\omega}$$

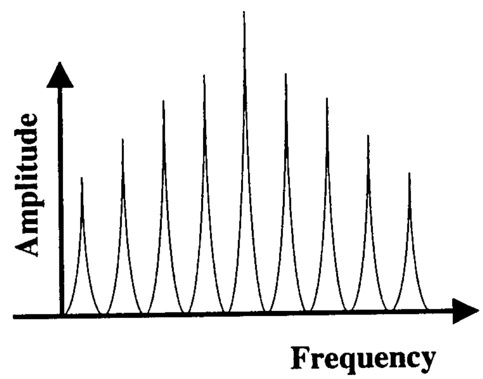

Lock in to mechanical resonance
Change external parameters (Temperature, Magnetic Field ...)

$\Delta f \rightarrow \Delta v$ $\qquad\qquad$ $\Delta A \rightarrow \Delta\alpha$

7

Sampled CW Experimental setup: transducer + crystal

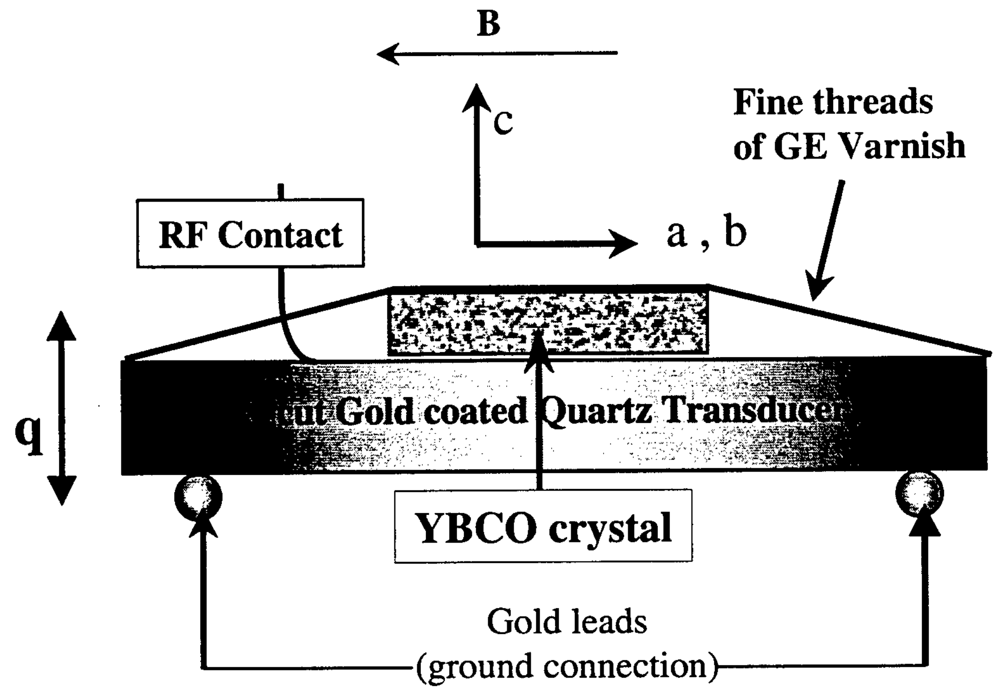

λ >> thickness of the sample assures no displacement gradient for the ions
sample thickness: ~50μm obtained through polishing (optical microscope for thickness)
sound velocity c:~ 5000 m/s, frequency: 5MHz $\Rightarrow$ $\lambda \approx 1$ mm >> sample thickness

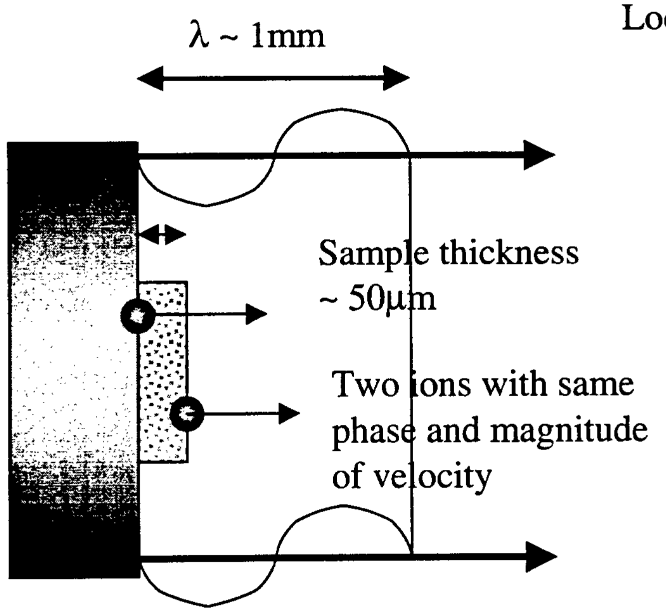

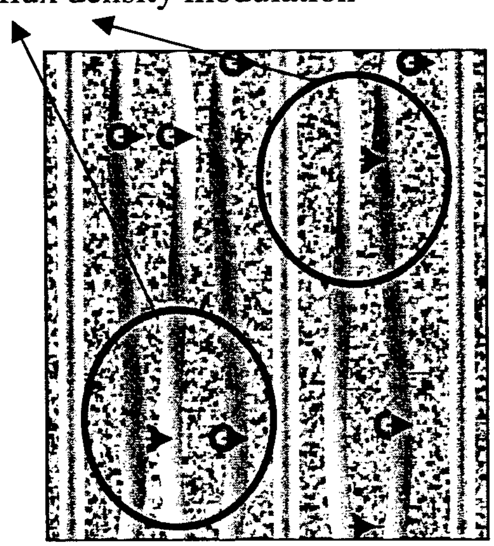

8

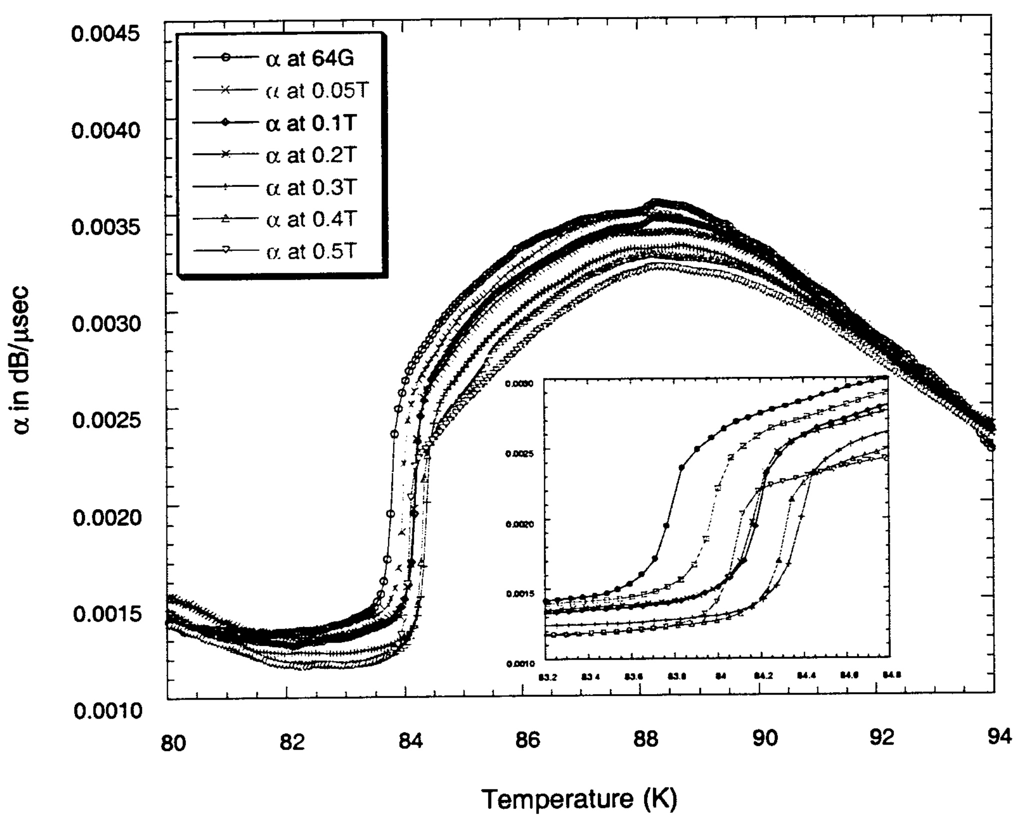

α at 64G
α at 0.05T
α at 0.1T
α at 0.2T
α at 0.3T
α at 0.4T
α at 0.5T
α in dB/μsec
Temperature (K)
0.0045
0.0040
0.0035
0.0030
0.0025
0.0020
0.0015
0.0010
80
82
84
86
88
90
92
94

9

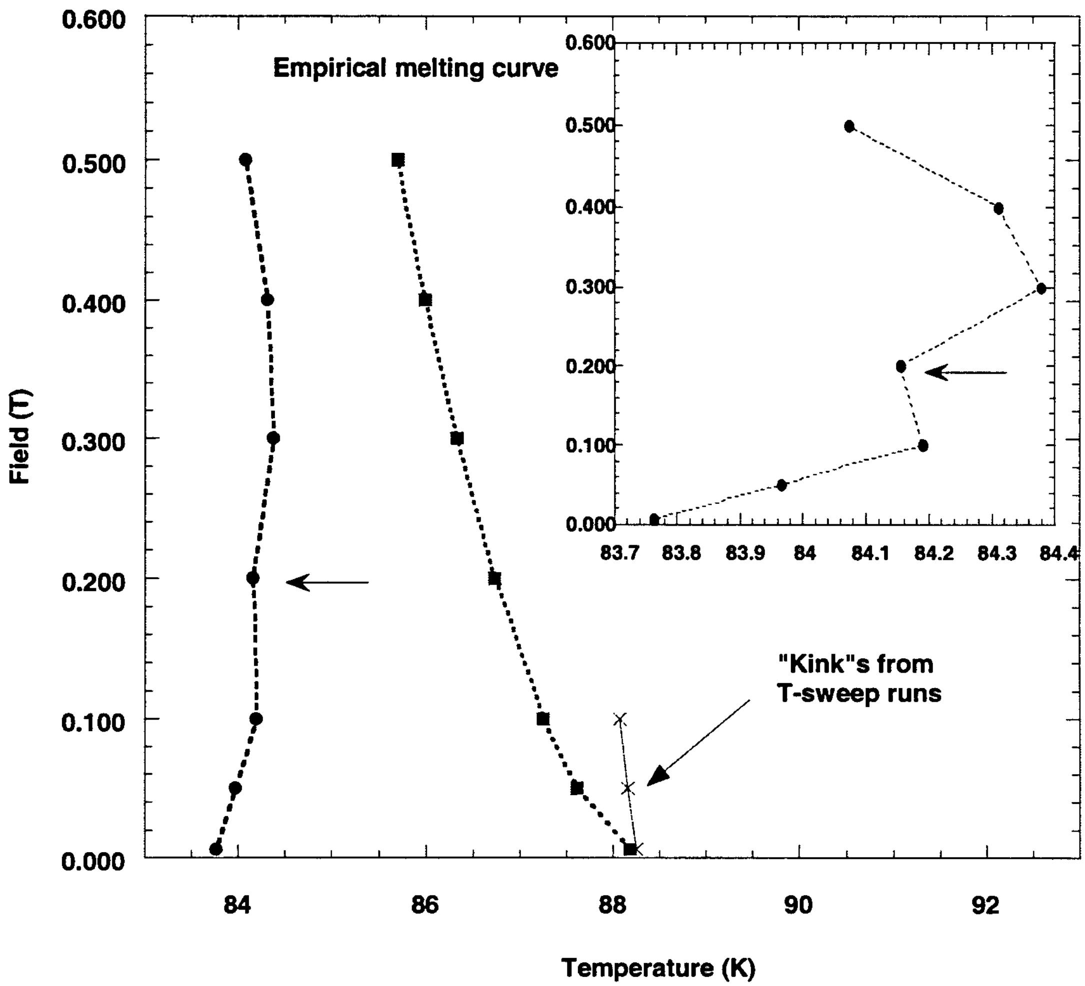
Empirical melting curve
"Kink"s from
T-sweep runs
Field (T)
Temperature (K)
0.600
0.500
0.400
0.300
0.200
0.100
0.000
84
86
88
90
92
83.7
83.8
83.9
84
84.1
84.2
84.3
84.4

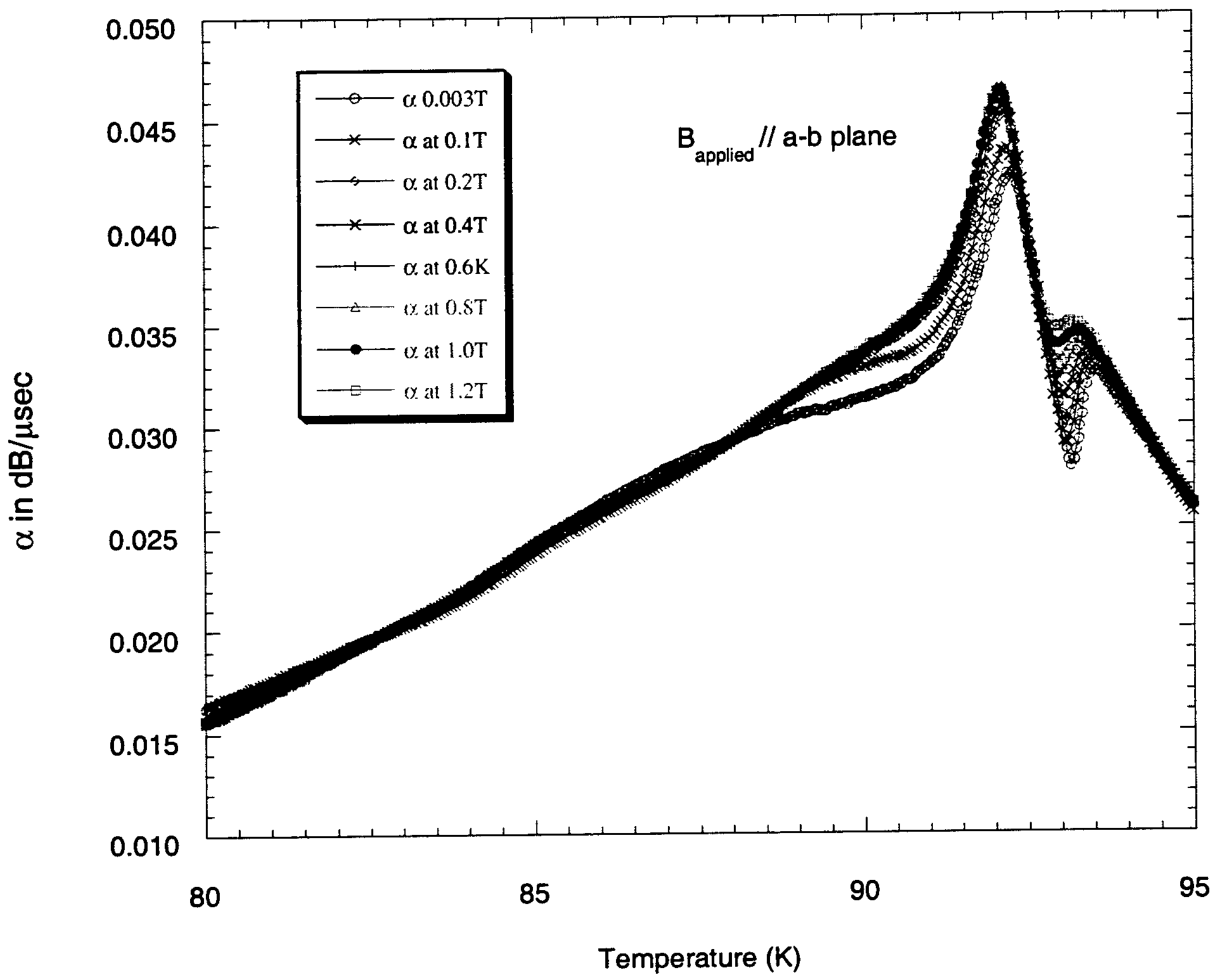
0.050
0.045
0.040
0.035
0.030
0.025
0.020
0.015
0.010
80
85
90
95
α in dB/μsec
Temperature (K)
α 0.003T
α at 0.1T
α at 0.2T
α at 0.4T
α at 0.6K
α at 0.8T
α at 1.0T
α at 1.2T
B applied // a-b plane

11

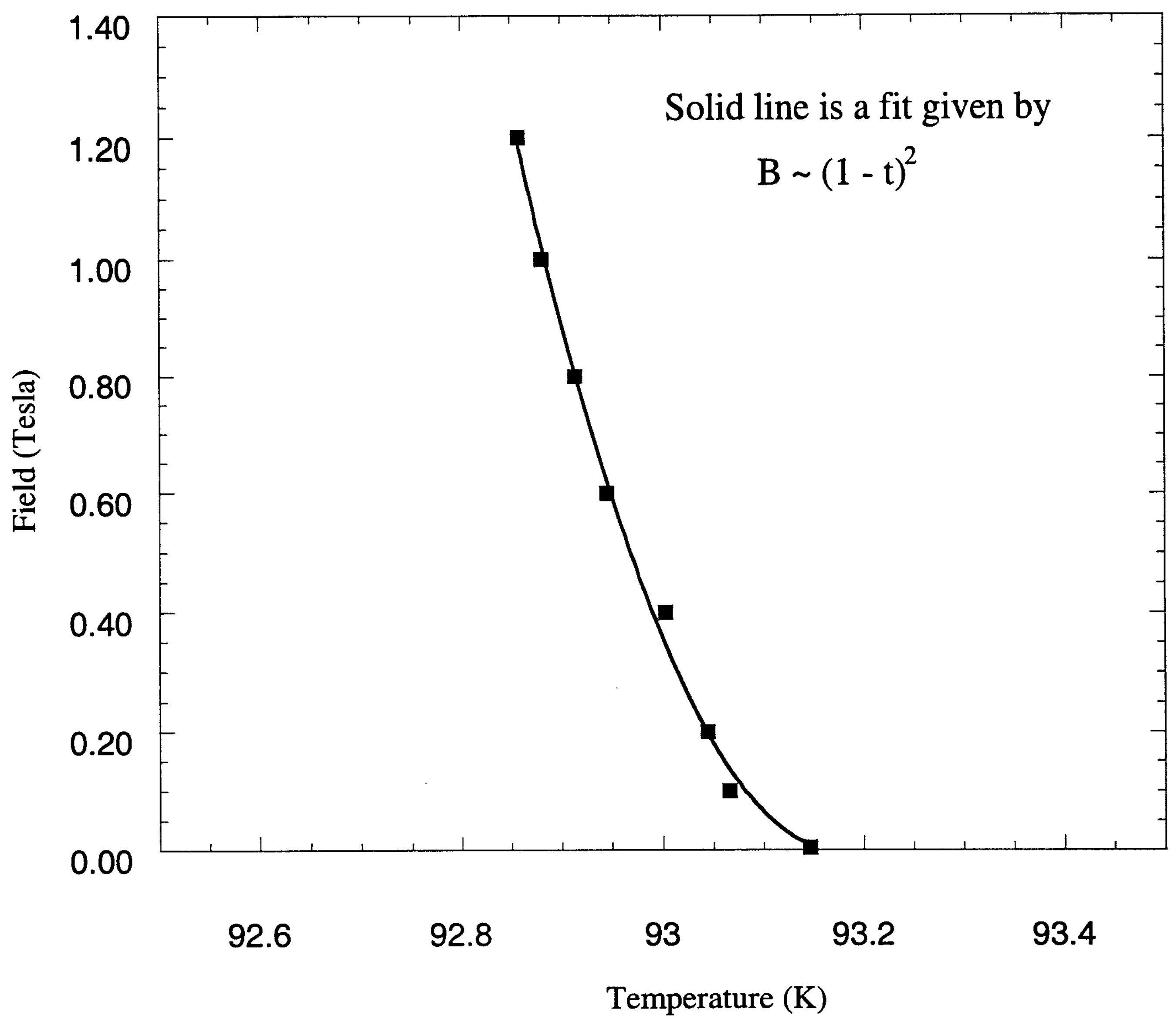
Solid line is a fit given by
B ~ (1 - t)^2
1.40
1.20
1.00
0.80
0.60
0.40
0.20
0.00
Field (Tesla)
92.6
92.8
93
93.2
93.4
Temperature (K)

12

H_{C2} and melting curves for a twinned YBCO crystal.
(H // c-axis)

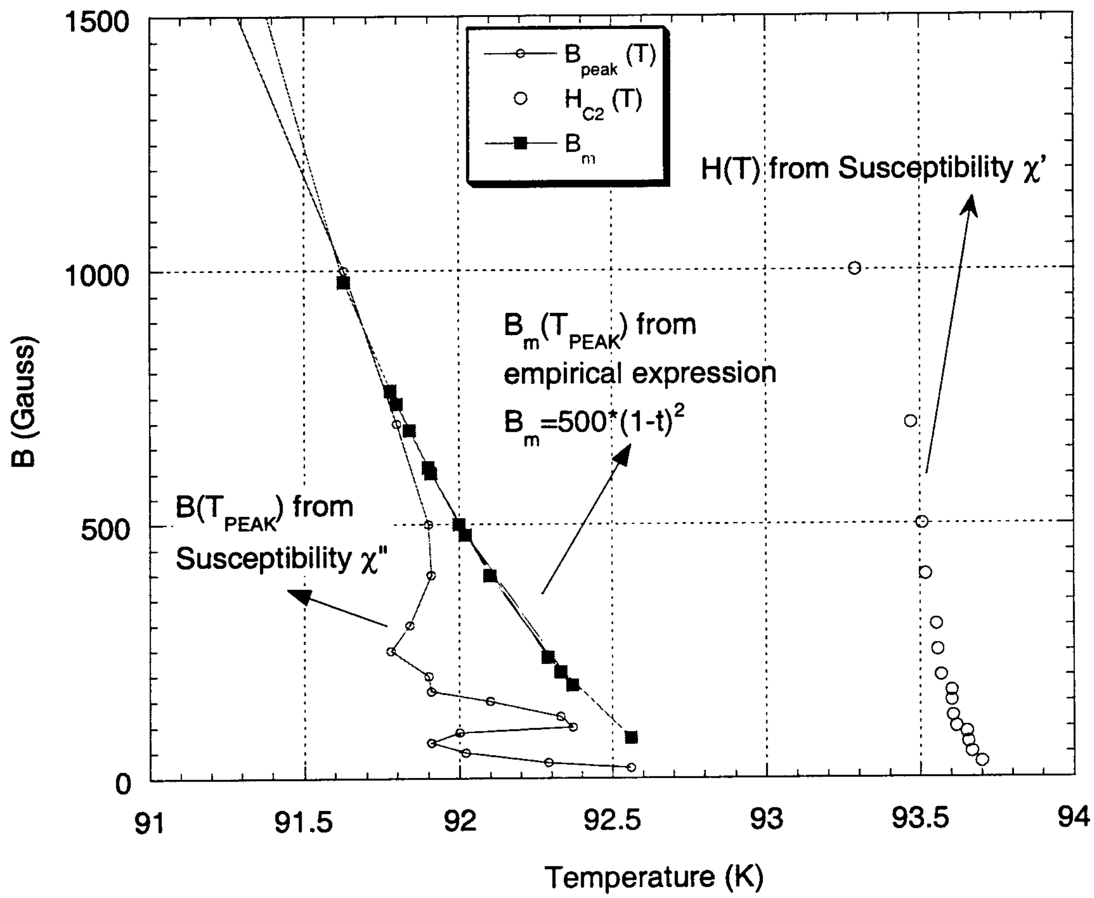

13

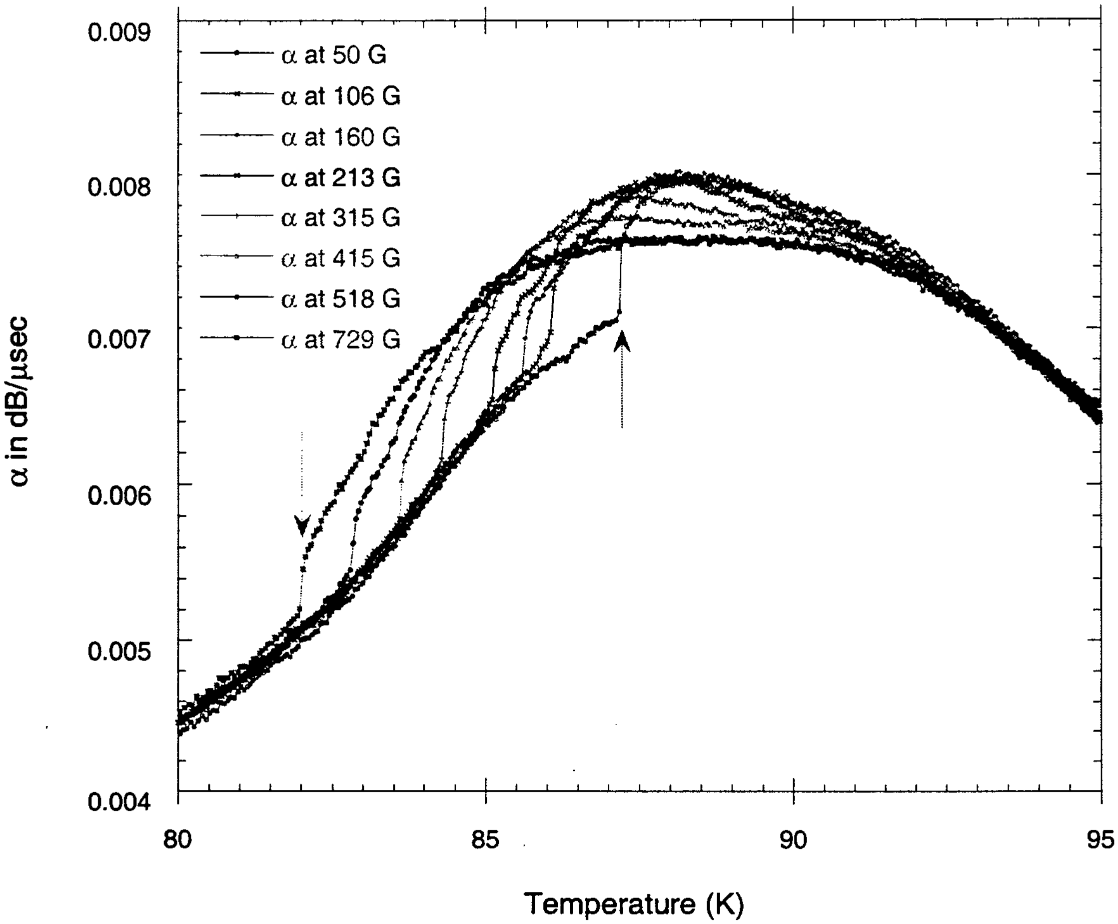
α at 50 G
α at 106 G
α at 160 G
α at 213 G
α at 315 G
α at 415 G
α at 518 G
α at 729 G
0.009
0.008
0.007
0.006
0.005
0.004
α in dB/μsec
80
85
90
95
Temperature (K)

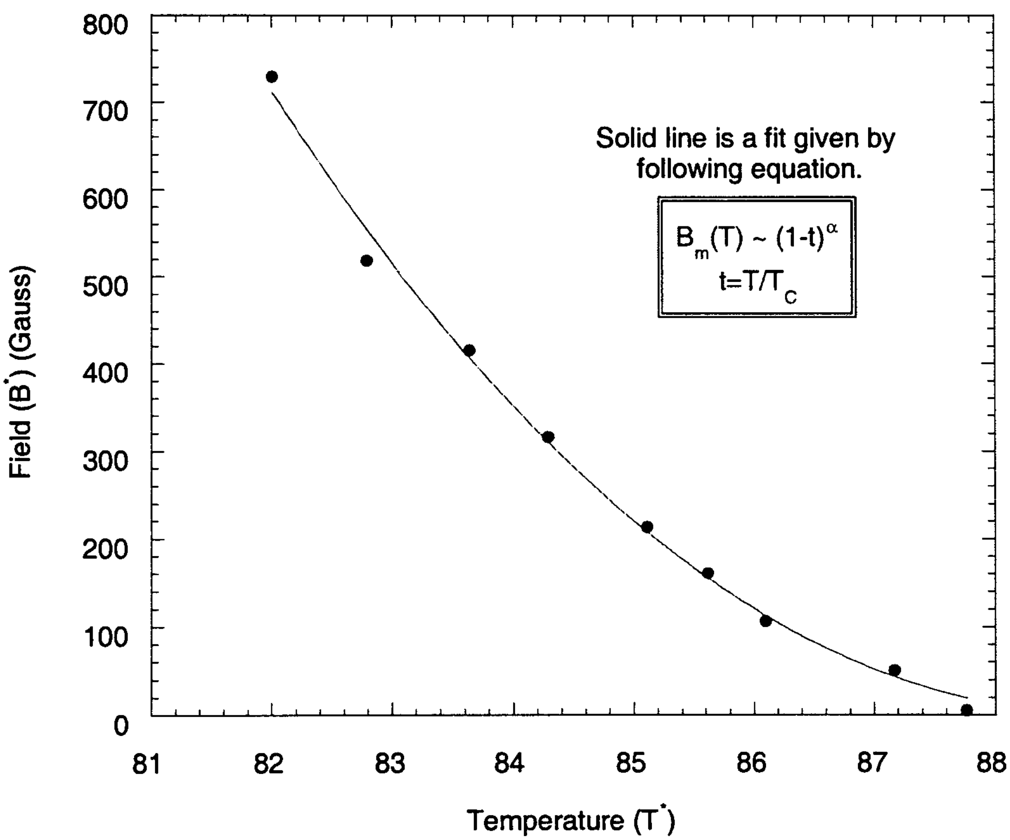
Solid line is a fit given by following equation.
$B_m(T) \sim (1-t)^{\alpha}$
$t=T/T_C$
800
700
600
500
400
300
200
100
0
Field (B^*) (Gauss)
81
82
83
84
85
86
87
88
Temperature (T^*)

14

Conclusions:

Sampled CW:

- "The ultrasonic technique"
- Minimum external perturbations →
  thermodynamic measurements
- Bulk elastic properties of flux lines
  - melting of flux lines in YBCO and BSCCO
  - soft lattice at low fields
  - rigid lattice at higher fields
  - possibly soft-rigid contour follows the melting curve with 0.3T as a turnaround field
- Sensitive to the "depinning" transition
  - change in activation energy around 0.3T for YBCO
- Basic electron-phonon interaction
  SC transition at H_{C2}

Susceptibility:

- Peak effect for YBCO
- Re-entrant nature of the peak effect has been observed

REPORT DOCUMENTATION PAGE

Form Approved
OMB No. 0704-0188

1. AGENCY USE ONLY *(Leave Blank)*

2. REPORT DATE
4 Jun 01

3. REPORT DYPE AND DATES COVERED
Conference Report, May 30 to Jun 30, 1999

4. TITLE AND SUBTITLE
Proceedings of the Resonance Meeting, Vol. 2. Transparencies

5. FUNDING NUMBERS
PE 61153N
N00014-98-1-0033

6. AUTHOR(S)
Elizabeth A. Furr, ed.

7. PERFORMING ORGANIZATION NAME(S) AND ADDRESS(ES)
Jamie L. Whitten National Center for Physical Acoustics
The University of Mississippi
University, MS 38677

8. PERFORMING ORGANIZATION REPORT NUMBER
LF1000-01

9. SPONSORING / MONITORING AGENCY NAME(S) AND ADDRESS(ES)
Office of Naval Research
ONR 331
800 North Quincy Street
Arlington, VA 22217-5660

10. SPONSORING / MONITORING AGENCY REPORT NUMBER

11. SUPPLEMENTARY NOTES

12a. DISTRIBUTION / AVAILABILITY STATEMENT
Approved for public release; Distribution unlimited

12b. DISTRIBUTION CODE

13. ABSTRACT *(Maximum 200 words)*
The Proceedings of the Resonance Meeting held May 30 to June 1, 1999 are in two volumes. Volume I of the proceedings contains verbatim transcriptions of the presentations given . This volume also contains a special appendix honoring Orson L. Anderson, Harold H. Demarest, Jr. and Ichiro Ohno for their contributions to the development of resonance techniques for determining elastic properties of solids.. Volume II of these proceedings contains copies of the transparencies used by the presenters.

14. SUBJECT TERMS **Resonance, Resonance Techniques, Acoustic Resonance, Resonant Ultrasound Spectroscopy, Elastic Properties**

15. NUMBER OF PAGES
25

16. PRICE CODE

17. SECURITY CLASSIFICATION OF REPORT	18. SECURITY CLASSIFICATION OF THIS PAGE	19. SECURITY CLASSIFICATION OF ABSTRACT	20. LIMITATION OF ABSTRACT
UNCLASSIFIED	UNCLASSIFIED	UNCLASSIFIED	

NSN 7540-01-280-5500

Standard Form 298 (Rev. 2-89)
Prescribed by ANSI Std. Z39-1
298-102